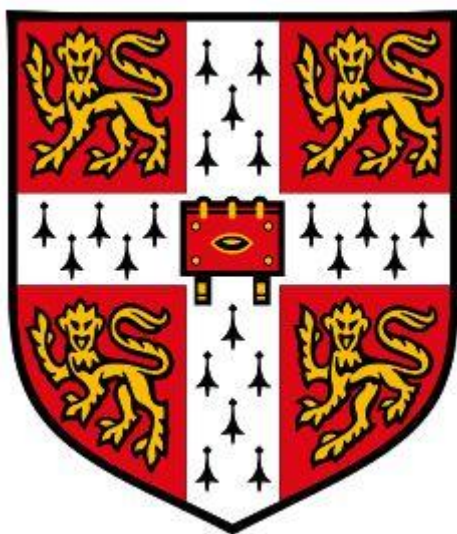


# **Rational Development of Small Molecules Targeting Virulence of *Pseudomonas aeruginosa***



**Rory Clifford Triniman**

**University of Cambridge  
Department of Pharmacology  
Hughes Hall College**

January 2021

This dissertation is submitted for the degree of  
Doctor of Philosophy



## **Preface**

### **Declaration**

This dissertation is the result of my own work and includes nothing which is the outcome of work done in collaboration except as declared in the Preface and specified in the text.

The following work was done in collaboration:

1. Molecular dynamic simulation conducted prior to this project by Dr Aneesh Chandran (University of Cambridge, UK).
2. Work on *Pseudomonas aeruginosa* was conducted in Dr Martin Welch's lab, department of Biochemistry (University of Cambridge, UK).
3. *Ex vivo* porcine lung experiments were conducted in Dr Freya Harrison's lab with Dr Marwa Hassan (University of Warwick, UK).
4. Transmission electron microscopy imaging during this project was done at the University of Cambridge core facility, CAIC with the help of Dr. Rita Monson (Department of Biochemistry)

This work has not been submitted for any other degree or qualification at the University of Cambridge, any other University or similar institution. This thesis does not exceed the prescribed word limit of 60,000 words set by the Biology Degree Committee. The work presented was conducted under the supervision of Dr Taufiq Rahman at the University of Cambridge, department of Pharmacology between October 2016 and January 2021.

## **Acknowledgements**

My first thanks and gratitude go to Dr Taufiq Rahman for providing me the opportunity to undertake this project as a member of his lab and of course his help and guidance throughout its duration. Secondly, to my collaborators, Dr Martin Welch who similarly provided a significant amount of guidance during my project, and Dr Freya Harrison and Dr Marwa Hassan who hosted me at Warwick University. I would like to thank Hughes Hall and the Department of Pharmacology for awarding me the Hughes Hall PhD Scholarship and the David James Bursary respectively, which have helped fund this work. Individuals that have contributed immensely to helping me with experimental techniques and advice are Dr Xavier Chee, Dr Stephen Dolan, Dr Rita Monson, Dr Alyssa McVey, Dr Eve Maunders and Dr Shunsuke Namata. Additionally, a huge thank you to the remaining members of the Rahman and Welch groups for the enjoyment day to day, a brilliant road trip across Ireland, visiting the south coast and a few liquid lunches on the river, amongst other memorable moments. Lastly, I would like to thank my parents for supporting my education as a seemingly perpetual student.

## Abstract

*Pseudomonas aeruginosa* is the leading cause of nosocomial infection in the UK and recognised as a critical priority pathogen in need of new antibiotics by the World Health Organisation. Its large genome allows it to adapt to a vast range of ecological niches meaning it is found almost ubiquitously in the environment, but as an opportunistic pathogen it poses almost no threat unless an individual is immunocompromised. *P. aeruginosa* causes a myriad of infections to burn, cancer, ventilated, and AIDS patients amongst many others. However, it is most associated with cystic fibrosis sufferers, colonising the lungs on average by 1yr of age and progressing to be the dominant infectious pathogen in the lungs for life. It is the leading cause of mortality in CF patients with ~80% dying from *P. aeruginosa* related lung failure.

*P. aeruginosa* is a multi-drug resistant pathogen with many intrinsic and acquired forms of resistance that can result in a cycle of infection, inflammation, tissue damage and scarring that ultimately results in lung failure. Without the development of any new commercial antibiotics for over 30 years focuses have shifted in the scientific literature to identifying new approaches to tackle infectious diseases. Targeting virulence factors poses many potential benefits, such as lower selection pressure driven resistance, shorter treatment times when used in conjunction with antibiotics, and preservation of gut microbiota to list just a few. *P. aeruginosa* has a large arsenal of virulence factors it uses to cause infections and the two major factors studied in this project are the type III secretion system and swarming motility.

During this project rational *in silico* drug discovery methods were used to identify small molecule inhibitors of ExsA, the master transcriptional regulator of the type III secretion system. The molecules were ordered from the Enamine and the NCI Diversity Set V libraries. Some small molecules were identified that bound to, but did not prevent activity of ExsA, and others that protected A549 lung epithelial cells *in vitro* from *P. aeruginosa* mediated cytotoxicity, but not by inhibition of ExsA. Upon further investigation it was found that phenyl piperazine molecules improved survival *in vivo* of *Galleria mellonella* in acute infection models by inhibiting the swarming activity of *P. aeruginosa*. How or if there is a link between the selection of compounds to inhibit ExsA and the inhibition of swarming is unknown, however the work in this project shows that phenyl piperazine molecules inhibit the expression of flagella under swarming conditions most likely by targeting a Class III or IV regulator in the

swarming regulatory hierarchy. This chemical class has therapeutic potential to be used as an anti-virulence treatment against *P. aeruginosa* infections and a full chemical assessment of the scaffold should be completed to move forward with patenting these compounds.

# Table of Contents

## Chapter 1: Introduction

<b>1.1 Antimicrobial resistance and its global threat</b> .....	<b>1</b>
1.1.1 Ancient resistance .....	1
1.1.2 Accelerating the rate of resistance .....	1
<b>1.2 An emergence of anti-virulence strategies</b> .....	<b>3</b>
1.2.1 A new approach to a growing problem .....	3
1.2.2 Anti-virulence therapies in the clinic .....	5
<b>1.3 <i>Pseudomonas aeruginosa</i></b> .....	<b>6</b>
1.3.1 An introduction .....	6
1.3.2 Acute and chronic <i>P. aeruginosa</i> infections .....	7
1.3.3 The cystic fibrosis lung .....	7
1.3.4 <i>P. aeruginosa</i> resistance mechanisms.....	8
1.3.5 Virulence mechanisms of <i>P. aeruginosa</i> .....	10
<b>1.4 The type III secretion system</b> .....	<b>12</b>
1.4.1 Evolution of the type III secretion system .....	12
1.4.2 Type III secretion system structure .....	12
1.4.3 Type III secretion system regulation.....	14
<b>1.5 Approaches to target the T3SS</b> .....	<b>17</b>
1.5.1 Targeting the regulation of the type III secretion system.....	17
1.5.2 Disrupting injectisome apparatus function.....	17
1.5.3 Effector proteins.....	19
<b>1.6 ExsA inhibition</b> .....	<b>20</b>
1.6.1 N-hydroxybenzimidazole inhibition of ExsA .....	20
<b>1.7 <i>In silico</i> drug discovery</b> .....	<b>22</b>
1.7.1 The rise of <i>in silico</i> .....	22
1.7.2 Ligand-based approaches .....	23
1.7.3 Structure-based approaches.....	24
1.7.4 Molecular dynamics .....	26
<b>1.8 Aims and objectives</b> .....	<b>26</b>

## Chapter 2: Materials & Methods

<b>2.1 <i>In silico</i> methods</b> .....	<b>29</b>
---	-----------

2.1.1 Protein structures and models .....	29
2.1.2 Sequence alignment .....	29
2.1.3 Prediction of ligand binding pockets.....	29
2.1.4 Electrostatic surface mapping .....	30
2.1.5 Ligand structures.....	30
2.1.6 Ligand docking .....	30
2.1.7 FA compounds selection.....	31
2.1.8 E compounds selection by molecular docking.....	31
2.1.9 NCI compounds selection .....	32
2.1.10 M compounds selection .....	32
2.1.11 Mutagenesis predictions for ExsA crystallography .....	32
<b>2.2 Bacterial techniques.....</b>	<b>33</b>
2.2.1 Bacterial strains.....	33
2.2.2 DNA extraction.....	35
2.2.3 Polymerase chain reaction (PCR) .....	35
2.2.4 Agarose gel electrophoresis .....	36
2.2.5 Restriction digest and ligation.....	36
2.2.6 Bacteria transformations .....	37
2.2.7 Phage transduction .....	37
2.2.8 DNA sequencing .....	38
<b>2.3 Mammalian cell culture techniques .....</b>	<b>38</b>
2.3.1 Mammalian cell line.....	38
2.3.2 Cell protection assay (CPA).....	38
2.3.3 Toxicity assay .....	39
<b>2.4 Protein purification.....</b>	<b>39</b>
2.4.1 Purification of ExsA.....	39
<b>2.5 Proteomic analysis .....</b>	<b>41</b>
2.5.1 SDS-PAGE .....	41
2.5.2 Secretome analysis.....	41
2.5.3 Liquid chromatography-tandem mass spectrometry (LC-MS/MS) .....	42
2.5.4 Electromobility shift assay .....	42
2.5.5 Western blot .....	42
2.5.6 ExsA X-ray crystallography.....	43
2.5.7 Intrinsic tryptophan fluorescence.....	44
2.5.8 Spectro fluorimetry .....	44
<b>2.6 Phenotypic assays.....</b>	<b>44</b>

2.6.1 Assay media and agar .....	44
2.6.2 Luciferase reporter assay .....	45
2.6.3 Growth curves .....	46
2.6.4 <i>Ex vivo</i> porcine lung.....	46
2.6.5 Protease activity .....	47
2.6.6 Biofilm formation .....	47
2.6.7 Twitching motility plate assay .....	47
2.6.8 Swimming motility plate assay .....	47
2.6.9 Swarming motility plate assay .....	47
2.6.10 Rhamnolipid production plate assay .....	48
2.6.11 Quorum sensing assay.....	48
2.6.12 Antibiotic minimal inhibitory concentration (MIC) assay .....	48
2.6.13 Transmission electron microscopy (TEM) imaging .....	48
<b>2.7 <i>In vivo</i> models .....</b>	<b>49</b>
2.7.1 <i>Galleria mellonella</i> killing assay.....	49

## Chapter 3: Compound Selection

<b>3.1 Binding site prediction of N-hydroxybenzimidazoles .....</b>	<b>51</b>
3.1.1 Background.....	51
3.1.2 Ligand binding pockets in AraC/Xyls proteins.....	52
3.1.3 Electrostatic surface mapping of AraC family proteins .....	58
3.1.3 Blind docking of N-hydroxybenzimidazoles .....	59
<b>3.2 Purification of ExsA.....</b>	<b>62</b>
3.2.1 Purification, function, and crystallization of ExsA .....	62
3.2.2 Evaluation of ExsA function.....	63
3.2.3 ExsA crystallography screen and stabilising mutagenesis predictions .....	67
<b>3.3 Compound selection.....</b>	<b>69</b>
3.3.1 Receiver operating characteristic (ROC) curve analysis.....	70
3.3.3 Ligand-based approaches .....	71
3.3.4 Structure-based approaches.....	73
3.3.5 Combined approaches ligand search.....	76
<b>3.4 Discussion.....</b>	<b>81</b>

## Chapter 4: Compound Screening

<b>4.1 Initial compound screening.....</b>	<b>84</b>
--	-----------

4.1.1 Background .....	84
4.1.2 Luciferase reporter screen .....	84
4.1.3 Protection against <i>P. aeruginosa</i> mediated cytotoxicity .....	92
<b>4.2 Further investigation of selected hits .....</b>	<b>97</b>
4.2.1 Growth curves .....	97
4.2.2 Evaluation of dose response and toxicity of selected compounds .....	99
4.2.3 Effect of compounds on T3SS expression .....	102
<b>4.3 <i>Galleria mellonella</i> acute PA01 infection models .....</b>	<b>104</b>
4.3.1 Animal models used in drug discovery against <i>P. aeruginosa</i> .....	105
<b>4.4 Discussion.....</b>	<b>110</b>

## Chapter 5: Alternative Virulence Mechanisms

<b>5.1 Phenyl piperazines .....</b>	<b>116</b>
5.1.1 Background .....	116
5.1.2 Assessment of NCI18 analogue activity .....	116
<b>5.2 Investigation of virulence mechanisms .....</b>	<b>120</b>
5.2.1 Protease activity .....	120
5.2.2 Biofilm formation .....	121
5.2.3 Motility related virulence.....	122
<b>5.3 Further investigation of swarming inhibition by NCI18<sup>1A</sup> .....</b>	<b>129</b>
5.3.1 Biosurfactant production.....	129
5.3.2 <i>gacA</i> hyper swarming mutant .....	130
5.3.3 <i>Pseudomonas tolaasii</i> swarming .....	132
5.3.4 QS activity .....	133
5.3.3 KEGG GENOME search for potential targets .....	136
<b>5.4 Discussion.....</b>	<b>139</b>

## Chapter 6: Flagella synthesis and ChpD related virulence

<b>6.1 Chemotaxis signal transduction pathways .....</b>	<b>144</b>
6.1.1 Background .....	144
<b>6.2 Investigation of ChpD as the phenyl piperazine target.....</b>	<b>147</b>
6.2.1 $\Delta$ <i>chpD</i> swarming phenotype .....	147
<b>6.3 Further assessment of NCI18<sup>1A</sup> activity.....</b>	<b>148</b>
6.3.1 Antibiotic susceptibility .....	148

6.3.2 Transmission electron microscopy (TEM) imaging .....	150
6.3.3 Acute <i>P. aeruginosa</i> infection model.....	153
<b>6.4 Characterisation of ChpD mutants.....</b>	<b>158</b>
6.4.1 Growth of the <i>chpD</i> transposon mutant .....	158
6.4.3 ChpD is required for full virulence <i>in vivo</i> .....	159
6.4.4 <i>chpD</i> mutant swimming motility .....	161
6.4.5 <i>chpD</i> mutation effects on QS .....	162
6.4.6 Evaluation of protease activity.....	164
6.4.7 <i>chpD</i> mutant secretome profile analysis by LC-MS/MS .....	165
<b>6.5 Conclusion and future directions .....</b>	<b>167</b>
6.5.1 Conclusion .....	167
6.5.2 Future directions .....	170
<b>Bibliography .....</b>	<b>175</b>

## List of tables and figures

### 1. Chapter 1: Introduction

**Figure 1.1** Antibiotic discovery timeline (pg.2)

**Figure 1.2** Rise in anti-virulence targeting (pg.3)

**Figure 1.3** Gram-negative antibiotic resistance mechanisms (pg.10)

**Figure 1.4** *P. aeruginosa* virulence factors (pg.11)

**Figure 1.5** Type III secretion system structure and regulation (pg.14)

**Figure 1.6** Type III secretion system inhibition mechanisms (pg.20)

**Figure 1.7** Key project work areas (pg.27)

**Table 1.1** N-hydroxybenzimidazole 2D chemical structures (pg.22)

### 2. Chapter 2: Materials & Methods

**Figure 2.1** Lactate dehydrogenase detection reaction (pg.39)

**Table 2.1** Strains used in this study (pg.33)

**Table 2.2** Antibiotics used in this study (pg.35)

**Table 2.3** Plasmids used in this study (pg.36)

**Table 2.4** Primers used in this study (pg.37)

**Table 2.5** ExsA purification buffers (pg.40)

**Table 2.6** Buffers and solutions used in this study (pg.41)

**Table 2.7** EMSA buffers (pg.42)

**Table 2.8** Sparse matrix industry screens for crystallization (pg.44)

**Table 2.9** Phenotypic assay media and agar recipes (pg.45)

### 3. Chapter 3: Compound Selection

**Figure 3.1** Putative binding site of N-hydroxybenzimidazoles in ExsA (pg.53)

**Figure 3.2** Predicted ligand binding sites in MarA and Rob (pg.55)

**Figure 3.3** AraC CTD predicted ligand binding pockets (pg.56)

**Figure 3.4** Predicted ligand binding pockets in ExsA MD simulation models (pg.57)

**Figure 3.5** Electrostatic surface map of AraC (pg.59)

- Figure 3.6** Blind docking of N-HB40 in AraC conformations (pg.61)
- Figure 3.7** ExsA purification (pg.64)
- Figure 3.8** ExsA functional activity in electromobility shift assay (pg.66)
- Figure 3.9** Predicted stabilising mutagenesis for ExsA crystallization (pg.69)
- Figure 3.10** ROC curve analysis of GOLD scoring functions (pg.72)
- Figure 3.11** Ligand-based approaches (pg.74)
- Figure 3.12** NCI compound selection (pg.75)
- Figure 3.13** ExsA tryptophan fluorescence quenching (pg.77)
- Figure 3.14** Docked ligand poses of ExsA binding compounds (pg.79)
- Figure 3.15** 2D chemical structures of FA8 and FA15 (pg.80)

#### **4. Chapter 4: Compound Screening**

- Figure 4.1** Luciferase reporter assay screen (pg.86)
- Figure 4.2** YM64 luciferase transformant (pg.92)
- Figure 4.3** Optimisation of cell protection assay (pg.93)
- Figure 4.4** Cell protection assay compound screen (pg.95)
- Figure 4.5** PA01 compound affected growth curves (pg.98)
- Figure 4.6** Toxicity profiles of compounds against A549 lung epithelial cells (pg.101)
- Figure 4.7** Compound effects on type III secretion system expression (pg.103)
- Figure 4.8** M1 effect on type III secretion system expression (pg.104)
- Figure 4.9** *G. mellonella* LD<sub>50</sub> and acute infection model (pg.110)
- Figure 4.10** *G. mellonella* survival in NCI18 treated acute infection models (pg.111)
- Table 4.1** Luciferase reporter assay (pg.90)
- Table 4.2** Luciferase and cell protection assay comparison (pg.97)
- Table 4.3** EC<sub>50</sub> values for prevention of *P. aeruginosa* mediated cytotoxicity (pg.100)

#### **5. Chapter 5: Alternative virulence mechanisms**

- Figure 5.1** 2D phenyl piperazine analogue structures (pg.117)
- Figure 5.2** Toxicity and efficacy of NCI18 and analogues (pg.118)
- Figure 5.3** *In vitro* and *ex vivo* growth of NCI18<sup>1A</sup> treated *P. aeruginosa* (pg.119)
- Figure 5.4** NCI18<sup>1A</sup> effect on type III secretion system expression (pg.120)
- Figure 5.5** NCI18<sup>1A</sup> effect on PA01 protease activity (pg.121)

- Figure 5.6** NCI18<sup>1A</sup> effect on biofilm formation (pg.122)
- Figure 5.7** PA01 swimming control and motility (pg.124)
- Figure 5.8** Swarming inhibition by phenyl piperazines (pg.127)
- Figure 5.9** NCI18<sup>1A</sup> effect on rhamnolipid production (pg.129)
- Figure 5.10** *gacA* hyper swarming mutants treated with NCI18<sup>1A</sup> (pg.131)
- Figure 5.11** NCI18<sup>1A</sup> effects on *P. tolaasii* swarming (pg.133)
- Figure 5.12** NCI18<sup>1A</sup> effect on PA01 and PA14 QS molecule production (pg.135)
- Figure 5.13** PQS production during *P. aeruginosa* growth (pg.138)

**Table 5.1** PA01 twitching motility (pg.128)

## **6. Chapter 6: Flagella synthesis and ChpD related virulence**

- Figure 6.1** Chemotaxis signal transduction pathways (pg.145)
- Figure 6.2** *chpD* mutant swarming (pg.147)
- Figure 6.3** TEM images of *P. aeruginosa* in planktonic and swarming conditions treated with NCI18<sup>1A</sup> (pg.155)
- Figure 6.4** PA01 *G. mellonella* infection model treated with NCI18<sup>1A</sup> (pg.157)
- Figure 6.5** Growth of PA01 vs *chpD*::*Tn* (pg.158)
- Figure 6.6** *chpD* mutant *G. mellonella* infection model (pg.160)
- Figure 6.7** *chpD* mutant swimming motility (pg.161)
- Figure 6.8**  $\Delta$ *chpD* mutation effects on QS (pg.163)
- Figure 6.9** Protease activity of the *chpD* transposon mutant (pg.164)
- Figure 6.10** Secretome analysis of  $\Delta$ *chpD* mutant and NCI18<sup>1A</sup> treated cultures (pg.167)
- Table 6.1** Antibiotic susceptibility of *P. aeruginosa* (pg.148)
- Table 6.2** *chpD* mutant twitching (pg.159)

**List of abbreviations:**

2D – Two dimensional

3D – Three dimensional

AA – Amino acid

AHL – Acyl-homoserine lactone

AI – artificial intelligence

ALU – Arbitrary light units

AMR – Antimicrobial resistance

APBS - Adaptive Poisson-Boltzmann Solver

ASM – Artificial sputum media

AUC – Area under curve

BHL – N-butyryl homoserine lactone

BoNT – Botulinum neurotoxin

cAMP – 3'-5'-cyclic adenosine monophosphate

c-di-GMP – Cyclic di-guanylate

CF – Cystic fibrosis

CFTR – Cystic fibrosis transmembrane conductance regulator

CFU – Colony forming units

CHO – Chinese hamster ovary

CPA – Cell protection assay

CTD – C-terminal domain

DMSO – Dimethyl sulfoxide

DNA – Deoxyribonucleic acid

dNTP – Dinucleotide triphosphate

DTT – Dithiothreitol

EDTA – Ethylenediaminetetraacetic acid

EGTA – Ethylene glycol-bis( $\beta$ -aminoethyl ether)-N,N,N',N'-tetra acetic acid

EMSA – Electromobility shift assay

EU – European Union

FA – Field Align

FBS – Foetal bovine serum  
FDA – Food and Drug Administration  
GAP – GTPase-activating proteins  
gDNA – Genomic DNA  
GFP – Green fluorescent protein  
GPU – Graphics processing units  
HPLC – High performance liquid chromatography  
ICD – Isocitrate dehydrogenase  
INT – tetrazolium salt  
IPTG – isopropyl  $\beta$ -d-1-thiogalactopyranoside  
IQS – 2-(2-hydroxyphenyl)-thiazole-4-carbaldehyde  
kDa - Kilodaltons  
LB – Lennox broth  
LBA – Lennox broth agar  
LC-MS/MS – Liquid chromatography-tandem mass spectrometry  
LDH – Lactate dehydrogenase  
Lux – Luciferase  
MD – Molecular dynamics  
MDR – Multi-drug resistant  
MH – Mueller Hinton  
MIC – Minimum inhibitory concentration  
MOI – Multiplicity of infection  
NAD – Nicotinamide adenine dinucleotide  
NADPH – Nicotinamide adenine dinucleotide phosphate  
NCI – National Cancer Institute  
N-HB – N-hydroxybenzimidazole  
NMR – Nuclear magnetic resonance  
NS – Non-specific  
NTD – N-terminal domain  
OD – Optical density

OdDHL– N-(3-oxododecanoyl)-homoserine lactone

PA– *Pseudomonas aeruginosa*

PBS – Phosphate buffered saline

PCR – Polymerase chain reaction

PDB – Protein data bank

PSGL-1 – P-selectin glycoprotein ligand-1

PQS – *Pseudomonas* quinolone signal

PVDF – Polyvinylidene fluoride

QS – Quorum sensing

QSAR – Quantitative structure-activity relationship

RFU – Relative fluorescent units

RLU – Relative light units

ROC – Receiver operating characteristic

ROCS – Rapid overlay of chemical structures

SAR – Structure activity relationship

SDM – Site directed mutagenesis

SDS – Sodium dodecyl sulphate

SDS-PAGE – Sodium dodecyl sulphate polyacrylamide gel electrophoresis

ssDNA – sonicated salmon sperm DNA

T2SS – Type II secretion system

T3SS – Type III secretion system

T4P – Type IV pili

TAE – Tris-acetate EDTA

TC – TanimotoCombo

TCA – Trichloroacetic acid

TEM – Transmission electron micrograph

v/v – Volume/volume

w/v – Weight/volume

WHO – World Health Organisation

WT – Wild type

$\lambda_{\text{max}}$  – Maximum emission wavelength

# **Chapter 1**

## **Introduction**

## **1.1 Antimicrobial resistance and its global threat**

### **1.1.1 Ancient resistance**

Antibiotic resistance is a topic much misunderstood by the general public, but it is a problem that has been faced from just a few short years after the introduction of antibiotics to clinical medicine<sup>[1, 2]</sup>. This is not to suggest that the development of commercial antibiotics began antibiotic resistance, it has in fact existed for millennia and therefore long before Fleming's discovery of penicillin. The majority of antibiotics are naturally derived from bacteria and fungi that use them as a form of weaponry in the competition for resources. Microbes have therefore also needed to develop sophisticated defence mechanisms to combat these antibiotics and ensure survival. When a microbe develops resistance to a once effective treatment it is known as antimicrobial resistance (AMR). Antibiotic resistance is a subset of AMR referring specifically to bacterial resistance to antibiotic treatments. Genomic analysis of ancient bacteria found in permafrost and other preserved locations demonstrates this ancient origin of AMR, finding genes associated with resistance long before the clinical introduction of infection medicines<sup>[3, 4]</sup>.

Bacterial resistance comes in two forms, intrinsic and acquired. Intrinsic resistance is due to innate physical or functional characteristics that enable them to evade an antibiotic mechanism of action<sup>[5]</sup>. Acquired resistance may stem from spontaneous mutation or horizontal gene transfer of mobile genetic elements<sup>[6-8]</sup>. The most common acquisition of resistance is via horizontal gene transfer between microorganisms where conjugation, transformation and transduction allow sharing of genetic material that can result in a myriad of defence mechanisms. These include the manipulation of drug targets, reduced permeability, improved efflux, alterations to cellular metabolic pathways and deactivating enzymes<sup>[8, 9]</sup>.

### **1.1.2 Accelerating the rate of resistance**

The famous discovery of penicillin in 1928 by Alexander Fleming marked the beginning of 60 years of antibiotic discovery that revolutionised medicine by making previously lethal infections easily treatable. Antibiotic use today is largely taken for granted however, it has now been 30 years since the introduction of a new antibiotic for use in the clinic (see **figure 1.1**) and AMR has risen sharply over these decades, presenting one of the most challenging threats to global health today. Over-prescription, misuse, prevalence of use in

livestock farming, and the expansion of an immunocompromised population have all contributed to the accelerated rate of resistance<sup>[10]</sup>.

Hospitals are an environment of intense selection pressure which harbour accelerated resistance and the production of so called ‘super bugs’ with extensive multi-drug resistance<sup>[11, 12]</sup>. *Pseudomonas aeruginosa* (*P. aeruginosa*, henceforth ‘PA’) has asserted itself as one such ‘superbug’, being one of the most common nosocomial infections in the UK. In 2017 the World Health Organisation (WHO) released a list of the 12 bacteria most in need of new antibiotics with PA listed as critical and second overall<sup>[13]</sup>.

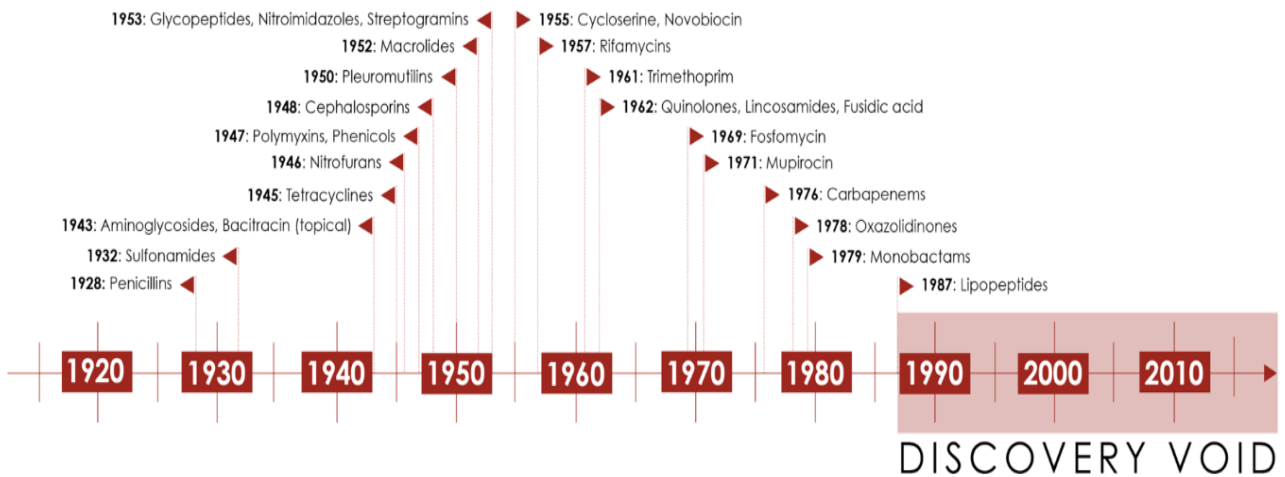


**Figure 1.1 Antibiotic discovery timeline:** Major antibiotic classes and their year of discovery from the first penicillin to the current day. There has been more than 30 years since a commercially available antibiotic has been introduced. Image was taken from Dickey *et al.*, (2017).

There is a substantial economic cost to AMR that impacts policy making, the behaviour of hospitals, other healthcare facilities and the funding bodies that support them<sup>[14–17]</sup>. The likelihood of hospitalisation and mortality are much higher in infection cases of resistant strains over treatment susceptible strains, as well as increased hospital stay lengths and longer treatment requirements. This amounts to costing between USD\$6,000-30,000 more per patient treated and in a wider context the WHO published the estimated societal cost of AMR to be €1.5 billion per annum for the European Union (EU) and up to €35 billion for the USA<sup>[17, 18]</sup>. Considering this, new antimicrobial treatments could have substantial positive impacts

economically as well as medically, and with AMR related deaths forecast to exceed cancer deaths by 2050 new treatment options are becoming increasingly urgent<sup>[14, 15, 19, 20]</sup>.

## 1.2 An emergence of anti-virulence strategies

### 1.2.1 A new approach to a growing problem

Exploration of pathways in bacterial metabolism that may reveal adjunctive or alternative therapies to antibiotics has exploded in recent years with the developing AMR problem. One of the main focuses has been targeting virulence components that are essential for bacterial pathogenicity. Since bacteria are capable of conferring virulence through numerous mechanisms, these budding approaches include targeting toxin delivery, bacterial adhesion, population density related virulence, and many more<sup>[21–23]</sup>. Examples for each of these are: the six secretion systems seen in Gram-negative bacteria (Type I–VI)<sup>[24]</sup>; the Dr family of adhesins in *Escherichia coli* associated with diarrhoea and urinary tract infections<sup>[25]</sup>; and quorum sensing controlling gene expression by autoinducer molecules, such as acyl-homoserine lactones (AHL) small molecules in Gram-negative or peptides in Gram-positive

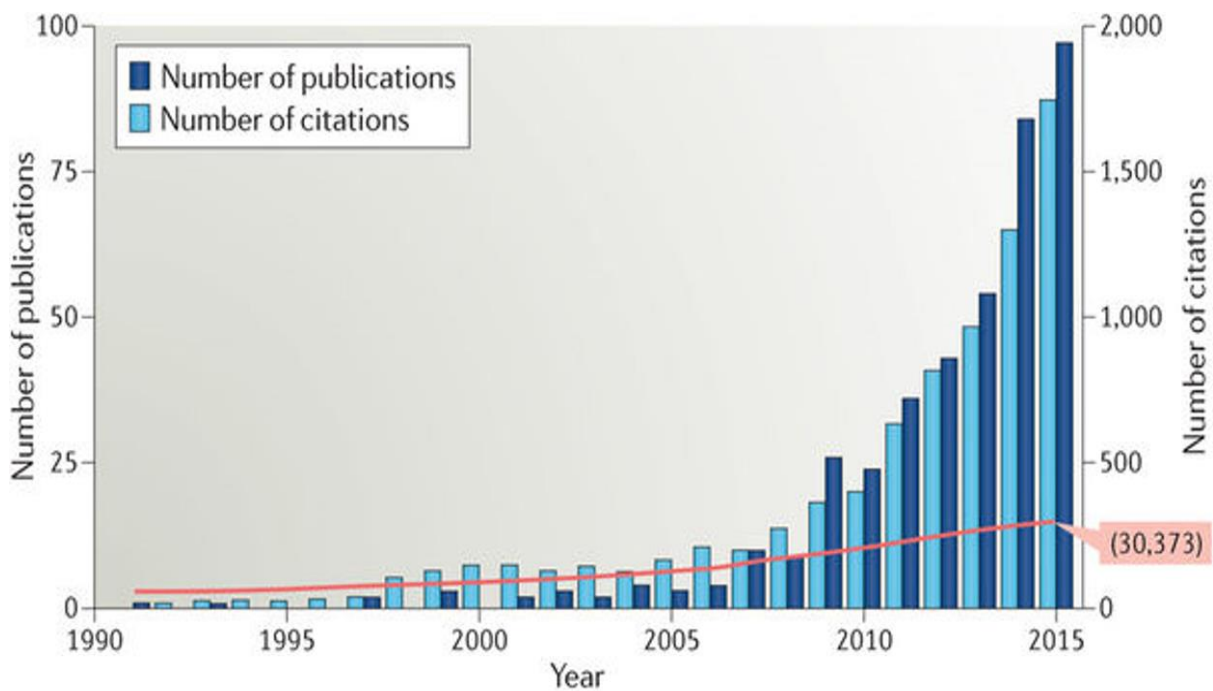


**Figure 1.2 Rise in anti-virulence targeting:** The rise in anti-virulence publications on Web of Science. The red line indicates the total number of publications scaled to the total in 2015. Figure taken from Peleg *et al.*, (2010).

bacteria<sup>[26]</sup>. **Figure 1.2** illustrates this recent increase in scientific literature published on anti-virulence.

In an infection scenario a pathogen must overcome several challenges presented by the host immune system and often by competing microbes as well. To establish an infection, it is critically important the pathogen can rapidly sense and adapt to the surrounding environment. Physical barriers, secretions such as mucus, pH changes and attacks by host immune cells are just some examples of how pathogens are prevented from successful colonization<sup>[21]</sup>. By targeting and blocking the array of strategies by which pathogens overcome these defences or outcompete other microbes offers new ways to fight infections. Without them the infective pathogen is susceptible to immune clearance or enhanced clearance by conventional antibiotic therapy<sup>[27]</sup>.

A number of potential advantages are envisaged by targeting virulence, with the primary hope being a substantial reduction in selection pressure. Antibiotics are identified via their bactericidal or bacteriostatic activity, targeting cell wall integrity, growth, protein synthesis, or DNA replication, but targeting virulence does not interfere with these growth and viability factors. Therefore, there should not be such pressurised selection for resistant bacteria as antibiotics create, by only killing those that are not resistant<sup>[27–29]</sup>. Virulence mechanisms also tend to be shared only in closely related species meaning resistance is less likely to be transferred horizontally into alternate species<sup>[23]</sup>. A major area that contributes to this selection pressure and AMR is the widespread use of antibiotics in livestock feed because of the growth benefits for the animals<sup>[22, 23, 30]</sup>. Anti-virulence therapies are unlikely to be used in this area since they would lack these growth benefits, meaning a dramatic reduction in exposure to initiate resistance.

Use as an adjunctive therapy to antibiotics or as a prophylactic have the potential to shorten treatment times and remove the need for antibiotic prescription; both would significantly reduce overall usage of antibiotics<sup>[22, 23, 31]</sup>. A further advantage is in the preservation of gut flora to which antibiotic treatment can damage and complicate recovery since broad spectrum antibiotics have no discrimination between pathogenic and resident microbes. Bacteria are able to seize an ecological niche as the flora are disrupted and secondary infections can occur; a notable example being diarrhoea caused by *Clostridium difficile* that disrupts intestinal function through two toxins, TcdA and TcdB<sup>[32–34]</sup>. Problems related to

digestion may become apparent as well as the benefits of ‘good’ gut microbes being lost following a course of antibiotic treatment<sup>[34]</sup>.

### 1.2.2 Anti-virulence therapies in the clinic

Antivirulence drugs already exist for some species, including *Clostridium botulinum*<sup>[35]</sup>. The botulinum neurotoxin (BoNT - eight types, A-H) disrupts the release of neurotransmitters at the neuromuscular junction, which can cause progressive paralysis and respiratory distress. Immunoglobulins purified from donor plasma that has been injected with pentavalent BoNT A-E inactivated toxins can neutralise the BoNT. The use of these immunoglobulins was the very first demonstration of efficacy by virulence targeting in a randomised clinical trial, showing a decrease in time required on mechanical ventilation and hospital stay<sup>[36-39]</sup>.

Following the success of inactivating toxins in acute infections, significant further work has been pursued using monoclonal antibodies to replicate this mechanism. One such example is the recently approved bezlotoxumab to treat *C. difficile* infections<sup>[40, 41]</sup>. However, despite monoclonal antibodies and toxin inactivation taking the lead to demonstrate antivirulence usefulness in the clinic, and biologics having grabbed the limelight in the media, it is still small molecules that rule the roost in new drug approvals. Between 2010 and 2017, the Food and Drug Administration (FDA) in the US approved 262 new molecular entities, of which 76% were small molecules<sup>[42]</sup>.

With only a small number of anti-virulence drugs in current clinical use, there is a lack of empirical data to determine whether resistance really is bypassed. Arguments exist for both scenarios, however, there is certainly no lack of ambition or drive in the research pursuing virulence mechanisms with small molecules. Drug repurposing and an expansion in using artificial intelligence (AI) to uncover new drugs is broadening the search and several common virulence mechanisms are being targeted.

Adhesion and biofilm formation play a key role in pathogenicity and are a focus of antivirulence research. Fimbrion (St Louis, MO) in collaboration with GlaxoSmithKline, for example, are developing mannophosphates as prodrugs and mannose C-glycosides to improve oral availability and *in vivo* metabolic stability after it was shown that biphenyl mannosides

were capable inhibitors of FimH mediated bacterial adhesion in mice, studying uropathogenic *Escherichia coli* (*E. coli*)<sup>[43, 44]</sup>. Direct toxin inhibition is not only being left to antibodies either, as cyclodextrins have been shown to successfully block pore forming toxins and treat *Staphylococcus aureus* (*S. aureus*) infections in mice<sup>[11, 45, 46]</sup>. Other mechanisms include toxin secretion and bacterial communication such as the type III secretion system (T3SS) and quorum sensing (QS), both of which are prominent virulence factors in PA.

PA virulence determinants have been a popular target given its prevalence and listing by WHO, as well as its extensive virulence arsenal. The T3SS in PA is the primary virulence factor it possesses and as it stands 12 small molecules have been identified that inhibit its expression or function causing a reduction in cytotoxicity to host cells<sup>[47-49]</sup>. The molecules range in their proposed mechanism of action from targeting T3SS regulatory systems, both directly and indirectly, blocking key structural or functional components of the injectisome, and inhibiting the activity of effector proteins. Only one of the small molecules has been tested *in vivo* but a bifunctional antibody that targets the translocation apparatus and a surface polysaccharide is currently in phase II clinical trials<sup>[50]</sup>.

### **1.3 *Pseudomonas aeruginosa***

#### **1.3.1 An introduction**

PA is a ubiquitous, Gram-negative, bacillus and mono-flagellated bacterium that acts as an often-lethal opportunistic pathogen in plants, animals and humans. First isolated in 1882 by Carle Gessard from soldiers' wounds whose bandages had turned blue-green, it belongs to the Pseudomonadaceae family and the  $\gamma$ -proteobacteria class. PA can often be isolated from healthy individuals, but it almost exclusively causes infection in immunocompromised or immunosuppressed individuals. It has become notorious and justifiably feared for its ability to persistently grow on medical equipment, particularly catheters and ventilators. Accounting for 10% of all nosocomial infections across the EU and boasting a staggering average mortality of 40-60% in hospitals, PA causes a broad range of infections with a prominent patient demographic being cystic fibrosis (CF) sufferers<sup>[51, 52]</sup>.

Containing a genome of between 5.5 and 7 million base pairs means, PA has one of the largest genomes among bacteria that allows it to operate a versatile metabolism with basic

nutritional requirements. The genome is split into a conserved core that is seen when sampled from a variety of patients, and an accessory genome that varies considerably even amongst species clones and contributes to its genetic plasticity. This adaptability permits the colonisation of numerous environments and hence the breadth of infections it may cause<sup>[53–55]</sup>.

### **1.3.2 Acute and chronic *P. aeruginosa* infections**

Acute infections are associated with highly virulent and planktonic cultures that results in direct decline in lung function by invading and damaging the lung tissue<sup>[43, 54–57]</sup>. PA has several virulence factors that enable it to evade the host immune system and outcompete other microbes in the lung. One virulence factor, the T3SS, has been linked to worse clinical outcomes and a mortality rate increased up to six times<sup>[52]</sup>. Direct injection of cytotoxic effector proteins into host cells by the T3SS causes the significant damage to tissue and evasion of the host immune response mentioned<sup>[43, 58, 59]</sup>.

Acute infections can often progress to chronic infections as a biofilm is established on the lung epithelium, however, the exact mechanism that causes this lifestyle change from a planktonic, mobile culture is not fully understood<sup>[60]</sup>. Cells adhere to the lung epithelium and begin to downregulate virulence and motility factors whilst upregulating production of a polysaccharide rich extracellular matrix. Microcolonies increase in size as the biofilm matures with a heterologous population, although, peripheral cells maintain the ability to disseminate under certain conditions by expressing enzymes which cleave the extracellular matrix. This dissemination may cause acute flare ups or allow the occupation of a new environmental niche<sup>[61, 62]</sup>.

### **1.3.3 The cystic fibrosis lung**

CF is caused by a hereditary mutation to the cystic fibrosis transmembrane conductance regulator (CFTR) gene, most commonly F508Δ. The mutations are divided into classes based on how they affect the expression, trafficking, or function of the protein. Class I mutations result in a complete loss of expression: class II cause misfolded proteins that never reach the cell surface: class III effect the function of the channel but do reach the cell membrane: class IV have functional problems specifically to do with opening the ion channel: and class V mutations cause insufficient quantities of the protein to be expressed. Under normal conditions the CFTR helps maintain the osmotic balance across cells membranes by allowing

chloride ions out of the cell, but when CFTR is absent or faulty a thick mucus builds up at the epithelial surface due to the water imbalance. Consequently, CF sufferers are prone to lung infections, have a persistent cough, are often short of breath, and can have gastro-intestinal and male fertility problems. CF is most associated with infections of the lung largely due to the impeded beating of cilia which are unable to clear bacteria.

Over the lifetime of a CF patient there is a gradual colonisation of the lungs by a variety of microorganisms that begins in infancy, with their population densities varying over the years<sup>[63]</sup>. By the time they are in their 20s most patients have PA as the prevailing microbial community in their lungs and it remains so for the rest of their lives. PA is the leading cause of mortality in immunocompromised patients and 80% of CF sufferers die from pulmonary obstruction; caused by a cycle of infection, inflammation and pulmonary obstruction, producing tissue damage and scarring that ultimately results in lung failure<sup>[64, 65]</sup>. Typically, treatment for CF patients with an acute PA infection involves anti-inflammatory drugs to prevent lung damage and aggressive antibiotic therapy. The latter, given the rates of resistance and the selection for those that develop resistance, or were already resistant, can exacerbate the disorder rather than help. Hospital stays are often extended as the lungs are quickly re-colonised by resistant bacteria, creating further risk to the patient the longer they remain in care<sup>[66-69]</sup>.

An important aspect of PA pathophysiology in the CF lung is that patients have accelerated decline in lung function and earlier mortality when monoclonal chronic infections undergo adaptive diversification of clonal variants. This is one of the reasons why it is treated so aggressively at initial and new-onset stages. The primary aim is to eradicate the infection at an acute stage before a chronic infection is established and adaptive responses by PA are made that severely hinder treatment. Additional changes that PA makes in establishing a chronic infection is the downregulating flagellum expression and overexpressing exopolysaccharides which confer a mucoid status and increases the chances of failing to eradicate the infection.

#### **1.3.4 *P. aeruginosa* resistance mechanisms**

Two major intrinsic resistance mechanisms contribute to the multi-drug resistant (MDR) nature of PA. Firstly, as a Gram-negative bacterium, it is less permeable to antibiotics than Gram-positive bacteria because of an additional lipopolysaccharide outer membrane that prevents the uptake of larger hydrophobic molecules, such as glycopeptide antibiotics<sup>[70-72]</sup>. The cell surface can be further modified by lowering the expression of porins or creating a

biofilm to prevent penetration by antibiotics<sup>[72, 73]</sup>. The second intrinsic resistance mechanism is the removal of antibiotics from the cell by expressing a host of MDR efflux pumps<sup>[66, 67, 69, 74, 75]</sup>. They are active in removing a wide range of compounds, metabolites, toxic entities and QS molecules. The MexAB-OprM, MexCD-OprJ, MexEF-OprN and MexXY-OprM are the most comprehensively researched efflux systems in PA; the MexAB-OprM being the most highly expressed and having the broadest range of activity against antimicrobial agents<sup>[75]</sup>. The others have a narrower range of substrates, but their activity is often seen to increase during an infection. Their activity serves to lower the intracellular concentration of the drugs and can confer resistance to  $\beta$ -lactams, tetracyclines, chloramphenicols and fluoroquinolones<sup>[76]</sup>.

Bacteria can acquire resistance by modifying enzymes, mutating the antibiotic target and changing the abundance or necessity of the target<sup>[71, 73, 76, 77]</sup>. Modifying enzymes that inactivate antibiotics are common and PA expresses some of these. AmpC  $\beta$ -lactamase is commonly found in PA that confers resistance to  $\beta$ -lactam antibiotics such as penicillin and its derivatives<sup>[78]</sup>. Point mutations that alter the DNA codon and cause an amino acid (AA) substitution in the target protein can lower the affinity of a drug for the target but maintain the protein's activity within the cell<sup>[79–82]</sup>. When necessary, bacteria may even make the drug target redundant or expendable through a variety of ways. This can include acquisition by horizontal gene transfer to create new metabolic functions, or from *de novo* mutations in the genome<sup>[83–85]</sup>. **Figure 1.3** gives an overview of these mechanisms of resistance in Gram negative bacteria and examples of the antibiotics they confer resistance to.

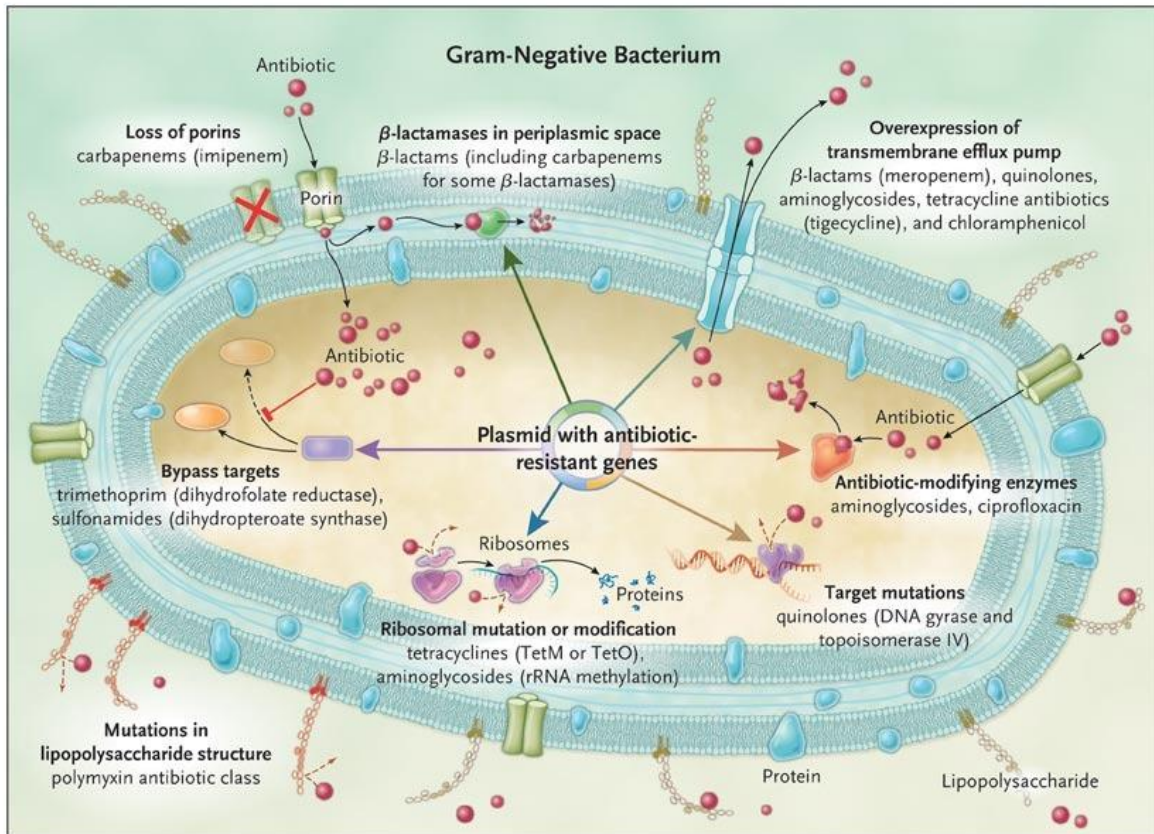


**Figure 1.3 Gram-negative antibiotic resistance mechanisms:** An overview of antibiotic resistance mechanisms in Gram-negative bacteria taken from Lee *et al.*, (2014). Mechanisms tackle the entry, accumulation, binding, and downstream toxicity of drugs as well as the necessity and abundance of drug targets.

### 1.3.5 Virulence mechanisms of *P. aeruginosa*

PA has a diverse arsenal of virulence factors that are deployed to outcompete other bacteria, evade immune responses and colonise host tissues during infection<sup>[86]</sup>. Numerous regulatory mechanisms interplay to govern expression levels of each according to environmental and population cues. An overview of PA virulence factors is shown in **figure 1.4** which reveals the diversity and breadth of its armoury. The T3SS is the primary cytotoxic virulence mechanism deployed by PA and is covered in next section.

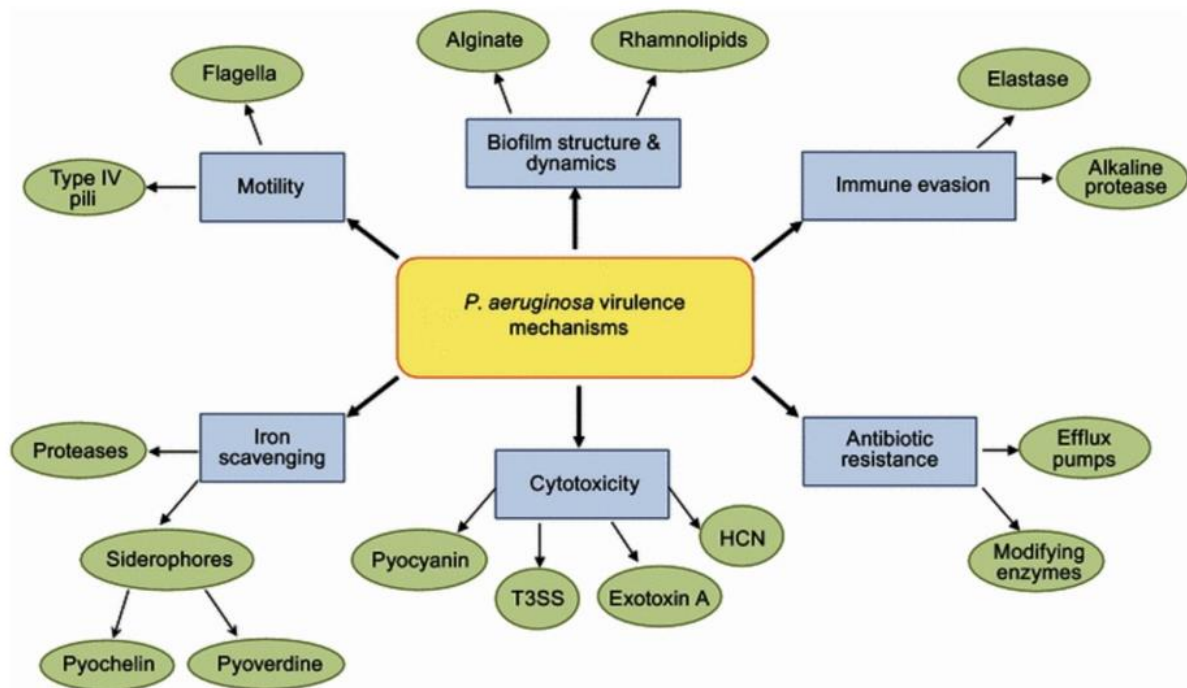


**Figure 1.4 *P. aeruginosa* virulence factors:** Virulence factors of PA used for colonisation of environmental niches, immune-evasion and to outcompete other species. This image was taken from Anantharajah *et al.*, (2016).

QS is an intercellular communication system that is cell density dependent and plays a vital role in the regulation of virulence and biofilm formation. Organised hierarchically between at least four signalling pathway mechanisms (las, rhl, quinolone based, and IQS systems), small chemical signals are released when population density is high, and this accumulation of signals interacts with cognate receptors to induce changes to gene expression[87]. The AHL signalling molecules that form complexes with the cognate receptors for the first three regulatory systems (LasR, RhlR and PqsR respectively) are, N-(3-oxododecanoyl)-homoserine lactone (OdDHL), N-butyryl homoserine lactone (BHL), and 2-heptyl3-hydroxy-4-quinolone (PQS). The fourth molecule, 2-(2-hydroxyphenyl)-thiazole-4-carbaldehyde (IQS) has been linked to integrating QS with environmental stress cues<sup>[88-90]</sup>.

Motility across surfaces is a key aspect of virulence, with swimming, swarming and twitching function being easily testable in the lab. Swimming and swarming are related to the complex control of the flagellum as an individual cell or in a bacterial population, whereas

twitching is controlled by the extension and contraction of the type IV pili (T4P). Swarming in particular has been associated with large changes to gene expression of virulence factors, including the T3SS and extracellular proteases<sup>[91]</sup>. The movement of PA in planktonic or biofilm cultures during infection plays a key part in the disease pathogenicity and is intricately linked with the cell-to-cell communication pathways<sup>[92]</sup>.

Proteases help PA invade tissues by cleaving components of the extracellular matrix and immune related factors like opsonin receptors. Proteases can also work to outcompete hosts for nutrients. By degrading host iron binding proteins PA gains a competitive advantage and uses iron for processes including respiration, biofilm formation and regulation of virulence factors<sup>[93, 94]</sup>.

## **1.4 The type III secretion system**

### **1.4.1 Evolution of the type III secretion system**

The T3SS is thought to have arisen from the exaptation of the flagellum, shifting its function from motility to effector protein delivery, quite probably with an intermediary translocation step<sup>[95, 96]</sup>. Predominantly obtained by horizontal gene transfer, there are many Gram-negative species that possess a T3SS that contributes towards their pathogenicity. Usually the system presents genetically as a large locus encoding the T3SS with a few effectors and smaller, individual loci encoding an effector each<sup>[97, 98]</sup>. Five main T3SS families have been identified, which are the Ysc, InvMxi-Spa and Ssa-Esc family of animal pathogens, and two Hrp T3SS families of plant pathogens. The PA Psc system is of the Ysc family<sup>[99]</sup>.

### **1.4.2 Type III secretion system structure**

Recent advances in cryo-electron microscopy have enlightened much of the macromolecular structure of the T3SS nanomachinery, which is often accurately referred to as a biological needle or molecular syringe<sup>[100]</sup>. Translocation, chaperone, regulatory, structural and effector proteins form a trans-membranous structure with an extracellular “needle tip” that injects cytotoxic effector proteins directly into the cytoplasm of host cells. **Figure 1.5** pictures the assembled structure of the T3SS machinery as well as the partner switching regulatory cascade discussed later in section 1.4.3.

The basal body of the injectosome is made up of around 25 proteins. It anchors the system and chaperones the cytosolic effectors through the needle complex. Two rings are embedded in the inner and outer membranes and a hollow cylindrical rod bridges the periplasm. The inner membrane ring is made of a lipoprotein, PscJ, whilst the outer is an oligomerised secretin, PscC<sup>[101-103]</sup>. ATPase activity by PscN at the cytoplasmic interface of the basal body facilitates recognition, separation from their chaperones, and translocation of effector proteins through the needle complex by assisting in their unfolding<sup>[104]</sup>.

The extracellular needle complex is a hollow tube which has recently been proposed to be formed by polymerisation of PscF, arranged so that the N-terminal region of each monomer is exposed on the outside whilst the C-terminal helix forms the inner core<sup>[101]</sup>. At the distal end of the needle complex are three translocation proteins, PcrV, PopD and PopB, which facilitate the perforation of the host cell membrane. PopD and PopB oligomerise to form the translocation pore and PcrV is necessary for the correct assembly and insertion of the two proteins into the host membrane. All three are required for effective translocation of effectors into the host cytoplasm<sup>[52, 101]</sup>.

Four exoenzyme effector proteins, ExoS, ExoT, ExoU and ExoY have been discovered in PA. It is rarely seen that all effectors are possessed in one strain and differing strains have either ExoS or ExoU<sup>[101, 105, 106]</sup>. The clinical outcomes of patients can differ based on which effectors are expressed<sup>[107-109]</sup>. ExoS and ExoT are GTPase-activating proteins (GAPs) that have activity against host cell GTPases. Host cells cannot migrate or phagocytose when injected with these toxins and become rounded and detached from neighbouring cells as the actin cytoskeleton is disrupted. Both these exoenzymes also have ADP-ribosyl transferase domains which have different functions in each. ExoS inhibits DNA synthesis, perturbs vesicular trafficking and causes cytotoxicity and apoptosis. In ExoT, the GAP and ADP-ribosyltransferase domains work in tandem to promote invasion, delay wound healing and prevent phagocytic activity<sup>[110-114]</sup>. ExoU exhibits phospholipase activity and causes acute lung injury and sepsis during infection by triggering an inflammatory response by enhancing transepithelial migration of neutrophils. Its phospholipase activity damages host membranes and causes necrotic cell death of epithelial cells, neutrophils and macrophages<sup>[115, 116]</sup>. Like the other effectors, ExoY has more than one active domain involved in its lethal activity against cells. Primarily, it possesses adenylate cyclase activity mediating cytoskeleton disturbance triggering cell necrosis<sup>[117]</sup>.

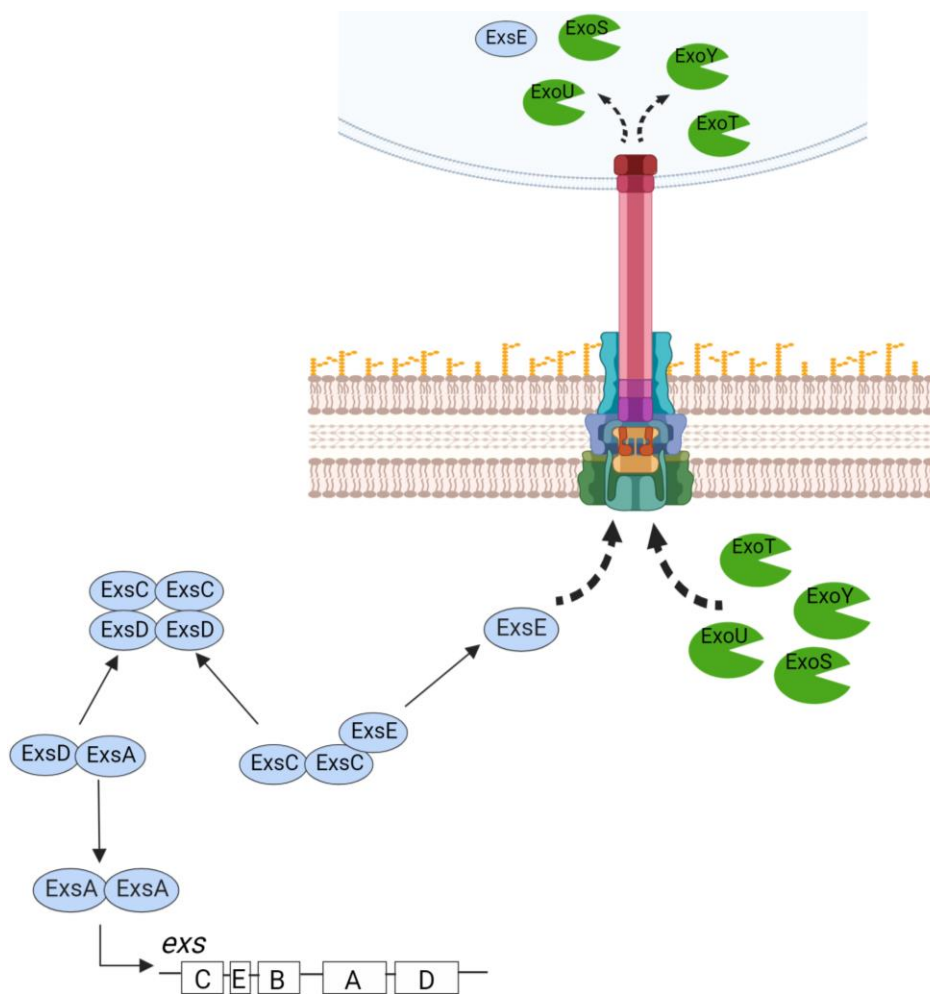


**Figure 1.5 Type III secretion system structure and regulation:** Image made using BioRender depicting the macromolecular structure of the T3SS and the partner switching regulatory mechanism ExsADCE cascade. Secretion of ExsE causes the sequestering of ExsD away from ExsA by ExsC, allowing dimerization of ExsA and transcription.

### 1.4.3 Type III secretion system regulation

Over 40 genes comprise the T3SS that is split across 5 operons<sup>[110, 115]</sup>. The master regulator of the T3SS is ExsA, an AraC/XylS family transcriptional regulator that transcribes all the genes involved, including its own. The mechanisms that trigger the induction of T3SS are not fully understood but the secretion of ExsE initiates a partner switching mechanism that allows the dimerization of ExsA to begin transcription. The induction may be by host cell contact or low calcium conditions, initiated by chelators such as Ethylenediaminetetraacetic acid (EDTA) or ethylene glycol-bis( $\beta$ -aminoethyl ether)-N,N,N',N'-tetraacetic acid (EGTA). The system is expressed at a low basal level under non-inducing conditions and unlike some

other virulence systems, induction results in increased expression of the entire system and not just the effector proteins<sup>[117]</sup>.

The partner switching mechanism can be seen with its correct stoichiometry in Figure 1.5 and is known as the ExsADCE cascade. Three proteins, ExsC, ExsD and ExsE interact to prevent or allow transcription by ExsA in response to the environment. When the injectisome is closed, ExsD acts as an anti-activator by forming a complex with ExsA, whilst ExsC chaperones ExsE. Under secretory conditions, ExsE is translocated through the T3SS and since the affinity of ExsD is higher for ExsC than ExsA, it switches partners releasing ExsA forming an ExsD·ExsC complex. ExsC is an anti-anti-activator and the cascade is dubbed a partner switching mechanism since both ExsC and ExsD may bind two partners, changing dependent on the intracellular concentration of ExsE<sup>[118]</sup>.

There have been 10 ExsA dependent transcriptional promoter sites identified. All have a region extending from the -35 to the -70 position relative to the transcriptional start site which included the consensus sequence for ExsA<sup>[119]</sup>. The size of this protected region alongside experimental evidence, markedly two shift products in electromobility shift assays (EMSA) and promoter truncation experiments, indicated two binding sites<sup>[119]</sup>. An ExsA monomer binds to the first promoter site and recruits a second monomer at the second binding site. This dimerization is regulated by the N-terminal domain (NTD) of the protein – the region with far less conservation within the AraC/Xyls family compared to the C-terminal domain (CTD)<sup>[120]</sup>. The ExsA proteins recruit RNA polymerase- $\sigma^{70}$  to begin transcription, however it remains uncertain as to whether one or both monomers are responsible for this<sup>[121]</sup>.

Besides ExsA, there is only one other transcriptional factor known to directly regulate the T3SS, PsrA<sup>[122]</sup>. It does so by binding the  $P_{\text{exsC}}$  promoter region and positively controlling transcription of the *exsCEBA* operon<sup>[122]</sup>. PsrA regulates motility, polysaccharide production and metabolism and is directly inhibited by long chain fatty acids, as is T3SS expression, although the implication of this finding is unclear<sup>[123, 124]</sup>.

In addition to these direct regulatory systems, a more global regulatory network exists for virulence factors in PA. Vfr is a global virulence factor regulator with over 100 genes under its positive control, including T3SS genes. Two genes, *cyaA* and, more importantly, *cyaB* encode two adenylate cyclases, CyaA and CyaB respectively. These are responsible for cAMP

production which acts as a cofactor to Vfr. Between CyaA, CyaB and a cAMP phosphodiesterase, CdpA, Vfr activity is regulated. Vfr can bind the  $P_{\text{exsA}}$  promoter site upstream of the *exsA* gene, as confirmed in EMSA experiments<sup>[125–127]</sup>. Non-functional mutants of these cAMP genes significantly reduced ExoS expression, although, double cAMP gene mutants or Vfr knock out is required for total abolition of ExoS. Over-expression of ExsA can re-establish a virulent phenotype in strains with non-functional cAMP-dependent regulatory networks, but over-expression of *cyaA* or *cyaB* does not cause increased ExoS production<sup>[128, 129]</sup>.

Further pleiotropic effects can be had on the T3SS as is the case for two additional systems, Muc/Alg and Gac/Rsm. Both can be described as affecting lifestyle choices of PA and likely intervene as a survival or protective mechanism during times of environmental stress due to the high energy demand the T3SS puts on the cell. Indeed, it has been demonstrated that PA has an inability to express the T3SS in inducing conditions under metabolic stress<sup>[130]</sup>. The Gac/Rsm pathway interaction with the T3SS is well characterised. The pathway is controlled by two components – a sensor histidine kinase, GacS and its cognate response regulator, GacA. GacS signalling is itself regulated by two kinases, RetS and LadS, which work antagonistically. The downstream effects of these pathways create an opposing expression effect on the T3SS and biofilm formation<sup>[131–141]</sup>. A biofilm triggering nucleotide, c-di-GMP reduces virulence by hampering cAMP production and even regulates secretion systems directly via the injectisome ATPase in some *Pseudomonas* species<sup>[142]</sup>. This serves to further support the inverse expression of virulence factors and biofilm formation. Many questions remain unresolved around the mechanisms of this interplay but a seesaw like interplay between T3SS virulence and biofilm formation irrevocably exists.

Contact with host cells and low  $\text{Ca}^{2+}$  have been the most extensively studied stimuli for T3SS induction, but conditions including high salt, DNA damage and metabolic stress have all been implicated too<sup>[143, 144]</sup>. Exactly how it is that these regulatory systems initiate the secretion mechanism remains elusive and all together it paints an extremely complicated picture for T3SS control.

## 1.5 Approaches to target the type III secretion system

### 1.5.1 Targeting the regulation of the type III secretion system

As discussed in previous sections, the expression of the T3SS is governed by a complex metabolic network and three chemical classes have been identified as influencing this expression, either by targeting the master transcriptional regulator, ExsA or by indirect mechanisms interfering with central metabolism.

N-Hydroxybenzimidazoles (N-HBs) have been demonstrated to reduce T3SS mediated cytotoxicity by binding to and inhibiting ExsA<sup>[145, 146]</sup>. These compounds bear the greatest relevance to the outset of this project and thus their activity is addressed independently and extensively in section 1.6.

Two phenolic compounds were identified as inhibitors of *exoS* transcription via screening of plant defence signalling molecules and their derivatives<sup>[147]</sup>. TS027 and TS103 were found to act on the GacSA-RsmYZ-RsmA-ExsA regulatory pathway. By promoting expression of two small regulatory RNAs, *rsmY* and *rsmZ*, *exoS* transcription was downregulated as these RNAs act to sequester the carbon storage regulator, RsmA. RsmA is an inducer of ExsA expression, but this activity is blocked via the sequestering by *rsmY* and *rsmZ*<sup>[147]</sup>.

Salicylidene acyl-hydrazides have been explored as T3SS inhibitors in other bacterial species and are suggested to target three enzymes in *E. coli* and *Yersinia pseudotuberculosis*<sup>[148–150]</sup>. The three enzymes, WrbA, Tpx and FolX most likely interfere with T3SS regulation through influences on cellular metabolism<sup>[149, 150]</sup>. Homologues of these proteins exist in PA and when screened, INP0341 was the most potent compound found and was subsequently shown to improve the survival of mice infected with PA by having dual activity against the T3SS and flagellar related swarming activity<sup>[151]</sup>.

### 1.5.2 Disrupting injectisome apparatus function

The T3SS injectosome shares close similarities with other secretion and motility systems due to evolutionary origins<sup>[95, 96]</sup>. Disrupting the function of the machinery by targeting the translocon, needle complex, or basal body have all been researched with some promising small molecule and antibody candidates.

Hydroxyquinolines were initially reported as inhibitors of T3SS expression in both *Y. pseudotuberculosis* and PA, but it was subsequently shown that this reduced expression was a downstream effect of blocking the secretion of ExsE, an effector protein and negative regulator<sup>[152, 153]</sup>. ExoS and FliC secretion were also inhibited by these compounds, as well as flagellar motility. The suggested mechanism in PA is the inhibition of the T3SS injectosome ATPase. The supporting evidence for this was that YscN ATPase activity, its *Y. pseudotuberculosis* homologue, was blocked by hydroxyquinolines as well as the demonstrable dual activity against the T3SS and the flagellar system<sup>[52, 152, 153]</sup>. The conclusion drawn was that they target a core constituent of the T3SS and the flagellar system with high homology – the ATPase<sup>[52, 152, 153]</sup>. The compounds exhibit protection of eukaryotic cells from T3SS-mediated cytotoxicity and improved survival of mice with an acute PA pulmonary infection<sup>[52, 152, 153]</sup>.

The only shared protein by the type II, III and IV secretion systems is secretin and this is therefore the predicted target of thiazolidinones<sup>[154, 155]</sup>. They have a broad spectrum of activity across Gram negative bacteria, and in PA prohibit secretory activity of all three systems<sup>[52, 154, 155]</sup>.

MBX1641 is a phenoxy acetamide discovered to decrease the secretion and translocation activity of the T3SS in PA<sup>[156]</sup>. Mutations to PscF, located in the needle complex of the nanomachinery, rendered the compounds inactive, suggesting this protein as their specific target<sup>[157]</sup>. Phenoxy acetamides reduce T3SS-mediated cytotoxicity and promote internalisation of bacteria in HeLa cells<sup>[157, 158]</sup>. They have also been shown to improve outcomes of mice with subcutaneous abscesses caused by PA infection<sup>[159]</sup>.

Separate to small molecules, antibody therapy has proven the most effective and promising approach to date, with two antibodies having reached clinical trials to combat PA infection. A rabbit polyclonal and a murine monoclonal antibody against PcrV were shown to be effective in reducing cytotoxicity, inhibit effector translocation, and restore the phagocytic activity of macrophages<sup>[160, 161]</sup>. Mice given anti-PcrV vaccination for acute and chronic pulmonary PA infection also displayed reduced tissue inflammation and injury<sup>[161, 162]</sup>. KB001 was developed from these studies and has completed phase II clinical trials on patients with ventilator-associated pneumonia and chronic pneumonia in CF patients<sup>[163]</sup>.

A bispecific monoclonal antibody, MEDI3902 targeting PcrV and PsI (an exopolysaccharide involved in adherence of PA) has also passed phase I clinical trials<sup>[164]</sup>. Having proved effective as a prophylactic and a treatment in reducing cytotoxicity against a wide range of clinical isolates *in vitro* and *in vivo* the phase II trial was completed in December 2019 and the publication of results is pending<sup>[165–167]</sup>.

### 1.5.3 Effector proteins

The effector proteins themselves have been shown to be targetable however, there is a significant drawback to this approach since not all effectors are expressed in each strain and so the breadth of clinical activity could be questionable<sup>[101, 105, 106]</sup>. Exosin is an ExoS inhibitor by competing with NAD<sup>+</sup> as a substrate for ExoS ADP-ribosyltransferase activity<sup>[168]</sup>. Exosin reduced the cytotoxicity of PA expressing ExoS in eukaryotic cells but had no effect on strains expressing alternative effectors<sup>[168]</sup>.

ExoU, a phospholipase A2 effector, has also been targeted by pseudolipasin which did not affect any other eukaryotic phospholipases that it was tested against<sup>[169]</sup>. ExoU expressing strains had decreased cytotoxicity when treated with pseudolipasin<sup>[169]</sup>. Arylsulfonamide compounds were also compared with pseudolipasin A for their inhibitory activity of ExoU but were ultimately found to be less potent in reducing ExoU-mediated cytotoxicity<sup>[170]</sup>.

The approaches discussed all target the bacteria, either through altering gene expression, system function or effector activity, but additional methods being explored are enhancing the host immune response and vaccinations, however neither will be discussed in this thesis. **Figure 1.6** summarises the targeting of the T3SS in PA by the mechanisms outlined above.

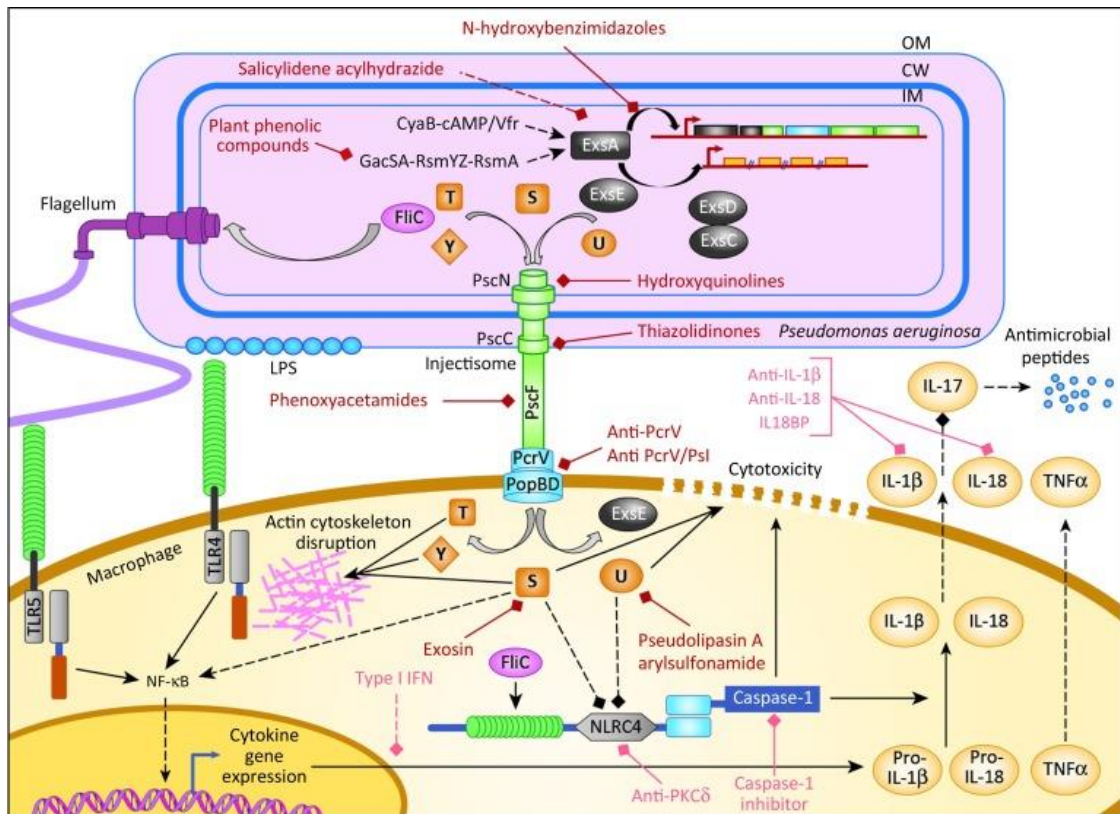


**Figure 1.6 Type III secretion system inhibition mechanisms:** Key inhibitory mechanisms of the T3SS in PA discussed in section 1.6. Abbreviations – OM: outer membrane, CW: cell wall, IM: inner membrane. Each small molecule or antibody target is indicated with their appropriate target. Image is taken from Anantharajah *et al.*, (2016).

## 1.6 ExsA inhibition

### 1.6.1 N-hydroxybenzimidazole inhibition of ExsA

To date, there is one known active class of small molecule inhibitors against ExsA, N-hydroxybenzimidazoles (N-HB). These compounds were initially identified as promiscuous inhibitors of the AraC/Xyls family proteins in *E. coli*. An *in silico* structure based screening approach was taken, using the crystal and nuclear magnetic resonance (NMR) structures of MarA and MarA related virulence regulators, Rob and SoxS, to build a model of the conserved DNA binding domain region. High scoring docked ligands were tested for the inhibitory activity on DNA binding by the three proteins using an *in vitro* chemiluminescent protein-DNA binding assay. Intrinsic antibacterial activity was tested by monitoring growth of antibiotic susceptible strains of *S. aureus* and *E. coli*, but no inhibition of growth was observed. Two compounds were next tested for activity of related AraC proteins, ExsA (PA), Rma (*Salmonella*

*typhimurium*) and PqrA (*Proteus mirabilis*). The two compounds were determined to have an IC<sub>50</sub> of 4μM and 1.9μM against ExsA binding<sup>[171]</sup>.

A following study acknowledged several N-HB analogues with greater activity against ExsA<sup>[172]</sup>. This paper reported testing previously established N-HB inhibitors of LcrF, a protein with a high degree of homology with ExsA, on a T3SS dependent PA macrophage whole cell cytotoxicity assay<sup>[173, 174]</sup>. Surprisingly, the compounds were ineffective against ExsA despite comparable IC<sub>50</sub> values established prior. The search for analogues was therefore expanded to find compounds effective in the whole cell assay via way of cell free ExsA-DNA binding assays.

A second follow up study looked more comprehensively at the interaction mechanism of these compounds with ExsA. T3SS dependent cytotoxicity was decreased by these molecules in a Chinese hamster ovary (CHO) cell assay *in vitro*. A green fluorescent protein (GFP) reporter showed a reduced expression of the T3SS and mutating the putative ligand binding site bolstered evidence of a DNA binding site interaction. The compounds remained promiscuous in their activity against related proteins, inhibiting other T3SS regulators in *Yersinia pestis*, *Vibrio parahaemolyticus*, and *Aeromonas hydrophila*<sup>[175]</sup>.

Compound	Structure
4816	
5330	
5631	
5707	
5784	
5816	

**Table 1.1 N-hydroxybenzimidazole 2D chemical structures:** This table is taken from Marsden et al., (2016) and contains the N-HB compounds used in the paper. It is noted in the paper that compound 5784 is the sodium salt of 5631, and 5816 is the sodium salt of 5707.

## 1.7 *In silico* drug discovery

### 1.7.1 The rise of *in silico*

The relationship between physicochemical properties and biological activity was being investigated as early as the 19<sup>th</sup> century, but it was the second half of the 20<sup>th</sup> century that saw remarkable advances in the drug discovery field. Initially the 2D and then the 3D conformations of ligands were credited with contributing to biological activity and once these had been tied together with the introductory concept of receptors to act as drug targets, the way was paved to elucidate specific structure activity relationships between the two<sup>[52, 142]</sup>. Scientists wasted no time in utilising advances in technology to economise this process. The term, *in silico*, begins

to make an appearance in the early 1990s and over the last three decades has established itself as an integral part of the drug discovery process<sup>[176]</sup>. Computational capabilities have expanded at an unprecedented rate, with the pharmaceutical and biotech industries benefiting enormously from these advances. The efficiency of the drug discovery process has been dramatically improved, increasing the return rate on wet lab experimentation, meaning lower costs and increased productivity<sup>[177, 178]</sup>. It is now possible to collate vast amounts of data on expansive compound libraries, enhance software algorithms with greater biophysical and biochemical detail and identify new targets with bioinformatics. *In silico* advances are allowing scientists to identify and screen more targets, more potential ligands, faster, in more detail, and more cheaply than ever before. Drug discovery is being revolutionised by these techniques at a time when the number and success rates of new drugs have dropped sharply. To date, most T3SS inhibitors have been discovered using *in silico*<sup>[179, 180]</sup>.

### 1.7.2 Ligand-based approaches

The overwhelming majority of drug discovery is focused on small molecules for a host of reasons: they are relatively easy to synthesize, have a high level of chemical stability, and can be characterised with comparative ease<sup>[181]</sup>. Ligand-based approaches are grounded on the concept that similar compounds tend to have similar biological properties. Ligand-based approaches therefore do not require knowledge of the target structure, but critically depend upon existing ligands with known pharmacological and biophysical characteristics.

Ligand-based approaches usually involve the virtual screening of chemical libraries using a known ligand as bait – named the lead query. The compounds can be ranked based on factors such as 2D or 3D similarity and electrostatic properties<sup>[182, 183]</sup>. Pharmacophore features of two or more chemically distinct but active ligands can also be used to generate a query and used to filter a chemical library<sup>[184, 185]</sup>.

Public databases such as, PubChem, ChEMBL and DrugBank, hold information on millions of compounds that far exceeds the number of crystal structures available in Protein Data Bank (PDB) (around 150,000 structures)<sup>[186]</sup>. Drug repurposing is becoming increasingly investigated as public databases of bioactive molecules expand and there are even now databases focused entirely on drug repurposing, containing failed drugs with their therapeutic indications and bioactivity data<sup>[187]</sup>. A shortfall of ligand-based approaches is that it does depend on the coverage of the known chemical entities and that even very small changes in the

structure or properties can have a significant influence on the activity compared to compounds with a high overall similarity<sup>[188]</sup>.

Much of the streamlining from computational usage comes during “hit” identification and optimisation, where disciplines such as cheminformatics can generate enormous libraries based on molecular attributes and chemical behaviour of an individual or group of compounds<sup>[189]</sup>. These may be direct measures of activity such as reactive groups or chemical constants, or indirect measures, which may be structural motifs, compound classes or higher order observations. There are innumerate attributes that can be used to generate or filter these libraries, but a good example is Lipinski’s “rule of 5” guideline. Supposedly “good” drug candidates for orally active molecules should fulfil certain criteria: a molecular mass of less than 500, a maximum of 5 hydrogen bond donors, a limit of 10 hydrogen bond acceptors, and a logP value of  $\leq 5$ <sup>[190]</sup>.

### 1.7.3 Structure-based approaches

A structure-based approach relies upon information on the target that has been derived experimentally or by computational methods generating homology models<sup>[191, 192]</sup>. As more structures are solved experimentally, generating homology models has become more popular in recent years. It uses related structures, often with ligands bound to provide conformational restraints, as templates for the final structure<sup>[193]</sup>. The goal of any structure-based method is to create an accurate conformation of the ligand binding site and thus the pose in which the ligand will occupy that site in. This process is called docking and may be blind, covering the whole protein surface, or focused, with only a defined region of the protein given for the ligand to occupy. The second goal is to score these poses – an estimation of binding affinity<sup>[194–196]</sup>. Attempts have been made to improve the enrichment of true positives by using a number of protein conformations and employing multiple scoring functions, known as consensus scoring<sup>[197]</sup>. As more structures are deposited to the PDB bound to ligands, analysis and implementation of this data is continuously being added to scoring functions<sup>[198]</sup>.

Commonly with molecular docking, the target protein is held static and the ligand is allowed to be flexible about the site to orientate itself to the most likely docking pose. Blind docking is often used to identify potential binding pockets, where ligands are likely to interact with the target. Because the protein is held static, it is feasible to dock whole libraries of compounds into the target<sup>[199]</sup>. Docking software produce conformational hits and scoring

functions based on varying predetermined criteria will score those conformations. The conformation of a compound is the 3D orientation it occupies in space and certain orientations are more energetically favourable than others. The flexibility of the ligand, and therefore the number of possible conformers it could have, or the binding site can have significant impacts on the predicted binding results. In a case where both target and ligand are already known or experimentally proven, docking can be used as a secondary validation tool or to investigate structure activity relationship (SAR).

At a more basic level, target structures can be compared with similar principle to ligand comparison methods, given structural likeness often means closely related functions and may recognise the same or similar ligands<sup>[200]</sup>. Phylogeny trees built on protein sequences can show that sequences can identify proteins with related functions and dual inhibitor molecules have been found via this hypothesis<sup>[201, 202]</sup>. The epidermal growth factor receptor and epidermal growth factor receptor B2 are such examples<sup>[203]</sup>. Programmes such as BLAST can perform multiple sequence alignments and are free through web servers. These should be used with caution in assuming activity of ligands as individual residue changes can entirely change the interaction of ligand binding<sup>[204–207]</sup>. Proteins often display reasonably similar or conserved regions but also heavily diverse regions around domains involved in regulation and it is at local binding sites that drug interactions must be investigated<sup>[208]</sup>. Take for example, AraC family proteins that exhibit a well conserved DNA binding domain with a classical helix-turn-helix that recognises DNA promoter sequences<sup>[209]</sup>. Changes to this region cause their specificity for promoter regions, however, the N-terminal regulatory domains of this family show an array of structural formations<sup>[210, 211]</sup>. Inhibitors that bind to the DNA binding domain are often promiscuous in their activity across the family such as seen with N-HB activity<sup>[212–214]</sup>.

Clear and obvious limitations can be seen for structural approaches, notably that all models are only models and not truly accurate structures. Small changes to binding sites can have large effects on ligand binding affinity and scoring functions are a product of the information and algorithms on which they run which are dependent on the input data which will always remain incomplete. Despite this though, structural approaches have been an effective methodology for drug discovery having contributed heavily to the benefits of a virtual approach. It has been used to identify a great number of new inhibitors including, human carbonic anhydrase II, cyclin-dependent kinases, epidermal growth factor receptor kinase and

vascular endothelial growth factor receptor 2 kinase<sup>[215]</sup>. Antagonists for neurokinin-1 and the  $\alpha$ -1-A adrenergic receptors were also found using structure-based methods<sup>[215]</sup>.

#### 1.7.4 Molecular dynamics

Molecular dynamics (MD) is the simulation of the interactions between the atoms and molecules present in a reaction, often including solvents, for a period of time. The intrinsic motion of proteins and the contribution this has to function is being increasingly incorporated into the drug discovery process. Large conformational changes like gating residues in ion channels or transporters are prime examples of these movements being critical to function and the principles remain for ligand binding pockets and expounding SAR<sup>[215]</sup>. Anytime a protein makes a complex with a substrate, ligand or protein there will be conformational changes within the protein, whether they be big or small. Hospital *et al.*, (2015) overlay PDB structures of acetylcholinesterase solved with different small molecule ligands which demonstrates this<sup>[216, 217]</sup>. No changes to the overall structure are seen, but minor alterations in the structures can be and these are often enough to hoodwink docking algorithms<sup>[215]</sup>. As mentioned in section 1.6.4, the target protein in docking is often held static based on the PDB crystal structures, or at best may have algorithms to select from a small number of conformations that have been pre simulated<sup>[218]</sup>. MD simulation lengths have increased substantially from picoseconds to more biologically relevant times of over one millisecond<sup>[219]</sup>. On the microsecond scale, conformational changes and ligand binding can be simulated with good effect and as computational power increases, especially through graphics processing units (GPU) use, MD simulation can be further optimised. Still a way away from being routine, MD has become more accessible to non-experts, has been and will continue to be, an invaluable addition to those in drug discovery<sup>[220]</sup>.

#### 1.8 Aims and objectives

The aims and objectives at the beginning of this project were to firstly use *in silico* methods to select chemical scaffolds with potentially inhibitory activity against ExsA function. The second was to assess these molecules for such activity and verify through biophysical and functional assays that the inhibition of ExsA results in the downregulation of the T3SS and protection of eukaryotic cells *in vitro*. Provided the first two aims were successful the final aim of this project was to begin optimisation of hit compounds by ordering second generation

analogues and characterising activity of each molecular scaffold *in vivo*. The major themes and key areas of the project are outlined in **figure 1.7** below.

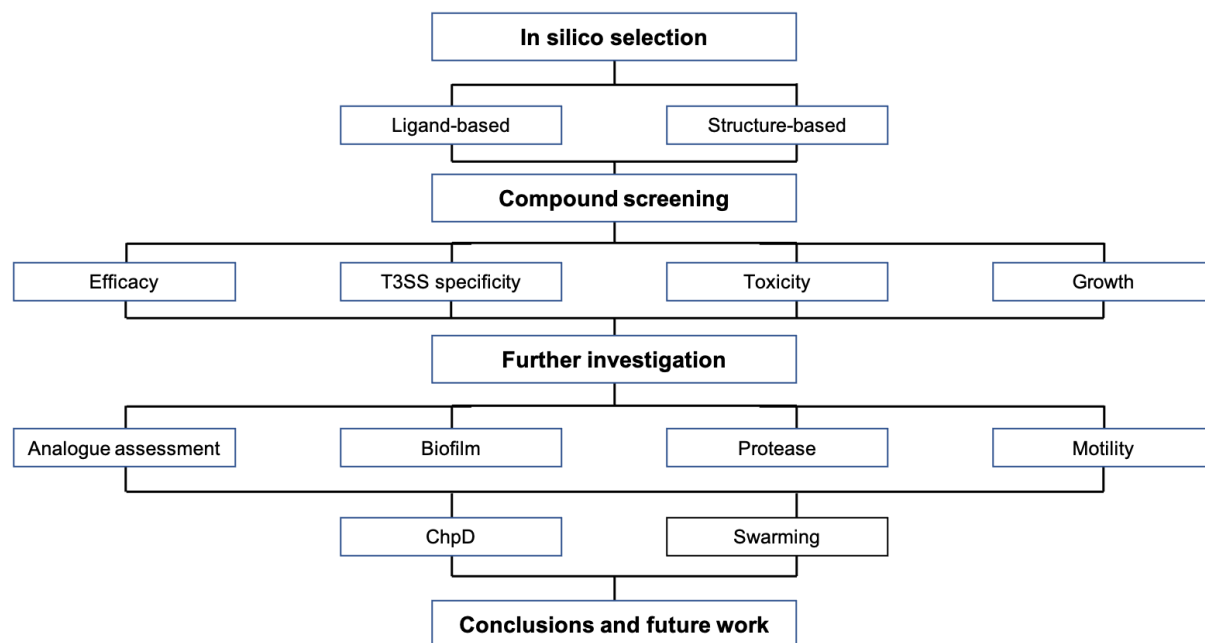


**Figure 1.7 Key project work areas:** Overview of the project workflow with the key areas addressed at each stage.

# **Chapter 2**

## **Materials & Methods**

## 2.1 *In silico* methods

### 2.1.1 Protein structures and models

The structure-based approaches utilised the ExsA NTD crystal structure, full length ExsA models, and several crystal and NMR structures of homologue *E. coli* proteins. Several website servers and software programmes were used to view and analyse these structures. The following protein structures were obtained from the Protein Data Bank ([www.rcsb.org](http://www.rcsb.org)):

- Solution NMR structure of DNA-binding domain of *E. coli* AraC (PDB ID: 2K9S)<sup>[221]</sup>
- X-ray structure of MarA protein from *E. coli* in complex with the target DNA sequence (PDB ID: 1BL0)<sup>[222]</sup>
- X-ray structure of the N-terminal regulatory domain of ExsA (PDB ID: 4ZUA)<sup>[223]</sup>
- X-ray structure of Rob protein from *E. coli* in complex with the target DNA sequence (PDB ID: 1d5y)<sup>[223]</sup>

ExsA MD models were created using I-TASSER Web Modeller (<https://zhanglab.ccmb.med.umich.edu/I-TASSER/>) and simulated for 10ns to create five additional conformers<sup>[224]</sup>. This MD simulation was done previously by post-doctoral fellow, Dr Aneesh Chandran Akathoot.

Viewing, editing, alignment, overlay and imaging of structures and docked ligands was done using PyMol<sup>[225]</sup>.

### 2.1.2 Sequence alignment

Multiple sequence alignment between ExsA, Rob, MarA and AraC was done using ClustalOmega (<http://www.ebi.ac.uk/Tools/msa/clustalo/>).

### 2.1.3 Prediction of ligand binding pockets

FTSite (<http://ftsitesite.bu.edu/>) was used to predict potential small molecule binding pockets on the protein structures used<sup>[226]</sup>.

#### 2.1.4 Electrostatic surface mapping

The electrostatic surface maps of protein structures were made using the Adaptive Poisson-Boltzmann Solver (APBS) executed on the PDB2PQR server ([http://nbcrc-222.ucsd.edu/pdb2pqr\\_2.1.1/](http://nbcrc-222.ucsd.edu/pdb2pqr_2.1.1/)) using the default set up<sup>[227]</sup>.

#### 2.1.5 Ligand structures

Ligands used for docking experiments in this study were drawn as 2D structures in Marvin Sketch (<https://chemaxon.com/products/marvin>) and were energy minimised into 3D structures using MMFF94 force field as implemented in MOE (2014 version)<sup>[228]</sup>. N-HBs used in this study for docking were selected based on reported AraC family inhibitory activity and ExsA IC<sub>50</sub> values<sup>[146, 208]</sup>.

A decoy set of ligands was created using DUD-E (<http://dude.docking.org>)<sup>[229]</sup> which used five known active inhibitors of ExsA listed in Marsden *et al.*, (2016), (note 5784 and 5816 were excluded as they are salts of 5631 and 5707 respectively), to generate 243 false, inactive ligands. This decoy set was run in ROCS (<https://www.eyesopen.com/rocs>) using three scoring functions (ShapeTanimoto, ColourTanimoto and TanimotoCombo) and the output scores were plotted with ROC (receiver operating characteristic) curve analysis. The decoy set was also screened in GOLD<sup>[231]</sup> and analysed in the same way with three scoring functions present in GOLD suite (Chemscore, Goldscore, and ChemPLP).

#### 2.1.6 Ligand docking

Ligand docking was executed using AutoDock Vina<sup>[230]</sup> or GOLD suite<sup>[231]</sup>. AutoDock Vina is a blind docking (un-biased) software programme allowing surface docking across the entire protein surface. 9 conformers of each docked ligand were generated in Omega version 2.0 (OpenEye Scientific Software Inc, Santa Fe, USA). 100 copies of the query were then docking with exhaustiveness setting 8 with docked poses ranked by predicted binding affinity. GOLD is a focused docking programme allowing specification of a ligand docking site allowing rotation of side chains within the docking site. 3 scoring functions are available within the programme – Chemscore, Goldscore and ChemPLP. Query molecules were docked into protein conformers at the specified DNA binding site and ranked by selected scoring function.

### 2.1.7 FA compounds selection

This methodology relied heavily on the only currently known inhibitor class of ExsA, N-HBs. An energy-minimized 3D structure of N-HB40<sup>[208]</sup> was used as a 3D query to virtually screen the Enamine Diversity conformer library using ROCS software program (<https://www.eyesopen.com/rocs>). Conformers of the Enamine Diversity Library ([www.enamine.net](http://www.enamine.net)) were made using Omega version 2.0 (OpenEye Scientific Software Inc, Santa Fe, USA). Hits were ranked by a TanimotoCombo (TC) Score - a 3D shape Tanimoto score (maximum value 1 for 100% overlap in 3D shapes between the bait and the hit) and ColourTanimoto score (maximum value 1 for 100% similarity in chemical groups present in the bait and the hit)<sup>[232]</sup>. The first 200 hits from the ROCS-based screening were then subjected to alignment based on electrostatic field<sup>[233]</sup> using FieldAlign (FA) version 2 (<http://www.cresset-group.com/>). This alignment selection was done manually and subjectively. A total of 18 compounds were ordered using this methodology and are referred to throughout this thesis as FA(X), where X represents a number 1-18.

### 2.1.8 E compounds selection by molecular docking

N-HB40<sup>[208]</sup> was docked in an unbiased manner (“blind docking”) into the 20 conformers of the *E. Coli* AraC CTD, MarA and Rob using AutoDock Vina<sup>[230, 234]</sup>. Docked poses of three ligands, N-HB40, FA8 and FA15 were aligned in MOE and four pharmacophore features predicted to be playing key roles in binding to ExsA were observed. These pharmacophore features, two aromatic regions and two electron acceptor groups, were used as queries to filter the Enamine library leaving 91,000 compounds. Conformers of these compounds were generated using Openeye systems and these conformers were screened in ROCS using N-HB40 as bait. The top 500 hits were subsequently run in both EON (<https://www.eyesopen.com/>) and GOLD suite version 1.7.0 (CCDC, Cambridge, UK)<sup>[231]</sup> (ChemPLP scoring function). Output scores from all three scoring functions were normalised and converted to a Z score<sup>[235]</sup>, the sum of which was used to rank the 500 compounds. The equation for normalisation and Z scores was as follows:

$$\text{Normalised score} = \frac{(\text{score} - \text{min})}{(\text{max} - \text{min})} \quad \text{Z score} = \frac{(\text{score} - \text{mean})}{(\text{standard deviation})}$$

Molecules with LogP and LogS values of less than 5 and greater than -5 respectively and had distinctly different chemical scaffolds to N-hydroxybenzimidazoles were ordered for

testing. There were 59 compounds ordered using this method and are referred to throughout this thesis as E(X) where X represents a number 1-59.

### **2.1.9 NCI compounds selection**

Conformers of the National Cancer Institute (NCI) Diversity set V library (<https://wiki.nci.nih.gov/display/NCIDTPdata/Compound+Sets>) were made using Omega version 2.0 (OpenEye Scientific Software Inc, Santa Fe, USA). These conformers were screened against the DNA-binding domain of six ExsA I-TASSER MD models using GOLD<sup>[231]</sup>. Three scoring functions (Goldscore, Chemscore, and ChemPLP) were used and the scores were normalised using the Z score function. The top 10% of hits were run in ROCS using compound 5631<sup>[146]</sup> as bait and scored by TC. Molecules were chosen based on their combined scores between GOLD and ROCS and those that fell within a LogS range of between -1 and -5 and a LogP score between 1 and 5. There were 40 compounds ordered using this method and are referred to throughout this thesis as NCI(X) where X represents a number 1-40.

### **2.1.10 M compounds selection**

M compounds were selected from visual inspection of ligand based virtual screening using an energy minimised 3D structure of N-HB40 as a query as described in section 2.1.7. Compounds were selected from the Chembridge (Express Pick®; [https://www.chembridge.com/screening\\_libraries/](https://www.chembridge.com/screening_libraries/)) and Specs® (<https://www.specs.net/>) libraries. Chosen hits were purchased through Molport (<https://www.molport.com/shop/search-in-progress?searchtype=text-search>).

### **2.1.11 Mutagenesis predictions for ExsA crystallography**

Stabilising mutagenesis predictions were done by submitting the ExsA AA sequence to three servers: UCLA SERp Server (<http://services.mbi.ucla.edu/SER/>), STRUM<sup>[236]</sup> (<https://zhanglab.ccmb.med.umich.edu/STRUM/>), and Site Directed Mutator (SDM) (<http://www-cryst.bioc.cam.ac.uk/~sdm/sdm.php>). Mutation predictions were compared between the 3 servers and collaboratively assessed for likely stabilising mutations of ExsA for future crystallization attempts.

## 2.2 Bacterial techniques

### 2.2.1 Bacterial strains

Several bacterial strains were used throughout this project and a full list can be found in **table 2.1**. All strains were stored at -80°C in 25% (v/v) glycerol solution.

**Table 2.1 Strains used in this study**

Strain	Genotype	Reference
<i>Pseudomonas aeruginosa</i>		
PA01	Wild type	Jacobs <i>et al.</i> , (2003)
PW6882 <i>rhlR::Tn</i>	PA01 with transposon insertion in <i>rhlR</i>	Jacobs <i>et al.</i> , (2003)
PW8716 <i>lasR::Tn</i>	PA01 with transposon insertion in <i>lasR</i>	Jacobs <i>et al.</i> , (2003)
PW2981 <i>fleQ::Tn</i>	PA01 with transposon insertion in <i>fleQ</i>	Jacobs <i>et al.</i> , (2003)
PW1764 <i>chpD::Tn</i>	PA01 with transposon insertion in <i>chpD</i>	Jacobs <i>et al.</i> , (2003)
PW4025 <i>exsC::Tn</i>	PA01 with transposon insertion in <i>exsC</i>	Jacobs <i>et al.</i> , (2003)
<i>PpcrV-lux</i>	PA01 gene fusion of <i>pcrV</i> promoter sequence and <i>luxCDABE</i>	Dr Stephen Dolan
<i>PlacZ-lux</i>	PA01 gene fusion of <i>lacZ</i> promoter sequence and <i>luxCDABE</i>	Dr Stephen Dolan
<i>PpqsA-lux</i>	PA01 gene fusion of <i>pqsA</i> promoter sequence and <i>luxCDABE</i>	Dr Stephen Dolan
YM64	PA01 $\Delta$ mexAB- <i>oprM</i> $\Delta$ mexCD- <i>oprJ</i> $\Delta$ mexEF- <i>oprN</i> $\Delta$ mexXY deletions	Morita <i>et al.</i> , (2001)
YM64 <i>PpcrV-lux</i>	YM64 gene fusion of <i>pcrV</i> promoter sequence and <i>luxCDABE</i>	This study
PA01 $\Delta$ <i>pqsA</i> <i>pqs::lux</i>	PQS biosensor strain	Flethcher <i>et al.</i> , (2007)

**Table 2.1 continued**

PA01 ATCC (15692)	Wild type	Prof. Cynthia Whitchurch, Quadram Institute Bioscience, Norwich
<i>ΔchpD</i>	PA01 ATCC allele exchange mutant	Professor Cynthia Whitchurch, Quadram Institute Bioscience, Norwich
PA103	Wild type	Prof. Yahr, University of Iowa
PA14	Wild type	Prof. Frederick M. Ausubel, Harvard Medical School
<i>ΔrhlR-ΔlasR</i>	PA14 containing double deletion of RhlR and LasR genes	Prof. Frederick M. Ausubel, Harvard Medical School
<b><i>Escherichia coli</i></b>		
DH5α	Competent <i>E. coli</i> strain	Prof. Yahr, University of Iowa
JM109	F' <i>traD36 proA+B+ lacIq Δ(lacZ)M15/ Δ(lac-proAB) glnV44 e14-gyrA96 recA1 relA1 end A1 thi hsdR17</i>	Steindler <i>et al.</i> , (2007)
Rosetta	(F-) <i>ompT hsdS<sub>B</sub>(r<sub>B</sub><sup>-</sup> m<sub>B</sub><sup>-</sup>) gal dcm</i> (DE3) pRARE (Cam <sup>R</sup> )	Novagen
<b><i>Pseudomonas tolaasii</i></b>		
2192T	Wild type	Dr Rob Jackson, University of Reading
<b>Bacteriophage</b>		
φMSPA63	Wild type	Maria Stroyakovski
φMSPA46	Wild type	Maria Stroyakovski
φMSPA18	Wild type	Maria Stroyakovski
φMSPA17	Wild type	Maria Stroyakovski

Glycerol stocks were streaked using a sterile loop spreader for use on 25mL Lennox broth agar (LBA) in 10cm petri-dishes with appropriate antibiotics as necessary and stored at 4°C for no longer than one week. Unless stated otherwise overnight cultures were grown for 12-16hrs in 50mL falcon tubes in 10mL of LB media with appropriate antibiotics as necessary

on a rotating wheel at 37°C. A list of the antibiotics and the respective working concentrations used is represented in **table 2.2**.

**Table 2.2 Antibiotics used in this study**

Antibiotic	Solvent	Working concentration (mg/mL)	
		<i>P. aeruginosa</i>	<i>E. coli</i>
Carbenicillin, Cb	50% (v/v) ethanol	250	50
Gentamicin, Gm	Water	50	10
Tetracycline, Tc	50% (v/v) ethanol	50	10
Chloramphenicol, Cpl	70% (v/v) ethanol	n/a	34
Rifampicin, Rf	95% (v/v) ethanol	500	n/a

### 2.2.2 DNA extraction

Genomic DNA (gDNA) extractions were performed using GeneJET Genomic DNA Purification Kit and plasmid DNA was extracted from bacterial cultures using GeneJET Plasmid Miniprep Kit. Concentrations of the extracted DNA were determined using a NanoDrop ND-1000 Spectrophotometer and were stored at -20°C. A list of plasmids that appear in this study can be found in **table 2.3**.

### 2.2.3 Polymerase chain reaction (PCR)

PCR were performed using 50µL reaction mixture volumes containing up to 250ng template DNA, 0.5µM of forward and reverse primers, 200µM dNTPs, Phusion HF buffer, 1.5µL dimethyl sulfoxide (DMSO), and Phusion DNA polymerase (1 unit). Reaction conditions were adjusted for amplicon length and annealing temperature of primers. A list of the primers that were used in this study appear in **table 2.4**.

Colony PCRs were carried out by diluting a single colony in 100µL of sterile dH<sub>2</sub>O. In a 50µL reaction, 2µL of diluted cells were added to PCR mixture in place of DNA template. **Table 2.4** contains a list of all primers used in this study.

**Table 2.3 Plasmids used in this study**

<b>Plasmid</b>	<b>Description</b>	<b>Source</b>
pET16b	<i>exsA</i> full length	Timothy Yahr, University of Iowa
pUCP20	<i>E. coli</i> to PA shuttle vector	Westa <i>et al.</i> , (1994)
pSB536	BHL biosensor	Winson <i>et al.</i> , (1998)
pSB1075	OdDHL biosensor strain	Winson <i>et al.</i> , (1998)
Mini-CTX	PQS sensor stain	Fletcher <i>et al.</i> , (2007)
Tn7 helper plasmid	Tn7 helper plasmid	Choi <i>et al.</i> , (2005)

#### **2.2.4 Agarose gel electrophoresis**

Agarose gel electrophoresis was performed by dissolving agarose in 1x Tris-acetate-EDTA (TAE) buffer supplemented with 0.4mg/mL ethidium bromide. 6x DNA loading dye (Thermo Scientific) was mixed with samples and loaded into 0.8% (w/v) agarose gels. Band sizes were measured by 1kb Hyperladder (Bioline) and gels were run at 80V for 1hr. Visualisation was by UV transilluminator. To purify DNA from within agarose gels, the desired bands were excised using a scalpel and DNA extracted by GeneJET Gel Extraction Kit. Sample concentration was determined by Nanodrop as previously mentioned and stored at -20°C.

#### **2.2.5 Restriction digest and ligation**

Restriction enzymes were used to digest according to manufacturer instructions and checked for successful digestion by gel electrophoresis followed by gel DNA extraction. Ligation of DNA fragments into plasmid DNA was also carried out in accordance with manufacturer instructions using T4 ligase. Mixtures were incubated for 1hr on ice before another 1hr at room temperature. Ligation mixtures were stored at -20°C if not used directly for transformation by electroporation.

## 2.2.6 Bacteria transformations

For *E. coli*, samples were sub-cultured from an overnight for 3hrs to harvest cells during exponential growth phase. Cells were pelleted (4000 x g) and washed 3x in MgSO<sub>4</sub> before resuspension in 100µL dH<sub>2</sub>O and mixed with 0.2-1mg plasmid DNA or 2µL ligation mixture and transformed by electroporation (2.5kV, 25mF, 200Ω). Immediately following electroporation, mixtures were added to 1mL pre warmed (37°C) LB and incubated rotating for 1hr at 37°C for recovery. Cells were then plated on antibiotic selective agar and incubated overnight at 37°C. PA transformations were performed by sub culturing PA overnights in LB with static incubation overnight at 42°C before following steps mentioned as above.

**Table 2.4 Primers used in this study**

Primer Name	Sequence
<i>pcrV</i> Tn7T lux F BamHI	AAACGCGGATCCGTTCCGGTGACCTGGGTG
<i>pcrV</i> Tn7T lux R XhoI	AAA <u>ACTCGAG</u> AAAAGGCGAAGGTCAGCTCT
<i>lacZ</i> F BamHI	ATATATACGGATCCACGCAGATACAGTGTCCCC
<i>lacZ</i> R XhoI	ATATATA <u>CTCGAGG</u> ATCGCCCTTCCCAACAGTT
<i>P<sub>exsC</sub></i> F	ATGGATTTAACGAGC
<i>P<sub>exsC</sub></i> R	TCAAACCCTCATGCC
<i>P<sub>exoT</sub></i> F	AATATCCCATCGGGTTCTCC
<i>P<sub>exoT</sub></i> R	GATGATTGACGTCTCCTGATGTTTC
<i>P<sub>katA</sub></i> F	ACGTGTGGTT CCTCGAGAAG
<i>P<sub>katA</sub></i> R	GACCTGGGAG AAGATCTTCG

## 2.2.7 Phage transduction

Lytic phage were added to LBA plates with a PA01 *exsC::Tn* lawn and left overnight. Phage lysates were then prepared by scraping the top layer off semi confluent plates (i.e. overlapping plaques with small areas of bacterial lawn remaining) into 2mL of phage buffer [10mM Tris-HCl (pH7.4), 10mM MgSO<sub>4</sub>, 0.01% gelatin] and 500µL chloroform. This was then vortexed for 2mins and centrifuged (4,500rpm, 20mins, 4°C). The supernatant was transferred to a glass bijou with 100µL chloroform for sterility and stored at 4°C.

Phage transduction was attempted by adding 100µL of phage lysate to an overnight of the recipient strain (PA103) with static incubation at 37°C for 30 minutes followed by 20 minutes shaking. The overnight was then pelleted and the supernatant discarded before resuspension in 300µL LB before plating onto antibiotic selection plate. Colonies growing on selection plates were checked for transduction by PCR.

### **2.2.8 DNA sequencing**

DNA sequences were determined by Sanger sequencing conducted by GATC Biotech as per company instructions.

## **2.3 Mammalian cell culture techniques**

### **2.3.1 Mammalian cell line**

The human lung carcinoma cell line, A549 (ECACC 86012804) was maintained using DMEM media (high glucose, pyruvate, Thermo Fisher #41965039) supplemented with 10% foetal bovine serum (FBS) (heat inactivated, Sigma #F9665) and penicillin-streptomycin (100x solution, Sigma #P433-100ML). Trypsin-EDTA (Sigma #T4174-100ML) was used during passages.

### **2.3.2 Cell protection assay (CPA)**

The CPA was used to establish which compounds had a protective effect *in vitro* against acute PA103 infection.  $5 \times 10^4$  A549 cells per well (counted using 4% trypan blue solution, Sigma #T8154-20ML) were allowed 24 hours to adhere in a 96 well plate (37°C, 5% CO<sub>2</sub>) before washing with calcium and magnesium free PBS (Sigma #D8537-500ML). DMEM media (high glucose, pyruvate free, Thermo Fisher #21063-029) supplemented with 10% FBS was then added. Overnight bacterial cultures were diluted and grown to mid-exponential growth phase before washing in PBS and resuspension in DMEM media (high glucose, pyruvate free, Thermo Fisher #21063-029 supplemented with 10% FBS). Bacterial cultures were then added to wells at a multiplicity of infection (MOI) of 5:1 and DMSO or compound (1% v/v) were also added before static incubation at 37°C for 4hrs. Full lysis controls were also used to ensure PA mediated cytotoxicity achieved a minimum of 40% relative to full lysis. Lysis buffer was added to the necessary control wells 45mins before the end of incubation as

per assay kit instructions. Results were quantified by the detection of lactate dehydrogenase (LDH) in a BMG Labtech FLUOstar Omega microplate reader using CytoTox 96® Non-radioactive Cytotoxicity Assay kit (Promega, #G1781, #G1780) measured at 492nm. Results are presented as percentages normalised against wild type (WT) infection controls (100%) and EC<sub>50</sub> values calculated using GraphPad Prism 6.0 non-linear regression analysis log(inhibitor) vs normalised response – variable slope.

### 2.3.3 Toxicity assay

Basic initial toxicity profiles of compounds were determined by LDH detection as in the CPA except for no bacterial cultures were added.. **Figure 2.1** visually represents the detection of LDH by the CytoTox 96® Non-radioactive Cytotoxicity Assay kit. Results are presented as percentages normalised against full lysis controls (100%).

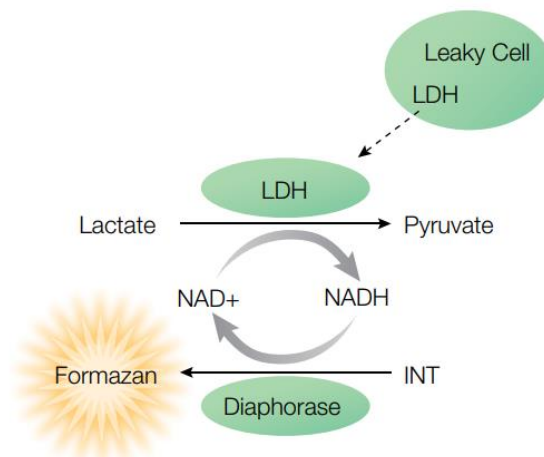


**Figure 2.1 Lactate dehydrogenase detection reaction:** LDH is released by damaged cells and is proportional to the quantity of formazan detected at 492nm. Formazan is red and formed when lactate, NAD<sup>+</sup> and INT dye act as substrates in the presence of LDH and diaphorase.

## 2.4 Protein purification

### 2.4.1 Purification of ExsA

ExsA contains rare codons making expression better suited in Rosetta cells than DH5a, so the plasmid encoding full length ExsA was extracted from DH5α cells using a Miniprep kit

and confirmed by Sanger sequencing. Plasmids were then successfully transformed into Rosetta cells using carbenicillin and chloramphenicol selection.

Overnight cultures of transformed Rosetta cells were added to 1L flask cultures of LB and grown shaking (200rpm) at 37°C until OD<sub>600</sub> 0.6, at which point cultures were induced using 1mM isopropyl β-d-1-thiogalactopyranoside (IPTG). Cultures continued to be incubated overnight shaking at 18°C. Cultures were then pelleted (4000 x g) and resuspended in lysis buffer before sonication. Following sonication cultures were pelleted again (20,000 x g, 4°C) and lysates were filtered using a 0.22µm syringe filter (Sartorius). Samples were then purified using Ni<sup>2+</sup> affinity chromatography technique (Qiagen AKTA, Ni-NTA Superflow Cartridge). The eluate (in elution buffer) was then dialysed at 4°C in dialysis buffer before being loaded onto a HiTrap™ heparin HP cation exchange column. ExsA was eluted using heparin column elution buffer and then re-dialysed at 4°C in ExsA storage buffer. VivaSpin columns were then used to separate ExsA monomers from dimerised ExsA. Purified protein was snap frozen in liquid nitrogen and stored at -80°C. A list of all the buffers used during the purification process are in **table 2.5**.

**Table 2.5 ExsA purification buffers**

<b>Buffer</b>	<b>Components</b>
Lysis	[500mM NaCl, 25mM imidazole, 50mM Tris-HCl (pH7.4)] + protease inhibitor tablets
Ni <sup>2+</sup> elution	Lysis buffer except 250mM imidazole
Dialysis	[200mM NaCl, 25mM Tris-HCl (pH7.4), + 1mM DTT]
Heparin elution	Dialysis buffer except 2M NaCl
Storage	[500mM NaCl, 25mM Tris-HCl (pH7.4), + 1mM DTT]

## 2.5 Proteomic analysis

### 2.5.1 SDS-PAGE

Purified ExsA samples were confirmed by running on 12% SDS-PAGE at 150V for 90mins. Purified samples were mixed with 4x loading dye and size determined by the relative position on the gel to a Precision Plus Protein Standard (BioRad). Gels were stained using Coomassie Blue before a two-step destaining process, first incubating overnight with Destain I and then with Destain II. SDS gel recipes and buffer compositions can be seen in **table 2.6**.

**Table 2.6 Buffers and solutions used in this study**

Buffer / Solution	Components
<b>SDS-PAGE</b>	
6% stacking gel	[7mL dH <sub>2</sub> O, 2mL 30% Bis-acrylamide solution (Severn Biotech), 1mL 5x stacking buffer, 50 $\mu$ L 20% (w/v) SDS, 100 $\mu$ L 8% (w/v) APS, 5 $\mu$ L tetramethylethylenediamine]
12% resolving gel	[1mL dH <sub>2</sub> O, 4mL 30% Bis-acrylamide solution (Severn Biotech), 5mL 5x resolving buffer, 50mL 20% (w/v) SDS, 100 $\mu$ L 8% (w/v) APS, 5 $\mu$ L tetramethylethylenediamine]
4x SDS loading dye	[2.4mL 1M Tris-HCl (pH6.8), 0.8g SDS, 4mL glycerol, 1mL 0.5M EDTA, 4mg bromophenol blue, 3.1mL H <sub>2</sub> O] + DTT
Coomassie Blue	[1g/L Coomassie Brilliant Blue G (Sigma), 50% (v/v) methanol, 10% (v/v) acetic acid]
Destain I	[50% v/v methanol, 7% (v/v) acetic acid]
Destain II	[10% v/v methanol, 7% (v/v) acetic acid]

### 2.5.2 Secretome analysis

Cultures were grown in LB shaking at 200rpm in 200mL flasks overnight at 37°C before normalisation and pelleting (4000 x g). Supernatants were then filtered using 0.22 $\mu$ m syringe filters (Millipore) and protein was precipitated overnight at 4°C by addition of 12%

(w/v) trichloroacetic acid (TCA). Samples were then pelleted (15,000 x g) at 4°C before washing 3x with 80% (v/v) acetone with pelleting between each wash. The pellets were then air dried and resuspended in PBS and 4x loading dye. Samples were then run on a 12% SDS gel and stained as in section 2.5.1.

### 2.5.3 Liquid chromatography-tandem mass spectrometry (LC-MS/MS)

LC-MS/MS was done by the Cambridge Centre for Proteomics with MS/MS fragmentation data searched against the National Centre for Biotechnology Information (NCBI) database using MASCOT (Matrix Science) search engine.

### 2.5.4 Electromobility shift assay

To test whether purified ExsA samples were active an EMSA was optimised. Two probes were generated tagged with a Cy5.5 fluorescent dye on the 5' end - a specific 200bp *P<sub>exoT</sub>* probe containing an ExsA binding region and a 150bp non-specific (NS) *katA* probe. The EMSA reaction mixtures can be found in **table 2.7**. Samples were incubated for 5mins at room temperature after ExsA and compound were added before the addition of any probes. On addition of probes samples were left for an additional 15 minutes at room temperature before being loaded into the gel. Reaction mixtures were had a 20µL final volume and were loaded onto a 4% native acrylamide gel run at 50V for 4hrs at 4°C. Gels were imaged on a BIO-RAD ChemiDoc.

**Table 2.7 EMSA buffers**

Buffer	Components
EMSA buffer	[10mM Tris pH7.5, 50mM KCl, 1mM EDTA, 1mM DTT, 5% glycerol, 0.5mg/mL ssDNA]  5nM ExsA, 100µM compound (when appropriate), 10ng <i>exoT</i> or NS probe and made up to 20µL with $dH_2O$
Reaction mixture (20µL)	[EMSA buffer 10µL, 100µM compound (1% v/v) or DMSO, 5nM ExsA, 10ng <i>P<sub>exoT</sub></i> or NS probe]

### 2.5.5 Western blot

Western blots were conducted in line with standard lab protocols. For bacterial samples, overnight cultures were normalised to OD<sub>600</sub> 0.05 in AGSY media and grown to the late mid log-rhythmic phase in a BMG Labtech FLUOstar Omega microplate reader, shaking 500rpm, 37°C. T3SS was induced by 5mM EGTA and DMSO controls or compound were added (1% v/v). Samples were normalised by OD<sub>600</sub> and pelleted with the supernatant added to SDS loading dye to create secretome samples. Pellets were resuspended in PBS and SDS loading dye was added for intracellular samples. For total protein samples, whole cell lysates were added directly to SDS loading dye after growth and normalisation.

All samples were boiled for 30mins at 95°C after addition of SDS loading dye and were run in a 12% SDS-PAGE before being transferred using a BIO-RAD Trans Turbo Blot Transfer onto a high fluorescence PVDF membrane. Following blocking (5% milky PBS), primary antibodies were incubated with the membrane in blocking buffer for 1hr and then washed 3x in PBS. Secondary antibodies (IRDye 680RD Li-Cor) were added and incubated in blocking buffer for 45mins before a secondary round of washing. Blots were imaged using a BIO-RAD ChemiDoc.

### 2.5.5 ExsA X-ray crystallography

Crystallization of purified ExsA (2.5mg/mL) was attempted using high throughput industry screening plates using sitting drop vapour diffusion. A sparse matrix index approach was used for ExsA. Screening plates (**table 2.8**) were thawed and 200nL of protein was added to wells with addition of either 200nL or 100nL of reservoir solution dropped using a Mosquito crystal liquid handling robot (TTP Labtech). All plates were sealed using clear package tape and a roller before being placed in a Rock Imager 1000 automated imaging and hotel system (Formulatrix) to equilibrate at 19°C. Images were captured every 24hrs for 3 weeks and plates were discarded after 3 weeks if no crystals were formed.

**Table 2.8 Sparse matrix industry screens for crystallization**

Supplier	Screening plate
Qiagen	Classics
Qiagen	PEGS Suite I
Molecular Dimensions	JSCG+
Molecular Dimensions	PACT <i>premier</i> Suite

### 2.5.6 Intrinsic tryptophan fluorescence

Decreases in tryptophan fluorescence were measured as an indicator of ligand binding. FA compounds or DMSO were added (200 $\mu$ M, 2% v/v) to ExsA (2.5 $\mu$ M) in storage buffer in a 96 well plate and tryptophan fluorescence using a BMG CLARIOstar Plate Reader. Excitation wavelength 295nm and emission 330-410nm. Curve fitting was done using GraphPad Prism 6.0 linear regression (non-binding) or nonlinear regression (binding).

### 2.5.7 Spectro fluorimetry

Spectro fluorimetry was performed using a FP-8300 Spectrofluorometer (JASCO), excitation wavelength of 295nm and emission wavelengths range of 305-400nm (0.5nm intervals, 100nm/min, triplicate measurements), 25°C. Compounds were titrated into the sample up to 2 $\mu$ M with a fixed protein concentration of 500nM. Ligands were also titrated into the buffer alone and used to normalise reads. Binding equilibrium constant ( $K_d$ ) values were calculated by plotting  $\theta$  vs [L], where  $\theta$  is equal to the fraction of bound ligand and [L] is the concentration of ligand. Curves were fitted in GraphPad Prism 6.0 non-linear regression analysis. Scatchard plots were also made plotting ratio of specific binding to concentration free ligand against specific binding.

## 2.6 Phenotypic assays

### 2.6.1 Assay media and agar

**Table 2.8** contains a complete list of the media and agar recipes mentioned throughout section 2.6.

**Table 2.9 Phenotypic assay media and agar recipes**

AGSY media	[56mM L-alanine, 17mM K <sub>2</sub> HPO <sub>4</sub> , 86mM NaCl, 3g L <sup>-1</sup> yeast extract, pH7.0] + (addition after autoclaving) [100µM CaCl <sub>2</sub> , 10mM MgSO <sub>4</sub> , 5µM FeCl <sub>2</sub> , 7.5µM ZnSO <sub>4</sub> ]
Artificial sputum media (1L)	[5g mucin type II (porcine), 4g fish sperm DNA, 1.25mM Na <sub>2</sub> HPO <sub>4</sub> , 0.348mM KNO <sub>3</sub> , 0.271mM K <sub>2</sub> SO <sub>4</sub> , 2.28mM NH <sub>4</sub> Cl, 14.94mM KCl, 51.85 NaCl, 10mM MOPS, 1.45mM Ser, 1.55mM Glu-HCl, 1.66mM Pro, 1.2mM Gly, 1.78mM Ala, 1.12mM Val, 0.63mM Met, 1.12mM Ile, 1.61mM Leu, 0.68mM Orn-HCl, 2.13mM Lys-HCl, 0.31mM Arg-HCl, 0.013mM Trp, 0.83mM Asp, 0.8mM Tyr, 1.07mM Thr, 0.16mM Cys-HCl, 0.53mM Phe, 0.52mM His-HCl·H <sub>2</sub> O, 3mM Dextrose (D-glucose), 9.3mM L-acetic acid (pH7), 1.754mM CaCl <sub>2</sub> ·2H <sub>2</sub> O, 0.61mM MgCl <sub>2</sub> ·6H <sub>2</sub> O, 0.0036mM FeSO <sub>4</sub> ·7H <sub>2</sub> O, 0.3mM N-acetylglucosamine, 5mL egg yolk emulsion (Sigma)] filter sterilised 0.22µm
Swimming agar (1L)	[4g tryptone, 2g NaCl, 1.2g agar]
Swarming agar (1L)	[1.07g NH <sub>4</sub> Cl, 1.7g Na <sub>2</sub> HPO <sub>4</sub> , 0.5g NaCl, 1.98g glucose, 5g casein hydrolysate, 5g agar] + (addition after autoclaving) [1mM MgSO <sub>4</sub> , 1mM CaCl <sub>2</sub> ]
Rhamnolipid agar (1L)	[20g glucose, 0.7g KH <sub>2</sub> PO <sub>4</sub> , 0.9g Na <sub>2</sub> HPO <sub>4</sub> , 2g NaNO <sub>3</sub> , 0.4g MgSO <sub>4</sub> ·H <sub>2</sub> O, 0.1g CaCl <sub>2</sub> ·2H <sub>2</sub> O] (addition after autoclaving) 2mL trace elements [2g FeSO <sub>4</sub> ·7H <sub>2</sub> O, 1.5g MnSO <sub>4</sub> ·H <sub>2</sub> O, 0.6g (NH <sub>4</sub> ) <sub>6</sub> Mo <sub>7</sub> O <sub>24</sub> ·4H <sub>2</sub> O] + [12g agar, 0.2g cetyl trimethylammonium bromide (CTAB), 0.005g methylene blue (MB)]
Mueller Hinton media	Oxoid CM0405

### 2.6.2 Luciferase reporter assay

A luciferase (*lux*) promoter reporter assay was used as an initial screen to identify compounds inhibiting T3SS expression measured by a reduction in *lux* signal normalised to growth. All luciferase strains used were previously generated by Dr. Stephen Dolan. Primers listed in **table 2.4** were used to fuse *luxCDABE* with upstream promoter sequences. Promoter regions were amplified using the primers and BamHI and XhoI digest sites added to the 5' and 3' ends of the promoters respectively. Purified PCR products were digested and ligated

directionally into the multiple cloning site of the pUC18T-mini-Tn7T-lux-Gm plasmid. The mini-Tn7-lux element was integrated into the PAO1 chromosome downstream of *glmS* at a conserved site by electroporation with helper plasmid pTNS2, previously described by Dolan *et al.*, (2020). Recombinants were selected using 50µg/mL gentamicin on LBA plates and confirmed by PCR. The upstream promoter sequences were examined for the PA *popN* and *exsC* type III secretion operons. A *lacZ* promoter was cloned from plasmid pUCP20 as a constitutive positive control.

Overnight lux cultures were normalised to OD<sub>600</sub> 0.05 and compound or DMSO were added to wells (1% v/v). Samples were grown in a BMG Labtech FLUOstar Omega microplate reader (shaking 500rpm, 37°C) and values were measured as relative light units (RLU) which were a factor of arbitrary light units (ALU) relative to culture growth, calculated:  $RLU = \frac{(OD_{600} \times 10^4)}{ALU}$ . For *PpqrV-lux* strains cultures were grown in AGSY media and induced with 5mM EGTA. LB media was used for investigation of *PpqsA-lux* and *PlacZ-lux* strains.

### 2.6.3 Growth curves

Growth curves were conducted by normalising overnight cultures to OD<sub>600</sub> 0.05 and compound or DMSO added as appropriate (1% v/v). Plates were grown shaking at 500rpm, double orbital shaking in a BMG Labtech FLUOstar Omega microplate reader. Colony forming units (CFUs) were counted as CFU/mL by 10-fold serial dilution of cultures and plating on LBA plates with antibiotic selection as appropriate.

### 2.6.4 *Ex vivo* porcine lung

Lungs were obtained as fresh as possible from John Taylor & Son and prepared as described in Harrison *et al.*, (2014). All lung preparations and incubation were performed at Warwick University in Dr. Freya Harrison's lab. Briefly, the main bronchiole section was cut out of each lung and alveolar tissue removed before washing and dicing into even sized chunks of tissue (5mm square). The tissues were infected by picking individual colonies of PA103 on insulin syringe needle tips and stabbing the tissues. Every 24hrs tissue samples were moved to a new plate and fresh artificial sputum media (ASM) added with the appropriate 100µM of compound (or v/v DMSO control). The tissues were incubated statically at 37°C. CFUs of tissue homogenates and supernatants were plated on *Pseudomonas* isolation agar after 10-fold serial dilutions.

### **2.6.5 Protease activity**

Overnight cultures were grown to stationary phase in flasks at 37°C, 200rpm and normalised to OD<sub>600</sub> 1.0 before pelleting and filtering supernatants (0.22µm Millipore). Equal volumes (100µL) of supernatant and 1.5% milk solution were mixed and OD<sub>595</sub> was measured using BMG Labtech FLUOstar Omega microplate reader (shaking 200rpm, 37°C).

### **2.6.6 Biofilm formation**

Overnight cultures were diluted 100x in LB with compound or DMSO added as appropriate (1% v/v) before being grown shaking (200rpm, 37°C) in 96 well plates for 48hrs. Cultures were then removed and wells washed 3x with dH<sub>2</sub>O before staining with 0.1% crystal violet (10mins). Following air drying after crystal staining wells were again washed 3x with dH<sub>2</sub>O before solubilisation of biofilms using 30% acetic acid. Biofilm formation was determined by OD<sub>550</sub> in a BMG Labtech FLUOstar Omega microplate reader.

### **2.6.7 Twitching motility plate assay**

Overnight cultures were normalised to OD<sub>600</sub> 1.0 and spotted onto the base of a 1% LBA plate with compound or DMSO added when appropriate (<1% v/v). Following overnight incubation at 37°C LBA was removed and the plate stained with 0.1% crystal violet. Twitching distance was determined as the widest diameter of stained twitching zone.

### **2.6.8 Swimming motility plate assay**

Overnight cultures were normalised to OD<sub>600</sub> 1.0 and pipetted into the centre of swimming agar plates and incubated overnight at 37°C. When appropriate, compound or DMSO was added to swimming agar (<1% v/v).

### **2.6.9 Swarming motility plate assay**

Overnight cultures were normalised to OD<sub>600</sub> 1.0 and spotted onto the surface of a swarming agar plate with compound or DMSO added as necessary (<1% v/v). Plates were then incubated at 37°C overnight.

### **2.6.10 Rhamnolipid production plate assay**

Overnight cultures were normalised to OD<sub>600</sub> 1.0 and spotted onto rhamnolipid agar plates. Small wells were made in the agar with a 5mL stripette heated tip. Plates were then incubated for 48hrs at 37°C followed by 48hrs at 4°C. This assay was adapted from Pinzon *et al.*, (2009).

### **2.6.11 Quorum sensing assay**

QS assays were conducted in line with a previous protocols and strains established by Dr. Peter Davenport. Cultures were grown in flasks overnight (shaking 200rpm, 37°C) and normalised by OD<sub>600</sub> before pelleting (4000 x g), supernatants filtered (0.22µm Millipore), and diluted 10x. Overnight cultures of sensor strains (PQS: PA01 *ApqsA pqs::lux*, BHL: JM109 pSB536, and OdDHL: JM109 pSB1142) were diluted 25x and grown to mid-logarithmic phase before mixing (1:1 volume ratio 60µL) with filtered supernatants in 96 well plates. PQS and BHL sensor plates were incubated static for 3hrs at 30°C and OdDHL sensor plates for 4hrs. Sensor strains contain lux plasmids that are induced by their namesake autoinducer QS molecules. Measuring of normalised lux was detected by BMG Labtech FLUOstar Omega microplate reader and was used as a determinant of autoinducer expression. This procedure was carried out as explained except in cases where growth times of flask cultures are specifically indicated.

### **2.6.12 Antibiotic minimal inhibitory concentration (MIC) assay**

Cultures were grown overnight in Mueller Hinton (MH) media and diluted 100x into 96 well plates with increasing concentrations of antibiotics (2-fold serial dilution). Compound or DMSO were added when appropriate (1% v/v). Plates were incubated static for 24hrs at 37°C. MIC was determined as the first concentration at which no growth was observed.

### **2.6.13 Transmission electron microscopy (TEM) imaging**

TEM imaging was conducted within the Cambridge Advanced Imaging Centre and this report acknowledges their support and assistance as well as that of Dr Rita Monson (Department of Biochemistry) in the image capturing process. Samples were attached to argon glow discharged carbon coated copper grids by 5min soaking of grids in sample culture followed by 3x HPLC water washes. Grids were then soaked for 2mins 30s in uranyl acetate.

Samples were either planktonic overnight cultures or taken from the leading edge of swarming projections on swarming agar plates by resuspension with 10 $\mu$ L of LB.

## **2.7 *In vivo* models**

### **2.7.1 *Galleria mellonella* killing assay**

Killing assays for *Galleria mellonella* were used to assess the toxicity of compounds and their efficacy at increasing survival time in an acute PA infection *in vivo*. Overnight cultures were washed and resuspended in PBS (Oxoid, #BR0014G) before normalising to OD<sub>600</sub> 0.1. Cultures were then diluted in a 10-fold series dilution and supplemented with rifampicin 0.5mg/mL. Larvae were ordered from BioSystems TruLarv and 10 $\mu$ L of desired dilution was injected into the haemocoel via the hindmost left proleg. An additional 5 $\mu$ L injection of compound (diluted in PBS) or PBS was given into the foremost right proleg when appropriate. The larger volume was injected first followed immediately by the smaller volume injection. Death was determined by an absence of movement in response to touch. Mock inoculation controls were performed in each experiment as well as no trauma controls to monitor killing due to physical trauma.

# **Chapter 3**

## **Results & Discussion**

### **Compound Selection**

## 3.1 Binding site prediction of N-hydroxybenzimidazoles

### 3.1.1 Background

The AraC/Xyls family are potentially good antimicrobial targets for drug development because they are only present in bacteria and fungi proteins and are not represented in higher eukaryotes<sup>[205]</sup>. A small sub-group of this family, in which ExsA is included, are regulated by protein-protein interactions rather than small molecule ligands, such as arabinose, which is usually the case for the family<sup>[205, 246–248]</sup>.

The first task of my project was to predict and purchase a small number of compounds that could have inhibitory activity against ExsA. Data that is available on a drug target, such as crystal structures, known active ligands, and SAR knowledge can be used to filter chemical libraries when searching for novel active compounds. The more that can be known about the target protein and preferably known active ligands too, the better informed *in silico* screening can be and therefore the chances of achieving “true hits” is increased. In the case of ExsA there is a distinct lack of such data. Only one class of chemical inhibitors of ExsA are published, N-HBs, and only the regulatory NTD has been successfully crystallized<sup>[223]</sup>.

A review of previous work indicated the putative binding site of N-HBs to be in the DNA binding domain of ExsA, predicted by FTSite<sup>[226]</sup> on a model of ExsA<sup>[146]</sup>. To confirm this experimentally residues around this region were mutated for either glutamic acid, a large bulky residue to occlude ligand binding, or alanine, to remove polar interactions<sup>[146]</sup>. Certain substitutions altered the ExsA sensitivity to N-HBs, decreasing their ability to prevent ExsA binding to promoter DNA<sup>[146]</sup>. **Figure 3.1** shows this putative binding pocket and the mutated residues from the paper<sup>[146]</sup>. A curiosity from this previous work is how N-HBs have activity against ExsA, LcrF and AscA, all with highly conserved DNA binding domains, but are also active against, Rma, PqrA, MarA, SoxS and Rob, which do not have these similarly conserved residues<sup>[146]</sup>. It was suggested that the pocket shape is the determining factor for N-HB binding to ExsA rather than specific residue interactions<sup>[146]</sup>.

Additional studies of ToxT, another AraC/Xyls family protein that controls the expression of virulence factors in *Vibrio cholerae*, showed an unexpected cis-palmitoleate in the NTD when the protein was crystallized<sup>[249, 250]</sup>. Work was carried out to identify compounds

that replicate the docked conformation of the *cis*-palmitoleate and were tested for an ability to inhibit ToxT activity<sup>[251–255]</sup>. In addition, AraC is regulated by arabinose in a binding pocket that replicates closely the region mentioned in ToxT<sup>[207]</sup>. Despite only having a low level of sequence conservation with the ExsA NTD, the overall structure of the three proteins are remarkably similar and there is suggestive data to show that the dimerization interface in both AraC and ExsA is also conserved. However, the ligand binding pocket that can be seen in AraC and ToxT does not seemingly play a role for ExsA in its binding to ExsD<sup>[223]</sup>.

MarA is an *E. coli* protein homologue of ExsA that does not have a regulatory domain as other members of the family do, only a typical AraC family DNA binding domain and is regulated at the transcriptional level<sup>[223]</sup>. It is often used as a template in the creation of ExsA models for the ExsA CTD<sup>[223]</sup>. Given previous work showing N-HB activity against MarA and Rob, as well as the sequence similarities to AraC, all these structures were used in the search for novel active ligands of ExsA.

In this chapter the aim was to illustrate the purpose and reasoning behind selecting one region of ExsA that would be used for structure-based docking. This selection utilised docking software and online servers and was a subjective choice based on balance of inputs from multiple *in silico* experiments as well as a review of current literature. The steps taken to purify ExsA and determine that it was active using an EMSA assay follows, before the final sections of the chapter address the selection of the compounds. This selection used a variety of techniques that included assessing the suitability of each scoring function of the focus-docking software (ROC curve analysis), and biophysical binding experiments of ordered ligands with purified and active ExsA (tryptophan fluorescence quenching).

### **3.1.2 Ligand binding pockets in AraC/Xyls proteins**

Initially, I wanted to test whether docking experiments would support the docking results seen in Marsden *et al.*, (2016) and the conclusions drawn from it. Therefore, I began by observing where binding sites were predicted on my own models and structures, the plausibility of these sites for ligand binding, and virtual docking of N-HBs to these structures. The resources available to this project meant only one region of the protein could be focused on for any structure-based methods and so the primary aim addressed in this section was to determine which region of ExsA to focus on for structure-based docking and virtual screening.

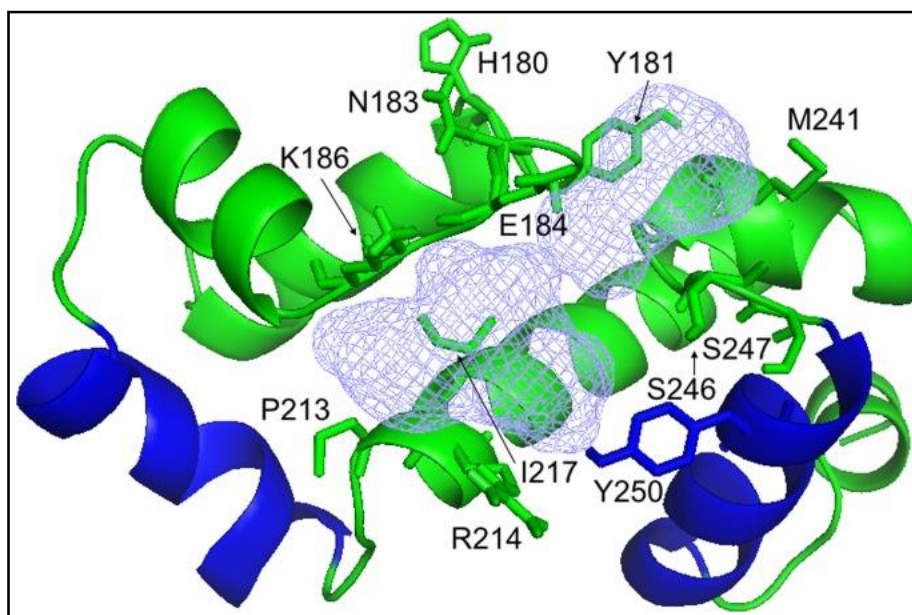


**Figure 3.1 Putative binding site of N-hydroxybenzimidazoles in ExsA:** The binding pocket of N-hydroxybenzimidazoles in the DNA binding domain of ExsA as predicted by FTSite. Blue residues represent those predicted to have base specific interactions with DNA and all labelled residues are those mutated in Marsden *et al.*, 2016. Image taken from Marsden *et al.*, (2016).

FTSite is a server that will identify potential ligand binding pockets on a protein surface by docking a number of solvents of varying polarity and observing cluster points<sup>[226]</sup>. 20 Conformations of the solution NMR structure of *E. coli* AraC CTD (PDB:2K9S) were submitted to FTSite along with 6 sampled conformations of ExsA from MD simulations (previously done by Dr Aneesh Chandran), MarA (PDB:1BL0) and Rob (PDB:1D5Y) structures. The MarA and Rob structures were solved bound to DNA which was removed from the models before submission. By submitting all the conformations for each protein, which pockets were predicted consistently across these AraC/Xyls family proteins could be seen.

Almost every structure was predicted to contain three potential ligand binding pockets. MarA and Rob proteins were predicted to have a pocket in the DNA binding domain located within the CTD. The MarA DNA binding domain pocket was significantly sized and the largest of the three indicated on the protein. Rob in comparison had an extremely small pocket predicted, it's other two ligand binding pockets within the NTD region also being small. The pockets predicted on these two proteins are visible in **figure 3.2**.

Of the 20 AraC CTD conformations submitted, a pocket within the DNA binding domain was predicted in all except conformation 15 (AraC\_15). The second persistently

predicted pocket was also in the CTD on the reverse side of the helix-turn-helix, so that two pockets existed like a saddle placed over the helix-turn-helix. A third pocket was predicted however, the NTD would likely significantly impact this third pocket. Three of the conformations and the pockets can be seen in **figure 3.3**.

None of the six ExsA MD models were predicted to have a ligand binding site in the DNA binding domain contrary the model seen in **figure 3.1**. Three pockets were indicated in all the conformations, but all were clustered in the NTD close to the CTD-NTD interface. This region is described in Shrestha *et al.*, (2015) and a hypothesis is that it became redundant as the protein evolved to be controlled by protein-protein interaction rather than ligand regulated or may hold unexpected regulatory secrets such as the *cis*-palmitoleate in ToxT. The region would be extremely interesting to investigate and target for small molecule intervention like the studies completed on ToxT<sup>[251, 253–255]</sup>. The available crystal structure of the ExsA NTD would also be a useful asset in the ligand search using this region. The absence of predicted binding pockets in the DNA binding domain of these ExsA models was troubling as it posed the question whether to focus on this NTD region with a crystal structure of the target protein, or to utilise a known active ligand class and rely primarily on related structures that support the proposed SAR of these known active ligands in a standard ligand-based drug discovery approach.

ExsA and other transcriptional factors can undergo dramatic structural changes differentiating ‘open’ and ‘closed’ conformations to bind promoter regions of DNA<sup>[207, 222, 248, 249]</sup>. Unfortunately, we could not be certain which of these conformations ExsA might be in, unlike for example with the Rob and MarA structures that were solved bound to DNA. The six models used were generated from a short (5ns) MD simulation likely showing the protein in a closed conformation.

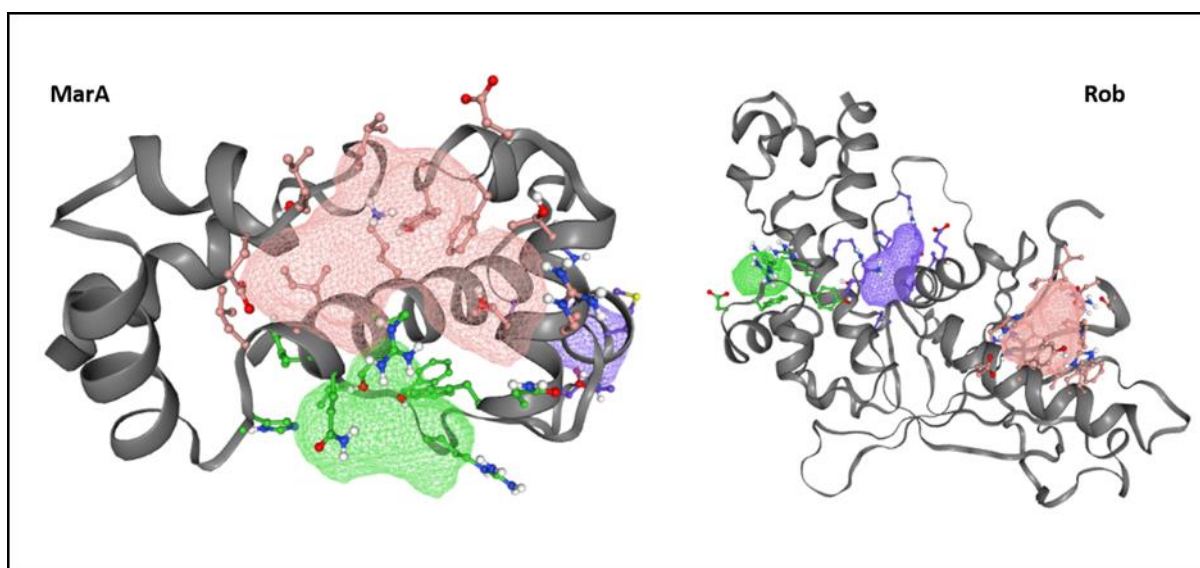


**Figure 3.2 Predicted ligand binding sites in MarA and Rob:** FTSite server ligand binding pocket predictions in MarA and Rob proteins. Both crystal structures were solved with DNA bound (removed before submission).

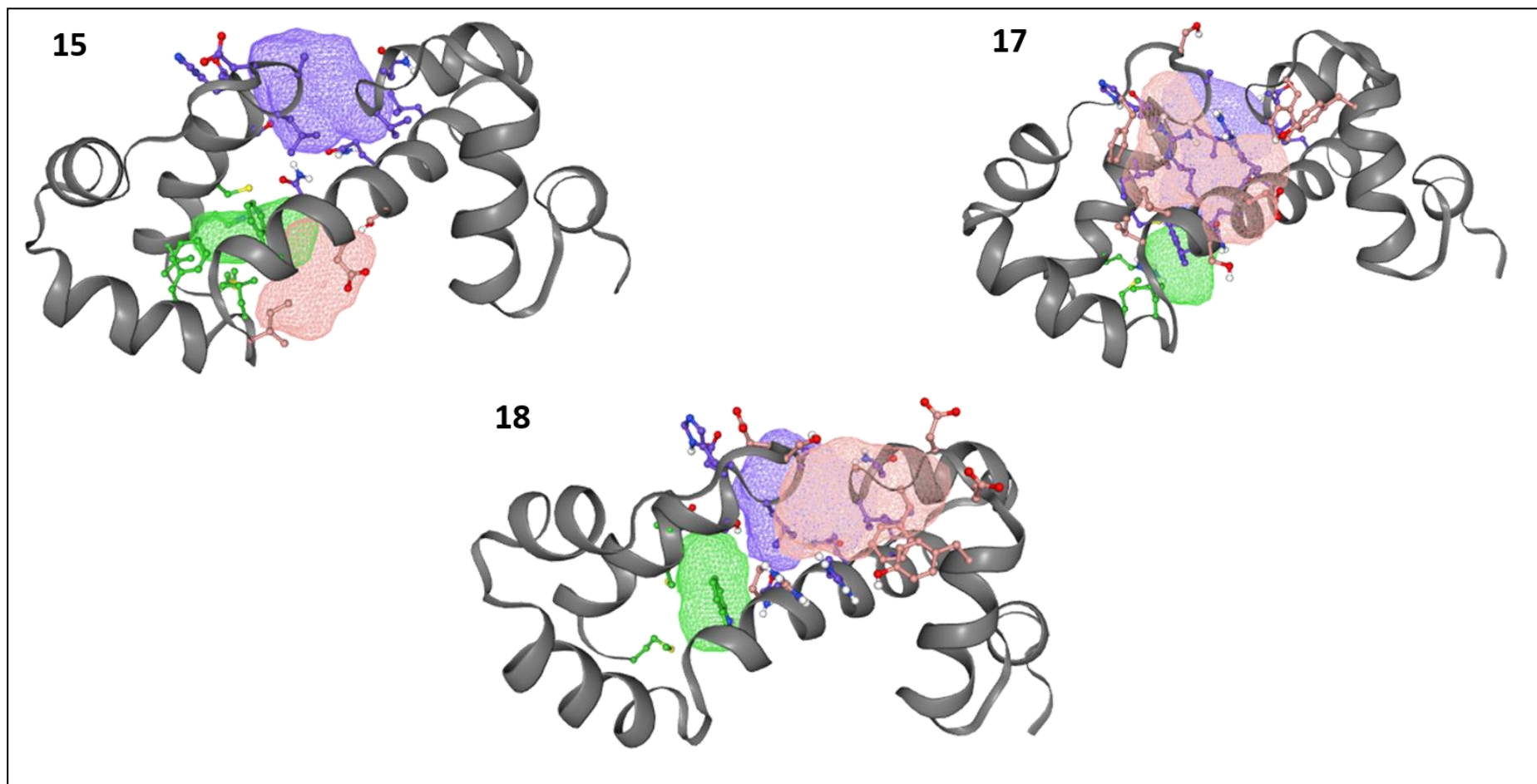


**Figure 3.3 AraC CTD predicted ligand binding pockets:** 3 conformations of AraC CTD submitted to FTSite (conformation 15, 17 and 18). Ligand binding pockets are indicated by coloured mesh. Structures are orientated in the same manner and the DNA binding domain is located at the site of pink mesh binding pocket in conformation 17 and 18.

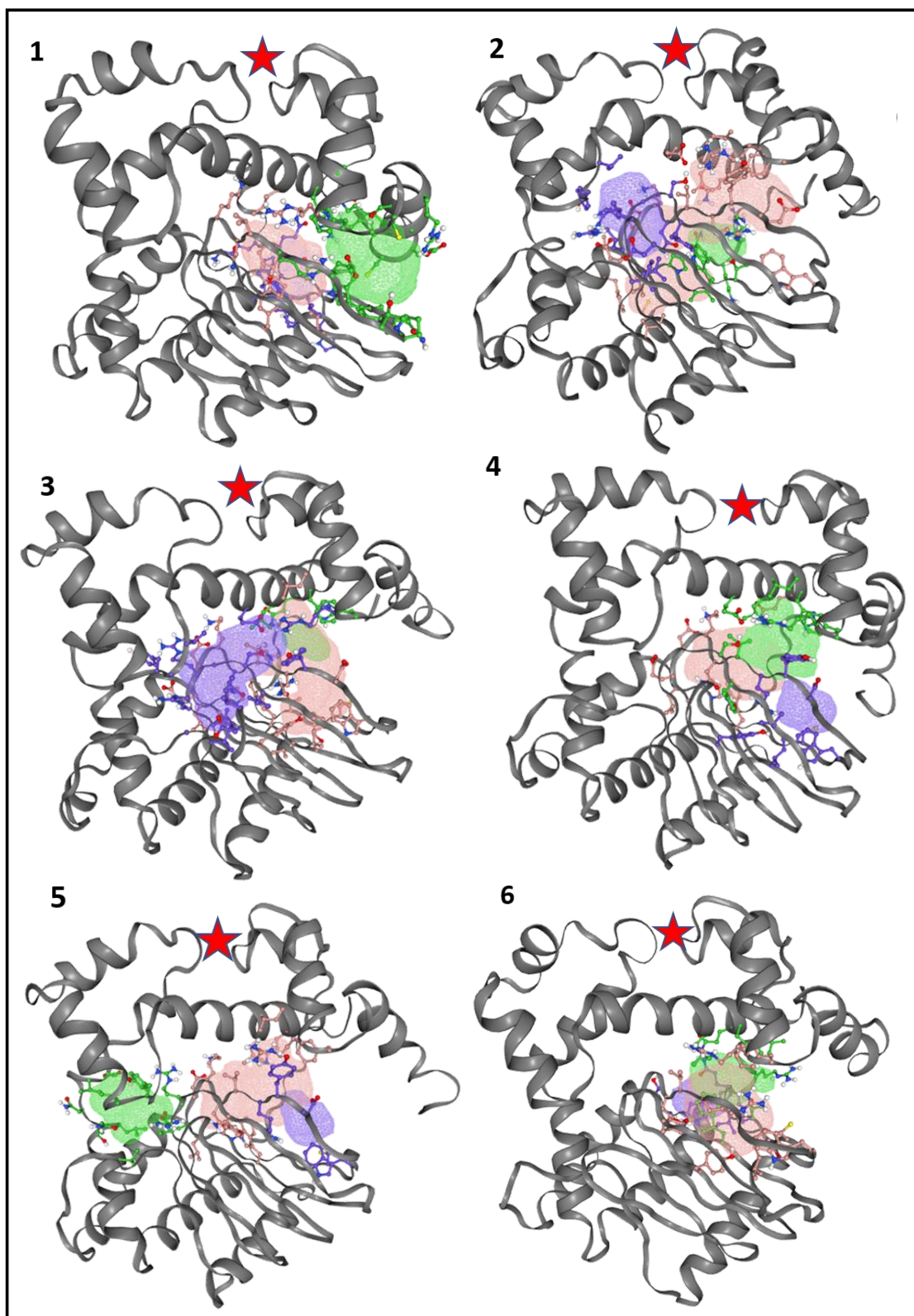


**Figure 3.4 Predicted ligand binding pockets in ExsA MD simulation models:** ExsA models refined through MD simulation were submitted to the FTSite server. Ligand binding pockets are indicated by coloured mesh and the DNA binding domain by a red star in each model.

The indication from these results is that ligand pockets are likely present at the DNA binding domain and the NTD within the AraC family, not unexpected given the ligand regulation of most of the family and additionally supportive of the broad family activity of N-HBs. As the 20 conformations of AraC show, there can be changes to the pocket sites between conformations and the proteins submitted are all inherently very flexible both around the CTD-NTD interface and around the DNA binding domain. Despite the ExsA MD models not having any pockets predicted in the DNA binding domain it does not exclude the possibility of one existing there in an alternate confirmation. Indeed, the model seen in **figure 3.1** has a such a pocket predicted from the FTSite server. The constraints, parameters and software algorithms used to build the models will all influence the conformations predicted and consequently the pockets.

### **3.1.3 Electrostatic surface mapping of AraC family proteins**

Following the absence of predicted ligand pockets in the DNA binding domain of the ExsA models I decided to map the electrostatic surface of the ExsA models along with an AraC model to observe whether it could potentially be a site for polar interactions. Electrostatic surface mapping<sup>[227, 256]</sup> of the AraC/Xyls family proteins revealed the DNA binding domain cavity to be a plausible site for polar interactions. **Figure 3.5** shows the electrostatic surface map of AraC with a predominance of electro-positivity, as expected for interactions with negatively charged DNA. The recess within which N-HB analogue 40 from Bowser *et al.*, (2007) (N-HB40, see **figure 3.6**) is docked has a contrast of positivity and negativity, meaning it is a plausible site for polar interactions. This technique was a further affirmation that the DNA binding domain would be a ‘druggable’ site. The process of docking N-HB40 is discussed in the next section.

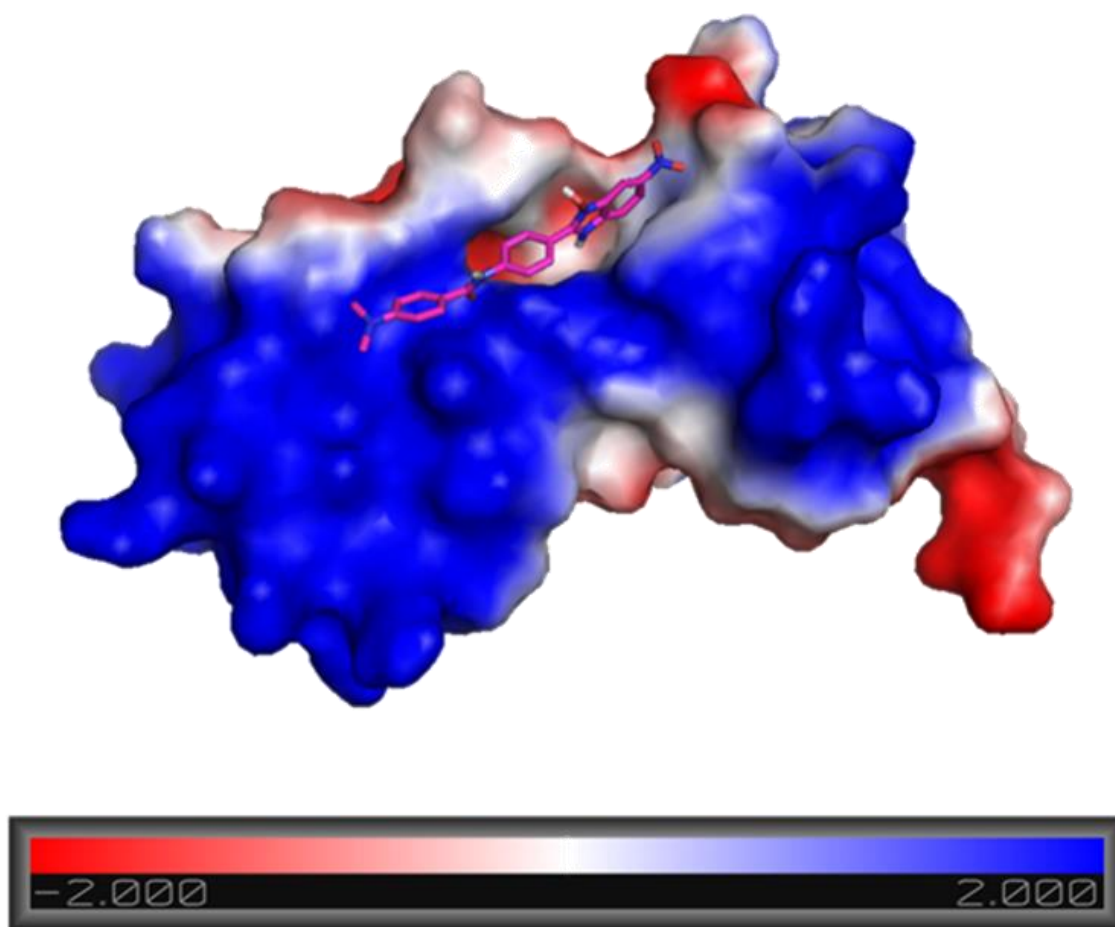


**Figure 3.5 Electrostatic surface map of AraC:** N-HB40 blind docked pose in the AraC DNA binding domain. Surface colours represent the electrostatic mapping of the protein. Blue = positive. Red = negative.

### 3.1.3 Blind docking of N-hydroxybenzimidazoles

To corroborate the binding pockets predicted by the FTSite server, N-HB40<sup>[208]</sup> (seen in **figure 3.6**) was blind docked (unbiased docking) using AutoDock Vina<sup>[230]</sup> to the entire surface of all the protein structures used in this project and the frequency with which each site was occupied was observed. AutoDock Vina is based on a stochastic algorithm<sup>[230]</sup> making it necessary to perform multiple independent docking runs to evaluate consistency in ligand poses to have greater confidence about the likely binding site for the selected ligand. The ligand (N-HB40) was docked 100 times to each protein conformation, with 9 conformations of the ligand generated each time. The top 100 poses docked were viewed in Pymol<sup>[225]</sup>.

N-HB40 docked largely in conjunction with the pockets projected by FTSite. Since the programme is stochastic, the proportions with each run differed, but the trends of frequency became apparent with independent docking repeats. When docked on the AraC protein conformations the ligand was docked at least once in the DNA binding domain in all but one conformation (AraC\_15), as well as being scattered between the alternative FTSite pockets and some individual poses in obscure positions on the protein surface. In AraC\_18, all poses were docked within the DNA binding domain, giving confidence to this being a likely binding site. The poses found in the DNA binding domain across all poses had 3 distinct orientations, the most common orientating the nitrite group toward the deepest recess of the cavity.

In the MarA and Rob protein structures the ligand was also found to dock consistently within the DNA binding domain, although poses within the other FTSite-suggested pockets or obscure positions on the protein surface were the most frequent cumulatively. In conjunction with AraC docking, the most frequent orientation of the ligand was to have the nitrite moiety aligned into the cavity region.

The ExsA MD models saw the ligands docked with a heavy priority to the NTD pockets and very few poses orientated in the DNA binding domain, although there was occasionally a docked pose here. This result was interesting and provided further evidence that the NTD region could be a druggable site on the protein, but also mimicked the smattering of DNA binding domain poses seen in the more closed conformations of the AraC structures.

The consistency of docking to the DNA binding domain amongst the homologue proteins suggested the region is a likely binding site for N-HBs and potential alternative inhibitors. However, to use the DNA binding domain would require greater reliance on homologue proteins over ExsA models itself in compound selection, which would significantly hinder any SAR elucidation. The NTD region of ExsA was also further affirmed for possible targeting if structure-based methods were to be used.

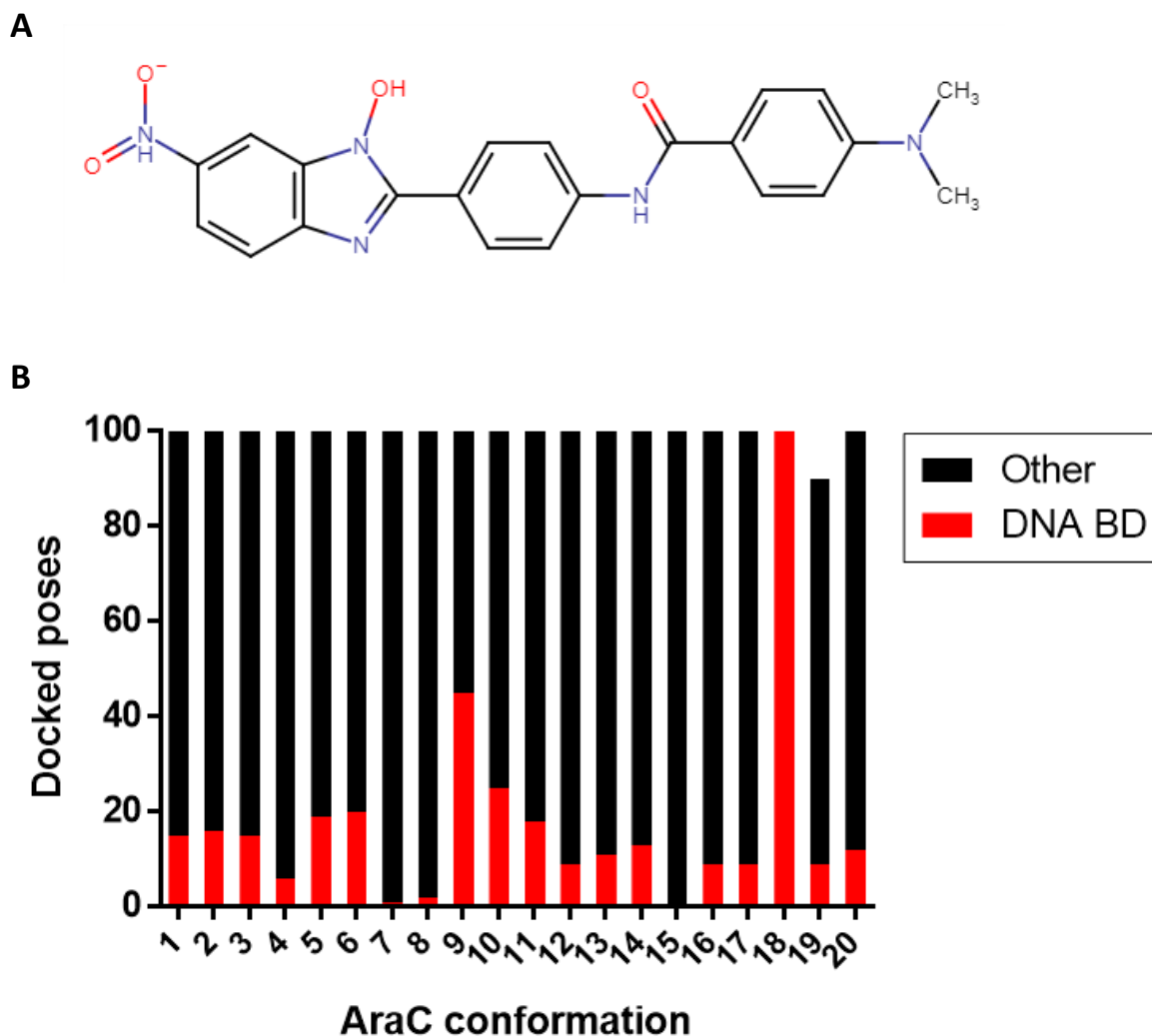


**Figure 3.6 Blind docking of N-HB40 in AraC conformations:** (A) A 2D structure of the N-HB40 molecule<sup>[208]</sup>. (B) The locations of the top 100 blind docked (AutoDock Vina) poses of N-HB40 in the 20 AraC conformations. DNA BD: DNA binding domain. This figure is representative of 3 repeat runs.

Since only a limited number of compounds could be purchased and the restricted amount of data available to utilise in a search, selection had to focus on just one region of the protein. A ligand binding pocket was predicted in the DNA binding domain of all the structures except the ExsA models, presenting a consistent picture across the family and a suspicion that the ExsA models were in ‘closed’ conformations. Virtual docking of N-HB40 in the AraC conformations and the FTSite pocket predictions indicated the drastic variability in ligand poses that can be seen between conformations, which highlights the difficulties faced in drug discovery when there is limited structural information. The electrostatic surface mapping aided the expectation that the DNA binding domain was a targetable region. It was therefore concluded the DNA binding domain was the most likely binding site of N-HBs and future *in*

*silico* screening involving both ligand and structure-based approaches should make use of the DNA binding domain of ExsA. This conclusion is further supported by the promiscuity of N-HBs across the AraC family alongside prior experimental data mentioned in section 3.1.1.

It must be noted that every model containing an NTD had a predicted ligand binding site in the NTD which warrants further investigation. This is supportive of the possibility that AraC family proteins have ligand regulation sites towards their NTDs and are targetable for small molecule intervention via these, such as with ToxT. The problematic nature of crystallizing these hydrophobic transcription factors frustrates structural investigation that would dramatically aid the search for such small molecules. An advantage to focusing on this region would have been the use of the crystal structure of the ExsA NTD and not the reliance on homologue structures. A deciding factor that prevented this option was that it would negate the use of N-HBs in a compound search given the conclusion of a DNA binding domain binding site for these molecules. Use of an ExsA structure itself over homologues would carry more weight in this circumstance if the pocket shape over specific interactions was not the prevailing hypothesis. Using a combination of structural and ligand-based approaches utilising the DNA binding domain and N-HBs had a greater chance of success in discovering novel ExsA inhibitors than to focus only on an NTD orientated structure-based approach. A project targeting the NTD would be a worthwhile future venture as a mechanism to inhibit ExsA.

## **3.2 Purification, function, and crystallization of ExsA**

### **3.2.1 Purification of ExsA**

ExsA contains rare codons which are associated with lower protein yields and so the plasmid containing the His-tagged full length *exsA* gene was transformed into Rosetta cells optimised for expression of genes containing rare codons. Numerous purification conditions were tried during the optimisation process including magnesium supplementation to media, alternate growth media, 3% alcohol, 3hr growth at 37°C after induction, and varied IPTG induction concentrations and time points were all tested. Yields were not noticeably different under the different conditions and so a protocol of induction with 1mM IPTG at OD<sub>600</sub> 0.6 and overnight growth at 18°C was followed. SlyD was a contaminant following Ni<sup>2+</sup> column purification but could be removed by excess washing on the heparin cation exchange column

and dimerised ExsA could also be removed by viva spin concentrator columns. Dimerised ExsA was probably not in itself a problem if isolated however, LC-MS/MS data showed that it was bound to chaperone proteins that were not removable after ATP washing and monomeric samples were shown to be active following electromobility shift assay (EMSA) experiments (section 3.2.2). A western blot was conducted using anti His antibodies in support of the LC-MS/MS data seen in **figure 3.7**.

Alternative methods that could have been tried in an attempt to increase purification yields included transforming the *exsA* plasmid into PA to express and purify the protein in its native species. Different plasmids could also have been used and several species have optimised plasmids for protein expression. Further changes such as adding or changing the tag on the ExsA might have improved the purification. A his-tag was used for Ni<sup>2+</sup> column purification that had the disadvantage of SlyD contamination. It was possible a change of tag might have helped purity to change the tag to glutathione-S-transferase for example. Additionally, generating an MBP fusion protein had the potential to improve the solubility which was another problem encountered. The MBP can be cleaved during dialysis, although with the hydrophobic nature of ExsA this might have meant it would not remain in solution after cleavage. Mutation of some of the more hydrophobic residues was also considered for the process and could have conferred better stability and potentially increased yields. These efforts are very typical solutions to yield or purity issues faced during a purification process and would have likely been the most efficient way to optimise a process given they have often-standardised protocols that go with certain plasmids, bacterial strains, and standard lab practice. It is not an exhaustive list however, and methods such as using denaturing conditions or resin-based techniques amongst many others could be tried if it had been necessary. Given the time constraints on the project, a priority was placed on investigating the activity of compounds and the process used was deemed adequate for the project with suitably pure and active ExsA, as determined by the EMSA assay in the following section.

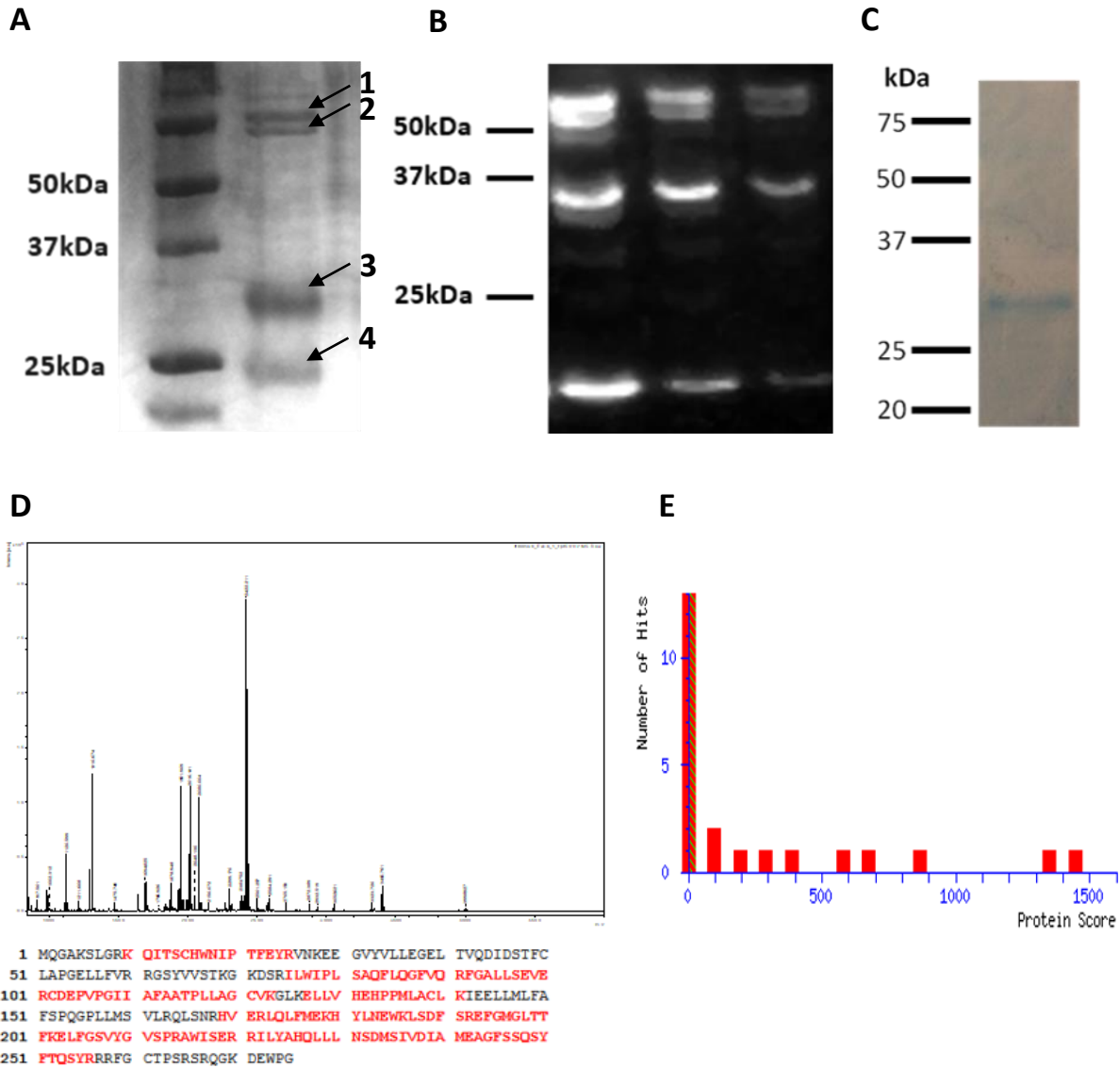


**Figure 3.7 ExsA purification:** ExsA was purified from *E. coli* Rosetta BL21 (DE3). AKTA HisTrap Ni<sup>2+</sup> column purification produced 4 bands determined to be ExsA monomer, dimer (2 bands) and SlyD contaminant. Additional purification steps using a Heparin cation exchange column and VivaSpin protein concentration columns improved ExsA monomer purity to >90%. **A)** 15% SDS-PAGE separation of HisTrap Ni<sup>2+</sup> column purified sample. The bands indicated by arrows and numbered were: **1 and 2** – ExsA dimer, **3** ExsA monomer, **4** SlyD. All bands were confirmed by MALDI fingerprinting or LC-MS/MS. **B)** Western blot of HisTrap Ni<sup>2+</sup> column purified ExsA sample using anti-His antibodies. The three lanes are 2x serial dilutions of the sample. **C)** 15% SDS-PAGE separation of sample purified using a HisTrap Ni<sup>2+</sup> column, a Heparin cation exchange column, and concentrated using a 50,000Da MW VivaSpin protein concentration column. **D)** LC-MS/MS trace of ExsA monomer band. **E)** MALDI fingerprint scoring of ExsA monomer sample.

### 3.2.2 Evaluation of ExsA function

To ensure that the purified ExsA samples were functional an electromobility shift assay (EMSA) was conducted using two fluorescently labelled DNA probes – an *exoT* promoter region probe and a non-specific *katA* promoter probe. EMSA gels are native, low percentage acrylamide gels that highlight DNA-protein interactions by slower migration through the gel matrix of DNA-protein complexes compared to DNA alone, observable by shifted bands when the gel is imaged. As can be seen in **figure 3.8**, there were shifts caused by the addition of ExsA to lanes containing *P<sub>exoT</sub>* probe. When excess unlabelled *P<sub>exoT</sub>* probe was added a knockdown is seen as ExsA binding is saturated by the unlabelled probe. The addition of DMSO did not affect the binding of the ExsA to the specific probe and no binding was seen between the non-specific *P<sub>katA</sub>* probe and ExsA. The final confirmation of activity was the addition of ExsA antibodies to the sample which causes super-shifts because of the added size of the product viewed by gel imaging and western blot (exsA antibodies). The different shift bands correspond to different ExsA products such as a monomer or dimer.

This assay was a robust measure of DNA-protein interaction and provides solid evidence in favour of active purified ExsA however, the method had some significant drawbacks for its use in this project. Ideally this assay could have been used to identify compounds inhibiting ExsA activity, but it was too low throughput to be used as a primary means of testing the compounds. Additionally, it is not quantitative due to dissociation of complexes as samples are not in chemical equilibrium and migration of complexes is influenced by many factors and not just size meaning shifts do not necessarily correspond to molecular mass. However, the intention in this project was to use the EMSA as a confirmation for molecular activity against ExsA function by using a dose inhibition curve, as well as being used to test if the purified ExsA was active. Titrating the compound into the samples at increasing concentrations should correspond with increased intensity of the unbound probe band and lower intensity in the shifted, protein-bound probe as ExsA binding approaches saturation. Using this technique has been reported previously in Marsden *et al.*, (2016) and is a good technique to demonstrate molecular activity following hit identification.

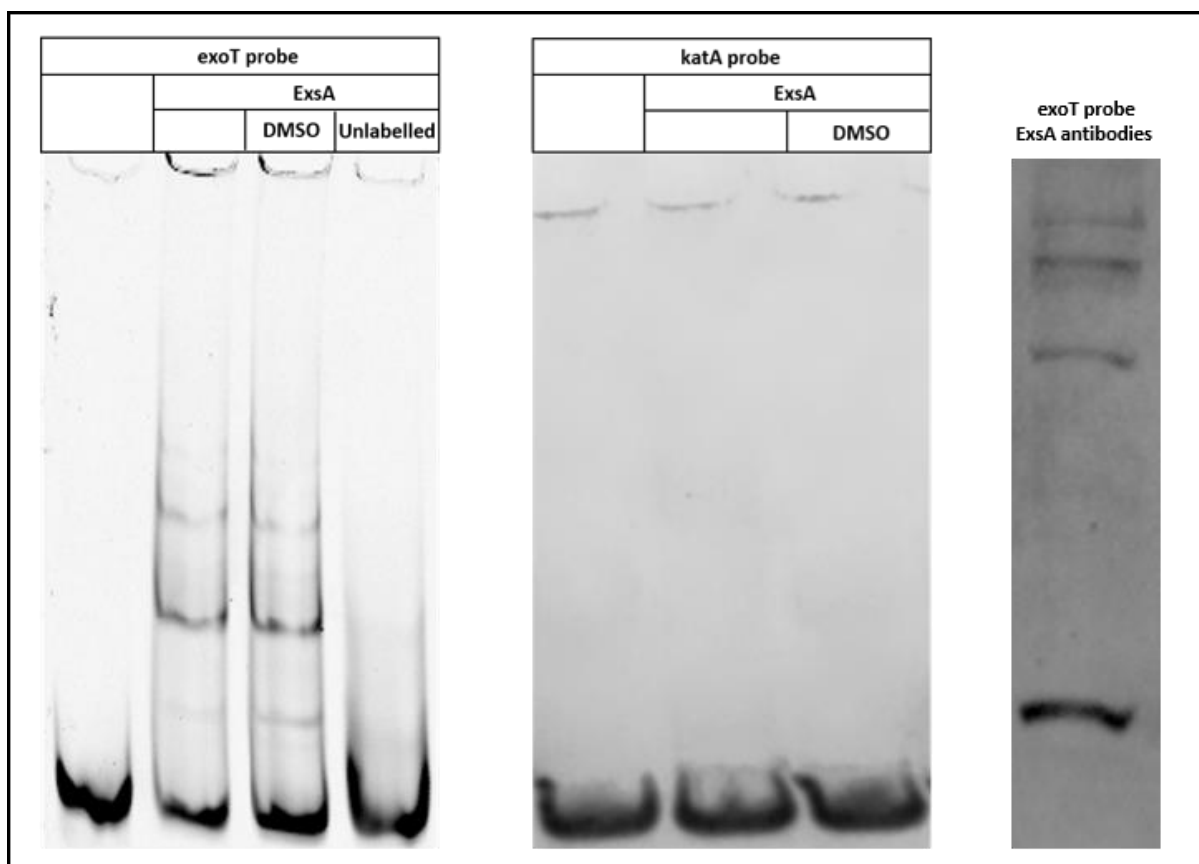


**Figure 3.8 ExsA functional activity in electromobility shift assay:** Specific and non-specific Cya5.5 fluorescently labelled probes were incubated with ExsA and separated by 4% native SDS-PAGE at 4°C. **(Left)** EMSA gel of  $P_{exoT}$  probe and lanes containing addition of ExsA, ExsA and DMSO, and ExsA and excess unlabelled  $P_{exoT}$  probe. Shift bands indicate DNA-protein interactions. **(Middle)** EMSA gel of non-specific  $P_{katA}$  probe with ExsA and ExsA and DMSO added. **(Right)** EMSA gel containing ExsA,  $P_{exoT}$  probe and anti-ExsA antibodies showed super shifts of bound complex. All images are representative of 3 independent experiments.

### 3.2.3 ExsA crystallography screen and stabilising mutagenesis predictions

Since no full length structure has been solved to date, I attempted to crystallize ExsA in order to gain valuable structural information that could be used to improve the modelling and search for new inhibitors. Four plates were prepared with purified ExsA (2.5mg/mL) and images were captured every day for 30 days. No crystals formed under any of the conditions tested. ExsA has a number of hydrophobic surface residues and a lot of inherent flexibility due to its tertiary structure making it an unlikely candidate for crystallization. Purification routinely returned low yields of less than 3mg/mL. which hampered crystallography efforts as well. For future attempts two main options were considered – co-crystallization with a strong inhibitor or site directed mutagenesis. Both aim to improve the stability of the protein and increase the likelihood of crystal lattice formation. Greater protein yields would have also benefitted attempts

Predictive computational work was done to identify potentially stabilising mutations for any future site directed mutagenesis work. The ExsA AA sequence was submitted to the UCLA SERp Server (<http://services.mbi.ucla.edu/SER/>) and clusters suitable for substitution were suggested. The three clusters flagged as suitable for alanine substitution can be seen graphically in **figure 3.9**. The first two clusters, 10-11 KQ and 28-30 KEE are located on a free loop at the beginning of the protein. The third is located close to the DNA binding domain.

To corroborate these predictions, I submitted three sequence regions of ExsA to STRUM<sup>[236]</sup>, a server that assigns a predicted stability score by using algorithms trained to predict Gibbs free-energy changes after single point mutations for a number of different point mutations for each residue within the target region. I submitted residues 2-30 housed in the free starting loop of the NTD, residues 150-200 covering  $\alpha$ -helices in the CTD and a second CTD  $\alpha$ -helices region of residues 230-260. As with the UCLA SERp Server predictions, these can be seen graphically in **figure 3.9**. Since each residue within the regions are given scores for 19 different substitutions, I noted those which were given improved stability values across most if not all substitution options. K5E in the first region, H180L and W185A in the second region, and T252A, Y255M, and R256I in the final cluster were all highlighted as the most effective mutation suggestions. These mutations were then all run in a third server, SDM (<http://www-cryst.bioc.cam.ac.uk/~sdm/sdm.php>) with STRUM suggested substitutions or with alanine substitutions. Residue mutations K5E, H180L and T252A were predicted to improve crystal formation as well as K5A, W185A and R256A.

Concluding from this iterative process is that the free starting loop of ExsA is likely to cause significant problems when it comes to crystallizing the protein, as well as at least two sites within the CTD, including the DNA binding domain, housing hydrophobic residues that could be mutated to improve efforts to crystallize the protein. Mutagenesis around the DNA binding domain would severely impact the benefit gained from SAR information gleaned from structural and docking information and I would therefore suggest that future attempts do not target those residues but instead look at T252A as a starting point for CTD substitutions.

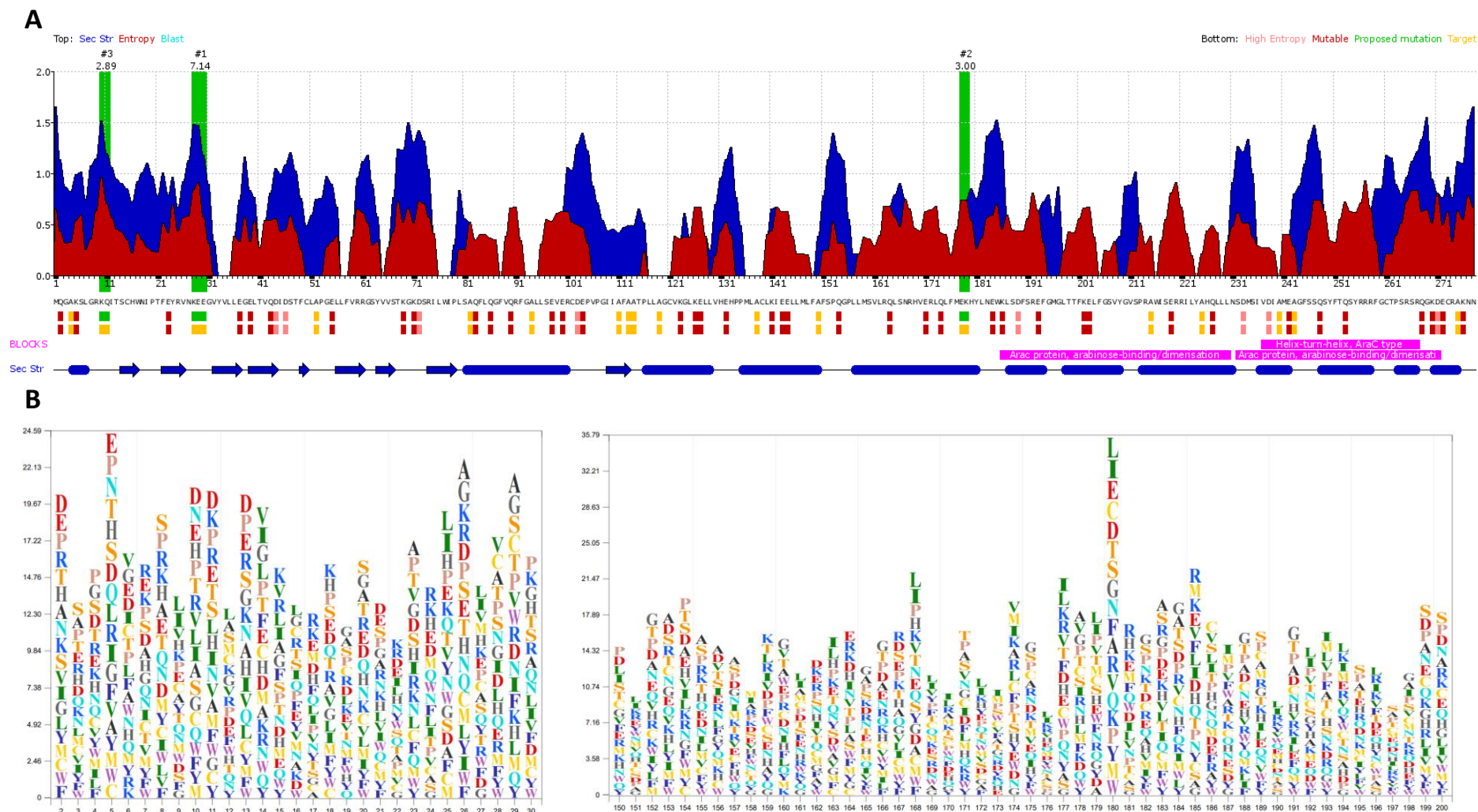


**Figure 3.9 Predicted stabilising mutagenesis for ExsA crystallization:** The ExsA AA sequences were submitted to UCLA SERp server and STRUM to predict mutations that would likely confer improved stability for crystallization. (A) UCLA SERp Server predicted three mutable regions (green bars). (B) STRUM scores of AA substitutions ranked vertically as a representation of predicted improved protein stability.

### 3.3 Compound selection

#### 3.3.1 Receiver operating characteristic (ROC) curve analysis

A combination of structural and ligand-based approaches was used to select the compounds ordered for testing. In total 131 initial compounds were ordered using 4 distinct methods. Throughout this project I refer to the compounds by the method in which they were chosen or the library from which they were selected. The compound groups are, FA, M, NCI and E. Compounds were named with their order category as a prefix followed by their number within that category. E.g. FA1, M2, NCI3 or E4.

As mentioned in section 3.1.1 additional active molecules would increase the chances of attaining more ‘true hits’ and if some were identified early on, they could be fed back into the selection process and assist in the search for more. The FA compounds were ordered first and tested using biophysical methods to identify molecules that were binding to ExsA. These molecules were incorporated into the selection and ordering of the E compounds.

Docking software programmes usually have changeable input parameters and more than one scoring function that will score differently for the same molecule docked in the same region of the same protein. This is because different scoring functions are weighted differently towards various binding forces, such as hydrogen bonds, electrostatic or hydrophobic interactions<sup>[194–197]</sup>. The optimal programme and scoring function to use in drug discovery will vary between proteins. To this end, I was careful to try and identify the “best” scoring functions to choose, as well as using a variety of selection techniques.

By using a false set of ligands (called a decoy set) generated from a collection of known active ligands, it is possible to test the global recognition and enrichment capabilities of a scoring function. Global recognition is testing whether the programme identifies all the active ligands within the set. For instance, if a library is generated consisting of 500 compounds (50 active and 450 inactive) and the top 200 ranked molecules were selected from the scoring function, but only 10 of the active compounds are present, then there is a global recognition problem. Enrichment is how highly the active ligands are ranked. For example, all 50 may be present in the top 200, but if they are ranked between 100 and 200, there is an enrichment problem. The known active and ‘inactive’ ligands are ranked by each scoring function and

analysed using ROC curve analysis. The inactive molecules are designed to be topologically distinct from the active molecules but share similar functional groups.

To do this for ExsA a decoy set of 243 ligands was generated based upon five N-HB compounds<sup>[146]</sup> and ROC curve analysis was performed on the GOLD software (CCDC Cambridge, UK) using an ExsA MD model, testing three scoring functions, Chemscore, Goldscore and ChemPLP<sup>[231]</sup>. Due to the relatively small number of compounds, all were ranked meaning global recognition was not truly tested. ChemPLP and Goldscore ranked all active compounds within the first 50% of molecules, whilst Chemscore ranked two active molecules outside of this first 50%. It was found chemplp overwhelmingly outperformed the other two scoring functions on enrichment and so was used in the selection of E compounds.

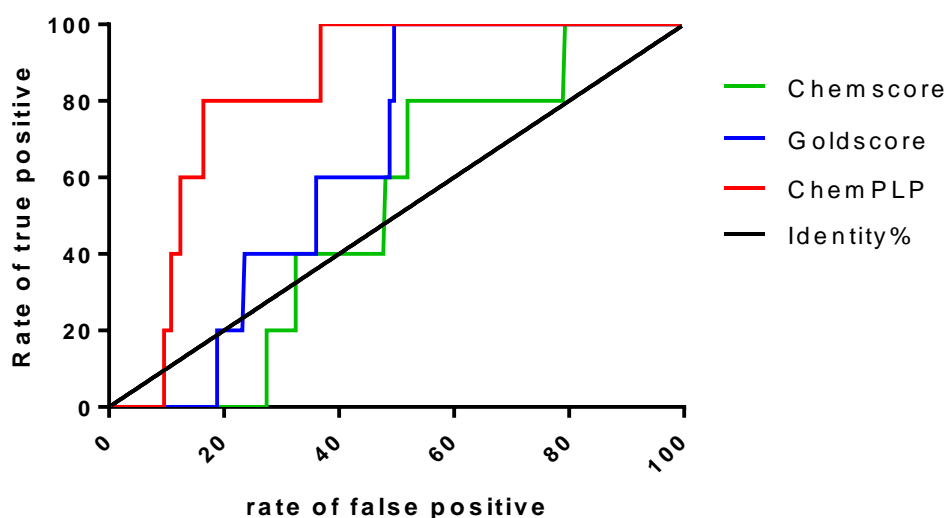
Although ChemPLP performed the best in the ROC curve analysis, “data fusion” methods combining different scoring functions during virtual screening has had reported success in the literature with regards to database enrichment<sup>[257]</sup>. Combining this with the small number of known active molecules, the NCI library was selected using all three of the scoring functions<sup>[257–260]</sup>.

The ROCS (Rapid Overlay of Chemical Structures) software (Open Eye Scientific, USA) gave perfect AUC (area under curve) scores of 1 for three functions, ShapeTanimoto, ShapeCombo and ColourTanimoto (<https://doi.org/10.1038/nchembio.150>). This is unsurprising given that ROCS scoring functions are based upon similarity to query molecule shape and the decoy set is created to be distinctly topologically different to the known active molecules. ROC curve analysis graphs were made in GraphPad Prism 6.0 using ROC curve and AUC analysis functions.

### **3.3.3 Ligand-based approaches**

The first ligand-based approach was to order the FA group of compounds which came from the Enamine hit locator® (Enamine HLL) library (<https://enamine.net/hit-finding/diversity-libraries/hit-locator-library-300>). The library was fed into ROCS using N-HB40 as a lead query and the top 200 output molecules, as determined by TanimotoCombo and ColourTanimoto scoring, were manually inspected in Field Align (Cresset, UK) for structural variance, but electrostatic similarity to the lead query. The TanimotoCombo score

will give a maximum value of 1 to a hit with 100% overlap in 3D shape to the query molecule. ColourTanimoto will do the same for a hit sharing 100% similarity in the chemical groups present. From this method 18 compounds were ordered. This subjective analysis is obviously a relatively low throughput method of selection although it has advantages in not selecting repeat chemical scaffolds, ability to spot enantiomers and groups or compounds known to be toxic can be removed too.



<b>GOLD scoring function</b>	<b>ROC AUC</b>
Chemscore	0.522
Goldscore	0.646
ChemPLP	0.828

**Figure 3.10 ROC curve analysis of GOLD scoring functions:** A ligand library containing decoy ligands and known active ligands were docked in the DNA binding domain of an ExsA MD model using GOLD. Each scoring function ranked the ligands and the output was analysed using ROC curve analysis. Chemscore (green), Goldscore (blue) and ChemPLP (red). Area under curve (AUC) calculations were conducted using GraphPad Prism 6.0 AUC analysis. This data is the result of one docking run for each scoring function.

A similar method was used to order the 14 M compounds with N-HB40 used as the lead query to scan the Chembridge CORE® ([https://www.chembridge.com/screening\\_libraries/](https://www.chembridge.com/screening_libraries/)) and Specs® ([www.specs.net](http://www.specs.net)) libraries. The libraries were screened in ROCS as ranked by scoring functions and assessed for scaffold overlap with previously purchased compounds

before being ordered through Molport. The user interfaces for ROCS and Field Align are shown in **figure 3.11**.

These ligand-based methods relied on the pocket shape hypothesis over specific interactions. With only one known active chemical class of inhibitors specific interactions or functional groups are elusive and it was not possible to further refine a ligand-based screen by using quantitative structure-activity relationship (QSAR) methods or similar to improve the likelihood of successful selection.

### **3.3.4 Structure-based approaches**

NCI Diversity set V (<https://wiki.nci.nih.gov/display/NCIDTPdata/Compound+Sets>) library conformers were docked into the DNA binding domain of six ExsA MD models using all three GOLD scoring functions (Goldscore, ChemPLP and Chemscore). The scores were normalised and the top 10% of hits were run in ROCS using N-HB5631<sup>[146]</sup> as bait and ShapeTanimoto scoring function. A Z score was generated between the GOLD and ROCS scores and this was used to rank the molecules, but any were excluded if the molecule possessed a LogS value outside the range of -1 to -5 and a LogP value between 1 and 5. In total, 40 compounds were ordered from the NCI library. GOLD is a focus docking software that allows the side chains of amino acids within the selected docking region to rotate<sup>[231]</sup> and so despite the lack of a predicted ligand binding pocket in the DNA binding domain of these ExsA models, this was conducted with the possibility this additional flexibility could expand the pocket into a more open conformation.

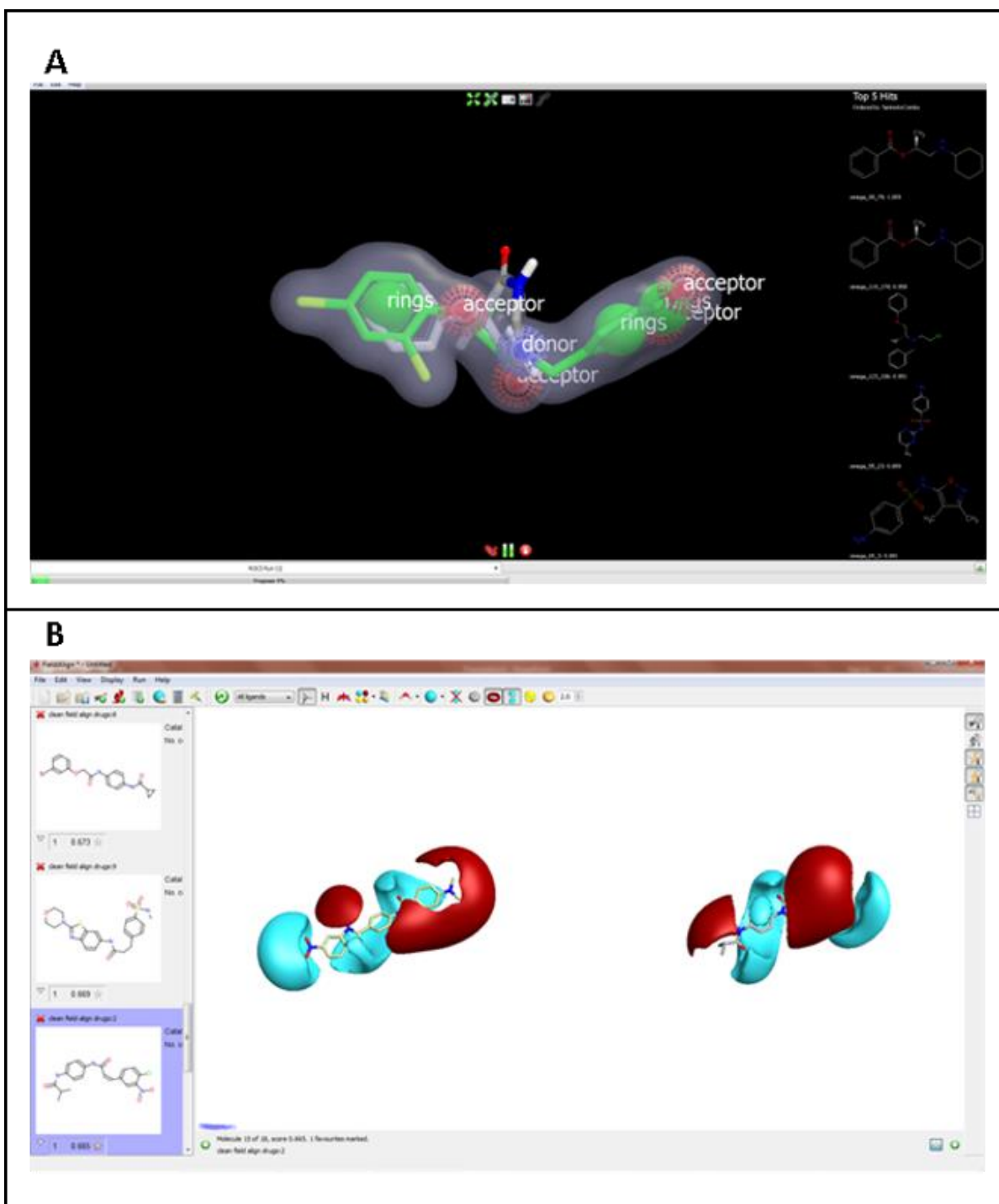
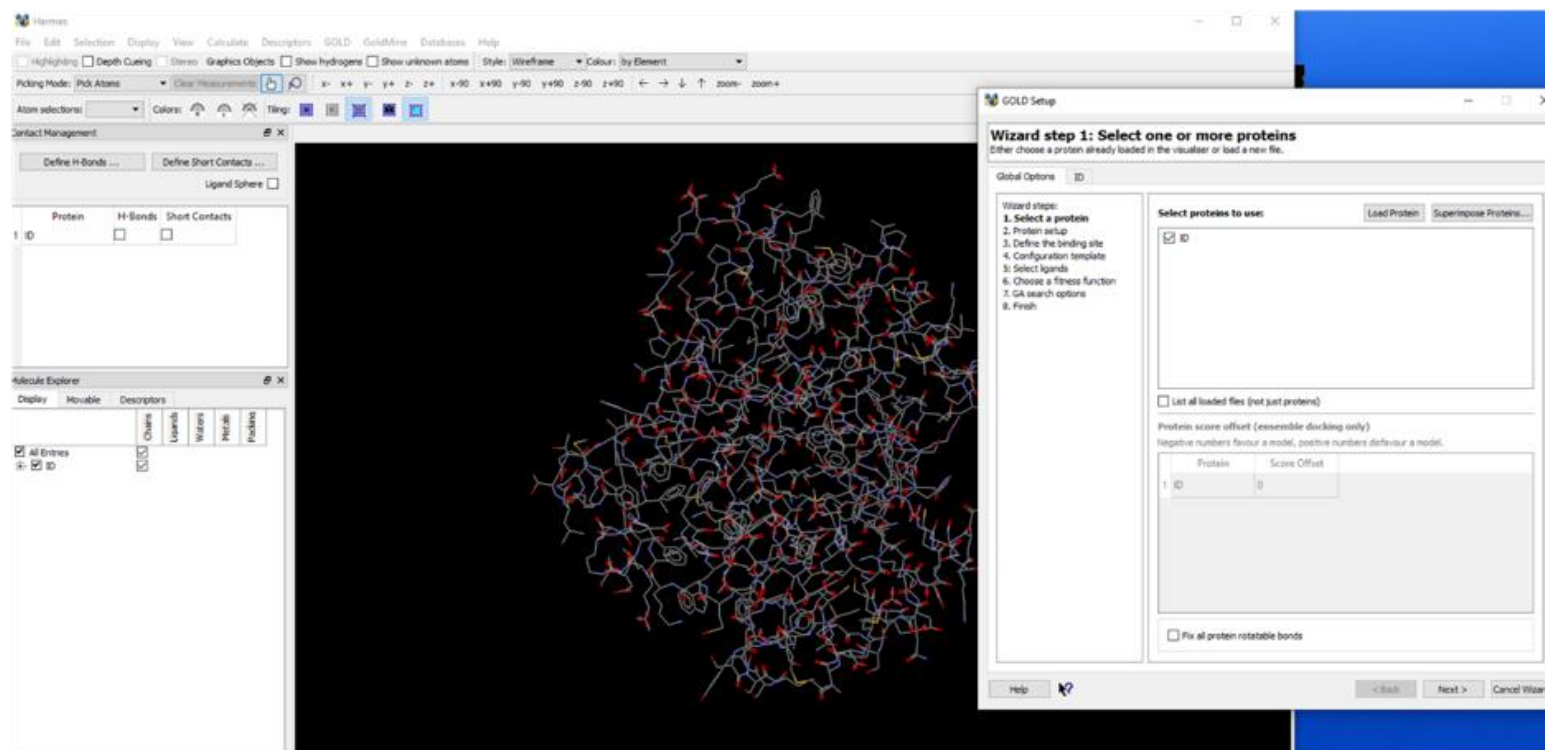


**Figure 3.11 Ligand-based approaches:** (A) The ROCS software user interface. A lead query molecule is entered and scoring functions are used to filter libraries based on similarity of desired properties to the lead query ligand. The results from ROCS can be input into another programme, EON (Open Eye Scientific, USA). (B) The Field Align software user interface. Electrostatic fields of the ligands can be viewed and aligned beside a lead query molecule. Inspection and selection of compounds in this software is manual and subjective. Red bubbles represent electropositive fields and blue electronegative fields.

A



B

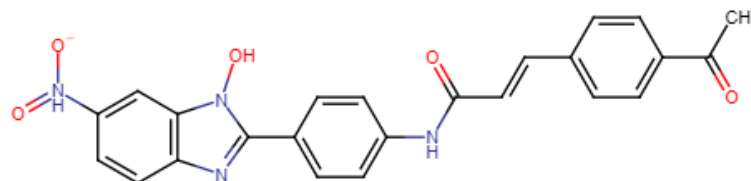


**Figure 3.12 NCI compound selection:** (A) The GOLD docking software user interface. ExsA MD models were uploaded and a central atom designated in the DNA binding domain with a radius of  $15\text{\AA}$  about the central atom. GOLD has three scoring functions – Chemscore, Goldscore, and ChemPLP. GOLD allows the rotation of side chains in the docking site and ligand conformations are kept static. (B) 2D chemical structure of N-HB5631<sup>[146]</sup> used as the lead query in ROCS screening of the NCI Diversity set V library.

### 3.3.5 Combined approaches ligand search

The final order of compounds was also from the Enamine library; selected using a combination of ligand-based and structure-based methods. Experimental binding data was gathered from the FA compounds, tested for their ability to bind purified ExsA by tryptophan fluorescence quenching. Two compounds that were positive for binding were overlaid with N-HB40 and their shared pharmacophore features were used to filter the Enamine library.

An intrinsic fluorescence assay was used, adding compounds at increasing concentrations to purified ExsA and measuring the reduction in tryptophan fluorescence. ExsA has four tryptophan residues and Trp-185 is located within the DNA binding domain, the other three are not surface accessible. These residues can be seen in **figure 3.13**. Reductions in fluorescence occur due to changes in polarity in the local environment to the residue from ligand binding, or from conformational change induced by binding. If no binding event occurs, the addition of material to the environment can cause the random blocking of fluorescence, presenting as a linear reduction in relative fluorescence units (RFU) relative to concentration. A potential flaw of fluorescence quenching is the inner filter effect; a ligand that absorbs close to the excitation or emission wavelengths can induce significant quenching without a binding event occurring. This can be accounted for by exciting the ligands alone and recording fluorescence to use as control titrations. Two compounds, FA8 and FA15 were found to bind ExsA, producing dose response curves. **Figure 3.13** shows these curves, as well as FA3 representing a nonbinding compound that inhibited fluorescence in a linear, concentration dependent manner.

FA8 and FA15 binding were investigated further using fluorimetry to establish a binding affinity. The two ligands were titrated into a buffer at 25°C containing ExsA and fluorescence was measured using a spectra fluorometer with  $\lambda_{\max}$  determined as 336.5nm. The binding affinity for both compounds was established to be in the low nanomolar range, 227nM and 140nM for FA8 and FA15 respectively. Interestingly, the data showed that FA15 had a curved scatchard plot, indicating two binding sites. Neither ligand caused a shift in  $\lambda_{\max}$ .

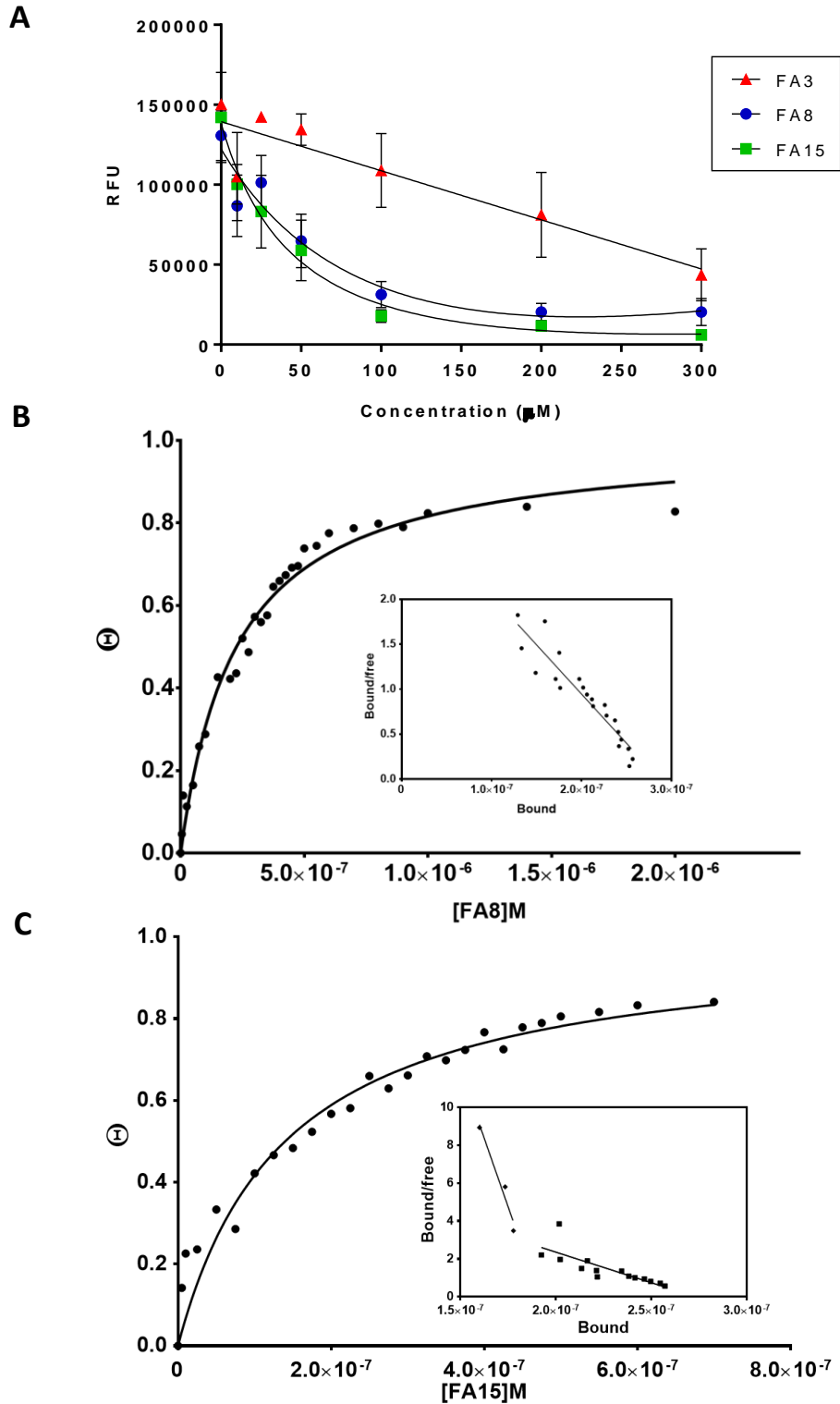
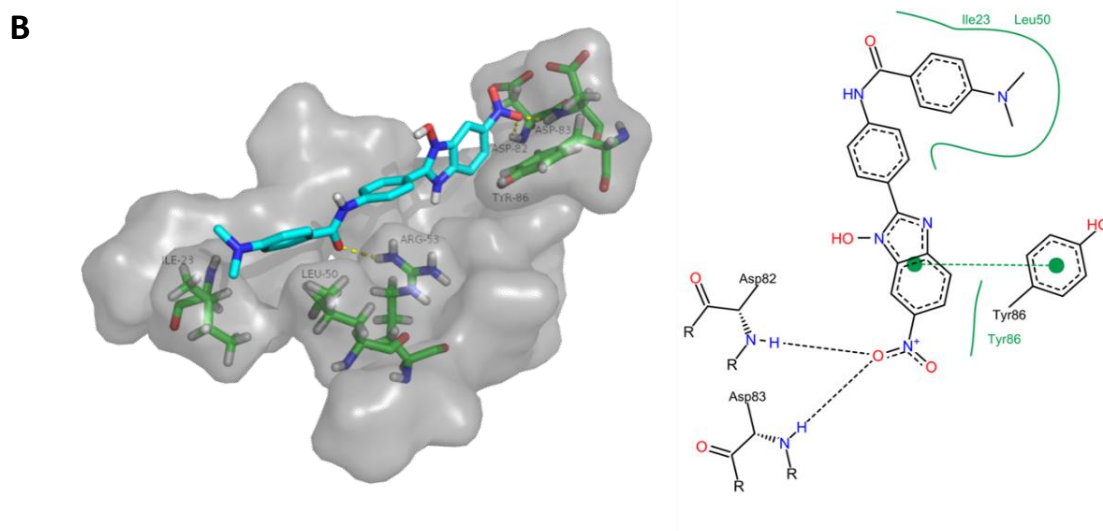
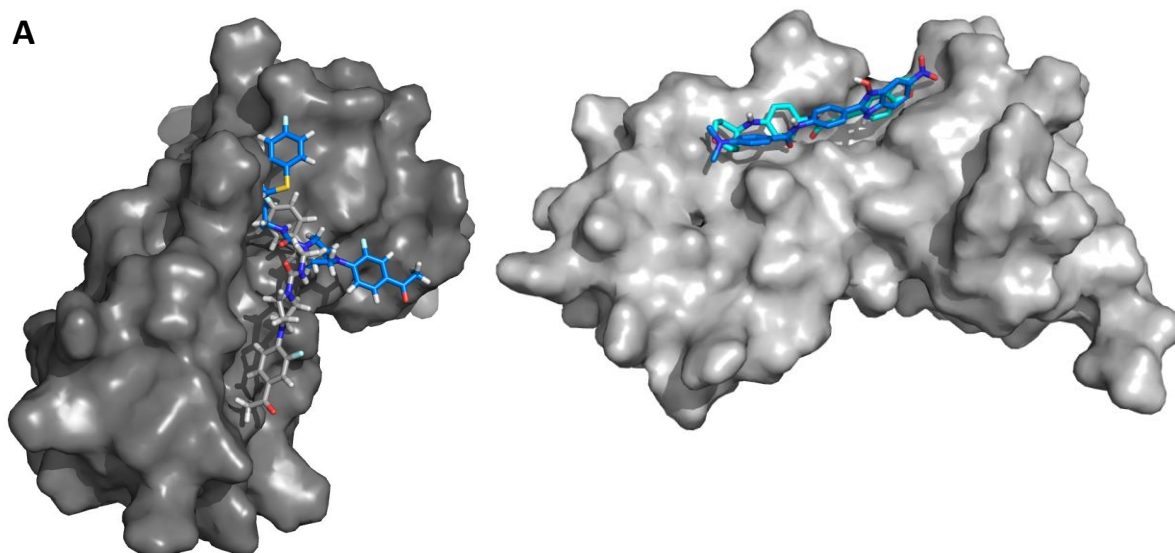


**Figure 3.13 ExsA tryptophan fluorescence quenching:** (A) Dose response curve of 3 FA compounds (FA3, FA8 and FA15) showing changes to tryptophan fluorescence with increased concentration of ligand. Excitation wavelength 295nm, emission wavelength 330-410nm. Data points are the mean  $\pm$ SEM of 3 independent experiments. (B and C) Fluorimetry binding data of ExsA to FA8 (B) and FA15 (C) using spectro fluorimeter.  $K_d$  values were calculated using GraphPad Prism 6.0 non-linear regression of  $\Theta$  vs [L]. Scatchard plots were analysed using GraphPad Prism linear regression. Data is representative of 3 independent experiments.

N-HB40 was docked in AraC\_18 using AutoDock Vina and the poses within the DNA binding domain were observed. The variability in the docked poses came primarily from rotation around longest axis of the molecule and therefore rotating the orientation of the amide and hydroxy benzimidazole groups that can form H-bonds. Additionally, the plane in which the aromatic regions are positioned changes with this rotation. Ultimately however, the docking was consistent in its overall orientation of the molecule to the region, with the nitrite group positioned towards a conserved section of the helix-turn-helix, shown in **figure 3.14**. Polar interactions between N-HB40 and the surrounding residues were predicted by PyMol as well as a submission of the docking to PoseView (<https://www.zbh.uni-hamburg.de/en/forschung/amd/server/poseview.html>) that provides 2D sketches of proposed interactions. Predicted binding included H-bonds between the acetamide oxygen and Arg-53, and the nitrite group and Asp-82 and Asp-83. Tyr-86 was predicted to have pi-pi interactions between the benzimidazole aromatic region in conjunction with the H-bonds mentioned. The end of the molecule was suggested to be coordinated by Ile-23 and Leu-50 residues. Alternative possibilities were that the molecule is shifted further along the region, meaning Arg-53 and Arg-57 formed H-bonds with the nitrite and hydroxyl groups, as well as an additional H-bond between the acetamide oxygen and Ile-23. The end of the molecule then being coordinated by Ile-23 and Phe-21. These predictions were based on AraC and so had to be compared for a likely semblance to docking in ExsA. Therefore, a sequence alignment was performed of the models used during this project in addition to alignment of AraC\_18 and the ExsA MD models in PyMol and residues that may play a role in binding were subjectively scrutinised. These specific interactions are the major shortcoming in this structure-based aspect and so the docking was utilised primarily to obtain docking poses that could be overlaid and compared to broaden the information available for a ligand-based search.



exsA:	IAMEA	<b>GFS</b>	SQSYFTQSYRRRFGCTPSRSRQG
AraC:	VGRNV	<b>GFD</b>	DQLYFSRVFKKCTGASPSEFRAG
MarA:	LAERY	<b>GFE</b>	SQQLTRTFKNYFDVPPHKYRMT
Rob:	IALQY	<b>RFD</b>	SQQTFTRAFKKQFAQTPALYRRS

**Figure 3.14 Docked ligand poses of ExsA binding compounds:** FA8, FA15, and N-HB40 were docked using AutoDock Vina into AraC\_18 conformation. (A) Left: Two top ranked poses of FA8 in the DNA binding domain. Right: N-HB40 and FA15 top ranked docking poses overlaid together in the DNA binding domain. (B) Left: N-HB40 binding pose docked in AraC\_18 with surrounding coordinating residues suggested by PoseView. Right: PoseView 2D representation of interactions for N-HB40 docked in AraC\_18 DNA binding domain. (C) Conserved residues in the DNA binding domain of ExsA, AraC, MarA, and Rob

It can be seen in **figure 3.14** that the FA15 docking aligned very closely to that of N-HB40. FA8 however, had more variation in the docked poses, two of which can be seen in **figure 3.14**. These poses all orientated the sulphide end of the molecule the same way as the nitrite group of N-HB40. The three most similar poses of the molecules were aligned together and overlaid in MOE with their pharmacophore features visually scrutinised for commonalities that may be involved in binding. All three molecules had electron acceptor groups at their ends orientated toward the conserved region of the DNA binding domain and therefore chosen as the first pharmacophore feature. Next were two aromatic regions that correspond to possible pi-pi interactions in binding since N-HB40 and FA15 both have two aromatic regions before an acetamide group, although FA8 only has one. Since all three compounds had an acetamide group the final pharmacophore feature was an electron acceptor group in the region of this acetamide when the compounds were aligned. Compound FA8 and FA15 can be seen in **figure 3.15**. The Enamine library was scanned and filtered down to 91,000 compounds using the selected pharmacophore features shared between the 3 molecules. Conformers of the filtered compounds were generated and a second screen in ROCS and Eon scored by TanimotoCombo and ET Combo (combination of shape Tanimoto and electrostatic Tanimoto) reduced this to 500. Structure-based focus docking using the ChemPLP scoring function in GOLD<sup>[231]</sup> given its preferable enrichment score and AUC in the ROC curve analysis was then used on these molecules. All scores were converted to a Z score, used to rank the 500 hits, provided they held LogP and LogS values of <5 and >-5 respectively. In total, 59 compounds were ordered from this screening method.

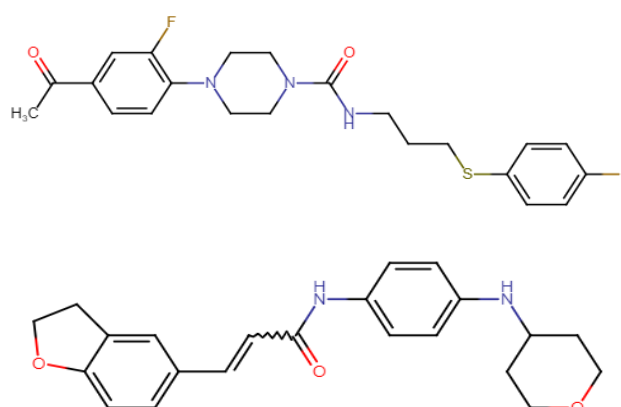


**Figure 3.15 2D chemical structures of FA8 and FA15:** 2D chemical structures of FA8 (*top*) and FA15 (*bottom*).

### 3.4 Discussion

The results discussed in this chapter were a positive start to the project despite challenges faced through lack of available structural data and low yielding purification. Compounds were selected and found to bind to ExsA with good affinity, with docking experiments supporting binding within the DNA binding domain as earlier experiments had concluded was the most appropriate region to focus on. Outlined in the relevant sections of this discussion were the plans or potential solutions for each of the techniques to carry the project forward should time or resources have permitted or during future work. Below addresses the individual assays and the conclusions drawn from them.

The aim in this chapter was to address the process and results of selecting compounds to be tested for inhibitory activity against ExsA. This was done by first defining which region of the protein to target before a variety of structure-based and ligand-based methods were employed to filter chemical libraries. ExsA appears to have at least two targetable sites, one in each of the CTD and NTD. Based upon this work and prior *in silico* and *in vitro* studies, this project focused on targeting the CTD, specifically the DNA binding domain.

The literature reports a surprisingly broad range of activity for N-HBs which made reporting results that suggested specific polar interactions within the binding site difficult to do with high levels of certainty, especially given the seemingly closed conformational pose of the ExsA MD model structures used in the early part of this project. To begin with the focus was to look for the most likely sight of interaction, not specific SAR interactions. As such, consistency was sought by using ExsA and relevant homologues to find results that would confer more probable chances of success. Although the structural information available around the NTD was unquestionably better for ExsA, having a known active ligand swayed the balance in favour of pursuing CTD targeting molecules after affirmation that the site was reliably predicted as a ligand pocket across the homologues and electrostatic mapping supported it as a site for polar interactions. The published literature also supported the hypothesis of binding by N-HBs here.

Given the relatively minimal structural data available on the target protein, attempts were made to crystallize ExsA, but to no avail. Purification of ExsA was a laborious and

difficult task, with low yields. Solving the crystal structure of ExsA would greatly improve ligand searches with homologues and short length MD models hardly optimal for an inherently flexible transcription factor. I was in the fortunate position to have access to the crystallization facilities at Cambridge University along with several members of the Welch lab (collaborator, Department of Biochemistry) with extensive crystallography expertise justifying a small venture of predicting stabilising mutations to ExsA for future efforts. Solving structures can take years and whilst having access to facilities it was not the primary objective of this project. Since the most likely chance of success was probably a co-crystallization effort with a tightly bound inhibitor crystallization efforts were chosen not to be continued until a suitable candidate for co-crystallization was found.

Fluorimetry binding experiments on compounds ordered using a ligand-based method of selection confirmed two molecules to bind in the low nanomolar range to ExsA. Using low concentrations of protein in the fluorimetry ensure saturation of binding sites however no data was perceivable on inhibition of activity nor of binding sites from this experiment. The choice to use binding data was an effort to increase the ligand-based information that could be fed into the compound search and a comparison of shared pharmacophore features was very useful in this case without known SAR information. Further analysis of the FA8 and FA15 activity is addressed in the next chapter although they are suspected to both have degraded rapidly after initial screening success was not repeatable.

Important for confirming the binding of the FA8 and FA15 molecules to ExsA was to verify that the purified protein was functional which was achieved by optimising an EMSA assay. Appropriate controls indicating binding of the protein to specific ExsA promoter sequences but not to random DNA promoter sequences showed the samples to be active. EMSA assays can have many pitfalls and are difficult to glean accurate quantitative data from however, they are an extremely robust measure of DNA binding by a target regulator<sup>[261]</sup>. The low throughput aspect of the assay meant it was not used as a preliminary screening tool to find molecules capable of preventing ExsA binding to DNA in this project, for the same reasons neither were the tryptophan fluorescence assays. The EMSA assay was planned to be used following the identification of hits by using dose response inhibition curves

# **Chapter 4**

## **Results & Discussion**

### **Compound Screening**

## 4.1 Initial compound screening

### 4.1.1 Background

Once all the compounds had been ordered an appropriately high throughput method of screening was needed that would indicate efficacy for both specific inhibition of ExsA and reduced virulence. Up-regulation of the T3SS can be induced *in vitro* by the chelation of extracellular  $\text{Ca}^{2+}$  ions with EGTA or by host cell contact. T3SS is particularly associated with acute infections and its increased expression has been linked with higher death rates in patients, especially in critical care units<sup>[52]</sup>. Biophysical screening methods were used in the initial selection of compounds (intrinsic fluorescence and spectrofluorimetric assays, section 3.3.5) however low yields of ExsA after purification and the timely expense of these methods was not optimal for screening a greater number of compounds. Two phenotypic screens were therefore optimised for this purpose that could identify both specific inhibition and virulence reduction. Of the 131 ordered compounds, 10 were not soluble in DMSO and so were excluded from investigation, leaving 121 compounds screened in total. Concentrations for screening were selected as 200 $\mu\text{M}$  and 50 $\mu\text{M}$  as they aligned to the higher end of concentrations used in similar drug discovery publications such as Zhao *et al.*, (2018). Since the number of tested compounds was very low in relative terms for drug discovery this increased the likelihood of identifying compound hits.

Overall, the experiments outlined in this chapter were designed to create a model framework for a selection process to determine which molecules to progress, using different criteria for each of the assays used. The criteria for each specific assay are outlined in the respective sections, but broadly the criteria fell into efficacy *in vitro*, specificity for T3SS, toxicity, growth, and efficacy *in vivo*. Ultimately, it was aimed for that experimental results were complementary to each other informing a decision of inclusion or exclusion.

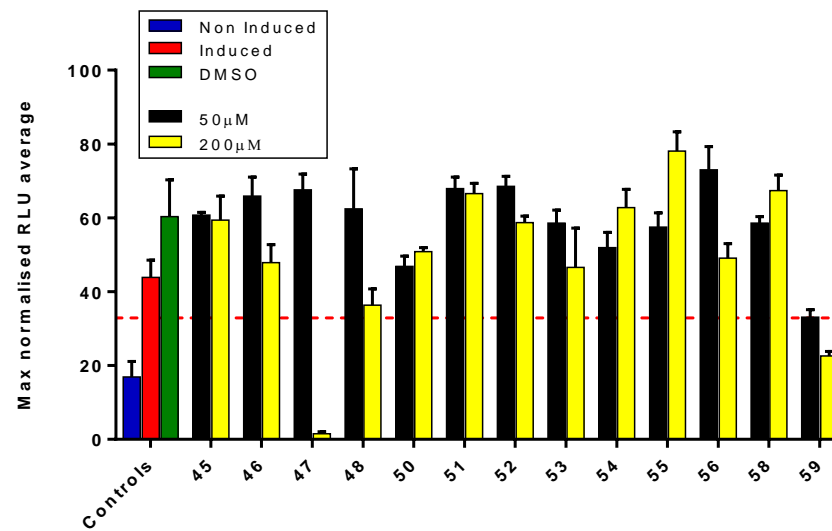
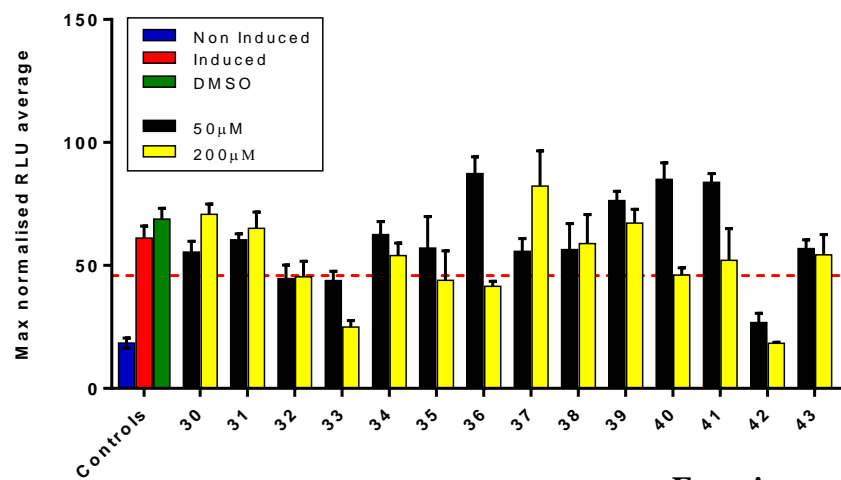
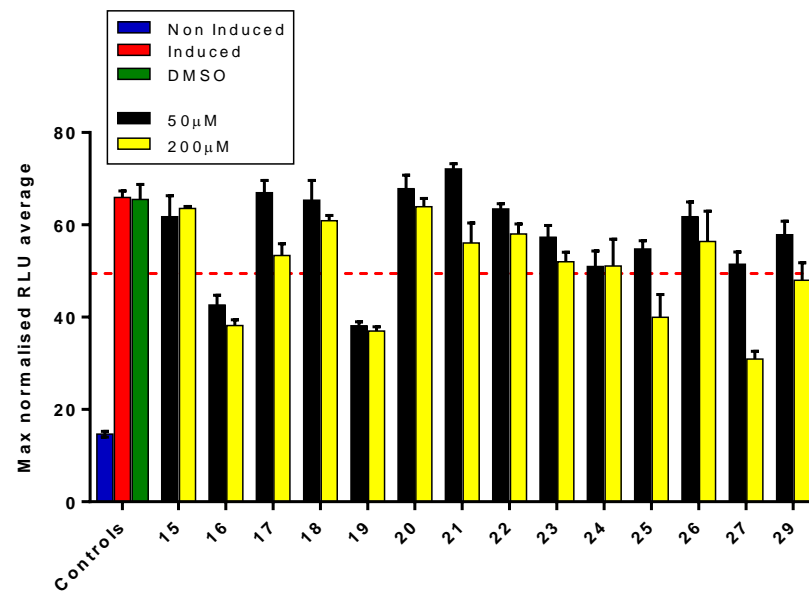
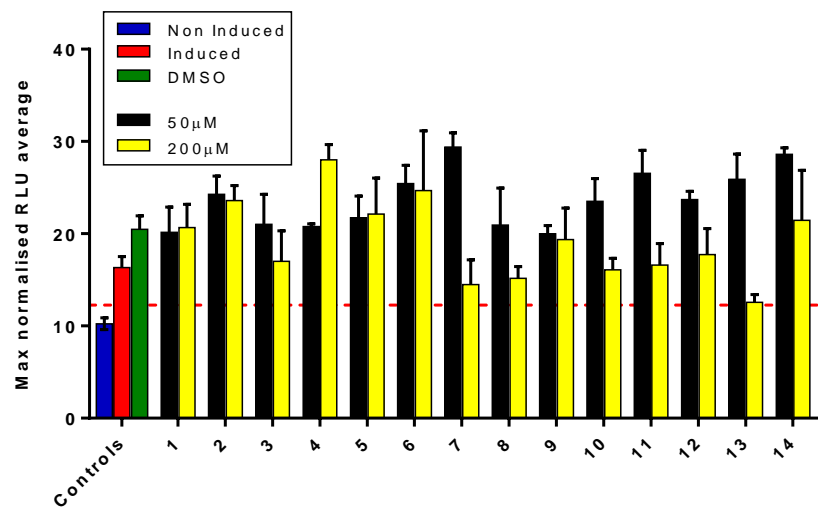
### 4.1.2 Luciferase reporter screen

The first assay chosen was a lux promoter reporter assay using a PA01 *PpcrV-lux* reporter strain (*see section 2.6.2*) previously generated by Dr. Stephen Dolan (Welch lab, Dept. of Biochemistry). PcrV makes up part of the translocation pore in the T3SS machinery and is transcribed by ExsA<sup>[100]</sup>. Induction with EGTA caused 2-4-fold increases in T3SS expression measured as an output of lux compared to non-induced controls. Decreases in the maximum

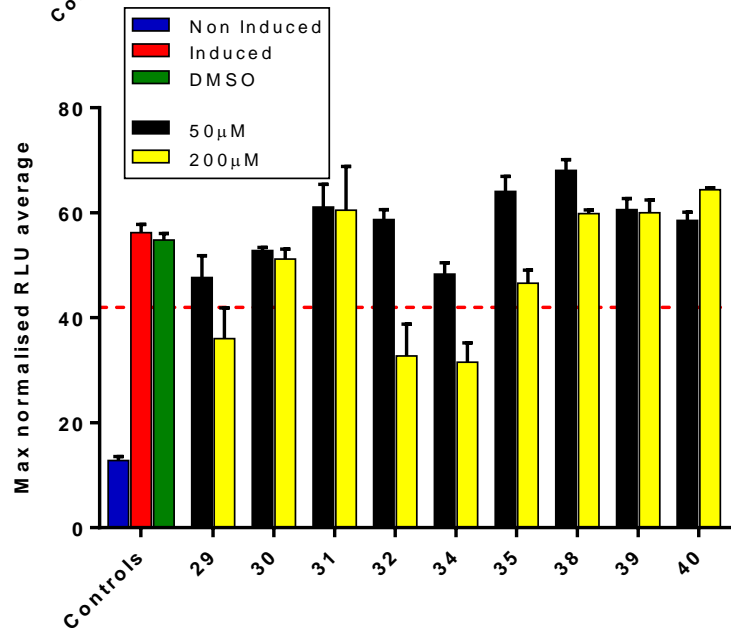
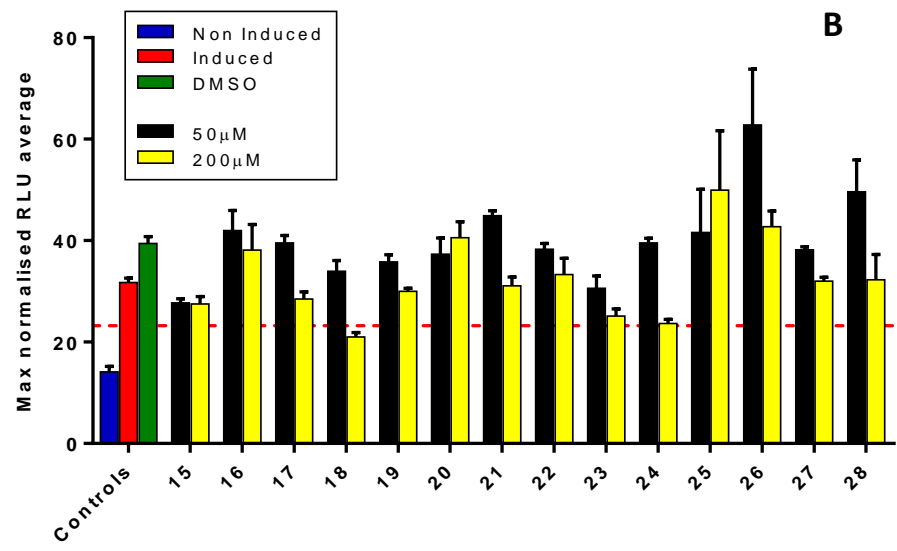
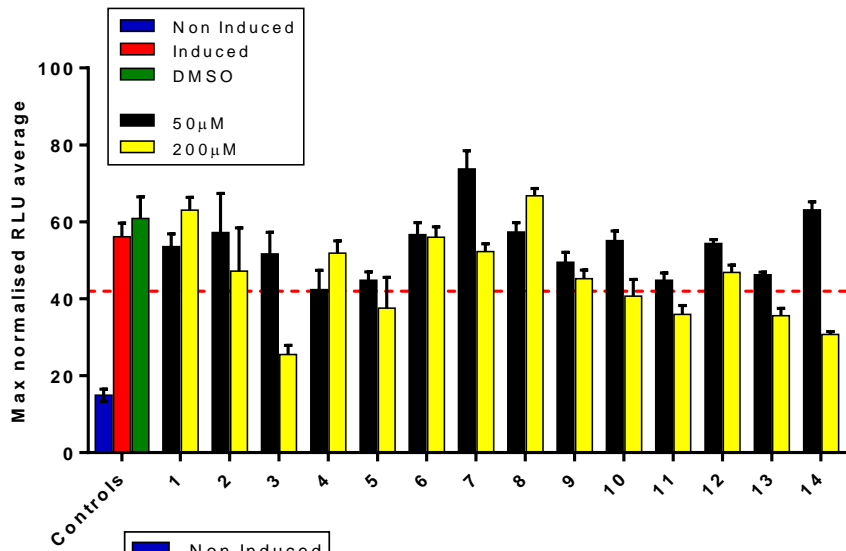
normalised lux signal caused by a compound could indicate ExsA inhibition resulting in a loss of transcriptional activity of the lux plasmid. Lux values were normalised against the OD<sub>600</sub> of each culture. Promoter assays are a commonly used technique to monitor transcriptional activity and a host of similar reporter systems have previously been used to study the T3SS, often utilising PcrV or ExoS as the focus genes<sup>[262–264]</sup>.

All compounds were tested at 200µM and 50µM and a reduction of 25% in the maximum normalised lux compared to an induced control was chosen as a threshold to warrant further investigation, provided a similar or greater reduction in virulence was seen in the second screening assay - an *in vitro* cell protection assay (CPA). **Figure 4.1** shows the maximum normalised lux signals for each of the compounds with their relevant controls.

**A**

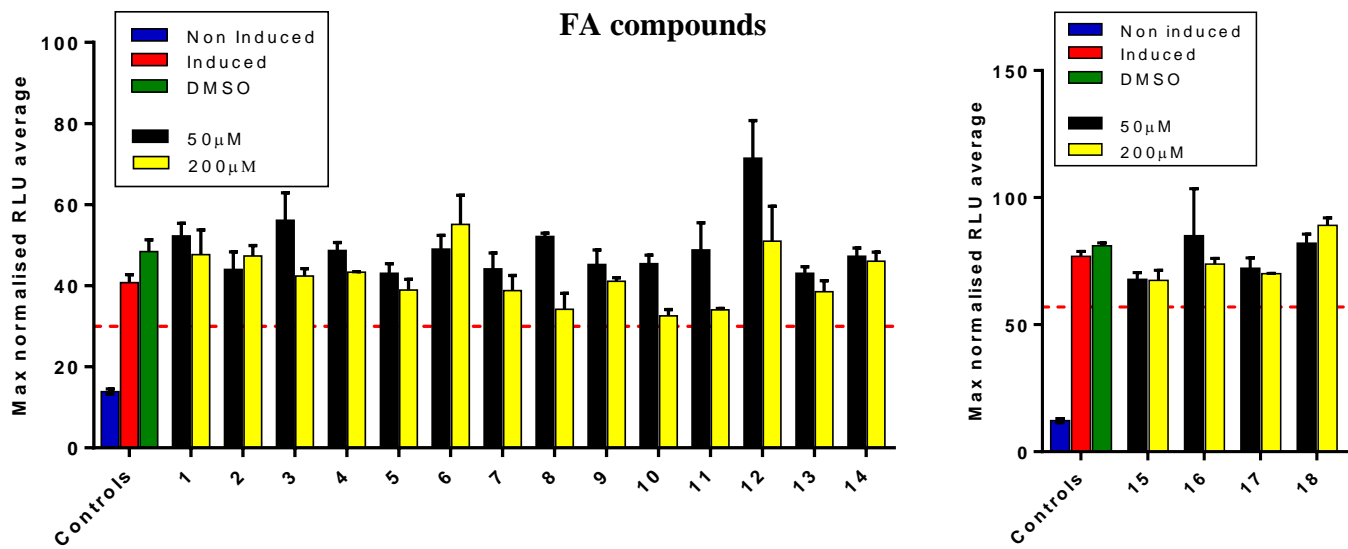


**Enamine compounds**

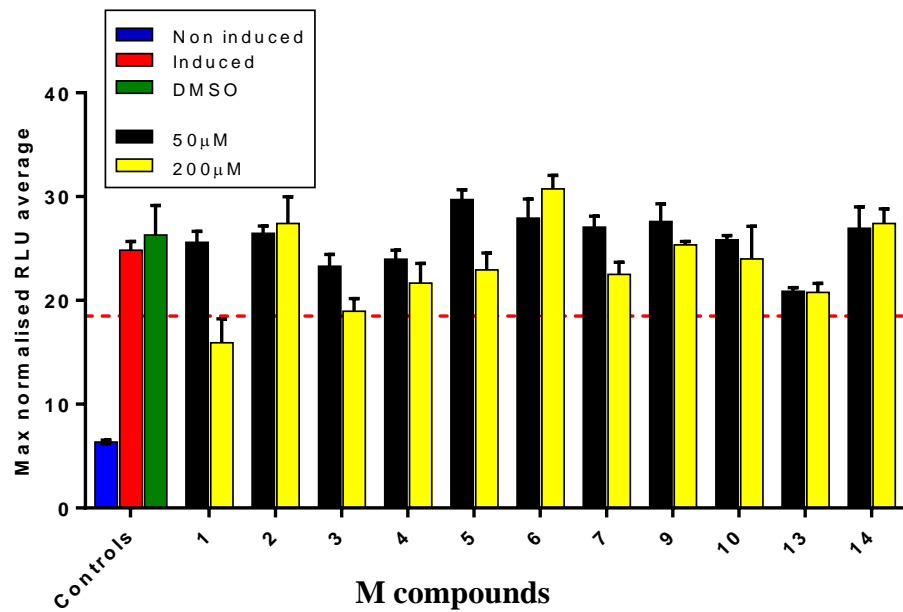


NCI compounds

C



D



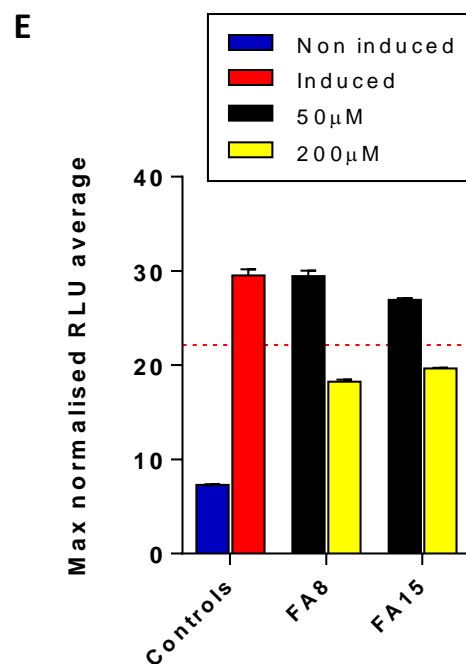


**Figure 4.1 Luciferase reporter assay screen:** Normalised PA01 *P<sub>prv</sub>-lux* reporter strain cultures were grown (AGSY media) with all of the purchased compounds at 200µM and 50µM (1% v/v both concentrations). EGTA (5mM) was used to induce T3SS expression in induced, DMSO (1% v/v) and compound treated samples. Non-induced sample media did not contain EGTA. Lux signals were normalised to growth by equation:  $\text{lux}/(\text{OD}_{600} \times 10^4)$ . Compounds that reduced normalised maximum signals by  $\geq 25\%$  (---) were taken forward for further investigation. Each bar represents mean  $\pm$ SEM (n=3). (A) Enamine compounds. (B) NCI compounds. (C) FA compounds. (D) Molport compounds. (E) FA8 and FA15 results tested earlier in the project than shown in C.

An interesting observation of the assay was that DMSO (1% v/v) slightly increased the lux signal in some cases. The average maximum normalised lux signal seen in non-induced controls was 32.5% of the induced controls when calculated from all the graphs shown above. **Table 4.1** highlights the compounds that produced a decrease in lux signals by 25% or more at each concentration tested, as well as the percentage signal compared to its induced control. Two compounds worth noting that are not in the table are FA8 and FA15 because they are speculated to have degraded. Early lux results for these compounds showed around a 50% reduction in lux signal, (shown in **figure 4.1**). In total 23 compounds breached the 25% threshold but only 5 of these were below this limit at 50µM as well as 200µM.

**Table 4.1 Luciferase reporter assay**

Compound	≥25% decrease		% vs induced control	
	200µM	50µM	200µM	50µM
E16	✓	✓	57.9	64.6
E19	✓	✓	56.1	57.8
E25	✓	✗	60.7	
E27	✓	✗	46.9	
E29	✓	✗	72.8	
E32	✓	✓	74.1	73.1
E33	✓	✓	40.9	71.8
E35	✓	✗	71.8	
E36	✓	✗	67.8	
E42	✓	✓	30.0	43.7
E47	✓	✗	3.5	
E59	✓	✗	51.5	
NCI3	✓	✗	45.4	
NCI5	✓	✗	66.9	
NCI10	✓	✗	72.5	

**Table 4.1 continued**

NCI11	✓	✗	64.0	
NCI13	✓	✗	63.4	
NCI14	✓	✗	54.8	
NCI18	✓	✗	66.3	
NCI29	✓	✗	64.1	
NCI32	✓	✗	58.2	
NCI34	✓	✗	56.1	
M1	✓	✗	64.0	

PA frustrates drug discovery with a strong propensity for developing antimicrobial resistance which in part can be attributed to overexpression of efflux pumps<sup>[66-69]</sup>. To identify compounds that may be active but cannot accumulate enough due to rapid extrusion by these efflux pumps a PA strain, YM64 which has deletions of the genes encoding these pumps, was transformed with the lux plasmid. Unfortunately, induction by EGTA caused an inversion of normalised lux signal, suggesting that the T3SS was inhibited under standard inducing conditions within this mutant.

There are several possible alternate reasons that could underlie these results aside from inhibiting ExsA function, which include toxicity to PA, post translational activity (i.e. interruption of luciferase enzyme activity), or effects on cellular ATP levels. Interestingly, some compounds increased the level of maximum normalised lux, but these were not investigated any further.

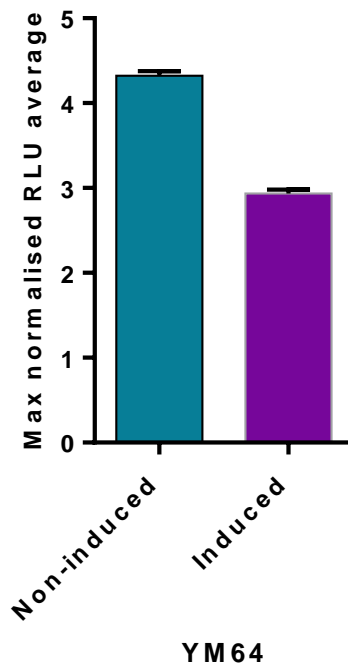


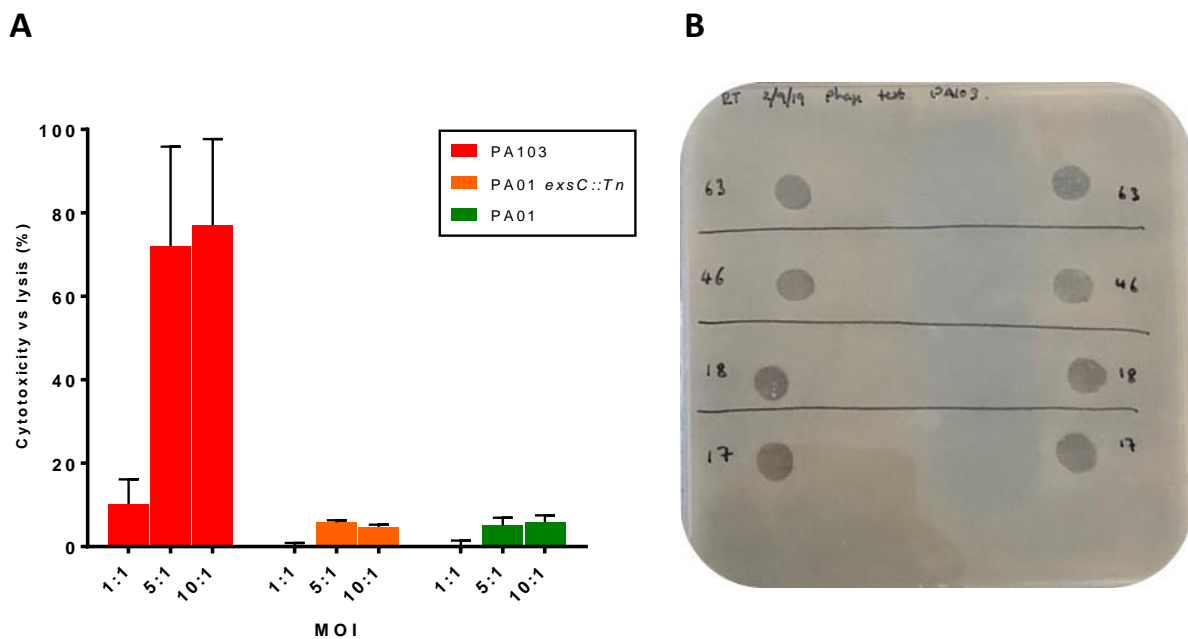
**Figure 4.2 YM64 luciferase transformant:** YM64, an efflux pump deficient strain of PA, was transformed with the *PpcrV-lux* plasmid and normalised lux signal output was measured under inducing and non-inducing conditions (5mM EGTA induction). Each bar represents the mean  $\pm$ SEM of 3 independent experiments.

#### 4.1.3 Protection against *P. aeruginosa* mediated cytotoxicity

The CPA used enzymatic LDH detection to measure virulence by cell damage when A549 lung epithelial cells were co-incubated with PA103. Compounds were tested at 50 $\mu$ M at a multiplicity of infection (MOI) of 5:1. A549 cells were chosen to represent an acute infection in the lungs. During optimisation of this assay PA01 failed to produce a threshold minimum of 40% LDH release compared to full lysis controls at appropriate MOIs. Therefore, PA103 was chosen for its greater T3SS expression and increased virulence, averaging 71.9% of full lysis at a 5:1 MOI.

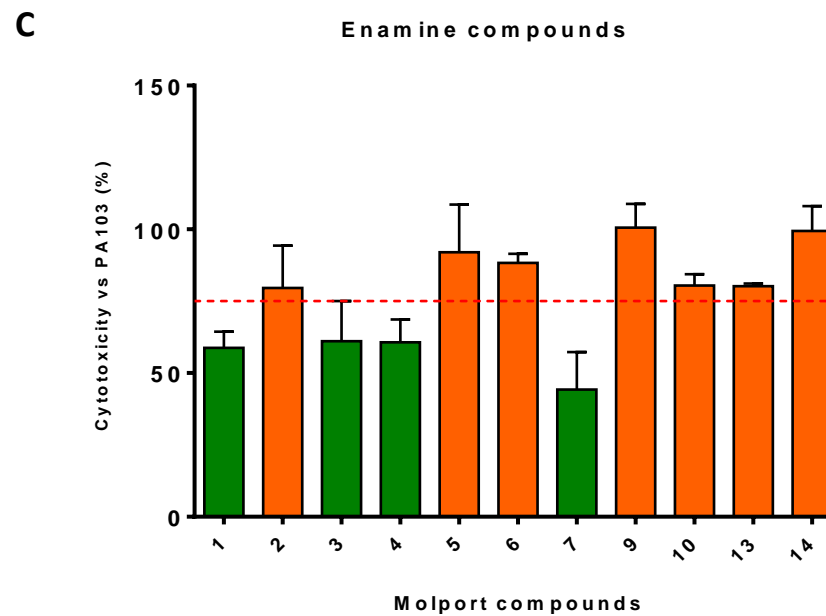
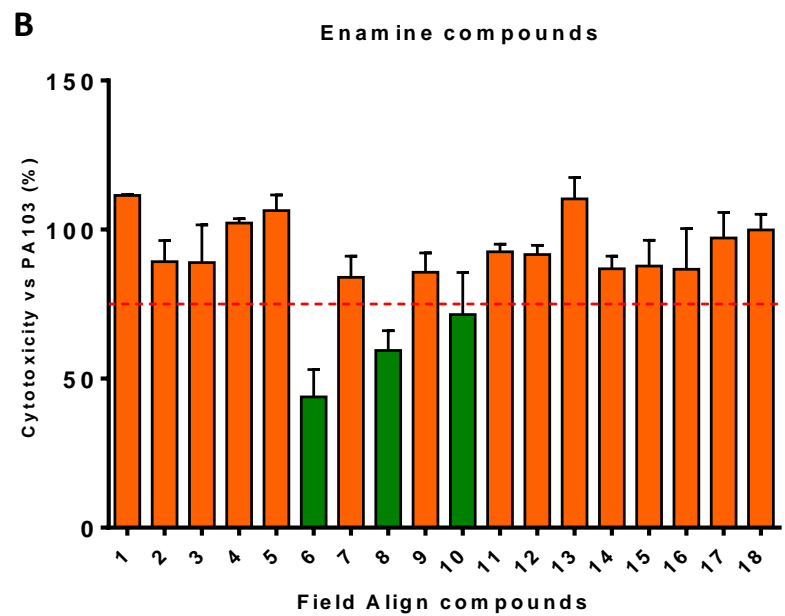
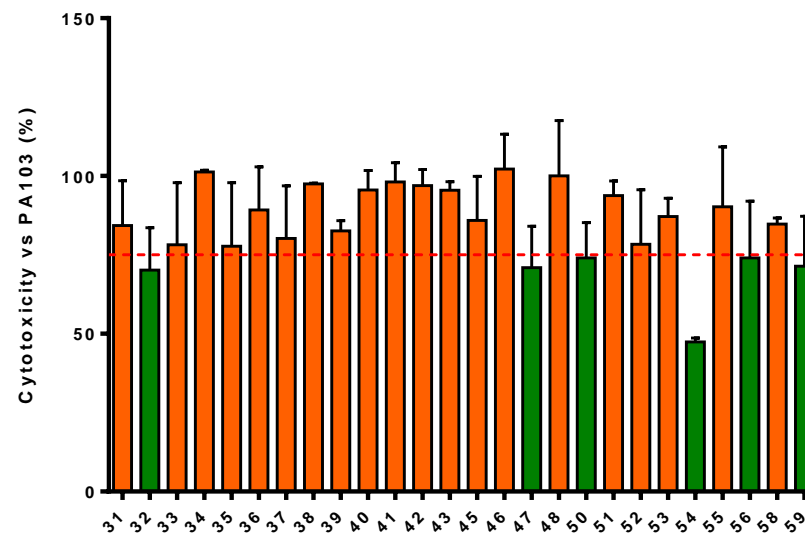
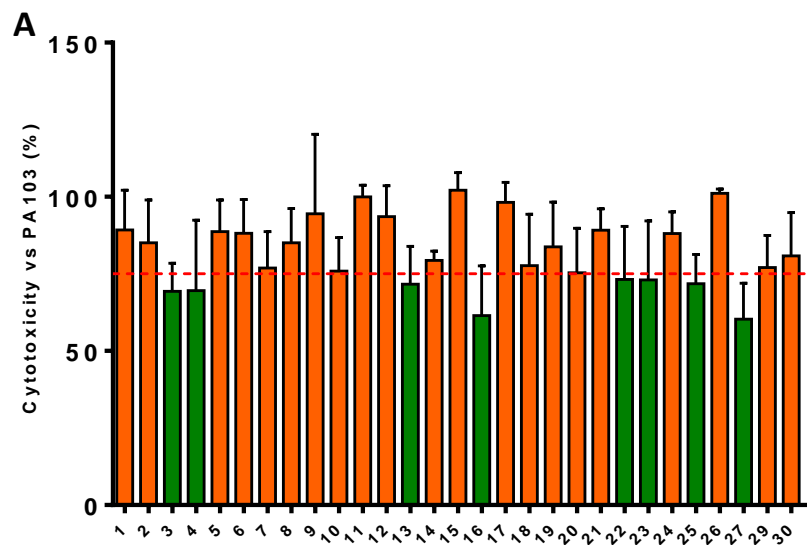
A PA01 *exsC::Tn* mutant deficient in T3SS expression was to be used as a negative control for this assay however, since the WT background was not virulent enough to be used a phage transduction technique to insert the transposon into the PA103 WT was attempted to be used as a negative control instead. Despite identifying four lytic phage no attempts were successful to transduce PA103 with the transposon insertion. **Figure 4.3** shows the lytic phage and optimisation efforts mentioned above.

DMSO controls (1% v/v) had no effect on LDH release relative to background levels from A549 cells and cytotoxicity was measured as a percentage of WT PA103. As for the lux assay a 25% reduction threshold was used for selection. In total, 32 compounds reduced PA103 induced cytotoxicity by more than 25% however, of these, only 10 met this cut off in the lux assay. These 10 compounds can be seen in **table 4.2** with their respective percentage compared to WT controls. The 25% reduction for lux was only required at 200 $\mu$ M, whereas 50 $\mu$ M was used for the CPA, meaning only two compounds, E16 and E32, had comparable reductions (<4% difference) across both assays at 50 $\mu$ M.



**Figure 4.3 Optimisation of cell protection assay:** (A) PA01, PA103 and *exsC::Tn* strains were incubated with A549 lung epithelial cells for 4hrs at increasing MOIs and cytotoxicity was measured by LDH detection in the media compared to full lysis controls (100%). Each bar represents the mean  $\pm$ SEM of 3 independent experiments. (B) 4 lytic phage ( $\phi$ MSPA63  $\phi$ MSPA46  $\phi$ MSPA17  $\phi$ MSPA18) were identified by spotting phage onto LBA plates covered with a PA103 lawn.

The assay was a robust test for the compounds ability to protect A549 cells from PA103 induced cytotoxicity, however, impacts on the bacterial growth, cytotoxicity of the compounds and the inhibiting or facilitating of the assays enzymatic reactions had to be considered before deducing a mechanism. It was impractical and financially prohibitive to test each of the compounds for their effect on the enzymatic reaction, but more experiments were utilised to investigate their mechanisms and provide supporting evidence that measured reductions in virulence were due to activity against PA and not the assay reaction. All the CPA results graphs can be seen in **figure 4.4**.



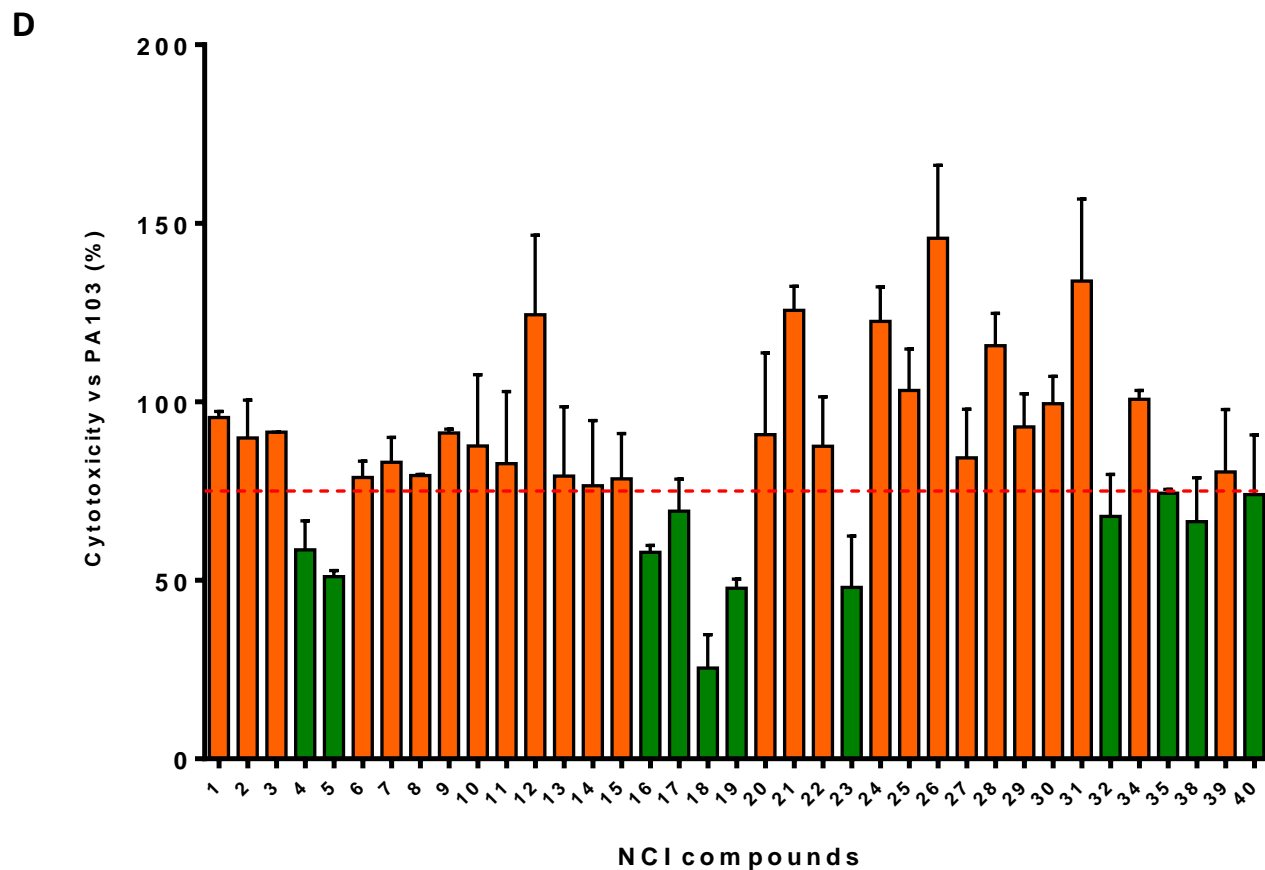


**Figure 4.4 Cell protection assay compound screen:** All ordered compounds were screened at 50 $\mu$ M for an ability to protect A549 lung epithelial cells from PA103 mediated cytotoxicity, measured by detection of LDH in the media after 4hrs of incubation. Results were normalised relative to WT PA103 infection (100%). Each bar represents the mean  $\pm$ SEM of 3 independent experiments. Only molecules that reduced cytotoxicity by  $\geq$ 25% (---) were investigated further. Compounds that passed this threshold are indicated by green bars. (A) Enamine compounds (B) FA compounds. (C) M compounds. FA8 and FA15 were not screened prior to assumed degradation. (D) NCI compounds.

**Table 4.2 Luciferase and cell protection assay comparison**

Compound	Lux % vs induced control (200µM)	LDH % vs PA103 control (50µM)
E16	57.9	61.5
E25	60.7	71.8
E27	46.9	60.3
E32	74.1	70.2
E47	3.5	71
E59	51.5	71.4
NCI5	66.9	51
NCI18	66.3	25.5
NCI32	58.2	67.9
M1	64	58.8

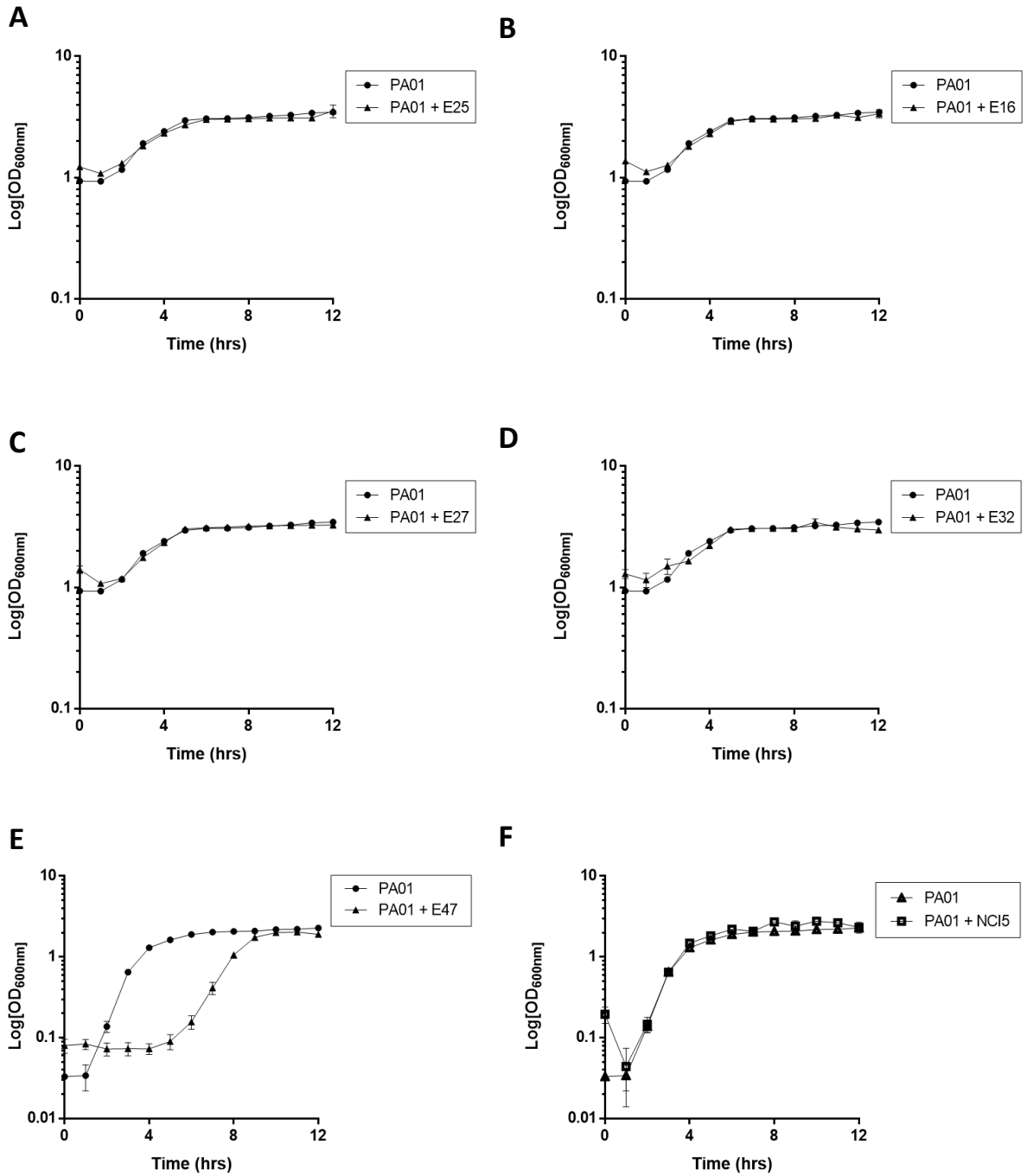
## 4.2 Further investigation of selected hits

### 4.2.1 Growth curves

Inhibiting ExsA, or other virulence determinants, should not influence the growth of PA and so simple growth curves in LB were used to further study the hit compounds. DMSO controls had no impact on growth at 1% v/v. Of the 10 hit compounds 7 had no effect on the growth of PA at 200µM. Compound E59 precipitated in LB and could not be resolubilised by warming and shaking during the assay and so was excluded from further investigation. The remaining two compounds that did have effects on PA growth were, E47 and M1.

Compound E47 caused a significant delay in growth at 200µM (**figure 4.5**), which likely accounts for the dramatic reduction in lux seen in **figure 4.1** to 3.5% of the induced control, and the reduced acute cytotoxicity in the CPA. M1 inhibited the total biomass of PA01

at 200 $\mu$ M without affecting early growth rate. Both compounds were excluded from further investigation because of the alterations caused to growth.



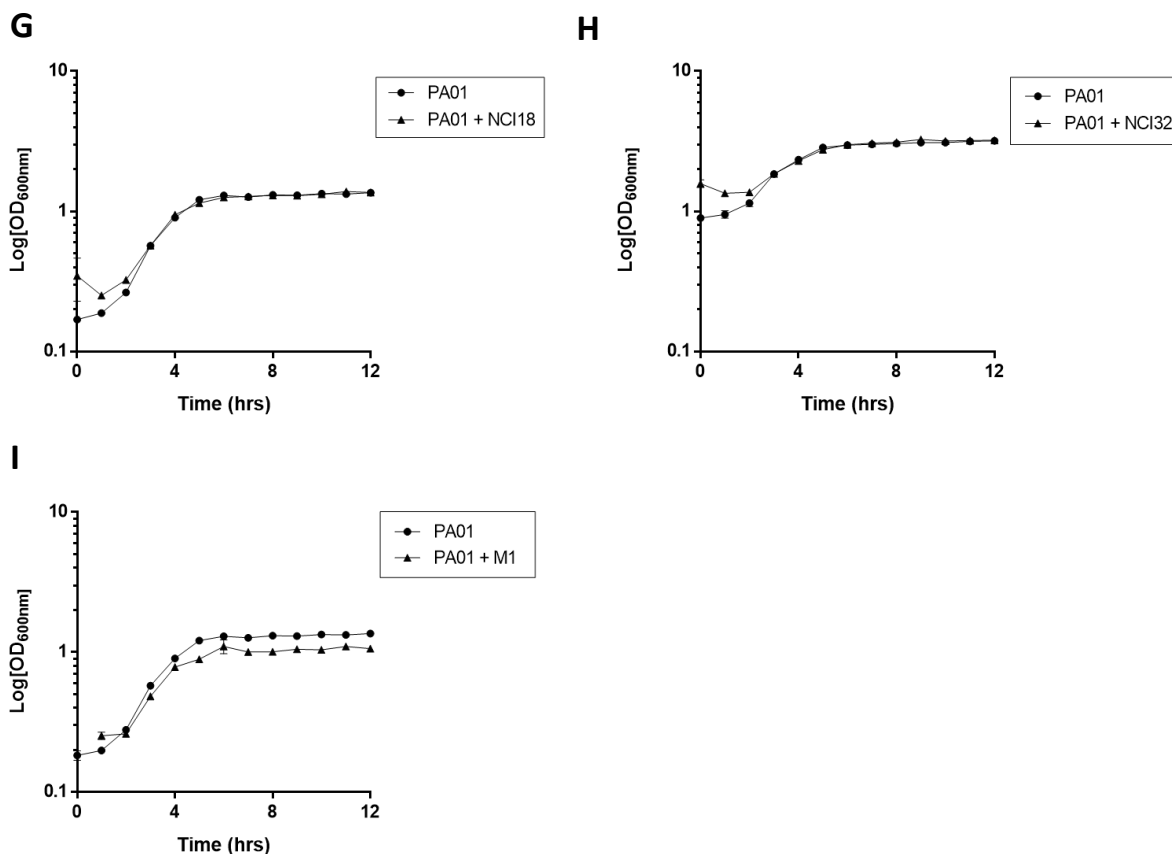


**Figure 4.5 PA01 compound affected growth curves:** Normalised PA01 cultures were grown in LB with compounds (200 $\mu$ M, 1% v/v) until stationary phase. Data points represent mean  $\pm$ SEM of 3 independent experiments. (A) Compound E16. (B) Compound E25. (C) Compound E27. (D) Compound E32. (E) Compound E47. (F) Compound NCI5. (G) Compound NCI18. (H) Compound NCI32. (I) Compound M1.

#### 4.2.2 Evaluation of dose response and toxicity of selected compounds

To establish a basic toxicity profile for the hit compounds and to determine EC<sub>50</sub> values the CPA was repeated in a dose-dependent manner. Compounds were added at 1% v/v in a 2-fold dilution series dose range of 200 $\mu$ M down to 750nM. Toxicity was measured against a full lysis control and cytotoxicity as in the initial 50 $\mu$ M screen vs a PA103 control. A rough guide for acceptable toxicity levels at this stage was set at 25% relative to a lysis control.

The assay was performed on some compounds that were active in the initial CPA screen despite not being active in the lux or had been ruled out because of effects on growth. At this stage I was still only looking for compound scaffolds for first generation compounds and so any that were active below 200 $\mu$ M where potential “side effects”, such as being deleterious to growth, may not be seen and could still be of interest. 4 compounds were found to behave in a

dose-dependent manner with acceptable toxicity profiles, however only 2 of these had EC<sub>50</sub> values worth pursuing. The EC<sub>50</sub> values are seen in **table 4.3** and their toxicity profiles in **figure 4.6**.

Compounds E16, E25, E27 and E32 did not act in a dose-dependent manner and were not sufficiently protective of PA103 mediated cytotoxicity to confidently establish an EC<sub>50</sub> value across the dose range and so were removed from the hit compound list as compounds not effective at concentrations below 200μM were deemed not worthy of further pursuit.

**Table 4.3 EC<sub>50</sub> values for prevention of *P. aeruginosa* mediated cytotoxicity**

<b>Compound</b>	<b>EC<sub>50</sub> (μM)</b>
NCI18	50
NCI19	670
NCI23	564
M1	10

Being extremely toxic at higher concentrations, NCI5 was also removed from the list of hit compounds. The toxicity profile of NCI5 can be seen in **figure 4.6**. Promising results came from NCI18, showing low toxicity even at high concentrations and a maximal reduction in the PA103 induced toxicity of 66%. An EC<sub>50</sub> of 50μM was established. NCI19 and NCI23 also displayed good toxicity profiles although their EC<sub>50</sub> values were far too high to be considered good candidates for continuation. NCI32 was not tested only because it became unfortunately impossible to obtain additional amounts of the compound since no vendor was able to provide it. M1 was the most effective compound giving an EC<sub>50</sub> value of 10μM. None of the compounds seen in **table 4.3** caused any serious toxicity to A549 cells.

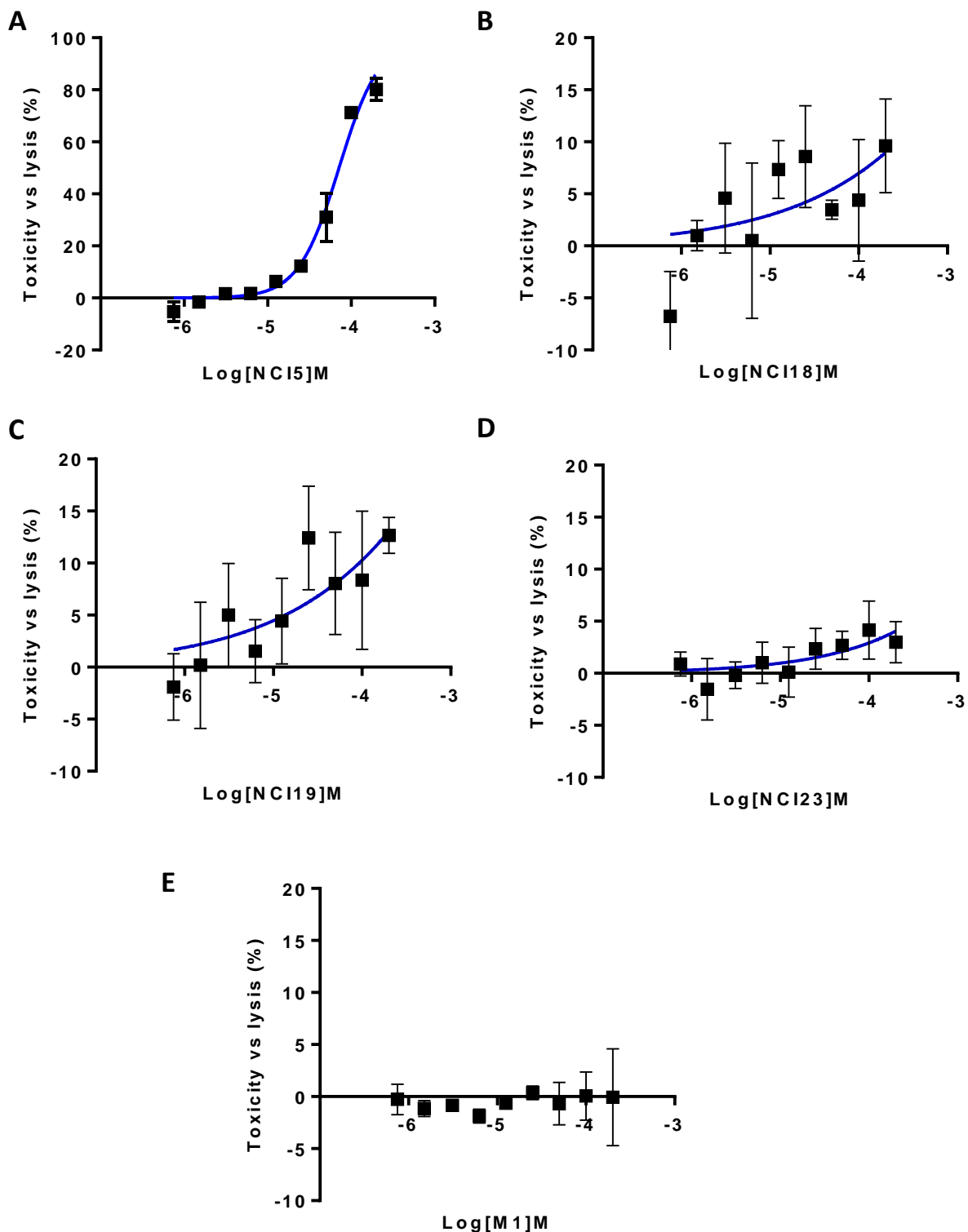


**Figure 4.6 Toxicity profiles of compounds against A549 lung epithelial cells:** Basic toxicity profiles were measured by detection of LDH released from A549 cells into the media compared to full lysis controls (100%). Compounds were added at 1% v/v (all concentrations) in 2-fold increases in concentration (750nM - 200 $\mu$ M). Graph curves were fitted using GraphPad Prism 6.0 log(agonist) vs normalised response – variable slope. Data points represent the mean  $\pm$ SEM of 3 independent experiments. (A) Compound NCI5 (B) Compound NCI18. (C) Compound NCI19. (D) Compound NCI23. (E) Compound M1.

### 4.2.3 Effect of compounds on T3SS expression

Having rapidly narrowed the search down to 1 compound fitting all criteria after the follow up assessments, it was necessary to determine whether NCI18 was protecting A549 cells by inhibiting expression of the T3SS. ExsA is the master transcriptional regulator of the T3SS<sup>[265]</sup> and its inhibition would result in a down regulation of PcrV expression<sup>[43, 117, 265]</sup> that can be observed by a western blot under inducing conditions. As before some additional compounds were also tested to ensure that no potential inhibitors were missed. PcrV was used as the marker for ExsA activity and subsequently T3SS expression with isocitrate dehydrogenase (ICD) loading controls. Since PcrV is part of the translocation pore of the T3SS machinery it is an extracellular protein which meant secretome, intracellular and total protein levels could be tested by western blot. Since it was difficult to use a reliable loading control for the secretome samples, all intracellular and secretome blots are taken from the same sample, therefore ensuring normalisation of the secretome by the ICD loading control in the paired intracellular sample. Taken together the blots are a representation of total protein. Induction by EGTA showed an upregulation of T3SS expression with no detectable levels in the secretome of non-induced samples. PA103 strain was chosen over PA01 because of its greater expression level of the T3SS and stronger signal in the assay.

NCI18 was tested in a concentration-response study but the compound was found not to cause any reduction in the expression of the T3SS. **Figure 4.7** shows the intracellular and secretome samples of NCI18 and the additional compounds tested which also showed no inhibition of T3SS expression except for M1 (**figure 4.8**), reducing T3SS expression at 200 $\mu$ M but not 50 $\mu$ M. Given no effect on growth is seen by M1 at 50 $\mu$ M (see **figure 4.8**) and having a calculated EC<sub>50</sub> of 10 $\mu$ M, if a reduction of T3SS had been seen at this lower concentration it might have suggested activity against ExsA. However, a decrease was only seen at 200 $\mu$ M meaning this result was most likely due to the inhibitory action of growth over any specific interactions with ExsA.

At this stage in the project no compounds were deemed active in inhibiting ExsA despite some promising results from early binding and *in vitro* assays. Given the encouraging results of the NCI18 compound, it was subjected to further *in vivo* investigation discussed in the next section. Revisiting the *in silico* work was also an option with a priority placed on addressing the structural issues facing ExsA docking. I was in fact awarded an HPC-Europa3

grant to visit Professor Antti Poso in Kuopio, Finland to generate long MD simulation models of ExsA that would tackle this exact issue, although this visit would subsequently be impossible due to travel restrictions introduced during the coronavirus global pandemic.

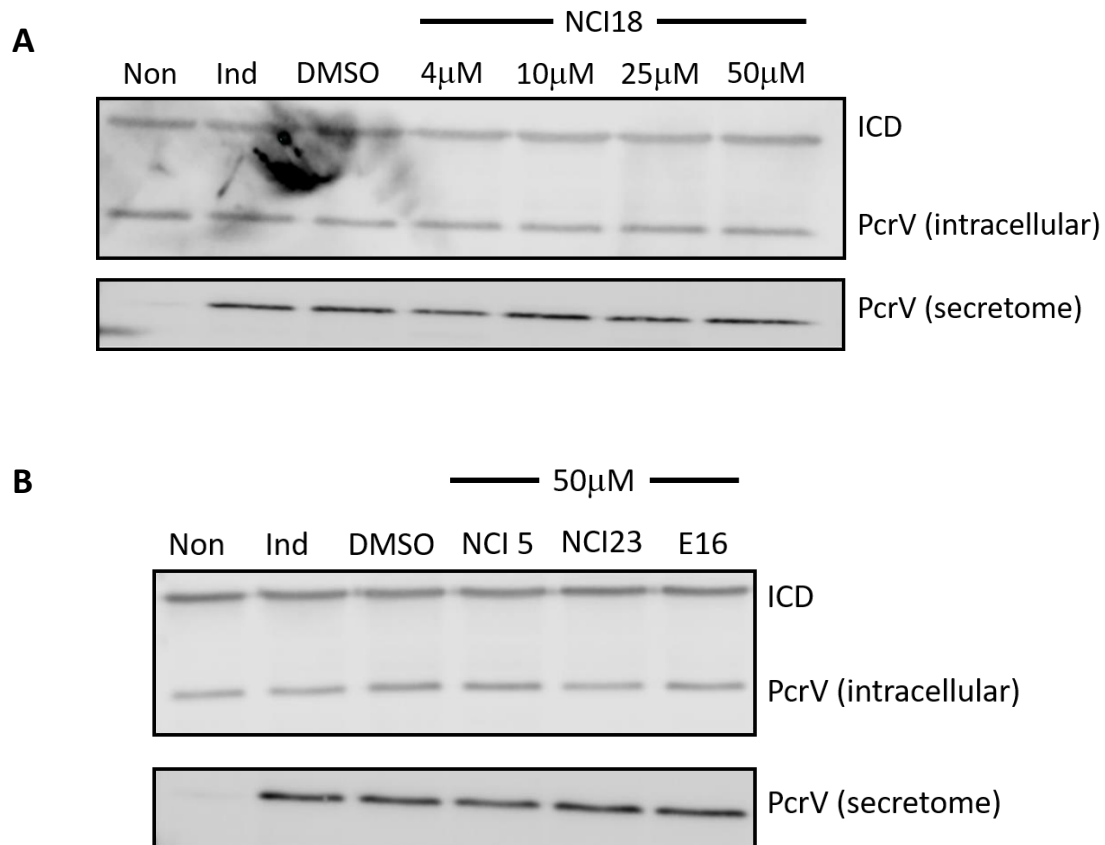


**Figure 4.7 Compound effects on type III secretion system expression:** Normalised PA103 cultures were grown (AGSY) until reaching stationary phase (~7hrs) and were normalised before western blotting. Isocitrate dehydrogenase (ICD) was used as a loading control. Secretome and intracellular fractions were taken from the same samples to ensure normalisation of secretome samples. Compounds and DMSO were added at 1% v/v (all concentrations). T3SS was induced (Ind) by 5mM EGTA in all conditions except in non-induced control lanes (Non). Images are representative of 3 independent experiments. **(A)** NCI18 dose dependent effect on PcrV expression. **(B)** Effect of NCI5, NCI23, and E16 (50 $\mu$ M) on PcrV expression.

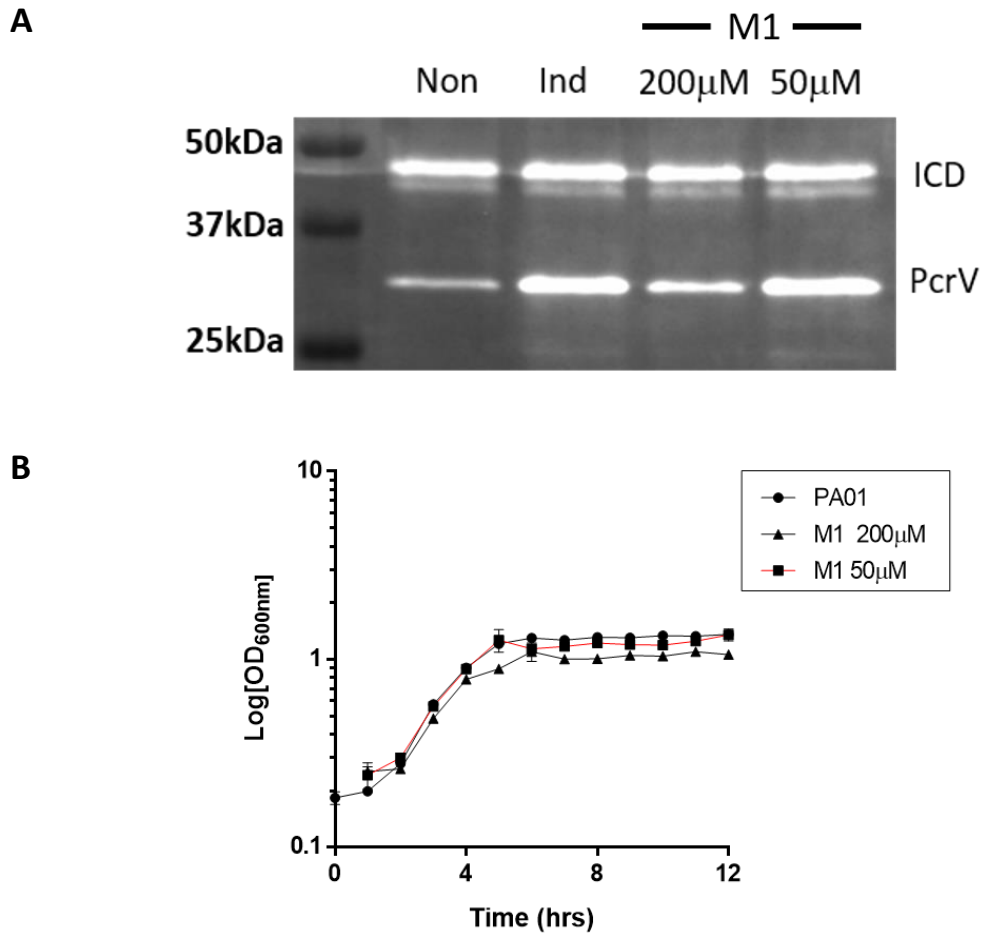


**Figure 4.8 M1 effect on type III secretion system expression:** (A) Normalised PA103 cultures were grown (AGSY) until reaching stationary phase (~7hrs) and were normalised before western blotting. Isocitrate dehydrogenase (ICD) was used as a loading control. M1 was added at 1% v/v (both concentrations). T3SS was induced (Ind) with 5mM EGTA in all conditions except non-induced control lane (Non). Image is representative of 3 independent experiments. (B) Normalised PA01 grown in LB with M1 (1% v/v, both concentrations) until stationary phase. Result is the mean  $\pm$ SEM of 3 independent experiments.

## 4.3 *Galleria mellonella* acute PA01 infection models

### 4.3.1 Animal models used in drug discovery against *P. aeruginosa*

The T3SS is an attractive virulence target since it has been shown across a wide number of bacterial species that express it, including PA, that when knocked out virulence is attenuated in a wide number of animal species<sup>[266]</sup>. This evidence is coupled against greater morbidity when expressed at higher levels, as mentioned previously.

Mice are the most commonly studied rodent for T3SS infection models for understandable reasons: they are relatively inexpensive compared to other animals, there are less stringent ethical ramifications around their use, they are well described in comparison to other models, and the ease of genetic manipulation<sup>[23]</sup>. However, cystic fibrosis transmembrane conductance regulator (CFTR) knockout mice do not present with an accurate representation of human CF lung disease, despite the appearance of severe intestinal disease<sup>[77]</sup>. Porcine models for CF research were first reported in 2008 and have proven immensely useful for comparing against rodent models and human clinical trials. CF pigs exhibit classical features of human CF lung disease suffering airway inflammation, remodelling, mucus accumulation, and infection<sup>[78]</sup>. Pigs were originally chosen for their similarity in respiratory anatomy to humans, as well as their closeness in physiology and size for translational imaging.

*Galleria mellonella* (greater wax moth) is an alternative *in vivo* infection model to rodents, pigs or other vertebrates. They are inexpensive, easy to obtain in large numbers, can survive at 37°C and do not require specialist lab equipment, nor ethical approval for use. Their life cycle is short and despite lacking an adaptive immune response, their innate response is remarkably similar to that of vertebrates<sup>[52]</sup>. Altogether, *G. mellonella* represents a valuable tool for studying infection models and have the potential to dramatically reduce the numbers of vertebrate animals used in early stage testing<sup>[267, 268]</sup>.

The innate immune response of insects is made up of a cellular and a humoral response<sup>[267]</sup>. The cellular response is mediated by phagocytic cells called haemocytes, which are found in the haemolymph – a liquid analogous to blood in insects. The humoral response refers to soluble effector molecules that immobilise or kill pathogens. Melanin, antimicrobial peptides and complement-like proteins are all examples of humoral response. Six haemocytes have been

identified in *G. mellonella*, but it is plasmatocytes and granular cells that play the predominant role in phagocytic cellular defence. Phagocytosis in insects and mammals is very similar and both involve these two cell types. A homologue of the human calreticulin protein found in neutrophils is expressed in *G. mellonella* haemocytes. Once phagocytosed, the internal killing mechanisms employable are varied but include reactive oxygen species generated by the NADPH oxidase complex. In neutrophils this complex involves proteins p47<sup>phox</sup> and p67<sup>phox</sup>, homologues of which exist in *G. mellonella*<sup>[269]</sup>. A demonstration of this similarity is that production of superoxide can be initiated and inhibited by 12-myristate 13 acetate and diphenyleneiodonium chloride respectively, in both neutrophils and *G. mellonella* haemocytes<sup>[270]</sup>.

The selection of species used in an infection model is critical to the translational relevance of the results. For instance, *G. mellonella* are subject to T3SS dependent killing, however, the invertebrate nematode *Caenorhabditis elegans*, which offers many of the same advantages listed above, is not<sup>[171]</sup>. For *G. mellonella* it was found that of the four T3SS effectors only ExoT and ExoU played a significant part in killing, with only one being needed to observe killing at WT levels.

Survival assays, usually referred to in insects as killing assays, are commonly used to measure the virulence of different strains or species, or the effectiveness of a treatment<sup>[265]</sup>. Small molecules can be injected into the larvae prior to, at the same time as, or after bacterial inoculation and the average survival time for each condition can be compared and analysed. Killing assays can be split into fast and slow killing, determined by the length of time for death to occur – hours vs days. This is especially easy in *G. mellonella* because the larvae dramatically melanise, and death is determined simply by a lack of movement in response to touch. In these assays either the bacterial load or the dose of the agent can be changed in the model with results presented as an LD<sub>50</sub> or survival time.

The pathway in which antimicrobial drugs are developed has been almost unchanged for decades however, the poor transition rate of moving from clinical trials to approval shows that the overall process is far from efficient. There is a significant chasm between expectant *in vitro* results and mammalian infection models. *G. mellonella* infection models may be able to bridge this gap somewhat. Basic pharmacodynamic and pharmacokinetic data such as half-life, bioavailability and protein binding from compounds can be gathered due to the size of the

larvae, since sufficient haemolymph can be extracted for this use. The stability in the larvae can be extrapolated to support *ex vivo* studies in mammalian serum as well. This data and more, determined in the model, can inform mammalian experimentation later with respect to therapeutic index, dosage and regimen<sup>[267]</sup>. Candidate therapies that are toxic or ineffective in *G. mellonella* are likely toxic or ineffective in mammalian models or humans. On this assumption, a decrease in the number of mammalian animals with greater ethical considerations could be seen, or conversely, provide a greater justification for the pursuit of a compound. Mammalian models will always be required as an interim step to humans, but as more research on *G. mellonella* is done and greater scrutiny placed on the translation and robustness of the model in comparison to human trials, there could be a positive outlook for the drug development pipeline.

Less commonly discussed than *in vitro* and *in vivo* models are *ex vivo* studies. By experimenting on tissues, the complex anatomical, 3D spatial structure of organs is maintained which cannot be replicated *in vitro*. Whilst *in vivo* models obviously represent the most accurate picture of a disease, the models are often limited by expense, ethical considerations, sample size, specialised facilities and the requirement for animal handling expertise. This section discusses the merits of invertebrate *in vivo* models bridging a gap in the drug development pathway, but *ex vivo* is a complimentary or alternative method to bridge this gap as well<sup>[245, 271]</sup>.

Pigs are almost certainly a more appropriate model for studying human lung disease than rodents<sup>[266]</sup>, and since lungs are a waste product in the food industry, they circumvent ethical problems encountered with *in vivo* models. In addition, they are very cheap, available at local butcher shops and can be studied in labs using basic to moderate laboratory techniques that do not require specialist training. Finally, the sections of tissue can be kept in culture for several weeks, microbes within the tissue can be analysed using conventional or confocal microscopy, histopathological changes can be monitored, and the 3D spatial structure of the tissue is maintained<sup>[243]</sup>. *Ex vivo* experiments are discussed in this project later in section 5.1.2.

#### **4.3.2 *Galleria mellonella* killing assays**

The killing assay was adapted from the previously described protocol in Cools *et al.*, (2019) with larvae supplied by BioSystems TruLarv. Since the larvae could only be injected once due to their size and because inhibition of virulence factors should not kill the bacteria

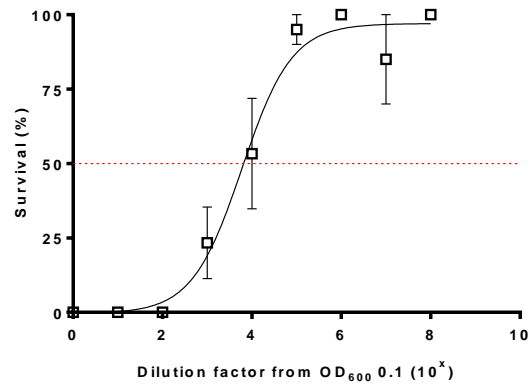
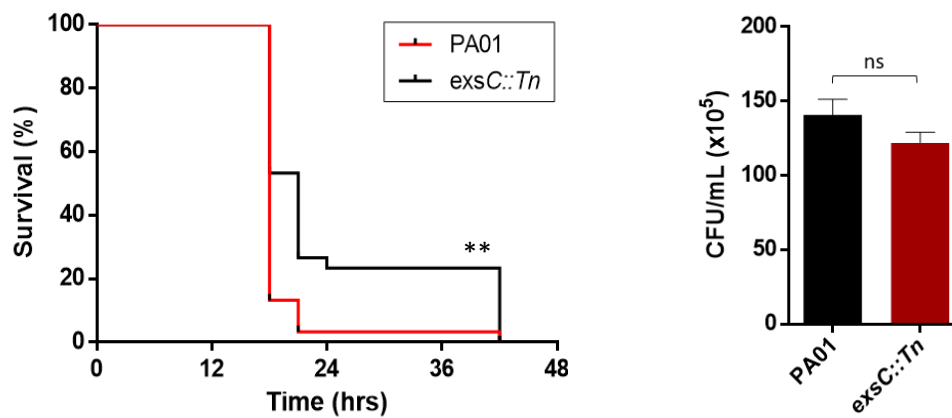
but is expected to reduce the virulence and assist the host's immune clearance, the assays were monitored over 48hrs. Therefore, an LD<sub>50</sub> was established to gauge a dose regimen for experiments where more than 75% of larvae died within 24hrs. A dilution of 10<sup>3</sup> from OD<sub>600</sub> 0.1 was chosen seen in **figure 4.9** after an LD<sub>50</sub> was calculated as 10<sup>4</sup> dilution. Larvae were kept at 15°C until used and were incubated at 37°C for the 48hr duration of the assay. Larvae were injected in the left hindmost proleg with 10µL of bacterial culture suspended in PBS or given a PBS only control injection. They were also injected with 5µL of either PBS or compound dissolved in PBS in the right front proleg immediately following infection. No trauma control groups were also used in each experiment and compound only controls. All 10µL injections contained rifampicin at 0.5mg/mL to ensure deaths were not by alternate infection. CFU counts were made of bacterial cultures determining an equal bacterial load between overnight cultures. All larvae supplied ranged between 0.18-0.35g therefore all mg/kg doses reported in this project were calculated assuming an average 265mg mass. Death of a larvae was determined by absence of movement when prodded. During the experiments no PBS nor any no trauma control larvae died at any timepoint and so are not shown in the graph data. Survival curves were analysed in GraphPad Prism 6.0 using Log-rank (Mantel Cox) test to determine significantly increased survival at  $p \leq 0.05$  certainty.

A PA01 *exsC::Tn* strain had significantly increased survival time ( $p = 0.0013$ ) compared to WT infections models and CFU/mL confirmed no difference in bacterial load between the strains for each larvae confirming that T3SS is required for full virulence in *G. mellonella* killing by PA. 30 larvae from 3 overnight single colonies cultures were used in each condition (10 larvae per culture) and survival curves are the combination of these results.

Two high doses of NCI18 were initially tested for an ability to improve survival time in acute PA infection models (**figure 4.10**) using 5µL injections of 50µM and 100µM based on EC<sub>50</sub> from **table 4.3**. Assuming an average mass of 265mg per larvae this is an equivalent dose of 950mg/kg and 1900mg/kg. At both doses NCI18 significantly increased survival time of *Galleria* ( $p < 0.0001$ ) with 1 larvae dying in each of the compound only control groups. 20 larvae were used in each group (injected from 2 single colony overnights). An additional two groups were injected with 200µM and 400µM of NCI18 in compound only control groups to assess toxicity with neither group seeing a single larvae death.

Given the extended survival of larvae at these higher doses a low dose experiment was done with 10 larvae per group. 3 additional doses of 1µM, 5µM and 10µM were given (19mg/kg, 95mg/kg and 190mg/kg). All significantly increased survival compared to acute WT infections ( $p < 0.0001$ ).

These results indicated that NCI18 was capable of increasing survival time of *G. mellonella* in acute PA infections. An additional assessment that was not monitored was bacterial load recoverable from the haemolymph of each larvae that would have shown whether treatment with NCI18 decreased colonisation by PA. Some of the PA virulence mechanisms that have been shown to be required for full virulence in *G. mellonella* include QS, T3SS and motility<sup>[268, 273, 274]</sup>.

**A****B**

**Figure 4.9 *G. mellonella* LD<sub>50</sub> and acute infection model:** Larvae were injected with 10 $\mu$ L of bacterial culture (PBS suspension, rifampicin 0.5mg/mL) and death was determined by no movement in response to touch. Bacterial loads were quantified between strains and single colony overnights by CFU/mL. **(A)** A 24hr LD<sub>50</sub> was established by injecting 10-fold serial dilutions of PA01 cultures normalised to OD<sub>600</sub> 0.1. 30 larvae were injected at each dilution from 3 single colony overnights (10 larvae per overnight culture). **(B)** 30 larvae were injected with PA01 and *exsC::Tn* (10<sup>3</sup> diluted cultures from OD<sub>600</sub> 0.1) from 3 overnight cultures (10 larvae per overnight culture) normalised by CFU (bars represent means of 3 overnight culture CFUs/mL  $\pm$ SD). \*\* indicates  $p = 0.0013$  as determined by Log-rank (Mantel Cox) between PA01 and *exsC::Tn* treated larvae GraphPad Prism 6.0. No PBS mock injection control larvae, nor no trauma control group larvae died during observation (30 larvae per group).

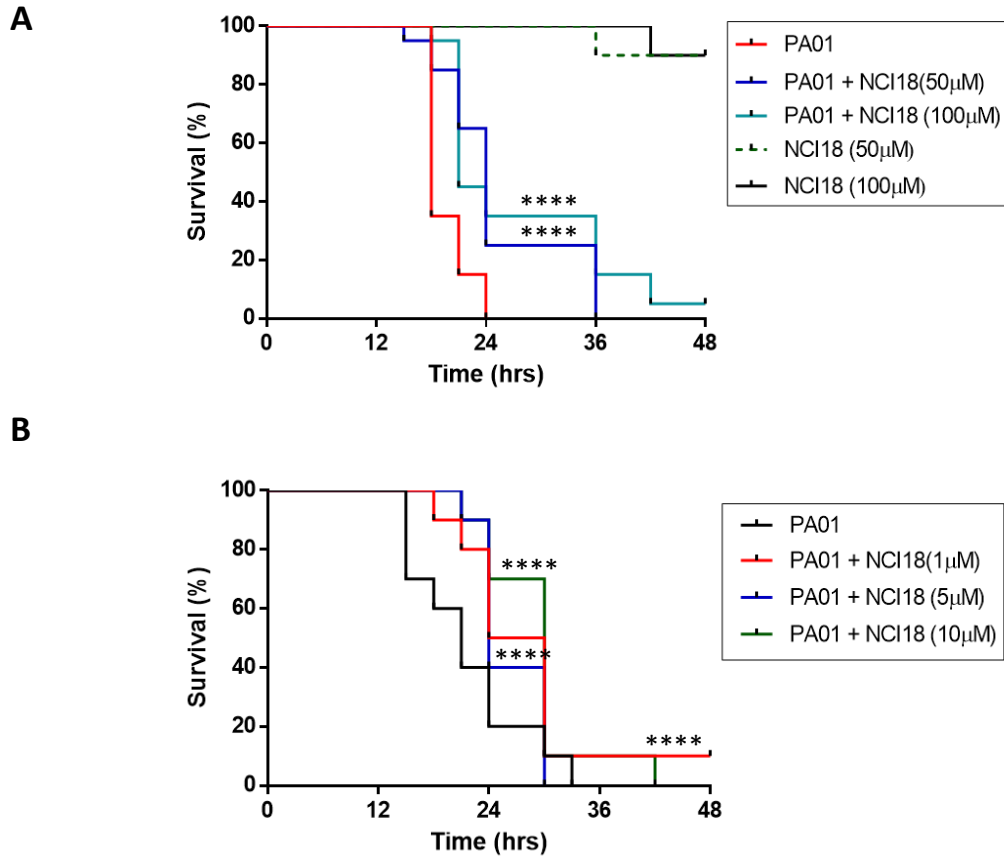


**Figure 4.10 *G. mellonella* survival in NCI18 treated acute infection models:** For both infection models, mock injection (PBS, 0.5mg/mL rifampicin) and no trauma control groups were used. No larvae in either of these control groups died during the experiments. All injected larvae were given two injections: 10µL of PA01 (PBS suspension, 0.5mg/mL rifampicin) or PBS mock injection, and 5µL of NCI18 (PBS suspension) or PBS (no rifampicin). PA01 injections were diluted  $10^3$  from OD<sub>600</sub> 0.1 and quantified by CFU/mL. **(A)** 20 larvae were used per condition from 2 single colony overnight cultures (10 larvae per overnight per condition). Results are the combined survival of all larvae per group. \*\*\*\* indicates  $p < 0.0001$  (PA01 vs PA01 + NCI18 50µM and PA01 vs PA01 + 100µM) determined by Log-rank (Mantel Cox) GraphPad Prism 6.0. **(B)** 10 larvae were injected with each NCI18 dose. 1 overnight culture was used per NCI18 dose. 30 larvae were used in the PA01 group and results are the combined survival of larvae from the 3 overnight cultures (10 larvae per overnight culture). \*\*\*\* indicates  $p < 0.0001$  (PA01 vs PA01 + NCI18 all doses) determined by Log-rank (Mantel Cox) GraphPad Prism 6.0.

## 4.4 Discussion

This chapter aimed to present outcomes of experimental validation of molecules purchased based on *in silico* screening (outlined in chapter 3) with unique chemical scaffolds to allow the expansion of research on ExsA small molecule inhibitors. In order to do so, reliable assays that could allow evaluation of efficacy and specificity to the T3SS were needed. Key experiments and milestones needed to be classified as a “hit” were a reduction of 25% relative to controls in both the lux and CPA assays, as well as acceptable levels of toxicity and no effect on growth. These criteria were the basis for a hit to be further tested for specific T3SS inhibition, the gold standard test for this being a western blot. An advantage of this method was that compounds that were not causing ExsA inhibition but were still efficacious in protecting PA mediated cytotoxicity proceeded to be investigated, which is discussed in the final paragraph of this discussion. Additionally, efficacy was investigated through *in vivo* experiments using *G. mellonella*. The conclusions from the individual assays are discussed below and the impact they had on decision making for the direction of the project.

Testing just over 100 compounds in drug discovery terms is an incredibly minute number. Since PA is so intrinsically resistant, notably because of its efflux pumps and the inner and outer membranes, attempts were made to find molecules that may be active against ExsA, but were unable to bypass the defensive strategies of PA. Unfortunately, the lux transformed YM64 strain did not have a compatible phenotype for the lux assay. Biophysical methods seen in chapter 3 were also hampered severely by the time consuming and low yield difficulties of ExsA purification.

The two aims were tackled first by the lux and CPA experiments. Both experiments are routinely used in published literature to assess the efficacy of compounds in drug discovery<sup>[263, 264, 275]</sup>. As previously mentioned, PcrV and ExoS are routinely used as indicators of T3SS expression and clear indications of its upregulation under assay conditions were seen in the normalised lux, as well as the western blots. A common request by reviewers for the CPA is whether the compounds themselves are indicated in changes in LDH detection. Unfortunately, the resources to test all the compounds again in this manner as a control were not available and therefore it was relied upon that the combination of assays, in addition to the growth and subsequent data to be confident in its results. Overall, the pair are robust assays commonly

used and were of reasonable high throughput for this project. The keystone experiment in this chapter was the western blots. Without evidence of T3SS downregulation there is no supporting a mode of action involving ExsA inhibition and after narrowing the hit compound search this was a compulsory experiment. M1 was the only compound to that caused a decrease in PcrV expression, although this was not attributed to activity against ExsA since it only occurred at concentrations that impacted PA growth.

Building on the toxicity profile of NCI18 the *G. mellonella* experiments showed the compound was not toxic *in vivo*, at least for *G. mellonella* at clinically relevant doses. Despite 1 death at 950mg/kg and 1900mg/kg, no deaths were recorded at much higher doses of 7,600mg/kg and efficacy was demonstrated at far lower doses. The first doses were based on the EC<sub>50</sub> value calculated from the CPA and improved survival at lower concentrations was pleasing. *G. mellonella* lack many advantages of larger animal models but there is a compelling argument for momentous uptake within drug discovery, especially in the early stages of development assessing efficacy and safety as argued in section 4.3.1. They have already been extensively used to assess various treatments against PA<sup>[267, 273, 276]</sup> and additionally one of the principals mentioned in chapter 1 is the adjunctive therapy use of anti-virulence molecules. These experiments could easily be designed using *G. mellonella*. For example, the rate of infection clearance by antibiotics only or by co-treatment with an anti-virulence therapy could be measured by recoverable haemocoel CFUs, as well as death rates. *G. mellonella* are susceptible to several PA virulence determinants<sup>[268, 274, 277, 278]</sup> which means the results do not pertain to a mode of action by NCI18 although this question is primarily addressed in the next chapter.

This project stood at a crossroads here with the original aim of identifying ExsA inhibitors having turned up nothing worthy of pursuit. Revisiting the *in silico* methods and ordering a new batch of compounds was one option. However, without additional computing power this seemed an unfavourable exercise given the limited ExsA structural or ligand information that could be utilised. An opportunity did arise with the HPC-Europa3 grant which would have provided just such computing power. The aim of the visit being to build a fresh homology model of ExsA and then refine it through long (~1 $\mu$ s) MD simulation. The refined model could then be used to perform new rounds of virtual screening. Unfortunately, this opportunity was not able to be taken due to the global pandemic. However, positive results in

the data showing that NCI18 could reduce PA virulence *in vivo* independent of affecting PA growth, as well as showing no substantial toxicity towards A549 cells, were interesting. The focus of this project shifted because of these promising results and it was chosen that the action of NCI18 would be explored by further characterisation of its role in targeting virulence in PA.

# **Chapter 5**

## **Results & Discussion**

**Alternative virulence mechanisms**

## 5.1 Phenyl piperazines

### 5.1.1 Background

Phenyl piperazine compounds have been linked with anti virulence activity in *Candida albicans* reportedly interrupting morphological transition<sup>[275]</sup>. A number of phenyl piperazine derivatives were tested for toxicity to A549 cells in the same manner as reported in this study except for an increased incubation time of 8hrs instead of 4hrs. The vast majority showed no toxicity towards A549 cells at high concentrations<sup>[275]</sup>. NCI18 is a phenyl piperazine very similar to, but distinct from, those tested in *Candida*.

Despite causing no decrease in T3SS expression, growth was unaffected by NCI18 and PA mediated cytotoxicity was significantly reduced *in vitro* and *in vivo*. I decided therefore, to pursue this compound and any analogues I could obtain to find improved reduction in PA cytotoxicity, as well as to elucidate a mechanism of action for the phenyl piperazine class.

Reviewing the NCI compound structures showed 3 analogues of NCI18 within the original order: NCI16, NCI17 and NCI19. The first CPA screen at 50 $\mu$ M showed NCI18 achieved a greater reduction in PA cytotoxicity compared to any of these molecules, therefore an additional two analogues were ordered for testing in a search for improved activity. Unfortunately, more NCI18 was not available to purchase and so the investigation of this drug class was continued using only NCI16, NCI17, NCI19 and the two additional analogues purchased, NCI18<sup>1A</sup> and NCI18<sup>2A</sup>.

### 5.1.2 Assessment of NCI18 analogue activity

**Figure 5.1** identifies the structural differences of the analogues to the original NCI18 compound. Of note for NCI18<sup>1A</sup> is the addition of a chlorine and bromine group, as well as the conjugation of the naphthalene group shifting one carbon further from the ether group. NCI18<sup>2A</sup> has no naphthalene group but is instead replaced by a phenyl acetamide group. The molecules contain a chiral carbon although unless the bond angle is indicated in **figure 5.1**. It is unknown whether the molecule came as a racemic mixture or one of its enantiomers. NCI16, NCI17 and NCI19 are all missing the chloride group within the phenyl piperazine core, instead possessing a methyl group on various carbons of the core. NCI16 and NCI17 do not have a naphthalene group either, instead only a single aromatic ring with either a chloride or methyl group addition.

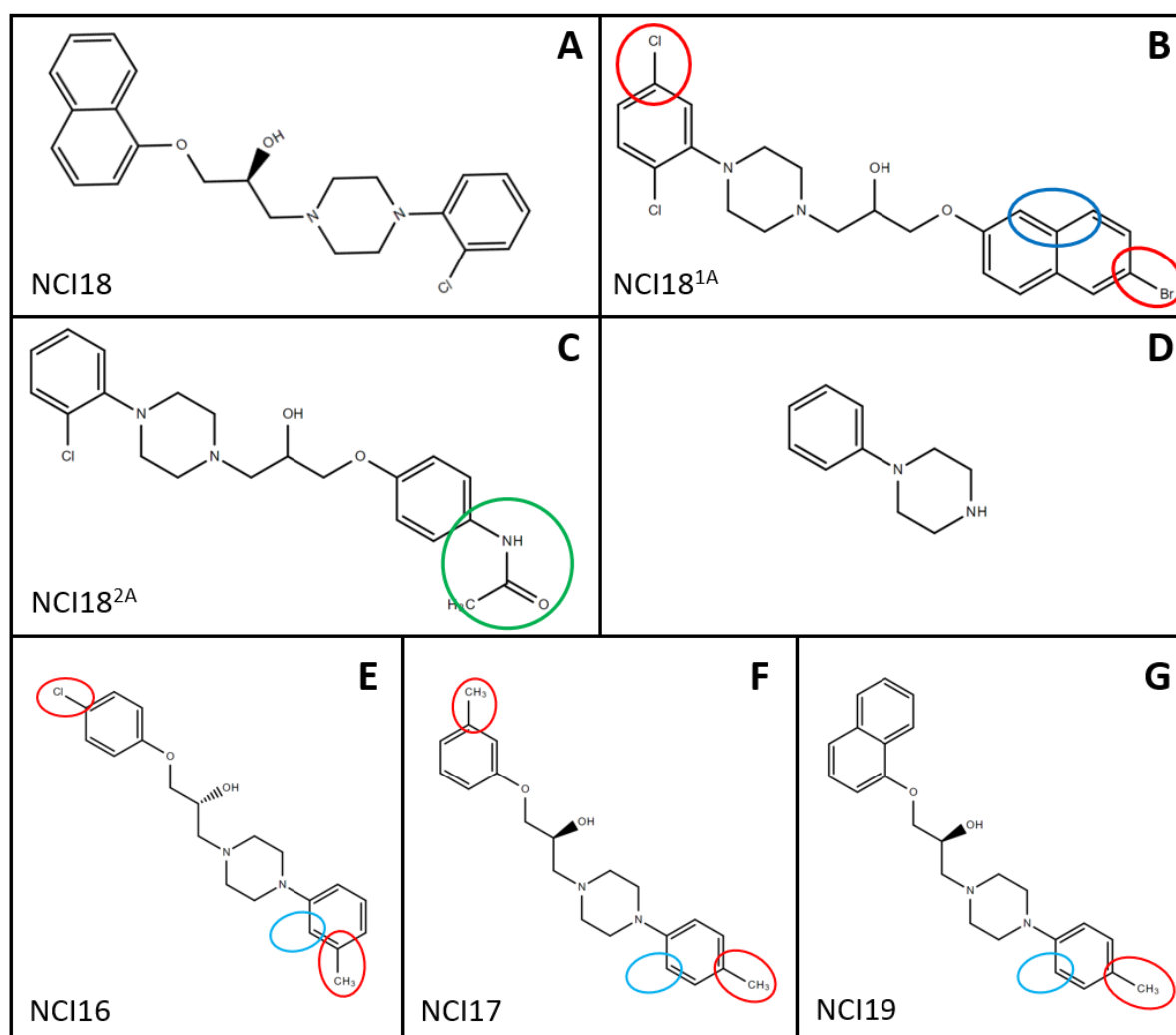


**Figure 5.1 2D phenyl piperazine analogue structures:** NCI18 is a phenyl piperazine compound. 3 analogues were identified in the original NCI order and 2 additional analogue molecules were purchased. Molecules in this figure are compared to NCI18. Red circles – Additional group. Dark blue circle – shifted carbon number for group. Green circle – acetamide group. Light blue circle – missing chloride group. (A) NCI18. (B) NCI18<sup>1A</sup>. (C) NCI18<sup>2A</sup>. (D) Phenyl piperazine class core structure. (E) NCI16. (F) NCI17. (G) NCI19.

NCI18<sup>1A</sup> and NCI18<sup>2A</sup> were initially tested for their ability to reduce PA103 induced cytotoxicity *in vitro* using the dose response CPA (see section 2.3.3). NCI18<sup>1A</sup> was found to be 15 times more potent than the original NCI18 molecule with an EC<sub>50</sub> in the low micromolar range and a maximal reduction in LDH detection of around 90%. NCI18<sup>2A</sup> was disregarded after this first assay because it failed to reduce PA103 mediated cytotoxicity in any capacity (data not shown). This lack of activity suggests that this portion of the compound may be essential for binding. The methyl groups on NCI16, NCI17 and NCI19 are non-polar as is the acetamide group on NCI18<sup>2A</sup> meaning the size and/or shape of the group is probably a factor in losing activity. The presence of an electronegative group on NCI18 and NCI18<sup>1A</sup> and their

improved efficacy would suggest these groups play a role in increasing binding affinity although the optimal position and group is unclear without testing of a much greater number of analogues. Additionally, the toxicity of NCI18<sup>1A</sup> appeared to be lower than NCI18 when tested in the same manner, with no toxicity detected at any concentration compared to the 10% seen at the highest concentration tested for NCI18. Results from the CPA and toxicity assays are shown in **figure 5.2**.

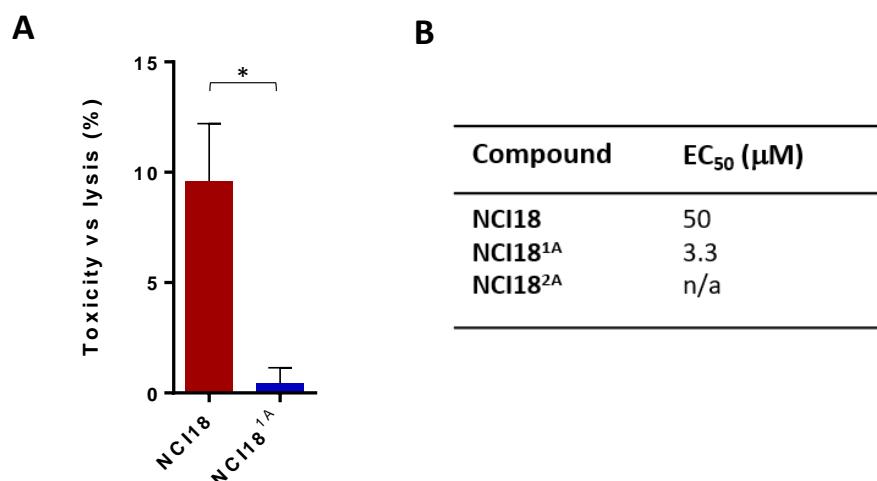


**Figure 5.2 Toxicity and efficacy of NCI18 and analogues:** (A) LDH released by A549 cells measured as a percentage vs full lysis controls (100%) when incubated (4hrs) with NCI18 and NCI18<sup>1A</sup> (200μM, 1% v/v). Bars represent the mean ±SEM of 3 independent experiments. \* indicates  $p = 0.025$  determined by unpaired student t-test (GraphPad Prism 6.0). (B) A549 cells infected with PA103 (MOI 5:1) treated with NCI18, NCI18<sup>1A</sup>, and NCI18<sup>2A</sup> in a dose dependent manner (750nM – 200μM, 1% v/v at all concentrations). EC<sub>50</sub> was determined as the concentration of compound at which 50% of LDH was released by A549 cells compared to untreated samples. Analysis conducted using GraphPad Prism 6.0 using log(agonist) vs normalised response – variable slope.

Growth curves demonstrated that NCI18<sup>1A</sup> had no effect on PA growth at a concentration of 200μM. In addition to a standard growth curve, I conducted an *ex vivo* growth experiment using porcine lung tissue as previously described by Harrison *et al.*, (2014). Outlined in section 4.3.1 are some of the substantial merits of using *ex vivo* models for investigation. Bronchiole tissue from fresh pig lungs were washed and infected with PA103 by stabbing with a single colony per tissue piece using an insulin needle. The tissue was incubated at 37°C in ASM and every 24hrs the tissue was washed and moved to a new plate with fresh media. At a concentration of 100μM NCI18<sup>1A</sup> had no effect on the colonisation of PA103 on bronchiole tissue after 48 or 96hrs as determined by CFU counts of tissue homogenate. DMSO

controls also had no effect on growth. **Figure 5.3** shows both the *in vitro* and *ex vivo* growth data.

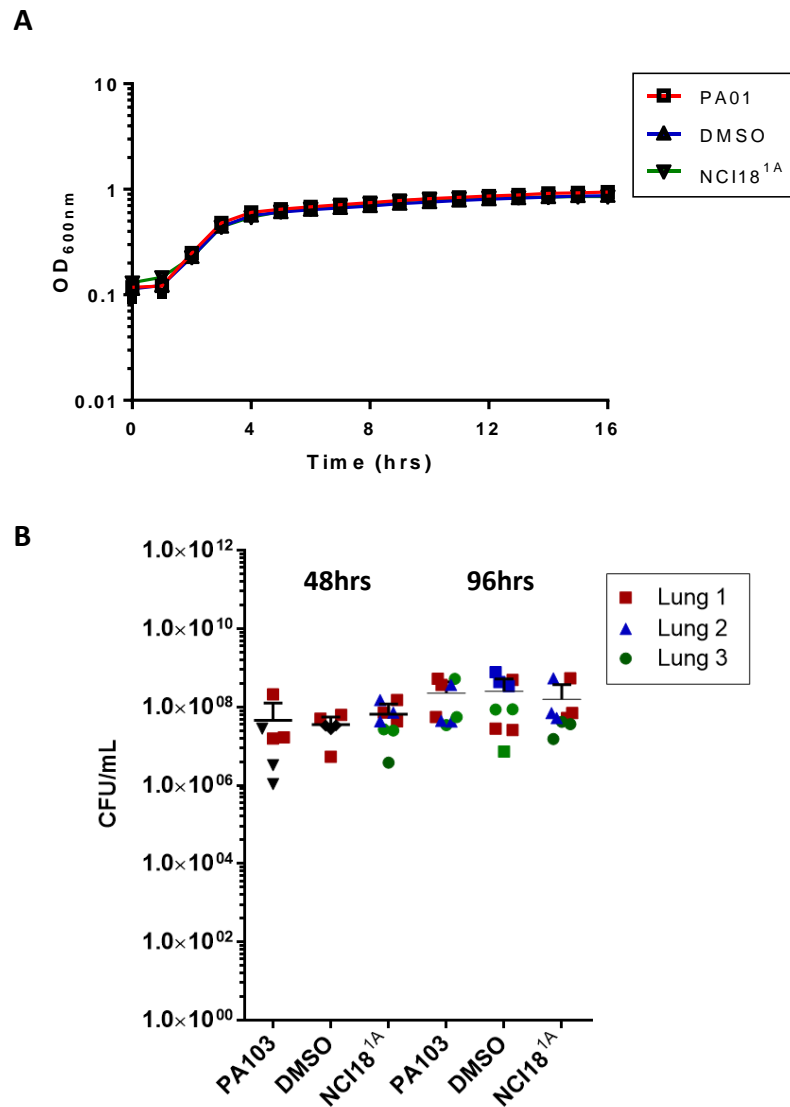


**Figure 5.3** *In vitro* and *ex vivo* growth of NCI18<sup>1A</sup> treated *P. aeruginosa*: (A) PA01 overnights were normalised to OD<sub>600</sub> 0.05 in LB and NCI18<sup>1A</sup> (200µM, 1% v/v) was added to appropriate wells. Growth was measured by OD<sub>600</sub>. Results are representative of 3 independent experiments. (B) Porcine lung tissue infected with PA103 was incubated in ASM treated with NCI18<sup>1A</sup> (100µM, 1% v/v) or DMSO (1% v/v). Lines represent means +SD of CFUs/mL from lung homogenates plated on *Pseudomonas* isolation agar. Each data point represents one piece of tissue. Results are from 3 independent experiments using 3 pieces of tissue per lung (except PA103 and DMSO 48hrs, n=2 lungs)

Confident that NCI18<sup>1A</sup> had improved activity *in vitro* without affecting growth, PcrV expression was measured using western blots to check activity against the T3SS (*see section 2.5.5*). As predicted, no change was seen in the expression levels of PcrV represented in **figure 5.4**. Without a reduction in T3SS expression it was apparent that these molecules did not act by inhibiting ExsA activity. Therefore, to proceed with the project their effects on a broad range of PA virulence factors were tested to clarify a mechanism by which the phenyl piperazine molecules were acting. Given the volume of compound stocks left at this point in the project only the best performing molecule (NCI18<sup>1A</sup>) was tested in every assay, followed up testing the other analogues only after positive results.

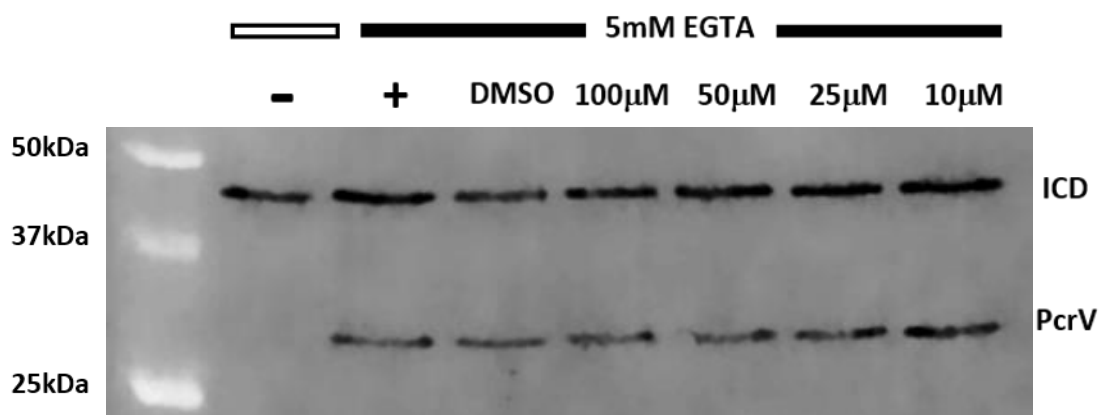


**Figure 5.4 NCI18<sup>1A</sup> effect on type III secretion system expression:** Normalised PA103 cultures were grown to the beginning of stationary phase (~7hrs) before normalisation for western blots. Induction of T3SS was by 5mM EGTA (all conditions except non-induced indicated by -). Addition of NCI18<sup>1A</sup> (all concentrations) and DMSO were at 1% v/v. Isocitrate dehydrogenase (ICD) was used as a loading control. Results are representative of 3 independent experiments.

## 5.2 Investigation of virulence mechanisms

### 5.2.1 Protease activity

Proteases are used by PA to disrupt host defence mechanisms and establish infection by breaking down the surrounding extracellular matrix and host defence molecules<sup>[279]</sup>. Reduced protease activity is well characterised for reductions in virulence<sup>[58, 279, 280]</sup> and therefore targeting production and/or activity of proteases is an established mechanism of reducing PA mediated cytotoxicity. Proteases are under the direct control of QS in PA and therefore mutants deficient in the main QS regulator *rhlR* are well characterised for losses in protease activity<sup>[281–283]</sup>. Consequently, I used a PA01 *rhlR*::*Tn* mutant as a negative control for this protease activity assay.

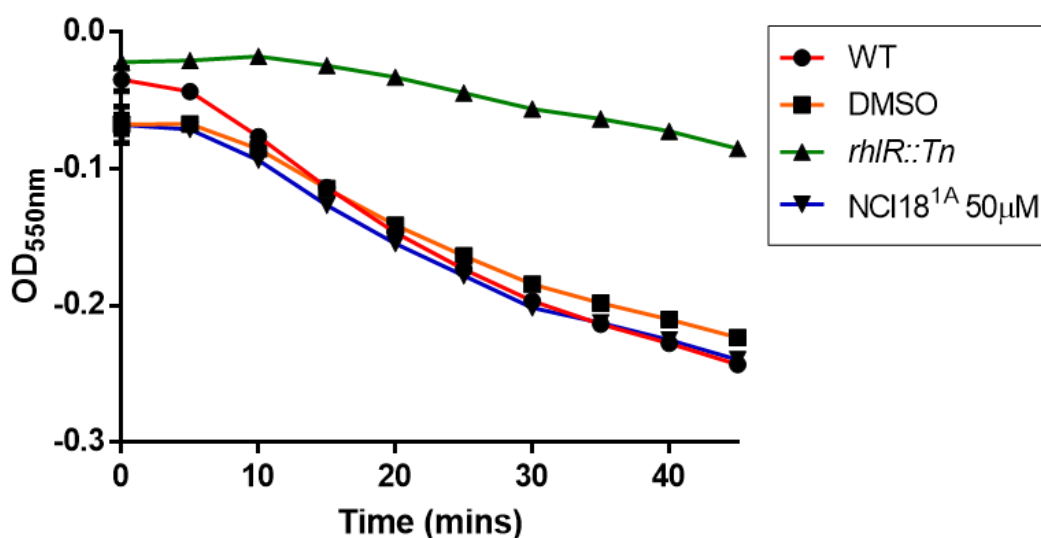


**Figure 5.5 NCI18<sup>1A</sup> effect on PA01 protease activity:** Normalised supernatant samples of overnight flask cultures were measured for protease activity by changes to OD<sub>595</sub> when mixed with 1.5% milk solution. DMSO and NCI18<sup>1A</sup> were added to growth cultures at <1% v/v. Results were normalised to LB only controls. Data is representative of 3 independent experiments.

Measuring the rate of casein breakdown in milk is a simple non-specific protease activity assay. As the casein substrate is cleaved by proteases the milk turns clear and colourless and OD<sub>595</sub> can be measured over time. Normalised secretome samples of overnight flask cultures added to milk showed that NCI18<sup>1A</sup> had no effect on protease activity in PA01 relative to WT and DMSO controls. A *rhIR::Tn* mutant had severely reduced protease activity, the results of which are seen in **figure 5.5**.

### 5.2.2 Biofilm formation

There is an inverse relationship between acute infection associated phenotypes and chronic infections, notably biofilm formation<sup>[127]</sup>. Results surrounding the relationship between these phenotypes in the presence of compound could provide clues to the mechanistic action by which these compounds act. Biofilms are associated with chronic infections and increased antibiotic resistance. Their formation is controlled by complex intersecting signalling pathways involving QS<sup>[55, 90]</sup>. The *las* and *rhl* system work in tandem to control genes associated with biofilm formation. *lasR* mutants are well characterised for a biofilm deficient phenotype and a transposon mutant was used as a negative control during this experiment<sup>[284–287]</sup>.

Overnight cultures were diluted 100x in LB and grown shaking at 37°C in 96 well plates for 48hrs, with biofilm formation quantified by OD<sub>550</sub> after staining with 0.1% crystal violet and solubilisation in 30% acetic acid (*see section 2.6.6*). Biofilm formation was shown to be unaffected by NCI18<sup>1A</sup> after 48hrs under assay conditions whereas the *lasR* mutant showed significantly reduced biofilm formation. DMSO did not affect biofilm formation (1% v/v). Statistical analysis was performed using GraphPad Prism 6.0 using an One-way ANOVA with Dunnett's post hoc analysis comparing multiple columns to WT control column (p < 0.0001).

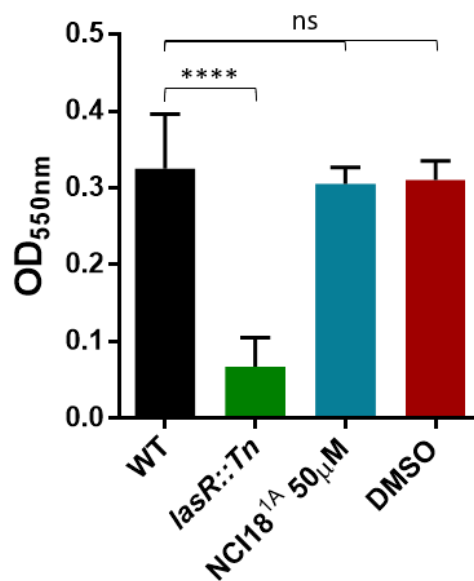


**Figure 5.6 NCI18<sup>1A</sup> effect on biofilm formation:** Overnight cultures were diluted 100x in LB and NCI18<sup>1A</sup> or DMSO (1% v/v) were added as appropriate. Plates were incubated shaking (200rpm) for 48hrs at 37°C. Biofilm formation was measured by OD<sub>550</sub>. Statistical analysis was performed in GraphPad Prism 6.0 using a One-way ANOVA test with Dunnett's post hoc analysis. \*\*\*\* represents p < 0.0001.

### 5.2.3 Motility related virulence

Motility is an essential part of virulence being crucial to surface adherence, invasion, biofilm formation, host recognition, nutrient acquisition and many other components of establishing infection<sup>[85]</sup>. PA moves across or through different surfaces using varying methods of motility, either as an individual cell or in a coordinated manner as a population controlled by cell to cell communication. The flagella and type IV pili (T4P) systems are the primary effectors in PA movement and give rise to several different modes of motility<sup>[85]</sup>. I focused on the three best established types of motility to investigate the action of phenyl piperazines on PA - swimming, swarming, and twitching. For each of the motility assays the overnight cultures

were not grown in the presence of any compound or DMSO, but these were added as appropriate to the assay specific agar.

Section 1.4.1 mentions the likely evolution of the T3SS from the exaptation of the flagellum, with a number of papers finding relationships between the expression of the two systems<sup>[83, 91]</sup>. The flagellum and the injectosome share some core components, such as the ATPase, and dual activity against both systems has been demonstrated by hydroxyquinolines targeting these core components. Evidently from section 1.5 there is intricate crosstalk between the flagellum and T3SS, and both swimming and swarming are dependent upon the flagellum. Due to this dependence, a *fleQ::Tn* transposon mutant was utilised as a negative control for both swimming and swarming assays. FleQ is a c-di-GMP responsive transcriptional regulator that presides as the master regulator for flagellum related genes in PA<sup>[288-290]</sup>. Transcriptional regulation of the flagellum is organised in a 4-tiered hierarchy of Class I-IV. FleQ is a Class I regulator, is constitutively expressed, and coordinates activation or repression of Class II regulators<sup>[288-290]</sup>. This hierarchy can be seen in **figure 5.7**.

Swimming motility is driven by the reversible rotation of PA's polar flagellum in acquiesce environments and swimming capability is tested using low percentage agar (0.1-0.3%). As with swarming and twitching, swimming deficient mutants are ineffective at biofilm formation and achieving full virulence<sup>[291-293]</sup>. Normalised cultures showed no change in swimming motility after overnight incubation when inoculated in swimming agar plates containing NCI18<sup>1A</sup> or DMSO controls. The *fleQ::Tn* mutant was entirely defective in swimming motility. The results of the swimming assay are seen in **figure 5.7**.

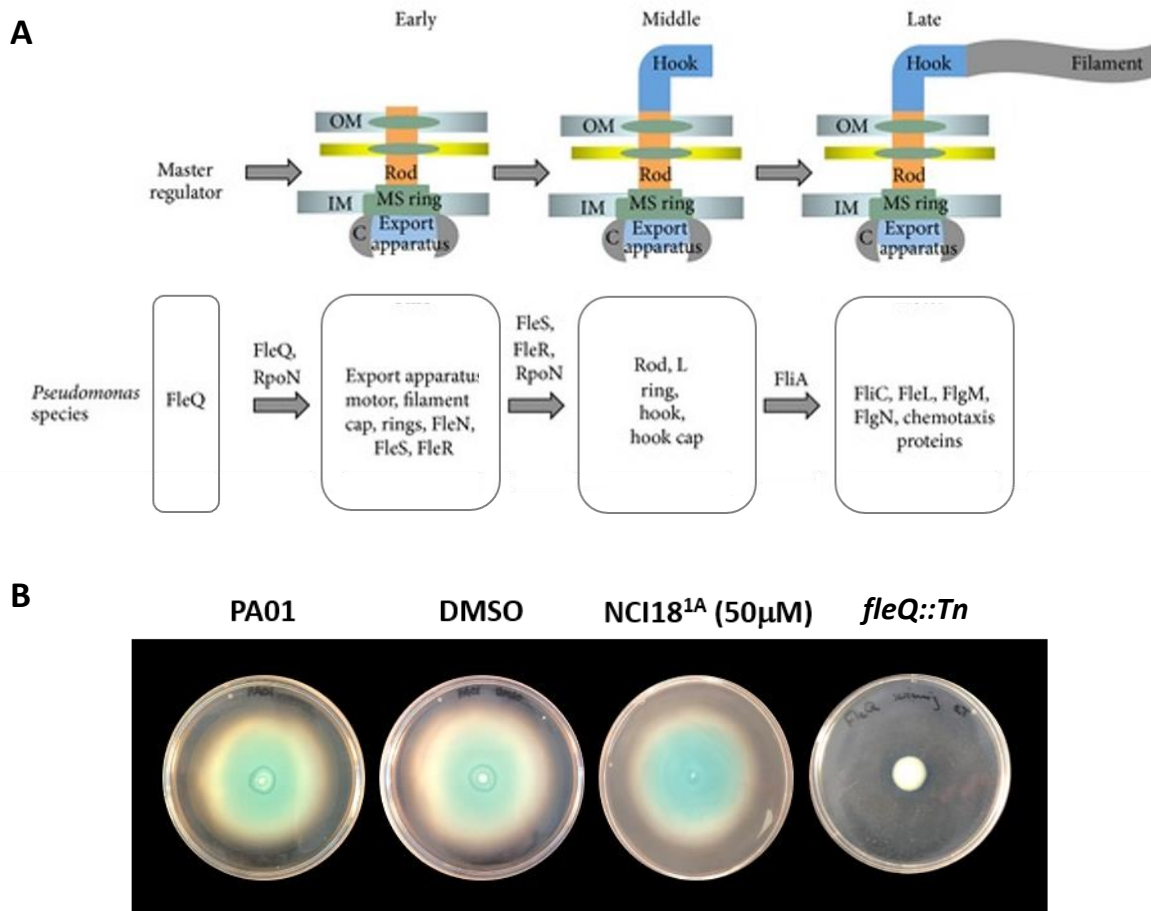


**Figure 5.7 PA01 swimming control and motility:** (A) Hierarchical regulatory control of flagella synthesis indicating FleQ as the master transcriptional regulator. Image adapted from Tsang *et al.*, (2014). (B) Overnight cultures were normalised to OD<sub>600</sub> 1.0 and inoculated into swimming agar plates (NCI18<sup>1A</sup> <1% v/v) and incubated overnight at 37°C. Images are representative of 3 independent experiments.

Studies have shown that swarming is required for full virulence by PA and the overexpression of the T3SS, extracellular proteases, and other virulence genes under swarming conditions have also been observed<sup>[83, 84]</sup>. Swarming is a social activity requiring coordination amongst the bacterial population. It is dependent upon QS signalling, chemotaxis regulation, and biosurfactant secretions such as rhamnolipids to overcome surface tension<sup>[294, 295]</sup>. Importantly, the conditions that are required for swarming seemingly replicate the mucous covered epithelial surface of a CF lung<sup>[296, 297]</sup>. Studies have shown that this type of movement over semi-solid surfaces is coordinated by both the flagellum and T4P and can be tested in laboratory conditions using semi solid agar (0.5%)<sup>[298]</sup>.

Swarming agar plates were inoculated with normalised cultures and incubated overnight (*see section 2.6*). Traditionally swarming is characterised by the neat projectile extensions branching towards the edge of a low percentage agar plate however, the complexity of swarming regulation and subtle changes in firmness to agar plates, as well as the specific strain or species, can result in varied swarming patterns<sup>[299]</sup>. Different swarming patterns were seen by the different strains tested in this assay. PA01 did not swarm with traditional dendritic features, taking longer to swarm than a PA14 WT strain also tested.

DMSO controls had no effect on swarming in either strain whilst the *fleQ* mutant control was devoid of any swarming motility as expected. Demonstrating that swarming is QS dependent a *rhlR* mutant was shown to be unable to swarm as well. NCI18<sup>1A</sup> inhibited swarming in both PA01 and PA14 at 10 $\mu$ M and after 48hrs swarming activity was not recovered by either strain. Further testing on PA14 revealed swarming was severely affected at concentrations as low as 500nM with complete inhibition seen in some plates, although at 1 $\mu$ M or below swarming activity was not always completely eradicated as seen in **figure 5.8**. Increased swarming motility was not regained after 48hrs of incubation at these lower concentrations. Two clinical isolates of PA were also tested for swarming inhibition however both were discovered to have non-swarming phenotypes.

The 3 other NCI18 analogues (NCI16, NCI17, and NCI19) also inhibited swarming although with less potency than NCI18<sup>1A</sup>. At 10 $\mu$ M only NCI19 eradicated all swarming activity whilst partial swarming at 1 $\mu$ M was seen in all plates with these compounds. This matches the level of decreased PA mediated cytotoxicity in the initial CPA screen when comparing activity across these analogues. Swarming inhibition is characterised by the reduction in the number of branches as well as the distance cultures swarm.

Having established the inhibitory action of these molecules on PA swarming, the next steps were to extrude a more specific mechanism and if possible find a link between the selection of these compounds and their activity. The N-HB molecules had a broad spectrum of activity across the AraC/Xyls family and the phenyl piperazine compounds were originally selected to inhibit the AraC/Xyls family T3SS regulator, ExsA. Given this, a plausible hypothesis was that they exhibited inhibitory activity against an AraC/Xyls family regulator

involved in swarming motility. A further assessment of swarming is discussed in the next section.

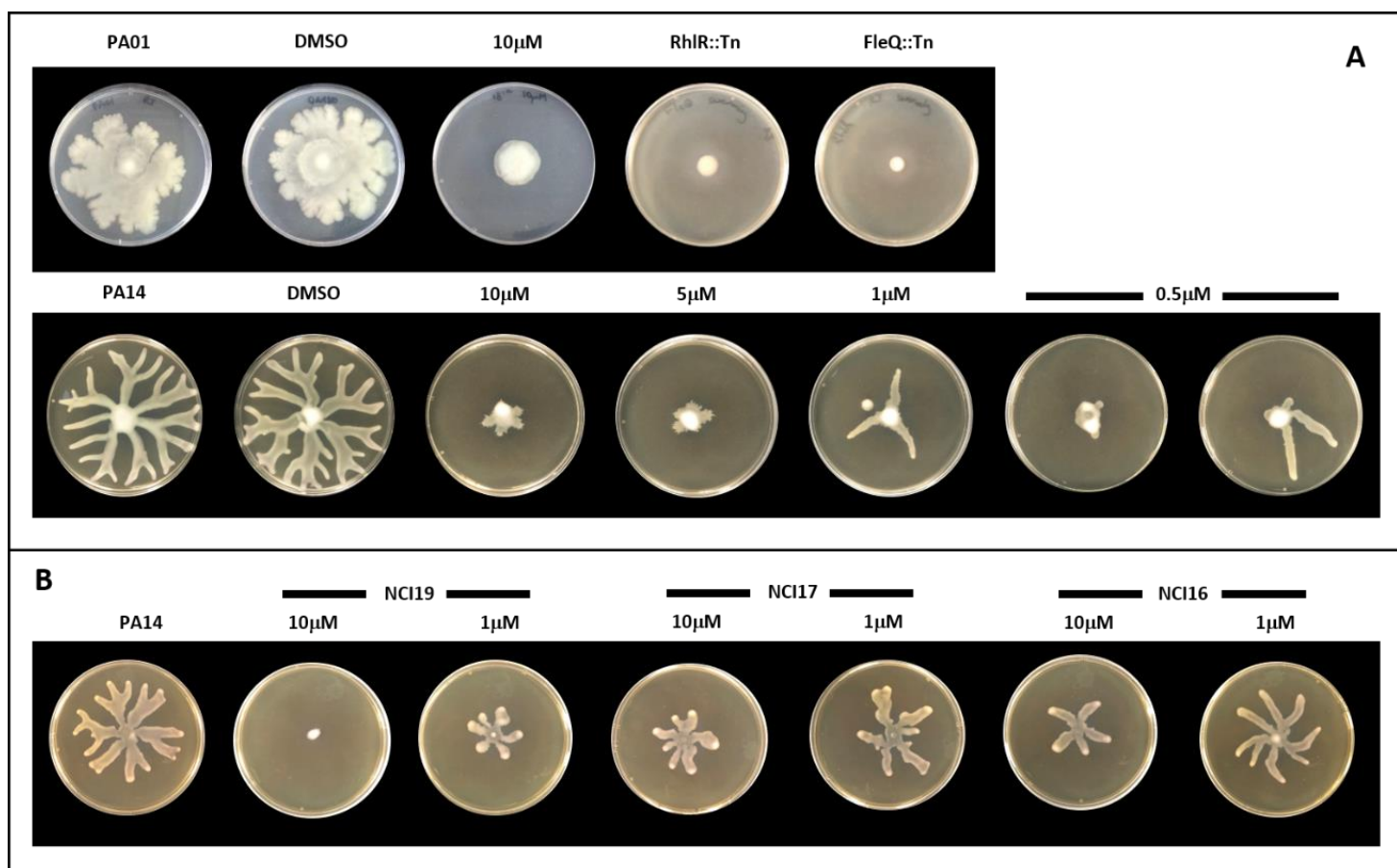


**Figure 5.8 Swarming inhibition by phenyl piperazines:** Overnight cultures normalised to OD<sub>600</sub> 1.0 were spotted onto swarming agar plates and incubated at 37°C overnight. Compounds NCI18<sup>1A</sup>, NCI16, NCI17 and NCI19 were added to swarming agar (<1% v/v). All images are representative of 3 independent experiments. **(A)** PA01 and PA14 strains treated with NCI18<sup>1A</sup>. *rhIR::Tn* and *fleQ::Tn* strains were used as negative controls. **(B)** PA14 swarming plates treated with two concentrations (10µM and 1µM) of NCI16, NCI17 and NCI19.

Twitching by PA refers to the its movement across a solid surface mediated by the extension and retraction of Type IV pili with cells moving linearly along their long axis<sup>[300]</sup>. T4P are under the control of the *pil-chp* chemotaxis system as well as the global virulence cAMP dependent regulator, Vfr<sup>[301, 302]</sup>. They play an important role in surface adhesion, cell aggregation, and biofilm formation in addition to specific twitching motility<sup>[300-304]</sup>. Mutants defective in twitching have a decreased ability to colonise hosts and are thus important for virulence<sup>[301, 302]</sup>.

Twitching assays were carried out in similar manner to swimming and swarming assays with normalised cultures inoculated onto motility specific agar and incubated at 37°C overnight. 1% LBA plates were used for twitching assessment and cultures were inoculated onto the base of the petri dish before incubation. Twitching motility was quantified by measuring the diameter at the widest point of the twitching zone visible by crystal violet staining. The results are seen in **table 5.1**. Twitching was unaffected by the NCI18<sup>1A</sup> with the *fleQ::Tn* mutant having partially reduced twitching motility.

**Table 5.1 PA01 twitching motility**

Sample	Ø (mm) ±SD
WT PA01	15.6 ±0.06
WT PA01 + 50µM NCI18 <sup>1A</sup>	14 ±0.2
PA01 <i>fleQ::Tn</i>	5.3 ±0.38

As stated above, swarming is usually considered dependent upon both flagella and T4P however, this is slightly more complex with some strains showing that T4P are not necessary for swarming function<sup>[293]</sup>. The partial reduction in swarming seen in the *fleQ::Tn* mutant highlights the overlap between these two systems although, since no effect was seen when treated with NCI18<sup>1A</sup> it appeared swarming inhibition was independent of T4P.

## 5.3 Further investigation of swarming inhibition by NCI18<sup>1A</sup>

### 5.3.1 Biosurfactant production

The exciting and stark activity of NCI18<sup>1A</sup> against swarming posed many questions about its mechanism. As previously mentioned, swarming motility is dependent on multiple factors which include regulatory control, function of the flagella, T4P, secretion of biosurfactants, and chemotaxis. Rhamnolipids are anionic biosurfactants secreted by PA to overcome surface tension as the population moves across a viscous surface<sup>[305]</sup>. PA01 was inoculated onto rhamnolipid agar plates and incubated for 48hrs at 37°C followed by 48hrs at 4°C before plates were imaged. The rhamnolipids produced by PA01 form a complex with the cationic CTAB and methylene blue in rhamnolipid agar which becomes visible as a blue halo around the culture and can be seen much more clearly using UV transillumination.

As for the swimming and swarming assays the *fleQ::Tn* mutant was used as a negative control and it can be seen in **figure 5.9** that the halo is absent from around the mutant. Since rhamnolipid production and secretion was unchanged by the presence of NCI18<sup>1A</sup> in this assay it indicated that the inhibition of swarming by NCI18<sup>1A</sup> was independent of this factor. Rhamnolipid production is, as for protease activity, under direct regulatory control of QS and *rhlR* mutants are deficient in rhamnolipid production<sup>[284]</sup>.



**Figure 5.9 NCI18<sup>1A</sup> effect on rhamnolipid production:** Overnight cultures normalised to OD<sub>600</sub> 1.0 were spotted onto rhamnolipid agar plates (NCI18<sup>1A</sup> <1% v/v) and incubated at 37°C for 48hrs followed by 48hrs at 4°C. Halo visibility was enhanced by UV transillumination. Images are representative of 3 independent experiments.

### 5.3.2 *gacA* hyper swarming mutant

*gacA* mutants have been characterised for hyper swarming phenotypes as they bypass the regulatory cascade defined by the Class I regulator, FleQ<sup>[297]</sup>. DMSO did not affect the swarming of the  $\Delta gacA$  strain and a PA01 WT was used as a control to display the characteristic poor swarming phenotype of PA01 which did not swarm after the same incubation time and has been shown in section 5.2.3 to be unable to swarm when treated with the compound. In the presence of 25 $\mu$ M NCI18<sup>1A</sup> the  $\Delta gacA$  strain was able to partially swarm (**figure 5.10**). This result suggests that the compound target is downstream of *gacA* in the swarming pathway and that mutations to the *gacA* gene can partially restore swarming capabilities of PA when treated with NCI18<sup>1A</sup>. Deletion of the *gacA* gene evidently cannot fully compensate for inhibition by the phenyl piperazine suggesting that the target is likely essential for full swarming motility.

A transposon mutagenesis study by Yeung *et al.*, (2009) gives an excellent indication of how complex swarming regulation is. Using a PA14 transposon mutant library they identified 233 mutants with altered swarming motility with insertion sites in genes associated with flagella and T4P biosynthesis, as well as a range of processes including secretion, transport and metabolism. 33 of the swarming deficient mutants had insertions in transcriptional regulator genes, including two-component sensors and response regulators. 27 of these were newly identified mutations to effect swarming. What is notable from the study is that of the 27 transcriptional genes characterised swimming and twitching motility were only minimally affected if at all and when assessed for biofilm formation it was found to be largely increased compared to WT controls, showing an inverse relationship between swarming motility and biofilm formation. Additionally, these swarming mutants had no changes to rhamnolipid production. Specifically, the study looks at rhamnolipid production in association with BHL and RhIR. These results backup the notion that the phenyl piperazine target is a regulator involved in the control of swarming that does not affect the associated phenotypes of swimming, twitching, biofilm formation, rhamnolipid production or QS. The effect of NCI18<sup>1A</sup> on QS and BHL production is discussed in section 5.3.4.

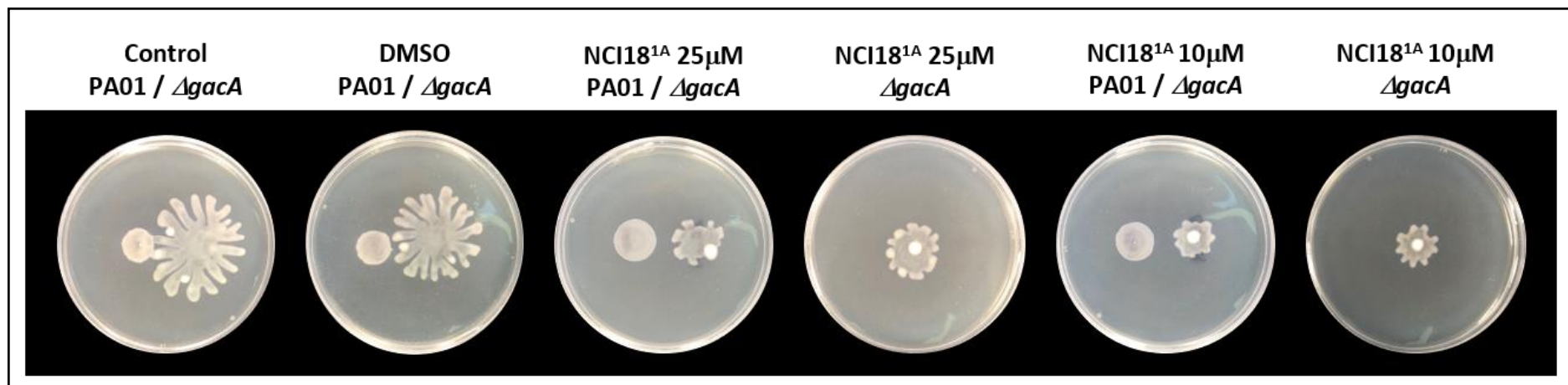


**Figure 5.10 *gacA* hyper swarming mutants treated with NCI18<sup>1A</sup>:** Normalised overnight cultures of PA01 and a  $\Delta gacA$  strain were spotted onto swarming agar plates treated with NCI18<sup>1A</sup> (10 $\mu$ M or 25 $\mu$ M, <1% v/v) or DMSO (<1% v/v). Plates were incubated overnight at 37°C. Images are representative of 3 independent experiments.

When looking in more depth at the list of mutants in Yeung *et al.*, (2009) one putative AraC family regulator stands out that is listed in the table figure – PA2332. In the paper, the mutant had no statistical difference in biofilm formation compared to WT, no change to swimming nor twitching motility, and secreted rhamnolipids equally to the WT. Another genomic analysis study of PA categorising essential conserved genes identified 980 genes with no variation at the amino acid level in the clinical isolate pool sequenced<sup>[306]</sup>. The paper sought to highlight that essential genes hold evolutionary importance and therefore could make good novel therapy targets. They also showed that essential and highly expressed proteins evolve more slowly compared to extracellular proteins. They reported that of the 980 conserved genes, those that were non-essential genes were primarily involved in regulation, motility and virulence. Listed in the paper is the previously mentioned putative AraC family regulator gene PA2332 stating that it was not found in any genus outside *Pseudomonas*, a point of importance surrounding non-specific drugs causing more side effects. This gene, PA2332 was a member of the 980 genes with no variation amongst the 36 sequenced clinical isolates and is also a non-essential gene.

Unfortunately, little else is reported in the literature on this uncharacterised gene and whilst it could be a good starting point to probe the link between compounds selected for ExsA inhibition and swarming inhibition by determining if the putative AraC regulator it encodes is the target of phenyl piperazines, it was not investigated further. Instead an alternative, slightly better characterised, potential target was explored which is discussed later in section 5.3.3 and the next chapter. The reported complexity and involvement of many regulators to control swarming motility, as well as evidence that PA2332 is a highly conserved protein, is extremely interesting though and future work should be carried out to characterise and assess this gene and its translated protein as a potential target for anti-virulence therapies in the future.

### **5.3.3 *Pseudomonas tolaasii* swarming**

Mechanisms of swarming are thought to be conserved across the *Pseudomonas* genus and so activity of these compounds in another *Pseudomonas* was tested. *P. tolaasii* is considered the biggest problem facing the European mushroom industry at this time, causing brown blotch disease which renders the economically important and nutritionally packed *Pleurotus* genus of fungi unappealing for human consumption. *P. tolaasii* is considered non-pathogenic to mammalian hosts and swarms, so as a preliminary test of broader activity and

potential application of phenyl piperazines, swarming assays were conducted in the same manner as for PA01 and PA14 with *P. tolaasii* 2192T strain.

NCI18<sup>1A</sup> entirely inhibited swarming of *P. tolaasii* at 1 $\mu$ M and was not recoverable after 48hrs of incubation. **Figure 5.11** shows the radial swarming phenotype of *P. tolaasii*. This activity against two *Pseudomonas* species would suggest its target is not specific to mammalian pathogenic strains and tests on alternate species would be extremely interesting to observe whether the action is genus specific or a more essential and universal element of swarming control.

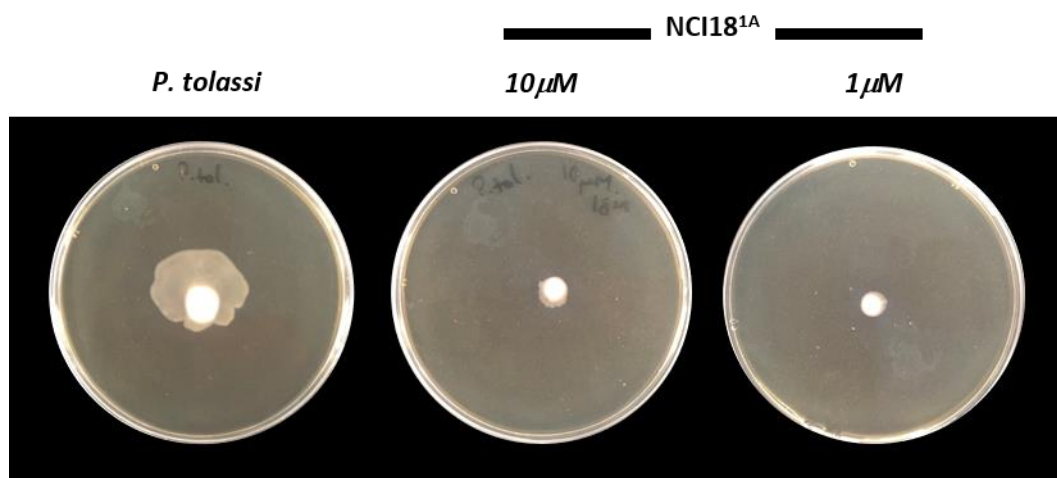


**Figure 5.11** NCI18<sup>1A</sup> effects on *P. tolaasii* swarming: Overnight cultures of 2192T were normalised to OD<sub>600</sub> 1.0 and spotted onto swarming agar plates treated or untreated with NCI18<sup>1A</sup> (10 $\mu$ M or 1 $\mu$ M, <1% v/v) and incubated at 37°C overnight. Images are representative of 3 independent experiments.

#### 5.3.4 QS activity

QS is a cell to cell communication system utilised by bacteria to coordinate virulence factor expression and biofilm formation<sup>[284–286]</sup>. The system is arranged in a complex hierarchy between the *las rhl* and *pqs* systems<sup>[286, 307, 308]</sup>. The *las* system resides at the top of the signalling pathway with LasR being the receptor for its autoinducer AHL molecule, OdDHL produced by LasI<sup>[308]</sup>. This system works in tandem with the *rhl* system; BHL being the autoinducer produced by RhlI and RhlR being the cognate receptor<sup>[308]</sup>. Finally, the *pqs* system involves PqsR and its autoinducer PQS<sup>[83]</sup>. Animal models have extensively shown the importance of QS for full virulence and roughly 10% of the PA transcriptome is under expression control of QS. Interruption of these pathways by phenyl piperazines could have significant impacts on virulence and as previously stated and shown, swarming is a population

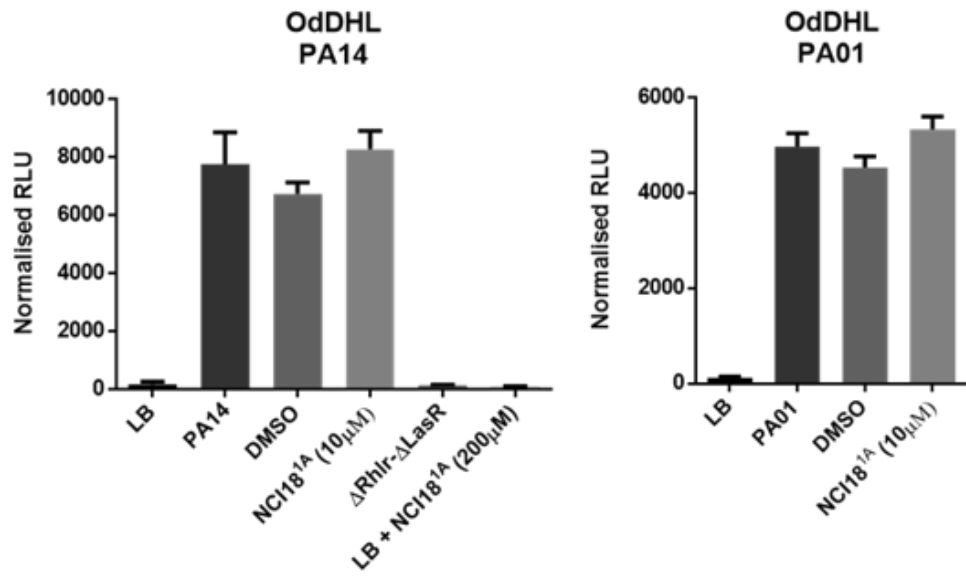
activity dependent on QS<sup>[280, 284, 285, 309–311]</sup>. **Figure 5.12** indicates the QS regulatory network and some of the downstream virulence factors they influence<sup>[287]</sup>.

Three lux sensor strains were used to detect the production of each of the three QS autoinducer signalling molecules<sup>[239, 240]</sup>. A lux signal is induced in each sensor strain by the cognate autoinducer molecule with increased or decreased levels of the molecule causing a corresponding increase or decrease in lux compared to controls. The secretome of each sample grown to stationary phase was incubated with the sensor strains, using a PA14 *AlasR-ΔrhlR* double mutant, LB, and LB with NCI18<sup>1A</sup> as control samples. By the addition of NCI18<sup>1A</sup> to each of the sensor strains it was shown that the compound does not cause any increase in lux signal by itself as levels were equal to that of LB alone. The *ΔrhlR-AlasR* double mutant produced lux levels equivalent to LB only controls when incubated with the OdDHL and BHL sensor strains confirming that an increase in autoinducer presence causes an increase in lux signal.

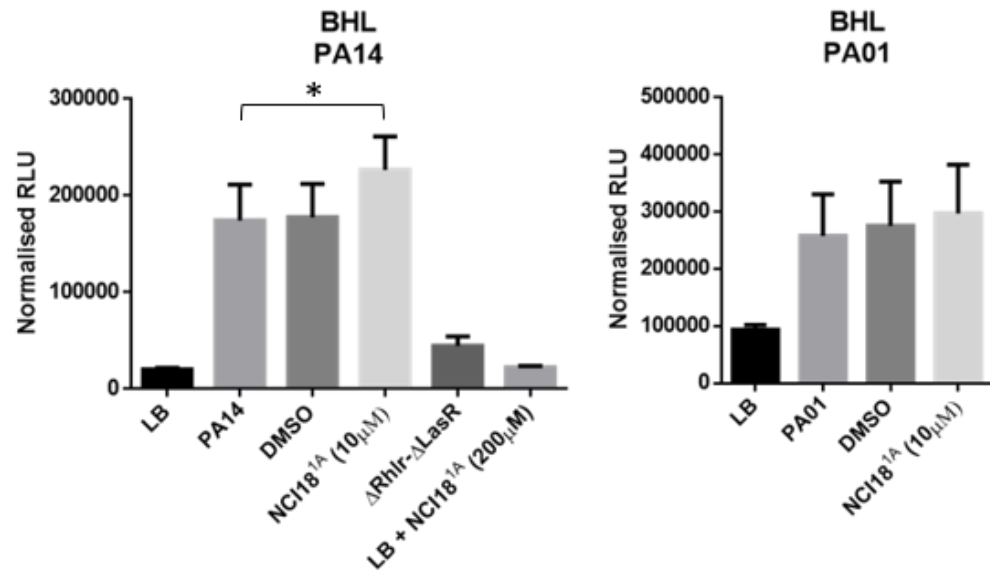
OdDHL production was unchanged by treatment with the compound in PA01 and PA14 when tested under assay conditions and was not investigated further (see **figure 5.12**). Results for BHL were difficult to interpret and posed a multitude of questions surrounding the effects on QS. Firstly, NCI18<sup>1A</sup> increased BHL production in PA14 but not PA01. Secondly, the results were not comprehensive, meaning that it was not reliably repeatable. The increase was seen more often than not however and is reported as such since numerous repeats were done of this experiment to be sure of the transient nature of the signal increase.

PQS production in both PA01 and PA14 strains was increased, however this increase was transient in the same manner as for BHL. Increased PQS has been previously shown to inhibit swarming in PA as a protective mechanism to avoid antibiotics or unfavourable environmental conditions<sup>[312]</sup>. This result was therefore investigated more rigorously and samples were tested during mid-log growth phase. No significant increase was seen in either strain at mid-log time points. Mid-log growth phase was chosen as QS molecule production is upregulated in high cell densities (i.e. stationary growth phase) and increased production at mid-log time points would suggest direct stimulation of PQS molecule production by the compound.

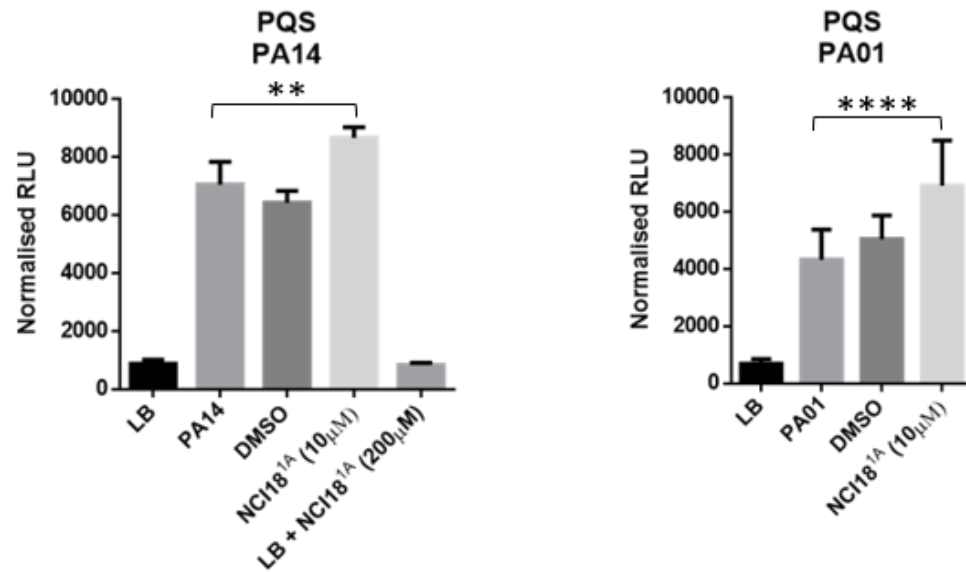
**A**



**B**



**C**



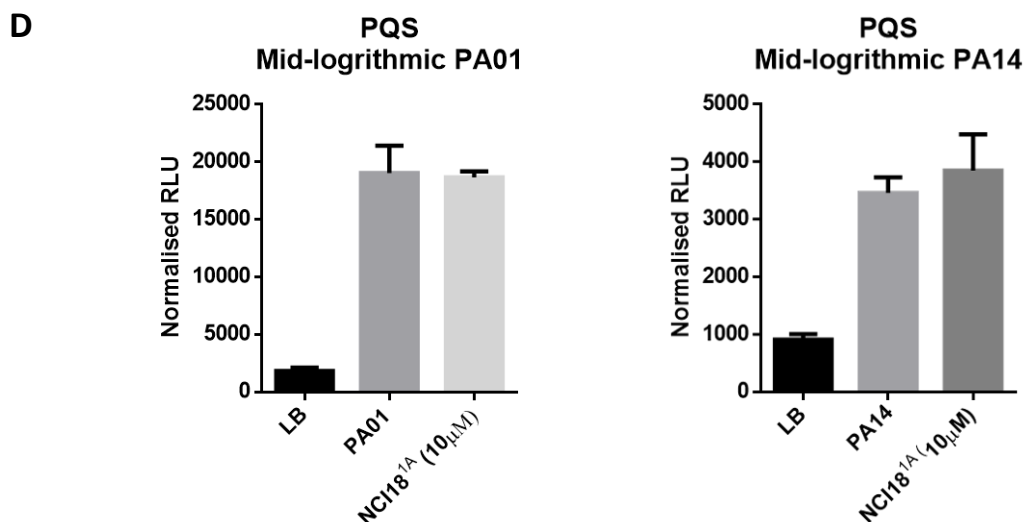


**Figure 5.12 NCI18<sup>1A</sup> effect on PA01 and PA14 QS molecule production:** The effect of NCI18<sup>1A</sup> (10 μM, <1% v/v) on the production of QS molecules (OdDHL, BHL, and PQS) was measured by incubation of supernatants with biosensor strains<sup>[240, 243]</sup> grown to mid log phase. Samples were incubated with biosensor strains for 3-4hrs (30°C) before measurement of lux. Statistical analysis was performed using GraphPad Prism 6.0 (student unpaired t-test). Columns represent means ±SEM of 3 independent experiments. (A) OdDHL measured at stationary phase. (B) BHL production measured at stationary phase. \* indicates p = 0.0301. (C) PQS production measured at stationary phase. \*\* indicates p = 0.0011 and \*\*\*\* indicates p < 0.0001. (D) PQS productions measured at mid log phase.

In addition to the mid-log time points PA01 *PpqsA-lux* strain was tested for changes in signal either by intensity or by timing of expression. The *pqsABCDE* operon is necessary for PQS production<sup>[313]</sup>, and therefore if a real increase was being seen in the assay, an increase would be expected under these conditions as well. The *pqsA* gene encodes a predicted protein with homology to acyl coenzyme A (acyl-CoA) ligases<sup>[313]</sup>. A PA01 *PlacZ-lux* control strain was also tested and NCI18<sup>1A</sup> was found to have no effect on the signal of either strain which can be seen in **figure 5.13**.

To further complicate interpreting these results it is important to consider the biosensor strains response to the compound and to each culture secretome. Every strain will have a slightly different secretome “fingerprint” not to mention that the compound is possibly influencing this fingerprint. Without dilution of the secretome the sensor strains are killed by the PA virulence components that have been secreted thus confirming the influence its components have on this assay. Without knowledge of how NCI18<sup>1A</sup> affects the secretion profile it is difficult to take a position on how much influence this may have. A solution could be direct detection of the QS molecules by assays such as quantitative LC-MS.

In addition, a common problem faced by lux reporter assays is fluctuation of signal strength. This assay would have benefitted from a positive control overexpressing the signalling molecules to help quantify what relative changes in expression can be expected under inducing conditions. Meaning whilst statistically significant mathematically, the results might not translate to significant phenotypic changes. Because of the extensive impact changes in QS have on population behaviour and cellular expression it is probable that the primary action of NCI18<sup>1A</sup> is not on a QS related target, nor is the primary cause of swarming inhibition due to changes in QS signalling. NCI18<sup>1A</sup> could have some pleiotropic effects on the QS signalling within PA under certain conditions though.

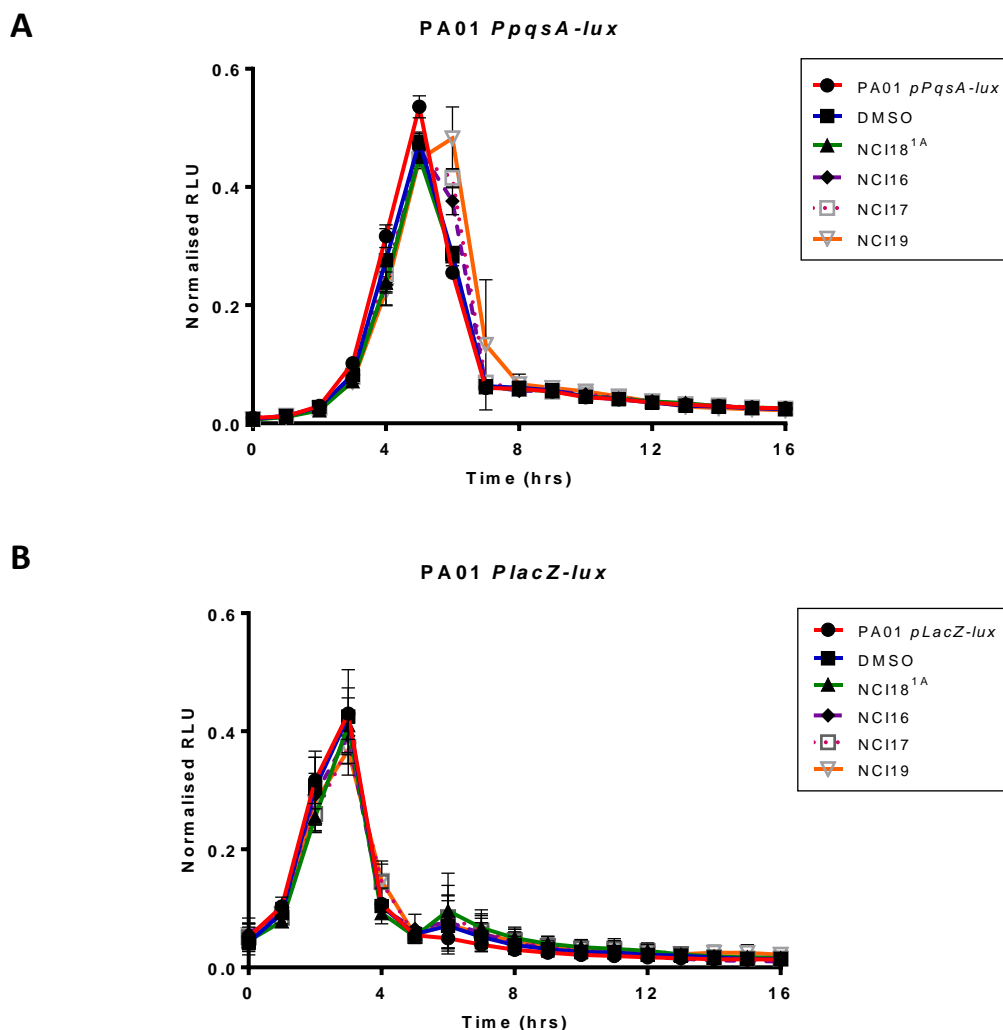


**Figure 5.13 PQS production during *P. aeruginosa* growth:** Normalised lux signals were measured from PA01 *PpqsA-lux* and *PlacZ-lux* strains treated with 10 $\mu$ M phenyl piperazine compounds (NCI18<sup>1A</sup>, NCI16, NCI17, and NCI19) added at 1% v/v in LB. Data points are the means of two independent experiments  $\pm$ SEM.

### 5.3.3 KEGG GENOME search for potential targets

Since all the compounds in this study (except for NCI18<sup>1A</sup> and NCI18<sup>2A</sup>) were originally ordered using ligand and structure-based approaches to inhibit an AraC family protein, I searched using KEGG GENOME for AraC family regulators in PA and identified those that may be involved in swarming motility. The search returned 13 hits of which 1 stood out as a possible target, ChpD. ChpD is part of the chemosensory *pil* system in PA. As mentioned in section 5.2.3, chemotaxis regulation is an integral part of swarming motility and thus was at this stage an interesting hit for investigation. Very little published research has been conducted on ChpD which is discussed in more depth in the next chapter. An advantage ChpD

had over investigating PA2332 was that it is marginally better characterised and verified mutants existed in the literature that I was able to acquire for this project.

## 5.4 Discussion

Following results that showed none of the ordered compounds inhibited T3SS expression by inhibiting ExsA activity, this chapter addressed the question of how NCI18 was protecting lung epithelial cells from PA mediated cytotoxicity *in vitro* and extending survival time of *G. mellonella* in acute PA infection models. PA has a lot of virulence factors and those tested in this chapter were chosen because they are major virulence determinants which have all been linked to changes in T3SS expression<sup>[110]</sup>. Since additional amounts of NCI18 were not produced by any vendors the project continued using previously purchased analogues and two available additional analogues.

The efficacy between the compounds only gave limited insights into the activity of the compound class and generating a full analogue library would be necessary to firmly establish essential scaffold components for activity. One place to begin in this assessment though would be determining which of the enantiomers is most active.

The results showed that phenyl piperazines seemingly have an extremely selective activity against swarming. This was suspicious since changes in swarming have been linked with several changes in the expression of other virulence factors. This is most likely due to assay conditions as to why no changes are seen since swarming control is extremely complex and requires semi solid surfaces. It is possible the target is only expressed or active under swarming conditions and future work should take this into account. The rhamnolipid assay clearly demonstrated that swarming inhibition was independent of biosurfactant production and secretion, and since no changes in swimming or twitching assays were seen we can be confident the target is not a Class I or II regulator within the regulatory hierarchy, since the *fleQ* mutant demonstrated that these higher-class regulators have impacts on each of the motility types. Further questions surrounding the expression and function of the flagella needed to be addressed at this point in the project, especially around the unaffected swimming motility.

Swarming has important implications for virulence within the CF lung and this role during infection consequently impacts on an inhibitors likely clinical use. Motility coupled with the secretion of toxins is considered imperative for acute infections and treatment methods prioritise eradication at initial and new-onset stages of infection, lending towards shorter length course treatment during acute flare-ups, or as a prophylactic to prevent colonisation and establishment of an infection outside of specific CF use, rather than long term usage of an inhibitor by patients. Indeed, it has been shown that flagellar expression is downregulated during chronic infection within biofilms and that clinical isolates not expressing flagella fail to activate the inflammasome. The flagella is a key structure for the immune system to detect and activate and therefore during chronic infection it may favour PA to avoid detection by downregulating its expression. In acute infections however, hyper-swarming isolates and strains are associated with increased antibiotic resistance and virulence<sup>[84, 312]</sup>, with the thick mucus lining in the CF lung providing a viscous environment required for swarming. This further supports clinical use of a swarming inhibitors for acute infections or flare-ups.

Experiments involving the *gacA* mutants and further study of the literature revealed that many additional regulators have been identified to play key roles in swarming without having significant impacts on other virulence factors tested in this project, such as swimming, twitching, biofilm formation and QS<sup>[297]</sup>. Dötsch *et al.*, (2010) stress the potential value in recognising specific targets for therapies to minimise the chances of treatment side effects. As mentioned previously, the AraC family of regulators are attractive because there are no homologues in the human genome. It appears that the compounds tested in this chapter show very specific activity to PA swarming and it would be extremely interesting to see whether the compounds inhibited swarming in any alternate genus having seen the conserved nature of many non-essential virulence and motility genes in Dötsch *et al.*, (2010). Elucidation of the target regulator of the tested molecules would be substantial in further understanding the intricate regulation of PA swarming in addition to holding a lot of potential for future therapies targeting these specific regulators if one was in fact the target. The absence of any AA variation in the screening of the clinical isolates within the study is also an interesting observation for the notion that antivirulence targeting would not exact the same selection pressures on bacteria. Testing the mutation rates of these swarming deficient mutants lacking specific regulators could be of value to antivirulence therapy development. Given the evidence of their conservation but also the non-essentiality of these proteins is worthy of further study.

The argument for fewer side effects seen treatments with highly specific targets overlaps with the need for a more extensive study of the toxicity profiles for phenyl piperazines. This project only covered a very basic assessment of toxicity with *in vitro* incubation with lung epithelial cells and monitoring *Galleria* larvae deaths after treatment. Establishing an LD<sub>50</sub> for the most effective compounds in addition to other toxicity tests would be important in taking this chemical scaffold forward towards clinical use, but also in observing and demonstrating the effectiveness of using *Galleria* to establish toxicity profiles over vertebrates.

ChpD is discussed in more detail in the next chapter but the obvious question mark over a gene included in a cluster known to regulate twitching is why no changes were seen in the twitching assay when treated with compound. As an AraC family regulator and with studies showing that swarming is dependent upon flagella and T4P it warranted significant further investigation. As mentioned little is reported on ChpD in published literature although, some noteworthy findings are the suggestion of a global regulatory virulence role and its requirement for full virulence as well as no changes seen in twitching motility in a knockout study<sup>[314–318]</sup>. ChpD was selected over gene PA2332 because of this marginally more advanced characterisation of the gene itself. Time limits prevented generating and appropriately characterising a deletion mutant of PA2332, whereas a clean deletion mutant of ChpD was available from Prof. Cynthia Whitchurch and was obtained extremely quickly with the added benefit of having supported published literature to corroborate its function and activity in a short time frame.

The QS assay probably generated more questions that it answered, and an overexpression positive control would be useful to gauge the relative increase in signal that would induce substantial phenotypic changes. Despite statistically significant differences in results the dynamic range of this assay may not be appropriate to detect small changes in QS expression. The relative fold changes are very small in the assays whereas overexpression controls may have much greater differences. A point discussed in more detail in the next chapter (section 6.4.5) is the necessity of host cell contact to cross a threshold of LasR activation, adding a layer of regulation to QS activity that may have implications on the relative increase of PQS seen in the assays. The absence of change seen in the *PpqsA-lux* strain test further supports that assay conditions are playing a part. There are substantial differences in conditions between flask grown and 96 well plates and no effect was seen at all in the *PpqsA* strain. I suspect that the conflicting and confusing results are due to assay conditions over any

specific inhibitory swarming related activity by the compound. Yeung *et al.*, (2009) reported no change in RhIR activity in relation to novel swarming regulator mutations but did not assess PQS or LasR.

At this point in the project my focus was to assess the phenotype of ChpD mutants and in the process conclude on whether it is the target of phenyl piperazine compounds in PA. Additionally, to further characterise the clinical relevance of swarming inhibition by phenyl piperazines.

# **Chapter 6**

## **Results & Discussion**

**Flagella synthesis and ChpD related virulence**

## 6.1 Chemotaxis signal transduction pathways

### 6.1.1 Background

Type IV pili (T4P) are the principle adhesins used by PA to facilitate its attachment to host epithelium<sup>[300]</sup>. They are filamentous projections located at the cell poles and coordinate the surface associated movement of twitching, which is mediated by their extension and contraction<sup>[317, 319, 320]</sup>. The biogenesis and function of T4P is controlled by signal transduction pathways that include the two-component sensor regulator systems, *pilSR*<sup>[321]</sup> and *algR/fimS*<sup>[322]</sup>, a global carbon metabolism regulator, *Crc*<sup>[323]</sup>, and the global virulence regulator *Vfr*<sup>[324]</sup>.

PA twitching motility is also under the control of a chemotaxis system, encoded partly by the previously characterised *pilGHIJK* gene cluster<sup>[325]</sup>, in addition to the less well understood *chpABCDE* cluster<sup>[316, 317]</sup>. This second cluster is located directly downstream of *pilK* and in combination they form a chemosensory signal transduction pathway that shares commonalities with those signalling pathways that regulate flagella rotation. PA has 4 chemosensory pathways it uses to respond to environmental stimuli that are critical to its ability to occupy a vast breadth of environments niches. These are the *che*, *che2*, *wsp*, and *chp* pathways.

The *che* chemotaxis pathway in *E. coli* is the best characterised and each of the 4 pathways in PA have homologous proteins to the components of the system. Briefly, using the *che* system and represented in **figure 6.1**, these systems work through methyl accepting chemotaxis proteins (MCPs)<sup>[326, 327]</sup>. A MCP detects a stimuli in the surrounding environment and relays the signal to a histidine kinase, CheA via a transducer protein, CheW. CheA auto phosphorylates before transmitting the signal by phosphorylation to the response regulator, CheY which transmits the signal to flagellar motors<sup>[295, 296]</sup>. The system also includes adaption enzymes, CheB and CheR which alter the methylation of the MCP, and CheZ phosphatase which dephosphorylates CheY<sup>[326, 327]</sup>.

Whitchurch *et al.*, 2004 proposed that the *chp* system comprises of the MCP, PilJ, a methyl transferase PilK (a CheR-like protein), 2 CheW homologues, PilI and ChpC, and a methyl esterase ChpB (homologue of CheB). Three response regulator homologues are

suggested – PilG, PilH and also the CTD of ChpA. ChpA is a CheA-like histidine kinase with 9 putative phosphorylation sites and it is suggested that it is responsible for the phosphotransfer with PilG and PilH on top of its autophosphorylation to its CheY domain. The system seemingly lacks a CheZ homologue to accelerate dephosphorylation of CheY, although it is possible the CTD of ChpA serves a similar function. PA encodes 26 putative MCPs<sup>[328, 329]</sup> and given the two CheW homologues in the *chp* system they may be used to complex multiple MCPs to ChpA, therefore enabling it to respond to many environmental stimuli<sup>[317]</sup>. A conclusion not drawn in Whitchurch *et al.*, (2004) is the role of ChpD and ChpE within this system other than its implication in liver colonisation.

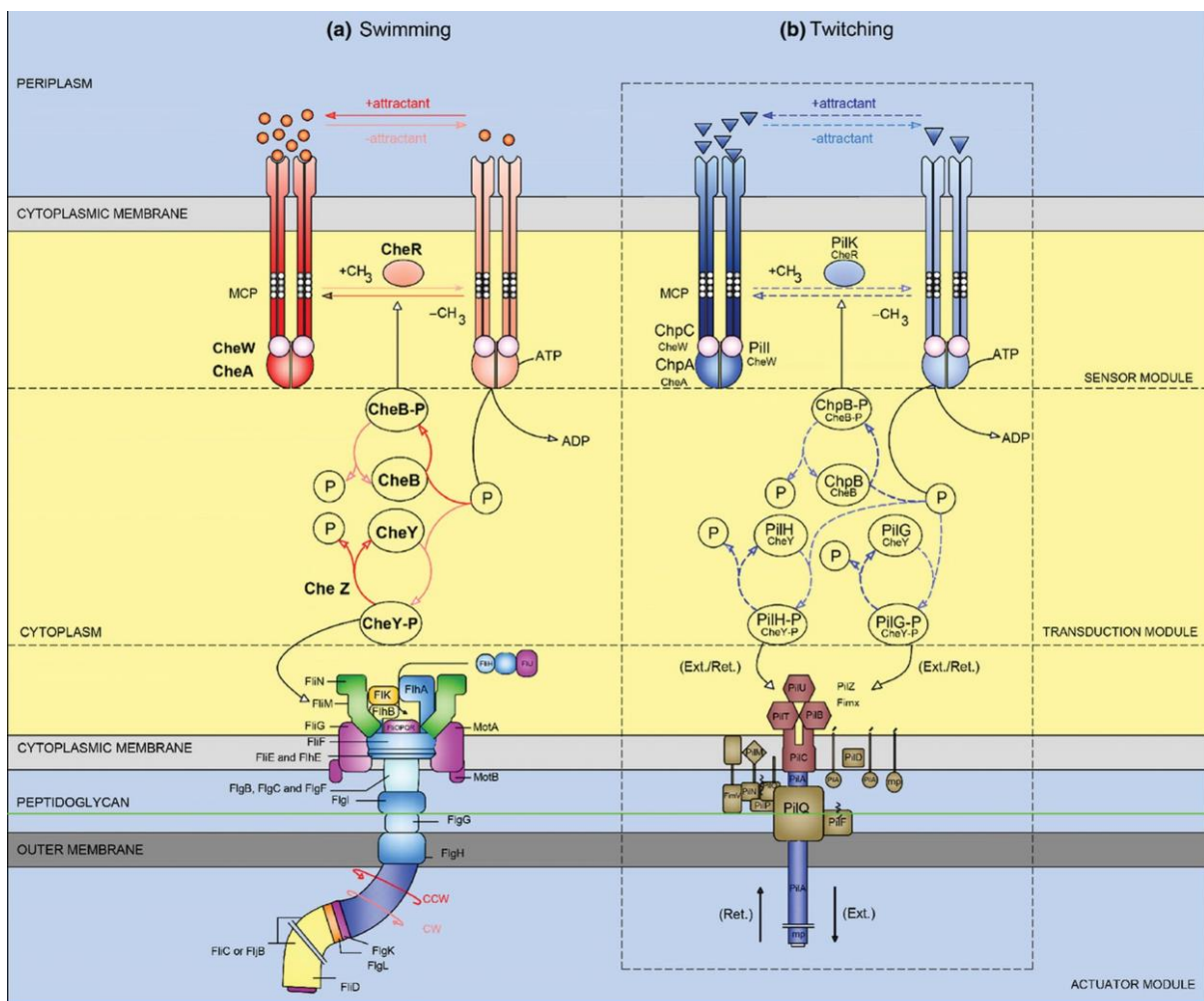


**Figure 6.1 Chemotaxis signal transduction pathways:** Swimming and twitching chemotaxis pathways in PA. MCPs recognise a cognate ligand and activate histidine kinases (CheA and ChpA) that transmit signal via phosphorylation to effector regulators (CheY, PilG and PilH). Relaying of signal causes changes to the frequency and direction of flagella or pili movement causing changes in motile behaviour of the cell. This figure was taken from Sampedro *et al.*, (2015).

More recent publications have made inroads into linking the role of the *chp* system to virulence within PA. These studies identify the mechano-sensing role of T4P to induce upregulation of cAMP related virulence factors. A transposon library was screened for mutants with reduced intracellular cAMP levels with the majority of insertions located within the *chp* system gene cluster<sup>[315]</sup>. Further analysis revealed the *chp* system was capable of both positive and negative regulation of intracellular cAMP by modulating CyaB activity. The paper found T4P dependent twitching motility to be independent of cAMP, but the production of T4P to be governed by cAMP modulation<sup>[330]</sup>. FimL, an accessory protein to the *chp* system with a previously unknown function, directly links the integral structural T4P complex, FimV with PilG, one of the *chp* system effector response regulators. FimL and PilG colocalise at the poles in a FimV dependent manner leading the authors to propose that FimL acts as a scaffold to colocalise the T4P and *chp* system components to organise signalling of cAMP-controlled virulence genes<sup>[330]</sup>.

Bioinformatic analysis showed that the *pil-chp* cluster was highly conserved amongst PA strains but varies more widely in other *Pseudomonads* and bacteria<sup>[314]</sup>, seemingly indicating that the presence of all 10 cluster genes overlaps with how closely related an organism is to PA. More specifically, it appears that *chpD* and *chpE* are only present in PA pertaining to a specific function for these genes. Neither are mentioned in Fulcher *et al.*, (2010) nor Inclan *et al.*, (2016), although it is not unthinkable to suppose that one or both genes are involved in the virulence expression in PA through cAMP related virulence factors.

The primary aim for this chapter was to first assess whether ChpD was the target of phenyl piperazine molecules causing an inhibition of swarming. Following this, to continue extruding a mechanism and understanding how ChpD is associated with virulence in PA. The second aim was to probe the further clinical relevance of phenyl piperazines by testing the sensitivity of strains to antibiotics when treated with NCI18<sup>1A</sup>. Lastly, this chapter will conclude on the major findings of this project and discuss the future directions that should be taken to progress this work.

## 6.2 Investigation of ChpD as the phenyl piperazine target

### 6.2.1 $\Delta$ *chpD* swarming phenotype

The most obvious and simple way to test for ChpD being the target of phenyl piperazine action was to measure swarming activity in a *chpD* mutant. For the *chpD::Tn* mutant the insertion site in the gene was at position 728 (795), which meant there was a possibility of residual activity within the transposon mutant. Therefore, a clean deletion was deemed necessary to properly assess the mutation phenotype. Professor Cynthia Whitchurch (Quadram Institute Bioscience, Norwich) kindly provided a  $\Delta$ *chpD* strain along with the PA01 WT background (referred to in this study as PA01 ATCC).

A deletion in *chpD* had no effect on the swarming of PA01 ATCC as seen in **figure 6.2**. The transposon mutant also displayed swarming activity and thus ChpD was revealed not to be the target of phenyl piperazines. It appeared from these swarming plates that ChpD is not involved in the regulation of swarming nor is there any reported effects of *chp* mutations affecting swarming motility in published literature, (although this was not a deterrent from investigating since so little was published). The transposon mutant when treated with NCI18<sup>1A</sup> was also inhibited of swarming activity. A test of the remaining mutants in the *chpABCDE* gene cluster for swarming motility would be an interesting and simple way to observe the independence or cross talk between the chemosensory signal transduction pathways.

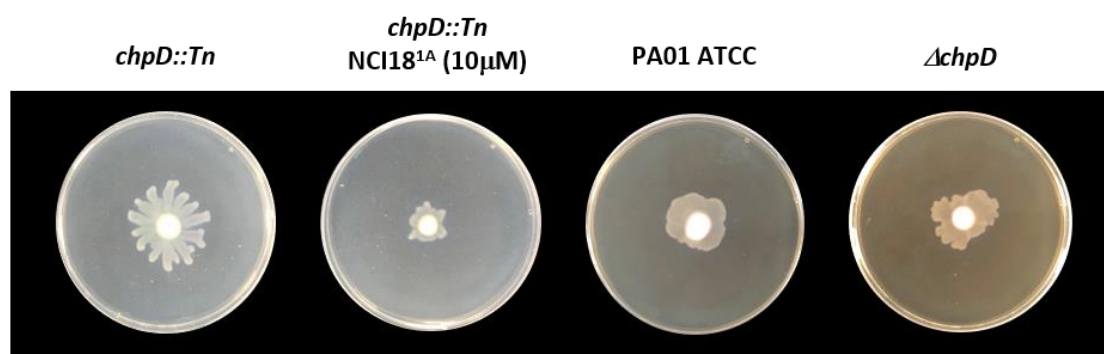


**Figure 6.2 *chpD* mutant swarming:** Normalised cultures of *chpD::Tn*, PA01 ATCC, and  $\Delta$ *chpD* were spotted onto swarming agar plates and incubated overnight at 37°C. *chpD::Tn* was also spotted onto NCI18<sup>1A</sup> treated plates (10μM). Images are representative of 3 independent experiments.

## 6.3 Further assessment of NCI18<sup>1A</sup> activity

### 6.3.1 Antibiotic susceptibility

An inability by PA and other pathogens to swarm has been reported to increase susceptibility to antibiotics, decreasing the minimal inhibitory concentration (MIC)<sup>[84, 312]</sup>. Knockouts of other virulence systems have also highlighted an increased sensitivity to antibiotics, whilst increased biofilm formation is heavily associated with resistance<sup>[12, 55]</sup>. Overnight cultures were diluted 100x in MH media in the presence of three antibiotics in a 2-fold serial dilution. MICs for gentamycin (aminoglycoside inhibitor of protein synthesis), ciprofloxacin (fluoroquinolone derivative inhibiting DNA replication), and meropenem (carbapenem drug disrupting cell wall synthesis) were calculated for PA01, *exsC::Tn*,  $\Delta$ *gacA*, and PA14 strains treated or untreated with NCI18<sup>1A</sup>.

**Table 6.1 Antibiotic susceptibility of *P. aeruginosa***

Strain	MIC (mg/mL)								
	Gentamycin			Ciprofloxacin			Meropenem		
	Control	DMSO	NCI18 <sup>1A</sup> (50 $\mu$ M)	Control	DMSO	NCI18 <sup>1A</sup> (50 $\mu$ M)	Control	DMSO	NCI18 <sup>1A</sup> (50 $\mu$ M)
PA01	1-2	1-2	1-2	$\leq 0.25$	$\leq 0.25$	$\leq 0.25$	4-8	4-8	4-8
<i>chpD::Tn</i> (PA01)	1	1	1	$\leq 0.25$	$\leq 0.25$	$\leq 0.25$	2-4	2-4	2-4
PA14	1	1	1	$\leq 0.25$	$\leq 0.25$	$\leq 0.25$	1-2	4	2-4
$\Delta$ <i>gacA</i> (PA01)	1-2	1-2	1-2	$\leq 0.25$	$\leq 0.25$	$\leq 0.25$	2-8	4-8	8

Ciprofloxacin had an MIC of  $\leq 0.25$ mg/mL to all strains in all conditions. PA01 WT resistance remained the same to each antibiotic under all conditions, not being affected by DMSO nor NCI18<sup>1A</sup>. An MIC of 1-2mg/mL was seen for gentamycin and 4-8mg/mL for meropenem.

The PA01 *chpD::Tn* strain was unchanged by DMSO or NCI18<sup>1A</sup>, but was more susceptible to both gentamycin and meropenem than the WT. For meropenem this was a clear 2-fold increase in sensitivity but, less abrupt for gentamycin with an MIC of 1-2mg/mL for WT vs 1mg/mL for the mutant. The mechanism for this increased sensitivity is unknown although it supports the validation of ChpD playing a role in antibiotic resistance in PA and should be investigated further.

Mutations to *gacA* are associated with reduced biofilm formation and hyper swarming. The PA01  $\Delta$ *gacA* strain was not conclusively shown to have increased resistance in the presence of NCI18<sup>1A</sup>. As with each strain results are reported from 3 independent experiments, meaning more repeats were needed to conclude on this result. Untreated repeats had an MIC of 2-8mg/mL however, no repeat had a resistance less than 8mg/mL when treated with compound. One repeat with DMSO had a lower MIC of 4mg/mL. NCI18<sup>1A</sup> therefore possibly increases resistance to meropenem, although more work is required to be sure. The MIC of PA14 was unchanged in gentamycin but increased in meropenem, however the 2-4-fold increase was seen in the DMSO control meaning the results cannot be attributed to compound activity. Having established that ChpD was not the target of the phenyl piperazine compounds, an interesting observation was that across 3 large studies screening for increased antibiotic resistance in PA, the PA2332 gene discussed in the previous chapter (section 5.3.2) is not listed on any as increasing resistance<sup>[331-333]</sup>.

From these experiments NCI18<sup>1A</sup> appears to have no effect on the antibiotic susceptibility of PA. Nevertheless, additional testing of MICs should be carried out for phenyl piperazine compounds under swarming conditions as this would be further evidence of a swarming specific target, expressed or active under swarming conditions. The role of ChpD in carbapenem resistance should also be explored, testing more carbapenem antibiotics. Clinical isolates with mutations in *chpD* would be extremely interesting to study in this aspect along with clinical outcomes. Chemotaxis can act as an evasion mechanism for cells directing it away from antibiotics or other unfavourable environmental conditions. This point makes it even more important to test this clinically relevant phenotype.

### 6.3.2 Transmission electron microscopy (TEM) imaging

TEM is most commonly used in biology to image stained samples utilising the short wavelength of electron beams to achieve sub nanometre resolution as contrast is created from the absorption and scattering of electrons<sup>[334]</sup>. TEM for this project was done at the University of Cambridge core facility, CAIC with the help of Dr. Rita Monson (Department of Biochemistry). Carbon coated copper discs were argon glow discharged by the CAIC before samples were attached. To load samples on to the discs 10 $\mu$ L of sample was spotted onto a wax surface and the disc placed in the culture for 5mins before washing 3x with HPLC water and a final 2min 30s staining with uranyl acetate. Conditions and strains imaged were as follows: PA01 in LB (planktonic) with and without NCI18<sup>1A</sup> (10 $\mu$ M), PA14 in LB (planktonic) with and without NCI18<sup>1A</sup> (10 $\mu$ M), and PA14 taken from the dendritic tip of a swarming colony on a swarming plate with and without NCI18<sup>1A</sup> (10 $\mu$ M). **Figure 6.3** represents images of each condition.

In planktonic culture PA01 were uniform in size and appearance. Cells were flagellated and around 1.5-2 $\mu$ m in length (cells measured in ImageJ software). This was comparable to the compound treated samples which were also flagellated. A noted observation was that cells seemed to have a prominent collapse or depression in the cell wall at the cellular poles; a subjective observation that was not absent in control samples but stood out during the image capturing process. PA14 planktonic samples yielded the same results, with both treated and untreated cells being flagellated with depressions at the cellular poles. The cell macrostructure was otherwise unchanged with no identifiable features that suggested compound activity.

Under swarming conditions, the characteristic elongation of cells and hyper flagellation<sup>[314, 335, 336]</sup> could be seen in the control sample however, a dramatic observation was the absence of flagella in the compound treated sample and neither was there the obvious elongation of cells. PA lacking fully formed flagella have been shown to cause no mortality and be 75% less likely to cause pneumonia in mice<sup>[337]</sup>. These images attest to the phenyl piperazine target being essential for the expression of flagella in PA under swarming conditions, but not in planktonic culture. The images show the flagella debris scattered around the cells in the untreated samples as well as their presence at the cell poles. Almost no complete flagella were seen in the compound treated samples with only some small fragments of flagella scattered or present, indicated in **figure 6.3**.

No pili were observed in any of the images which was an interesting observation given that several studies have shown swarming to require T4P<sup>[84, 298, 314, 338]</sup> but this is somewhat of a confusing area as a host of studies contradict this<sup>[314, 336, 339]</sup>, including these results. Here I present evidence that PA01 and PA14 are capable of swarming independently of T4P.

The observations from the TEM images were a significant breakthrough in elucidating a mechanism for the phenyl piperazine compounds and shed light on why no activity was seen in assays conducted in planktonic conditions. It heavily supports a target expressed or active only under swarming conditions as previously mentioned, but which is essential for the expression of flagella. As previously mentioned expression of flagellar is regulated in a 4-tiered hierarchy system, pictured in **figure 6.3**. FleQ is the master transcriptional regulator, externally negatively influenced by Vfr but positively regulated by  $\sigma^{70}$ <sup>[288, 340]</sup>. FleN inhibits FleQ post-translationally and losses of FleN result in increased numbers of polar flagella<sup>[288, 340]</sup>. Class II genes require both FleQ and RpoN for activation and include genes encoding the basal body, motor and export apparatus<sup>[288, 340]</sup>. Class III require FleQ, RpoN and FleR and encode the hook proteins, whilst class IV are transcribed after FliA activation and include the *fliC* gene encoding flagellin which makes up the length of the flagella<sup>[288, 340]</sup>.

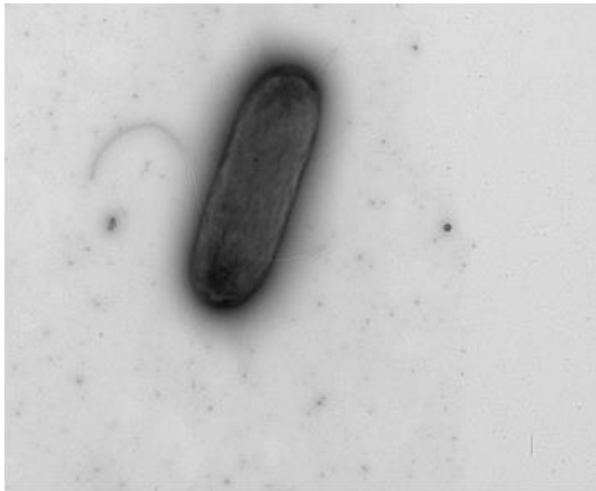
Whilst not usually specified, swimming and swarming flagella are not identical in their structure in PA. Studies have identified two different stators in the flagella to which mutations can cause loss of motility and biofilm formation<sup>[293, 341]</sup>. The stator is the stationary component of the flagella motor that helps generate torque for the flagella to rotate and variations amongst organisms allow activity in different salt, pH and viscosity conditions<sup>[342]</sup>. These studies found that either stator was sufficient for swimming in PA but that both were required for swarming motility. The two stators, MotAB and MotCD when deleted independently or as a pair did not result in a loss of flagella<sup>[293]</sup>, but a dual deletion or a single deletion of MotCD meant PA14 was unable to swarm on 0.5% agar<sup>[293]</sup>. Toutain *et al.*, (2007) reported that a mutation in either MotAB or MotCD impaired biofilm formation without affecting swimming. More recent electron cryo-tomography studies have also revealed that differences in structure pertain to evolutionary adaption such as increased stability to handle the greater viscosity PA would encounter in a pulmonary environment<sup>[342]</sup>. TEM images in Toutain *et al.*, 2005 revealed the flagella to be present in  $\Delta$ *motAB*,  $\Delta$ *motCD* and  $\Delta$ *motABDCD* mutants meaning that these are

not the targets of phenyl piperazine compounds. However, the importance of these findings lies in identifying swarming specific variants of flagella structural components essential for function. It is possible that a yet unknown target or regulator necessary for swarming but not swimming exists in the biosynthesis of PA flagella most likely at the lower Class III or Class IV level.

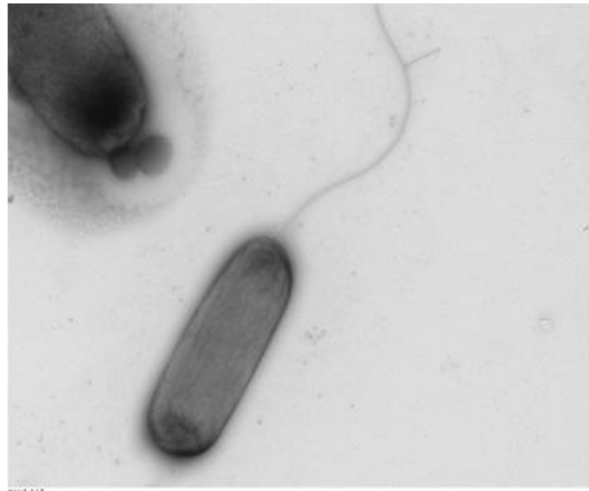
Unfortunately, it was not clear from these images whether the hook basal body is present in the compound treated cells which has significance for the level of hierarchy interruption. The presence of flagella in planktonic culture and partial fragments in compound treated samples suggests it may not be the prevention of hook basal body assembly nor of FliC expression which makes up the flagellin, but interruption of secretion by interference with a regulator or possibly structural component that is present or active specifically in swarming flagella. I therefore propose a hypothesis that NCI18<sup>1A</sup> and other phenyl piperazine compounds interrupt the latter stages of flagella biosynthesis by targeting a process independent or redundant for swimming motility.

Some interesting work by Jyot *et al.*, (2007) has proposed that accumulation of FlgM, (the repressor of FliA) due to proteolytic activity by neutrophils on the hook (FlgE), which is required for FlgM export, resulted in flagellin downregulation. The hook is regulated by Class III regulators<sup>[288]</sup> and nominates this component as being possibly involved in this investigation. This however is merely conjecture at this stage picked out from a thorough assessment of the relevant literature and more work must be done to verify what is happening at the molecular level.

### PA01 (planktonic)



pa01.tif  
Cat: 0.001574 nm/pix  
15:27:22 09/15/20  
500 nm  
HV-200.0KV  
Direct Mag: 4500x  
X=8.22944 Y=17.82288 T:0.00

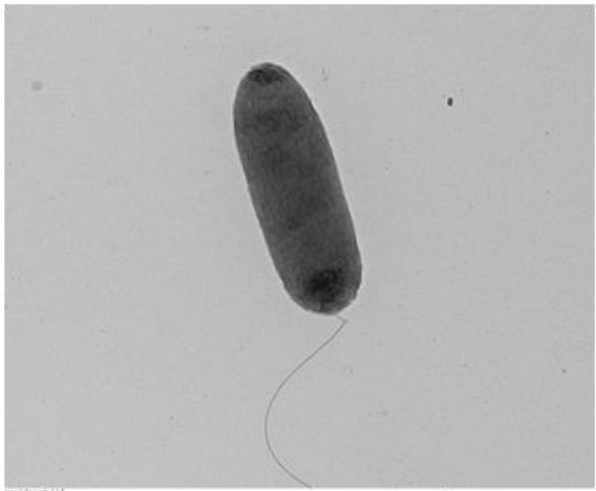


pa01.tif  
Cat: 0.001574 nm/pix  
15:28:22 09/15/20  
500 nm  
HV-200.0KV  
Direct Mag: 4500x  
X:174.1428 Y=-27.89434 T:0.00

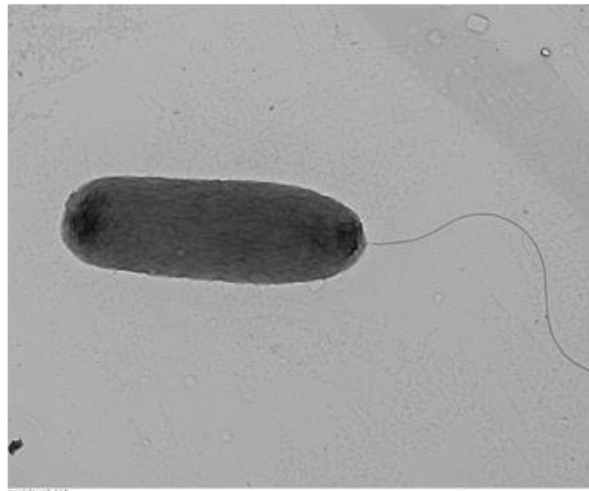


pa01.tif  
Cat: 0.001574 nm/pix  
15:28:38 09/15/20  
500 nm  
HV-200.0KV  
Direct Mag: 4500x  
X:215.0848 Y=-34.05588 T:0.00

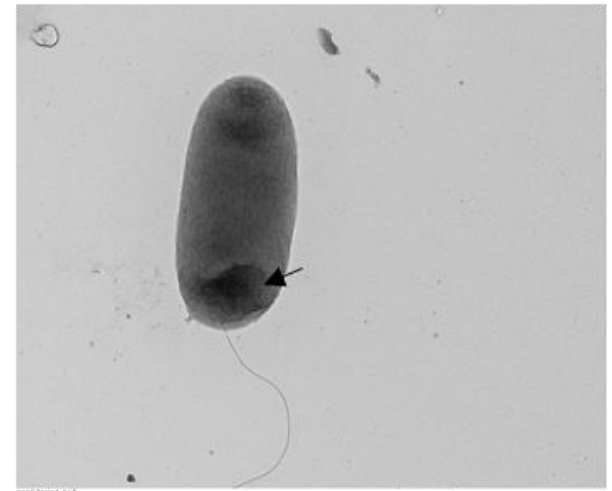
### PA01 + 10 $\mu$ M NCI18<sup>1A</sup> (planktonic)



pa01.tif  
Cat: 0.001574 nm/pix  
15:38:58 09/15/20  
500 nm  
HV-200.0KV  
Direct Mag: 4500x  
X=-75.88452 Y=104.84352 T:0.00

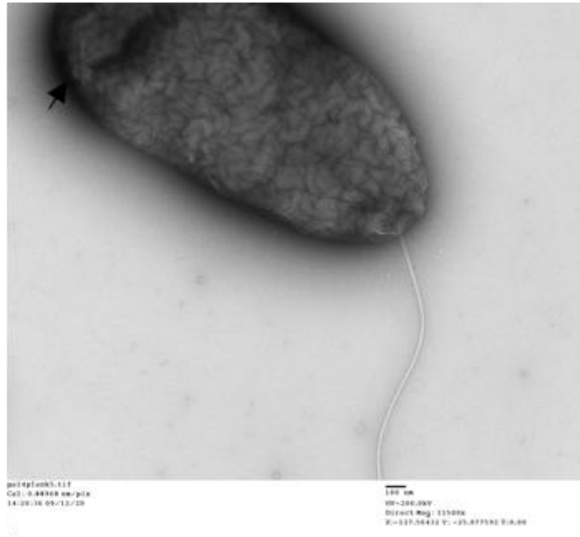


pa01.tif  
Cat: 0.001574 nm/pix  
15:49:04 09/15/20  
500 nm  
HV-200.0KV  
Direct Mag: 4500x  
X=-53.8848 Y=145.81248 T:0.00

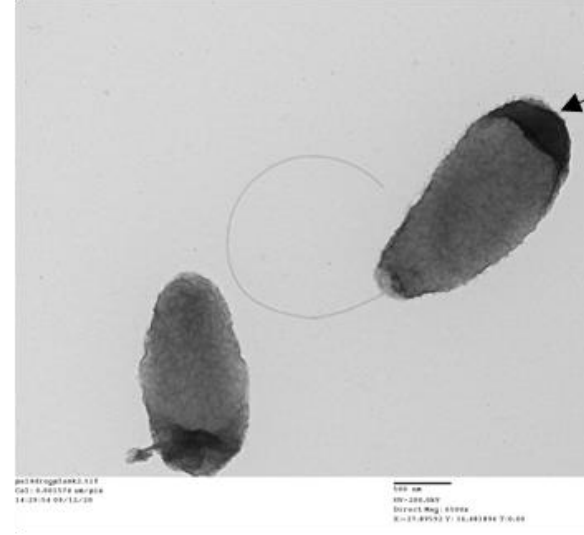


pa01.tif  
Cat: 0.001574 nm/pix  
15:48:34 09/15/20  
500 nm  
HV-200.0KV  
Direct Mag: 4500x  
X=-62.88154 Y=131.81248 T:0.00

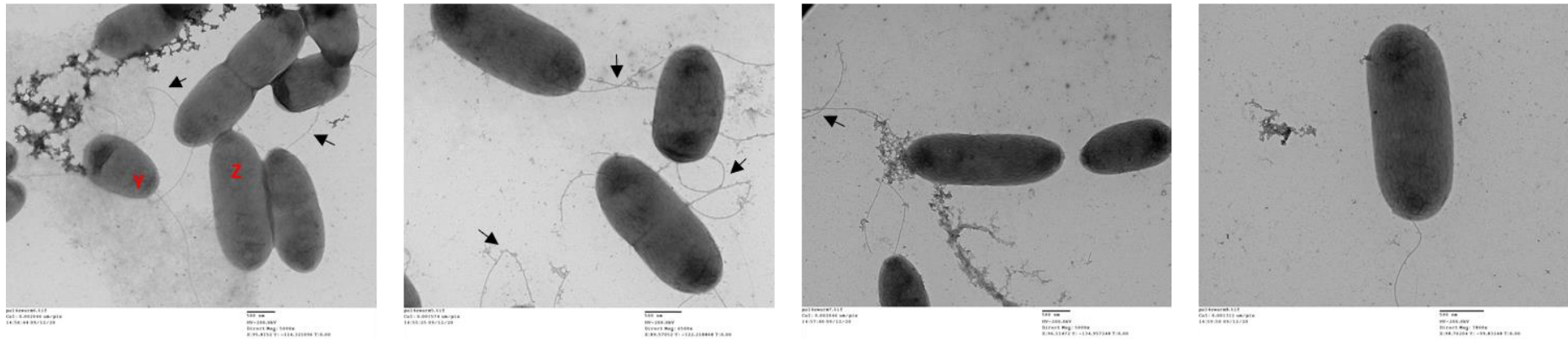
**PA14 (planktonic)**



**PA14 + 10 $\mu$ M NCI18<sup>1A</sup> (planktonic)**



### PA14 (swarming)



### PA14 + 10 $\mu$ M NCI18<sup>1A</sup> (swarming)

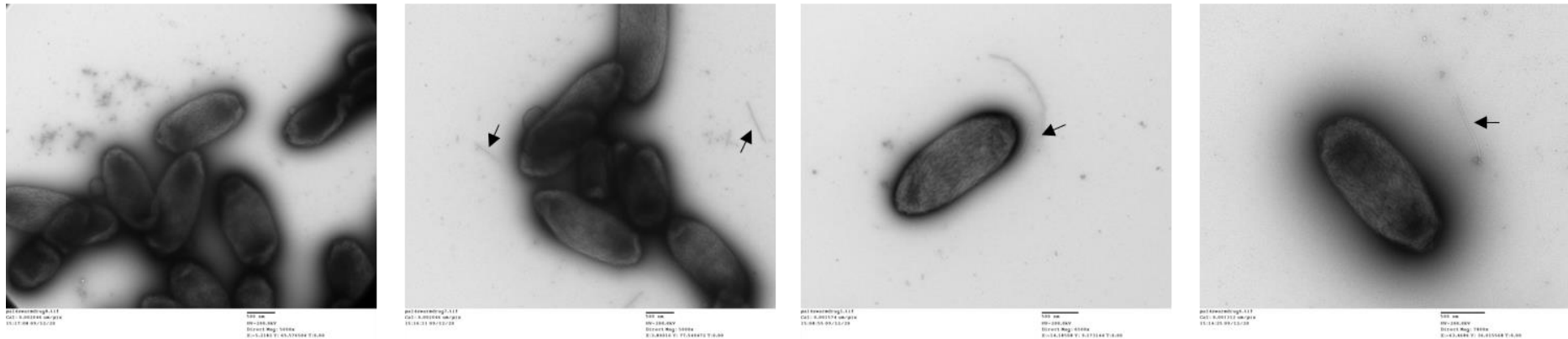


**Figure 6.3 TEM images of *P. aeruginosa* in planktonic and swarming conditions treated with NCI18<sup>1A</sup>:** TEM images were captured of PA01 and PA14 planktonic cultures (LB), and PA14 swarming cultures (swarming agar plate) with and without treatment with NCI18<sup>1A</sup> (<1% v/v in growth media or plate agar). Swarming cells were taken from the edge of a dendritic projection and from edge of colony growth in absence of swarming from NCI18<sup>1A</sup> (10 $\mu$ M) treated plate. Arrows in planktonic images indicate depressions at the cellular poles. Arrows in swarming plate images indicate hyper flagellation in untreated sample and flagellin fragments in treated sample. Cells labelled Y and Z highlight elongation of cells during swarming.

### 6.3.3 Acute *P. aeruginosa* infection model

NCI18<sup>1A</sup> outperformed NCI18 in both the initial toxicity screen and the CPA with no observable LDH release and a 15x greater potency for preventing PA mediated cytotoxicity. An acute infection model using *Galleria* was repeated as before with 30 larvae for each condition split across 3 groups of 10, each injected from 3 single colony PA01 overnights diluted ( $10^3$ ) from OD<sub>600</sub> 0.1. Larvae were given 5 $\mu$ L of 1 $\mu$ M NCI18<sup>1A</sup>, an equivalent dose of ~19mg/kg. One control larvae in the PBS group died during the experiment.

12 larvae died in the compound only control group displaying a level of toxicity not seen in the initial toxicity screen assay against A549 epithelial cells, nor in the original compound, NCI18. This was a disappointing result given the improved efficacy in the CPA and the nanomolar inhibition in the swarming assays. With regards to this nanomolar efficacy *in vitro* it would be desirable to repeat this model at a lower dosage to observe efficacy. A therapeutic window was not discussed in the results section of the dose response curves due to an absence of toxicity displayed by the compounds but, having now seen deaths in the acute model an LD<sub>50</sub> could be established and a therapeutic index determined *in vivo*. A therapeutic index is the ratio between efficacious and toxic drug doses calculated by LD<sub>50</sub>/ED<sub>50</sub>. In humans since we cannot establish an LD<sub>50</sub> a toxic dose is used indicated by symptoms (TD<sub>50</sub>). A visual representation of the therapeutic index is seen in **figure 6.4**.

Despite deaths occurring in the compound control group the deaths in the compound treated infection group were not over and above those in the untreated infection group, with no statistical difference as determined by Log-rank (Mantel Cox) test.

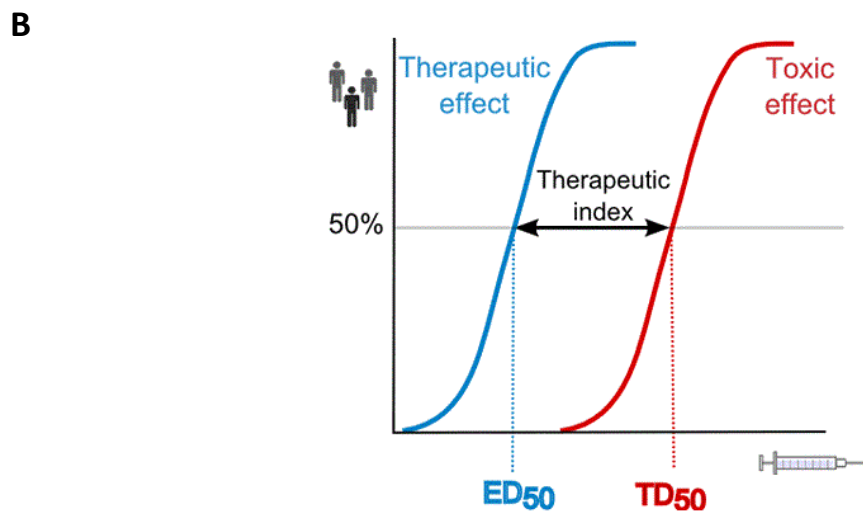
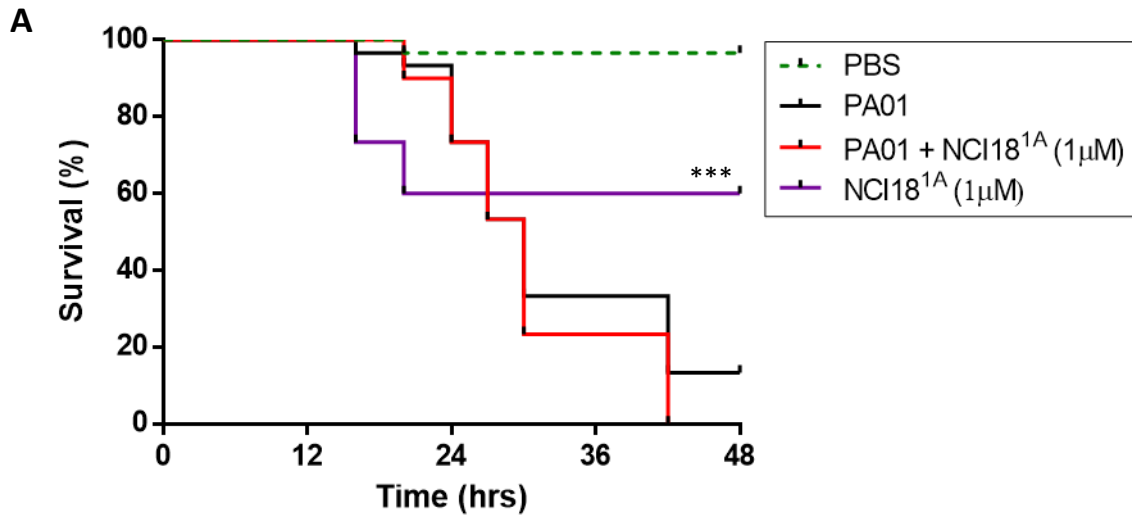


**Figure 6.4 PA01 *G. mellonella* infection model treated with NCI18<sup>1A</sup>:** Each larvae received two injections: 10μL of PA01 (PBS vehicle, 0.5mg/mL rifampicin, CFU/mL quantified) or PBS vehicle (0.5mg/mL rifampicin), and 5μL of NCI18<sup>1A</sup> (PBS vehicle, 1μM) or PBS vehicle. \*\*\* indicates  $p = 0.0005$  as determined by Log-Rank (Mantel-Cox) statistical analysis in GraphPad Prism 6.0 (PBS vs NCI18<sup>1A</sup> group). 30 larvae were used per condition with 10 larvae injected per overnight culture. Results are the combined survival of all 30 larvae in each condition. No trauma, PBS vehicle mock injections, and NCI18<sup>1A</sup> control groups were used. No larvae in no trauma control group died. **(B)** Schematic representation of how a therapeutic index is calculated by the LD<sub>50</sub>/ED<sub>50</sub> in animals or the TD<sub>50</sub>/ED<sub>50</sub> in humans indicating a dose range in which a treatment is therapeutically useful.

## 6.4 Characterisation of ChpD mutants

### 6.4.1 Growth of the *chpD* transposon mutant

The growth of *chpD::Tn* was unchanged compared to that of a WT in an *in vitro* growth curve measured by OD<sub>600</sub>. No effects on growth are reported in the literature concerning mutations to the *chp* gene cluster and mutants grew equal to WT rates within *Drosophila*<sup>[318]</sup>. There is also no proposed role for *chp* affecting growth and these results support this notion.

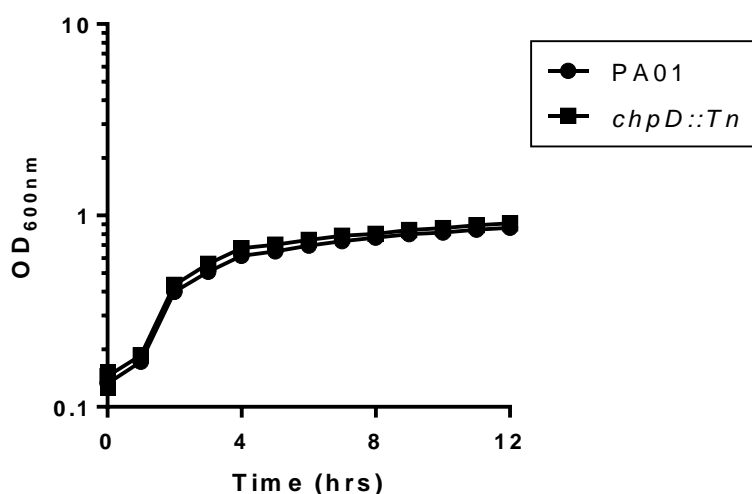


**Figure 6.5 Growth of PA01 vs *chpD::Tn*:** Overnight cultures of PA01 and *chpD::Tn* were normalised to OD<sub>600</sub> 0.05 and grown shaking (500rpm, 37°C) until stationary phase. Figure is representative of 3 independent experiments.

### 6.4.2 *chpD* mutant twitching phenotype

Twitching motility as in previous experiments was conducted by pipetting normalised overnight culture to the base of 1% LBA plates and incubating overnight. Twitching motility was determined as the greatest diameter across the twitching zone measured after crystal violet staining. In line with results seen by Whitchurch *et al.*, (2004), no difference was observed in twitching between  $\Delta$ *chpD* and the WT, also supported by no change in twitching between the transposon mutant strain and its WT background. This result confirms that ChpD is not required for twitching motility. Only a *chpA* mutant was reported to have reduced twitching motility in Whitchurch *et al.*, (2004) with all other mutants in the *chp* gene cluster exhibiting WT twitching motility.

**Table 6.2 *chpD* mutant twitching**

Strain	Ø (mm) ±SD
PA01	32.3 ±2.08
<i>chpD::Tn</i>	33 ±1
PA01 ATCC	26.8 ±2.79
Δ <i>chpD</i>	26.5 ±5.1

### 6.4.3 ChpD is required for full virulence *in vivo*

As for the other *G. mellonella* killing assays in this project, larvae were injected with  $10^3$  diluted cultures from OD<sub>600</sub> 0.1 suspended in PBS with 0.5mg/mL rifampicin. 30 larvae were used in each condition including no trauma and PBS controls. The bacterial loads of WT and *chpD::Tn* strains were checked by CFU and found to be equal to previous experiments. Survival in *chpD::Tn* infected larvae was significantly longer than WT infected larvae ( $p < 0.0001$ ) as determined by GraphPad Prism 6.0 Log-rank (Mantel Cox) survival analysis.

This result revealed ChpD to be essential for the full virulence of PA in *G. mellonella*. D'Argenio *et al.*, (2001) demonstrated in killing assays of the fruit fly, *Drosophila melanogaster* that mutations in the *pil-chp* gene cluster necessary for twitching reduced PA virulence however, twitching was also shown not to be required for full virulence of PA pushing the authors to speculate that the cluster is involved in expressing unknown virulence factors. The insertion sites in the *chp* cluster during this study were all in *chpA*, the insertion sites appear in **figure 6.6** taken from the paper. It is noted it was not known how the inserts affected the rest of the cluster but *chpA* is required for normal twitching motility<sup>[317, 318]</sup>.

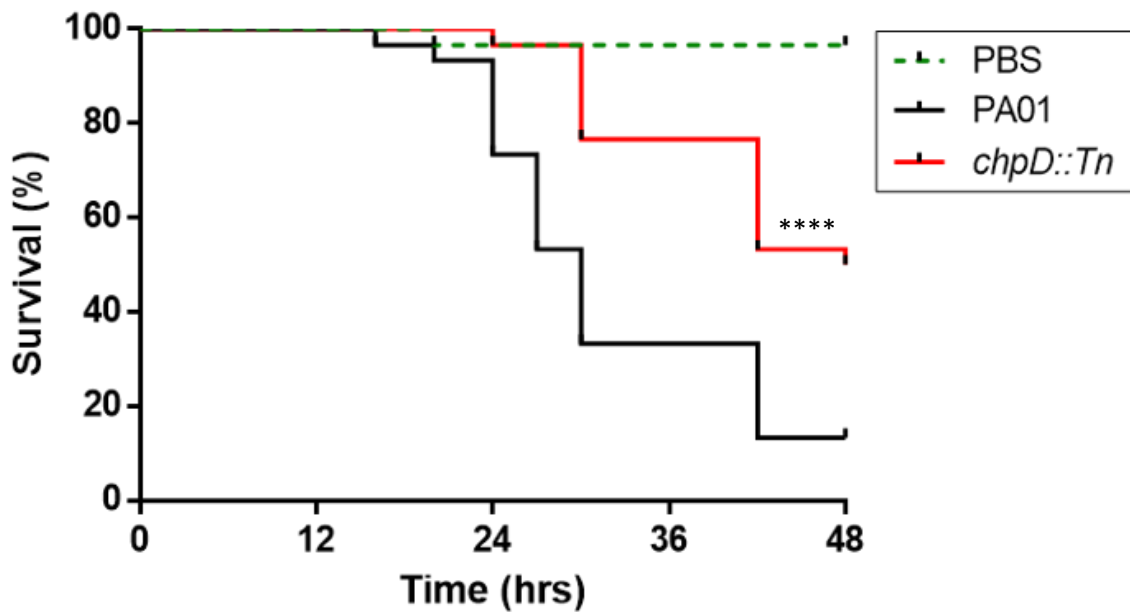


**Figure 6.6 *chpD* mutant *G. mellonella* infection model:** Larvae were injected with 10 $\mu$ L of PA01 or *chpD::Tn* (PBS vehicle, 0.5mg/mL rifampicin, CFU/mL quantified). \*\*\*\* indicates  $p < 0.0001$  as determined by Log-Rank (Mantel-Cox) statistical analysis in GraphPad Prism. 30 larvae were injected with each strain with 10 larvae injected per overnight culture. Results are combined survival of all 30 larvae for each strain after 48hrs. Control groups contained 30 larvae receiving no injection or a PBS vehicle (0.5mg/mL rifampicin) mock injection. No larvae in no trauma control group died.

Consequently, since *Drosophila* killing is independent of twitching and growth rate within the fly was also equal to WT in *chpA* mutants these mutations must cause a delay in killing via a separate mechanism. Whitchurch *et al.*, 2004 also proved that the *chp* system was required for full virulence in a murine model where *chpD* mutants were unable to colonise the liver as effectively as WT. A couple of hypotheses can be put forward for the involvement of *chpD* in virulence. The first is that it regulates the *chp* cluster itself, but no effector molecule or target genes are known<sup>[314, 317]</sup>. The second is that it transcribes unknown virulence factors and acts independently of the cluster. This initially seems unlikely as, except for *chpE*, the cluster is thought to be transcribed as an operon<sup>[314]</sup>. T4P have more than one function though and mentioned in section 5.4 is the role of host cell contact dependent cellular response. By having a potentially global virulence factor associated within a cluster responsible for host cell and surface recognition and attachment it would allow PA to have a robust and rapid response to improve its chances of occupying an ecological niche.

Since the *chp* system serves to complex a lot of MCPs to the histidine kinase ChpA the signal transduction pathway can respond to a large number of chemotactic stimuli, an area which is very poorly understood. Virulence related consequences transpire as a result of these responses to the environment that are not directly related to twitching. For instance, *pilD* encodes the primary peptidase which coordinates components of both the T4P and the type II secretion system (T2SS), whose substrates include phospholipase C, elastase, and exotoxin A<sup>[318]</sup>. It was extremely surprising therefore to see that a *pilD* mutant was unimpaired for killing of *Drosophila*<sup>[318]</sup>. Having established ChpD as an essential component of PA virulence, some factors likely to be involved were explored in a similar manner during the investigation of phenyl piperazine activity.

#### 6.4.4 *chpD* mutant swimming motility

The *chpD* transposon mutant displayed no changes to swimming activity under assay conditions. This was unsurprising and it reinforces the notion that there is no cross talk or co-dependency between *che* and *chp* signalling pathways, nor that ChpD plays a role in swimming flagella biosynthesis or function. Assays were conducted as previously by inoculating normalised cultures into swimming agar and incubating overnight.

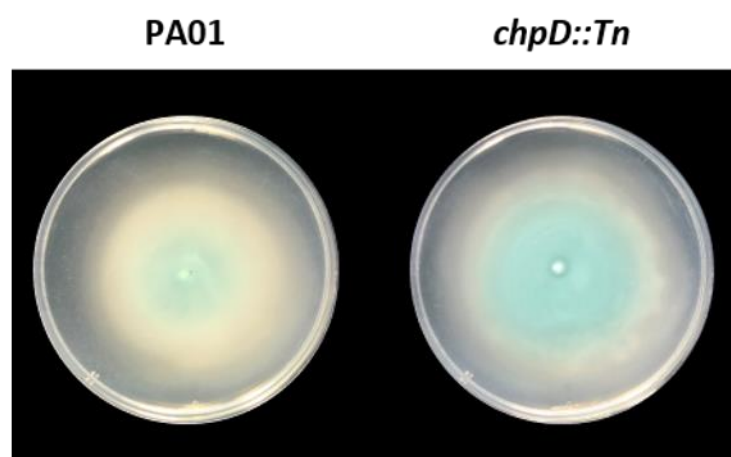


**Figure 6.7 *chpD* mutant swimming motility:** Normalised cultures of PA01 and *chpD::Tn* were inoculated into the centre of swimming agar plates and incubated overnight (37°C). Image are representative of 3 independent experiments.

#### 6.4.5 *chpD* mutation effects on QS

QS assays were repeated as in section 5.3.4 with overnight flask cultures grown for 12-16hrs to stationary phase before normalisation, followed by the filtered secretome samples being incubated for 3-4hrs with biosensor strains grown to mid-log phase. The experiments revealed that none of the QS molecules were significantly changed in the *chpD* deletion mutant compared to the WT. One-way ANOVA tests with Dunnett's post hoc analysis revealed significant differences only between control groups, but not PA01 and  $\Delta$ *chpD* (GraphPad Prism 6.0).

A recent publication showed that surface association of PA sensitises the cells to QS allowing the population to respond more robustly during important times of need, such as an infection scenario<sup>[344]</sup>. It was revealed that LasR is upregulated when surface associated and that LasR targets were induced more strongly in response to autoinducer by surface associated bacteria than those in planktonic cultures<sup>[344]</sup>. The experiments suggested a cap on the planktonic response with some LasR targets capable of activation in planktonic culture at low LasR levels, but a surface associated threshold was required to activate other LasR targets<sup>[344]</sup>. Several factors are known to influence LasR transcription including the cAMP dependent virulence regulator, Vfr<sup>[281, 308]</sup>. Surface recognition and association implicates T4P in all cases with virulence factor expression initiated by cAMP and Vfr, or c-di-GMP through PilY1<sup>[344-347]</sup>. Surface association is a non-twitching related role of T4P which links back to section 6.4.3 and the suggestion of alternative roles for this system. It would be worth repeating this assay under surface associated conditions to replicate work in Chuang *et al.*, (2019) and it would be fascinating to observe any involvement by ChpD as mysteries surrounding the *chp* system and virulence begin to be probed.

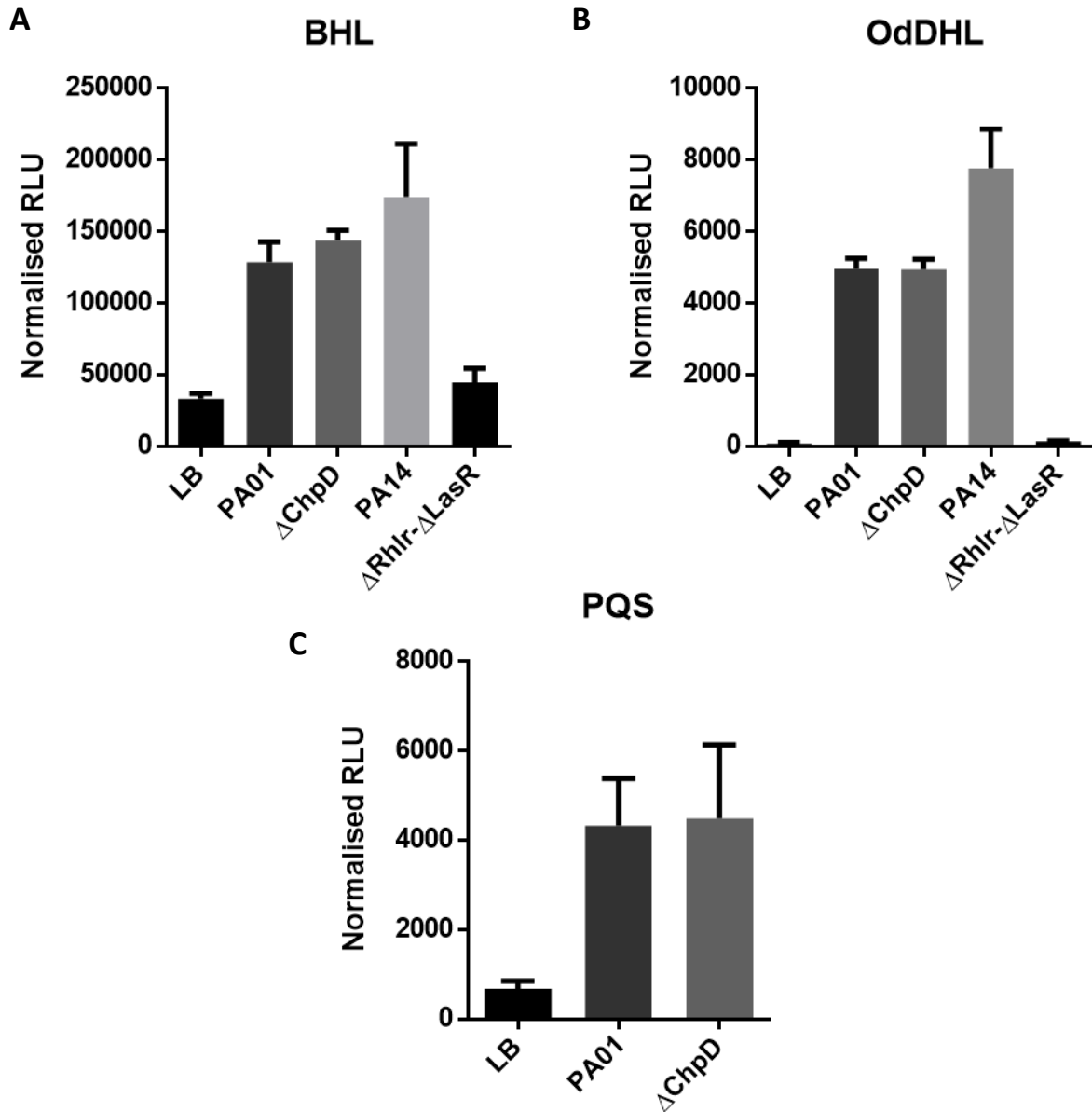


**Figure 6.8 *ΔchpD* mutation effects on QS:** Production of QS molecules (OdDHL, BHL, and PQS) was measured by incubation of stationary phase supernatants with mid log phase biosensor strain cultures for 3-4hrs. Control strains of PA14 and double deletion mutant *ΔrhlR-ΔlasR* were used for OdDHL and BHL detection. Bars represent means  $\pm$ SEM of 3 independent experiments. (A) BHL detection. (B) Detection of OdDHL. (C) Detection of PQS.

#### 6.4.6 Evaluation of protease activity

Proteases cleave peptide bonds and milk can be used to test non-specific protease activity; containing casein acting as the primary substrate that upon being cleaved by proteases the milk loses opacity as the resulting smaller products are more soluble. A test for changes in protease activity between the WT and the *chpD* transposon mutant strain revealed no differences in the level of activity. Repeating this experiment using a *pilD* mutant would be interesting to observe whether a reduced rate of activity would be seen since the mutant was unimpaired for killing in *Drosophila*, yet as mentioned in the previous section it encodes the primary peptidase components of the T2SS. This assay is a non-specific test and lower level regulation of particular proteases are unlikely to be identified relative to higher level regulation interruption, such as with mutations in *rhIR* that have been previously discussed in section 5.2.1. Given this result it was concluded that the reduction in virulence during the acute *G. mellonella* infection model was not due to decreases in protease activity as a result of *chpD* mutation.

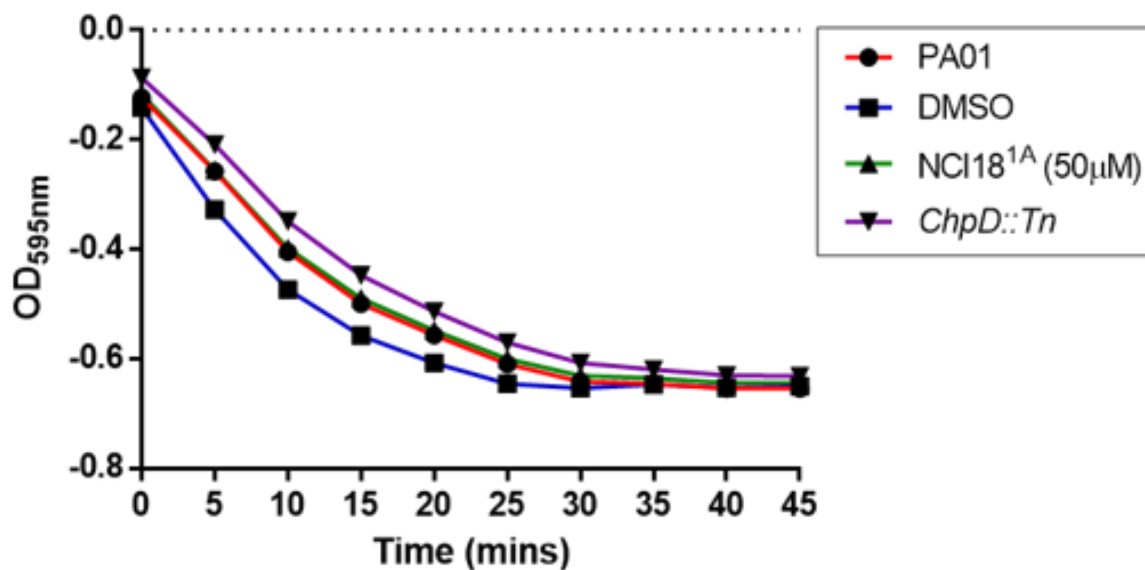


**Figure 6.9 Protease activity of the *chpD* transposon mutant:** Normalised supernatant samples of overnight flask cultures were measured for protease activity by changes to OD<sub>595</sub> when mixed with 1.5% milk solution. DMSO and NCI18<sup>1A</sup> were added to growth cultures (<1% v/v). Results were normalised to LB only controls. Data is representative of 3 independent experiments.

#### 6.4.7 *chpD* mutant secretome profile analysis

A further effort to find the mechanism by which *chpD* mutations cause a loss of virulence *in vivo* was done by analysing the secretome profiles of PA01 ATCC and the  $\Delta$ *chpD* mutant. Overnight flask cultures were grown and normalised before being pelleted and filtered. TCA precipitation was then used to concentrate the samples and they were separated by 12% SDS-PAGE. Three distinct changes could be seen on the gel. There was a downregulation of a large protein (~100kDa) and upregulation of two smaller proteins (~30kDa and ~20kDa). The three bands, indicated in **figure 6.10**, were submitted for LC-MS/MS analysis at the University of Cambridge Biochemistry Proteomics Core Facility.

The first band (band 1, **figure 6.10**) of ~100kDa was determined to be IMPa, an immunomodulating metalloprotease encoded by the gene *impA*. This protein has a prominent role in managing PA evasion of phagocytosis by neutrophils during infection by cleaving P-selectin glycoprotein ligand-1 (PSGL-1) on neutrophils<sup>[348]</sup>. The first step in neutrophil activity to fight infection is recruitment to the site of infection. This is coordinated by the interaction between P-selectin present on the surface of endothelial cells and PSGL-1 on neutrophils<sup>[348]</sup>. The binding event triggers extravasation of neutrophils to the infection site and by inhibiting this recruitment process, PA can avoid phagocytosis. IMPa was also shown to cleave CD44 on macrophages<sup>[348]</sup>. A very recent study revealed that *impA* is under regulation of ExsA with an ExsA promoter sequence upstream of the gene and binding was confirmed by EMSA[349]. This work established a novel ExsA regulated virulence factor and the cooperative inhibition of macrophages and neutrophils by the two systems. This raises the question as to which of the regulators, ExsA or ChpD, is the more dominant regulator of *impA* assuming that it is under direct transcriptional control of ChpD. Measuring the expression of IMPa in an  $\Delta$ *exsA*, a  $\Delta$ *exsA*- $\Delta$ *chpD*, and complemented mutants in addition to identifying ChpD promoter sequence regions would be revealing to their regulatory control. Mutations to T2SS machinery genes resulted in the loss of IMPa secretion suggesting it is a substrate of the T2SS<sup>[350, 351]</sup>.

Unfortunately, the second two bands were not as clear in their distinction of which proteins were upregulated. Band 2 gave hits for elastase, B-type flagellin, aminopeptidase, and chitin-binding protein D (CbpD). Within the thicker upregulated bands there are almost certainly multiple proteins since separation is only by mass meaning it is difficult to single out an individual protein from this list. LC-MS/MS analysis would be needed on multiple gels to

confirm in addition to western blot analysis. Based on the size of the bands the most likely candidate is probably CbpD. This is because in its full form it is a 43kDa protein that is cleaved by elastase into smaller fragments. These fragments include a 30kDa and a 23kDa fragment which aligns with the migration distances on the gel. Whether it is CbpD or not, these proteins are associated with or are secreted factors of the T2SS (except B-type flagellin), which is consistent with a link between the *pil-chp* system and the T2SS, as seen in the *pilD* mutant. Interestingly these factors are seen to be upregulated in the mutant and yet virulence is reduced in the infection model. This would support that loss of ChpD activity causes an upregulation of T2SS related factors, but that proteases do not play a role in virulence during PA infection of *Galleria*. Protease independent killing of *Galleria* is in fact supported by a study where protease deficient mutants (elastase knockout, assessed for absence of activity prior to infection models) had an equivalent LD<sub>50</sub> to WT<sup>[352]</sup>. The third band was also flagged as CbpD, elastase, and B-type flagellin, further supporting the likelihood that CbpD is the primary upregulated protein seen on the gel.

Given the results presented in this section, it is likely that *chpD* has a role in the regulation of the T2SS, possibly governed through sensing by the T4P via the *pil-chp* signal transduction pathway. Also, that the loss of virulence in *G. mellonella* infection models is not due to increased protease activity but due to a loss of perturbing host immune response, specifically recruitment of neutrophils and macrophages (or in the case of *G. mellonella*, haemocyte equivalents). How this relates to colonisation of the liver in murine models remains unknown and more research is required to confirm these findings.

An NCI18<sup>1A</sup> treated sample was also examined by SDS-PAGE although no changes in the secretome were apparent. This is probably due to the seeming absence of activity by the compound under planktonic conditions since flagella were present in the TEM images under such conditions, but not when taken from a swarming plate.

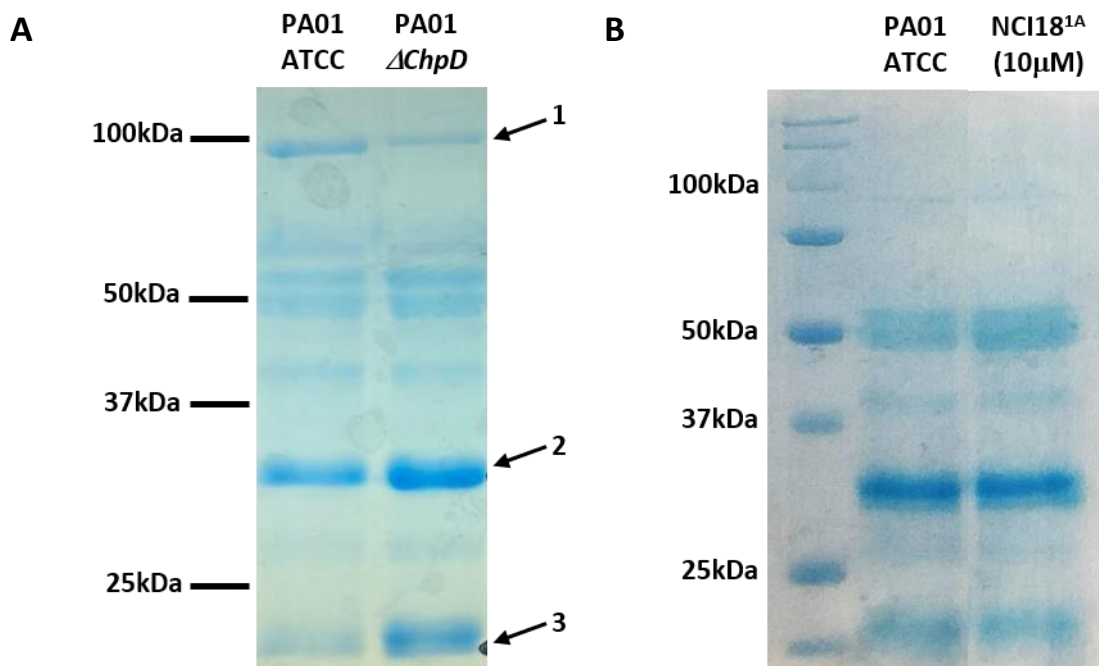


**Figure 6.10 Secretome analysis of  $\Delta chpD$  mutant and NCI18<sup>1A</sup> treated cultures:** Normalised secretome samples of PA01 ATCC,  $\Delta chpD$ , and PA01 ATCC NCI18<sup>1A</sup> treated (10 $\mu$ M, <1% v/v) cultures were separated by 12% SDS-PAGE. Bands indicated in gel A (**1**, **2** and **3**) were submitted for LC-MS/MS analysis. (A) Gel containing PA01 ATCC and  $\Delta chpD$  mutant secretome samples. Band **1** was determined to be IMPa. Bands **2** and **3** were most likely the cleaved products of chitin binding protein, CbpD. (B) Gel containing PA01 ATCC control and NCI18<sup>1A</sup> treated sample. Images are representative of 2 independent experiments.

## 6.5 Conclusion and future directions

### 6.5.1 Conclusion

With the hastening approach of an antibiotic resistant era, PA remains a major global concern for antimicrobial resistance related deaths. Its prevalence and adaptability have allowed it to capture a significant proportion of nosocomial infections and be placed on the WHO's highest priority list. While breakthroughs are yet to be seen in the development of novel antibiotics, attention has been turned to new approaches for combating infections, notably targeting virulence systems. In acute infection scenarios the T3SS has been shown to be the primary virulence factor associated with higher mortality and worse clinical outcomes for patients<sup>[52]</sup>. The study of this system has been the focus of much anti-virulence targeting based research in recent years with some progress in the discovery and development of small molecule and antibody therapies in attempts to tackle PA<sup>[52]</sup>.

This study began by attempting to build on previous work which identified N-hydroxybenzimidazoles as the only known inhibitors of ExsA - the master transcriptional regulator of the T3SS<sup>[117]</sup>. Mutations to the *exsA* gene are well established in significantly reducing virulence and therefore has validated the regulator as a drug target, with the added benefit of no mammalian homologues existing of the AraC/Xyls family of proteins. Varying levels of success have also been shown targeting related transcriptional factors, such as ToxT using similar rational drug development techniques<sup>[251, 254, 255]</sup>.

Early work in this project encountered typical problems when working with transcription factors and unsolved structures. Purification strategies of ExsA were tedious to optimise and low yielding, whilst *in silico* docking experiments were difficult to quantify for accuracy or extrapolate useful SAR knowledge from without high quality full length structural models of ExsA. Nevertheless, early binding experiments gave positive results with 2 compounds having high affinity for ExsA. Disappointingly, despite this reasonably good binding affinity and early efficacy *in vitro* during the *PpcrV-lux* screen, this activity was seemingly lost, most likely due to degradation of the compounds. An absence of activity against the T3SS by any of the hit compounds was established after the initial screen. This was primarily confirmed using western blots, with PcrV expression unchanged compared to WT in compound treated samples.

The project was pushed in a new direction after a broad screening of effects on virulence factors by one of the hit compounds, NCI18 since it was found that it reduced PA mediated virulence both *in vitro* and *in vivo* during a *G. mellonella* acute infection model at clinically relevant doses. This screening demonstrated that a novel chemical class, phenyl piperazines, selectively inhibited swarming in PA. What remained unknown is whether a causal link existed between the *in silico* selection for ExsA inhibitors and the swarming related target of these compounds. Work in this study showed NCI18 had no effect on the growth of PA confirmed by *ex vivo* porcine lung experiments in addition to standard *in vitro* growth curves. This is an important aspect of validating virulence targeting as it infers a specificity of activity over general toxicity which may be misleading when interpreting *in vitro* efficacy data. Since additional amounts of NCI18 could not be purchased, the pursuit of its mechanism was conducted using a small number of phenyl piperazine analogues.

Some of these analogues were found to inhibit swarming at nanomolar concentrations which was not recoverable over time. The principal molecule investigated, NCI18<sup>1A</sup> prevented expression of flagella under swarming conditions, but not in planktonic culture suggesting that the target is only expressed or activated under swarming conditions. The ability of a *ΔgacA* strain to partially swarm suggested that the target was essential for full swarming motility but could be partially compensated for by bypassing the characterised 4-tiered hierarchy regulatory pathway in PA. In addition, it was shown that phenyl piperazine inhibition of swarming was independent of rhamnolipid production. The absence of change in any of the alternative virulence factor assays, (specifically the T3SS, swimming, twitching, proteases and biofilm formation), alongside supporting evidence from Yeung *et al.*, (2009), Dötsch *et al.*, (2010), and the presence of flagella in planktonic conditions, indicate that the phenyl piperazine target is almost certainly an as yet unknown or uncharacterised swarming specific regulator; most probably at the Class III or Class IV level of hierarchy. Given the presence of flagella in planktonic conditions it is plausible that the regulator controls the expression of a specific component required in the structure of a swarming flagella given the bacteria has evolved to overcome the physics associated with motility in different conditions, exemplified by its two stators.

It did not appear that the NCI18<sup>1A</sup> caused any increase in resistance to antibiotics although, given the clear distinction between planktonic and swarming conditions in the compound activity this assessment should be repeated on plate assays. Additionally, it should be investigated using *in vivo* infection models, observing the potential to assist antibiotic clearance of infections.

The investigation into the effects that NCI18<sup>1A</sup> had on QS was interesting with regards to PQS and BHL production results. Discussed in this study is the recent finding of host cell contact removing a threshold barrier for QS signalling through LasR. This could have a considerable potential impact on these results if this is an additional layer of signalling control of virulence used by PA. Combining this with the absence of a positive control within the assay further work is needed to conclude on the effects NCI18<sup>1A</sup> had on QS autoinducer molecule production. However, the results did suggest there was perhaps at least some pleiotropic effects from the molecule that increased the production of PQS in both PA01 and PA14, and BHL in PA14 only.

Inhibition of swarming in *P. tolaasii* demonstrated that the phenyl piperazine compounds could have a broad level of activity across the *Pseudomonas* genus, however additional species would need to be tested for confirmation. This activity means these compounds have potential merit outside of human clinical use, for example preventing brown blotch disease which is incredibly costly to the mushroom industry.

As a result of searching for possible targets of phenyl piperazines and trying to identify the link between the *in silico* selection of these compounds and their swarming inhibition, this project stumbled upon a relatively unknown and poorly characterised AraC/XyIs family regulator, ChpD. ChpD became the focus as a potential target because swarming relies on chemotaxis control and it is related to ExsA. Part of the *pil-chp* cluster, ChpD function remained unknown with published literature tentatively proposing a role in global virulence. Examination of a *chpD* transposon and deletion mutant revealed it to be essential for full virulence in *G. mellonella* infection by PA, but not to play a role in swarming, nor to be the target of phenyl piperazine molecules. The secretome analysis revealed a downregulation of IMPa in the *chpD* deletion mutant. This result implies that ChpD plays a role in virulence by immune evasion since IMPa cleaves PSGL-1, which is used to recruit immune cells to the infection site. Additional work would be needed to confirm this mechanism however, the similarities in the innate immune response between vertebrates and *G. mellonella* strongly supports this from the evidence in this project. Additionally, relating to ChpD is that work surrounding T4P involvement in surface association is just beginning to be understood. How this relates to the induction of virulence factors is similarly only just starting to unravel. ChpD is a PA specific gene that has for the most part been ignored or overlooked in studies investigating these links. This project also revealed that ChpD could play a role in regulating the T2SS possibly mediated by T4P sensing since it seemingly is transcribed as part of the *chp* operon. A final inclusion for the findings in this study that *chpD* plays an important role in PA virulence is the increased sensitivity the *chpD::Tn* mutant had to gentamycin and carbapenem antibiotics compared to WT in this study.

### **6.5.2 Future directions**

At the time of writing this thesis is held under restricted access until a full chemical characterisation of the phenyl piperazine class can be completed in support of a patent filing for clinical use against PA infection. The creation of a complete analogue library in order to

characterise the chemical properties, method of synthesis and number of active analogues must be completed and will aid investigations of their activity. Isolating the “chemical warhead” of the molecule that confers specificity and activity, as well as probing which is the active enantiomer are important steps in the filing of a patent for these molecules.

Transcriptomics and/or proteomics are the next logical steps in uncovering the mechanism of these compounds. With the prominent lead being a transcriptional regulator active only under swarming conditions observing the transcriptional and translational changes after treatment with phenyl piperazines could offer insights into their mode of action. Similar methods to those used in the first two chapters of this thesis could be employed candidates once chosen, using purification techniques, biophysical and some functional assays to confirm the target. Further investigation of the PA2332 gene could be a starting point since this gene is selected on the back of the search for a link between the original compound selection and their target. Testing phenyl piperazine activity in alternative genus could help narrow the potential pool of candidates when allied with bioinformatics data similar to that which appears Yeung *et al.*, (2009) and Dötsch *et al.*, (2010).

The discussion in this project has focused on AraC/Xyls related targets with the justification of a search for the link between ExsA and the exhibited activity on swarming. It must be considered that this link does not exist, and methods should be explored to address that. Exposure of a whole transposon mutant library to the compound is another possibility. This would allow isolation of mutants that were able to swarm in the presence of compound. There has also been the assumption that the molecules act on an internal target, but surface receptors for example could be modulating the effects by interaction extracellularly.

Significant changes to related virulence factors are reported throughout the published literature when a virulence system is perturbed, one of the most prominent being the inverse relationship between biofilm formation and the T3SS<sup>[127]</sup>. This makes it very unlikely that no changes are occurring in the expression of at least some related virulence factors of PA when treated with any of the active compounds. More probable is that assay conditions did not replicate swarming conditions masking downstream or pleiotropic effects of swarming inhibition by the compounds. Future work should explore this since it has prominent clinical relevance with a priority on antibiotic susceptibility, as well as T3SS expression. Both have been linked to swarming and since MIC tests done during this project were in planktonic

culture, combined with the potential in utilising *G. mellonella*, more work is readily achievable to answer these important questions.

This project covered toxicity only minimally and progression on profiling this chemical class is needed to advance their development. Following the creation of an analogue library, examination of toxicity on a broad range of cell lines, establishing an LD<sub>50</sub> in *Galleria* and possibly additional species, and even *in silico* programmes exist to aid prediction in potential interactions with cytochrome P450 enzymes.

For future work addressing the original aims of this project, finding inhibitors of ExsA, every effort should be made to refine ExsA models, preferably through long MD simulations unless an experimentally solved 3D structure of ExsA becomes available with good resolution. If the opportunity arises to complete the work awarded in the HPC-Europa3 grant this would be a considerable step towards this. Additionally, making use of the predicted stabilising mutagenesis work in this thesis to attempt crystallization could be beneficial in supporting the computational methods.

ChpD has proven itself worthy of greater scrutiny after confirming its necessity for full virulence, with a starting point being the secretome changes reported in this study proposing a link to the regulation of the T2SS. To advance knowledge of this matter overexpression of ChpD would be a simple way to begin. Clarifying the effects of mutations upstream in the *chp* cluster would also help understanding of earlier work in *Drosophila* and future work looking at the chemotaxis pathway. The recently discovered implications that host cell contact can have for virulence factor expression should be taken into account for any future work on ChpD since it is encoded with a T4P cluster intricately involved in the sensing and association of host cells and surfaces. The results in this study suggest that it is not the active killing of host cells that ChpD regulation influences during *Galleria* infections, but instead the subversion of the host's immune response instead, at least in part by the immunomodulating metalloprotease, IMPa.

What is an important consideration is the broader context of anti-virulence targeting as a way of treating patients in the future. Relatively few therapies of the kind exist and consideration should be taken into assessing which method of use is the most effective. Prophylaxis, adjunctive, or replacement, as well as short- or long-term usage should all be considered. PA causes an enormous fraction of hospital acquired infections and almost

exclusively to the immunocompromised. A highly specific swarming inhibitor that drastically reduces the chances of PA being able to establish an infection could be a standard treatment for burn victims, cancer patients, AIDS patients and many more. As outlined in the section 1.3.3 this early treatment prior to establishing infection is a priority and a reason to treat aggressively at initial and new-onset stages to eradicate PA. This type of inhibitor offers an additional and novel option for this method of treatment. Similarly, long term usage for CF sufferers to prevent the cycle of acute flare ups resulting in an inflammation and scarring cycle – especially with new evidence to suggest that chronic infection bacteria stop expressing flagella and when they restart expression, it is the recognition of the flagella that instigates the inflammatory pathway. As the leading cause of mortality in CF patients, a treatment that could improve the prognosis for this demographic from a young age would have an immense impact. Adjunctive use could mean shorter dose regimens of antibiotics and a reduction in time the selection pressure to allow acquired resistance as well overall reduction usage which would again reduce selection pressure and costs. Benefits may be seen to the patient as well with less impact on gut microbiota for example. Even replacement of antibiotics could be possible with less severe infections treated with anti-virulence medication to assist with host immune clearance, thereby entirely negating the unnecessary or overuse of antibiotics and potentially slowing the spread of resistance. These uses are far ahead and should not only be considered for phenyl piperazine use but for all potential future anti-virulence therapies and can be addressed and studied during the lab stages of research and development to prepare for their use in advance.

Alternative uses for these molecules that could be their use in veterinary clinics as PA is a common infection in animals, or in agricultural industry such as the mushroom industry as PA is also a plant pathogen. Additionally, they could be explored for use in manufacturing of materials for sterile surfaces, incorporating the molecules into materials to prevent bacterial spread and improve cleaning.

Overall, PA is an especially nasty Gram-negative pathogen and notoriously difficult to kill. Any new antimicrobial agent against PA would be hugely beneficial to hospitals and patients globally. Swarming is the coordinated movement of a bacterial population across a semi solid surface, closely replicated by the thick mucus layer on the epithelium of a CF patient lung. Swarming is an essential part of PA virulence and is under incredibly complex regulatory control that includes highly specific regulators active only under swarming conditions. This

project has identified the phenyl piperazine chemical scaffold to be a promising lead for a novel PA virulence targeting small molecule, by inhibiting swarming motility.

## Bibliography

1. Davies, J.: Origins and evolution of antibiotic resistance., (1996)
2. Antibiotic Resistance: Multi-country public awareness survey. (2015)
3. Elena Kashuba, Alexey A. Dmitriev, Shady Mansour Kamal, Ojar Melefors, Gennady Griva, Ute Römmling, Ingemar Ernberg, Vladimir Kashuba & Anatoli Brouchkov (2017) Ancient permafrost staphylococci carry antibiotic resistance genes, *Microbial Ecology in Health and Disease*, 28:1, DOI: 10.1080/16512235.2017.1345574.
4. Perry, J., Waglechner, N., Wright, G.: The prehistory of antibiotic resistance. *Cold Spring Harbor Perspectives in Medicine*. 6, (2016). <https://doi.org/10.1101/cshperspect.a025197>
5. Giedraitienė, A., Giedraitienė, A., Vitkauskienė, A., Naginienė, R., Pavilonis, A.: Correspondence to Antibiotic Resistance Mechanisms of Clinically Important Bacteria. (2011)
6. Daubin, V., Szöllősi, G.J.: Horizontal gene transfer and the history of life. *Cold Spring Harbor Perspectives in Biology*. 8, (2016). <https://doi.org/10.1101/cshperspect.a018036>
7. Alekshun, M.N., Levy, S.B.: Molecular Mechanisms of Antibacterial Multidrug Resistance. *Cell*. 128, 1037–1050 (2007). <https://doi.org/10.1016/j.cell.2007.03.004>
8. Alekshun, M. N. & Levy, S. B. Molecular Mechanisms of Antibacterial Multidrug Resistance. *Cell* 128, 1037–1050 (2007).
9. Tenover, F. C. Mechanisms of Antimicrobial Resistance in Bacteria. *Am. J. Med.* 119, S3–S10 (2006).
10. Castro-Sánchez, E., Moore, L.S.P., Husson, F., Holmes, A.H.: What are the factors driving antimicrobial resistance? Perspectives from a public event in London, England. *BMC Infectious Diseases*. 16, (2016). <https://doi.org/10.1186/s12879-016-1810-x>
11. Lister, P.D., Wolter, D.J., Hanson, N.D.: Antibacterial-resistant *Pseudomonas aeruginosa*: Clinical impact and complex regulation of chromosomally encoded resistance mechanisms, (2009)
12. Taylor, P.K., Yeung, A.T.Y., Hancock, R.E.W.: Antibiotic resistance in *Pseudomonas aeruginosa* biofilms: Towards the development of novel anti-biofilm therapies. *Journal of Biotechnology*. 191, 121–130 (2014). <https://doi.org/10.1016/j.jbiotec.2014.09.003>
13. Tacconelli, E., Carrara, E., Savoldi, A., Kattula, D., Burkert, F.: GLOBAL PRIORITY LIST OF ANTIBIOTIC-RESISTANT BACTERIA TO GUIDE RESEARCH, DISCOVERY, AND DEVELOPMENT OF NEW ANTIBIOTICS.
14. Holmberg, S. D., Solomon, S. L. & Blake, P. A. Health and economic impacts of antimicrobial resistance. *Rev. Infect. Dis.* 9, 1065–78.
15. Maragakis, L. L., Perencevich, E. N. & Cosgrove, S. E. Clinical and economic burden of antimicrobial resistance. *Expert Rev. Anti. Infect. Ther.* 6, 751–763 (2008).
16. Holmberg, S.D., Solomon, S.L., Blake, P.A.: Health and economic impacts of antimicrobial resistance. *Reviews of infectious diseases*. 9, 1065–78

17. Maragakis, L.L., Perencevich, E.N., Cosgrove, S.E.: Clinical and economic burden of antimicrobial resistance. *Expert Review of Anti-infective Therapy*. 6, 751–763 (2008). <https://doi.org/10.1586/14787210.6.5.751>
18. Health and Food Safety.
19. ANTIMICROBIAL RESISTANCE Global Report on Surveillance.
20. Antimicrobial Resistance: Tackling a crisis for the health and wealth of nations.
21. Johnson, B.K., Abramovitch, R.B.: *Small Molecules That Sabotage Bacterial Virulence*, (2017)
22. Clatworthy, A.E., Pierson, E., Hung, D.T.: Targeting virulence: A new paradigm for antimicrobial therapy, (2007)
23. Dickey, S. W., Cheung, G. Y. C. & Otto, M. Different drugs for bad bugs: antivirulence strategies in the age of antibiotic resistance. *Nat. Rev. Drug Discov.* 16, 457–471 (2017).
24. Costa TR, Felisberto-Rodrigues C, Meir A, et al. Secretion systems in Gram-negative bacteria: structural and mechanistic insights. *Nat Rev Microbiol.* 2015;13(6):343-359. doi:10.1038/nrmicro3456.
25. Korotkova, N., Cota, E., Lebedin, Y., Monpouet, S., Guignot, J., Servin, A.L., Matthews, S., Moseley, S.L.: A subfamily of Dr adhesins of *Escherichia coli* bind independently to decay-accelerating factor and the N-domain of carcinoembryonic antigen. *Journal of Biological Chemistry*. 281, 29120–29130 (2006). <https://doi.org/10.1074/jbc.M605681200>
26. Rutherford, S.T., Bassler, B.L.: Bacterial quorum sensing: Its role in virulence and possibilities for its control, (2012)
27. Allen, R.C., Papat, R., Diggle, S.P., Brown, S.P.: Targeting virulence: Can we make evolution-proof drugs?, (2014)
28. Silver, L.L.: Challenges of antibacterial discovery. *Clinical Microbiology Reviews*. 24, 71–109 (2011). <https://doi.org/10.1128/CMR.00030-10>
29. Aminov, R.I.: A brief history of the antibiotic era: Lessons learned and challenges for the future. *Frontiers in Microbiology*. 1, (2010). <https://doi.org/10.3389/fmicb.2010.00134>
30. Voth, D.E., Ballard, J.D.: *Clostridium difficile* toxins: Mechanism of action and role in disease, (2005)
31. Allen, R.C., Papat, R., Diggle, S.P., Brown, S.P.: Targeting virulence: can we make evolution-proof drugs? *Nature Reviews Microbiology*. 12, 300–308 (2014). <https://doi.org/10.1038/nrmicro3232>
32. Alonso, C.D., Mahoney, M. v.: Bezlotoxumab for the prevention of *clostridium difficile* infection: A review of current evidence and safety profile, (2019)
33. Cornely, O.A., Mullane, K.M., Birch, T., Hazan-Steinberg, S., Nathan, R., Bouza, E., Calfee, D.P., Ellison, M.C., Wong, M.T., Dorr, M.B.: Exploratory evaluation of bezlotoxumab on outcomes associated with *Clostridioides difficile* infection in MODIFY I/II participants with cancer. *Open Forum Infectious Diseases*. (2020). <https://doi.org/10.1093/ofid/ofaa038>
34. Yoon, M.Y., Yoon, S.S.: Disruption of the gut ecosystem by antibiotics, (2018)

35. Kent, D.: Disruption and maturity: The next phase of biologics.
36. Mydock-McGrane, L., Cusumano, Z., Han, Z., Binkley, J., Kostakioti, M., Hannan, T., Pinkner, J.S., Klein, R., Kalas, V., Crowley, J., Rath, N.P., Hultgren, S.J., Janetka, J.W.: Antivirulence C-Mannosides as Antibiotic-Sparing, Oral Therapeutics for Urinary Tract Infections. *Journal of Medicinal Chemistry*. 59, 9390–9408 (2016). <https://doi.org/10.1021/acs.jmedchem.6b00948>
37. Cusumano, C.K., Pinkner, J.S., Han, Z., Greene, S.E., Ford, B.A., Crowley, J.R., Henderson, J.P., Janetka, J.W., Hultgren, S.J.: Treatment and prevention of urinary tract infection with orally active FimH inhibitors. *Science Translational Medicine*. 3, (2011). <https://doi.org/10.1126/scitranslmed.3003021>
38. Kleeb S, Jiang X, Frei P, Sigl A, Bezençon J, Bamberger K, Schwaradt O, Ernst B. *J Med Chem*. 2016;59:3163–3182. doi: 10.1021/acs.jmedchem.5b01923.
39. Klein T, Abgottspon D, Wittwer M, Rabbani S, Herold J, Jiang X, Kleeb S, Lüthi C, Scharenberg M, Bezençon J, et al. *J Med Chem*. 2010;53:8627–8641. doi: 10.1021/jm101011y.
40. Karginov, V.A.: Cyclodextrin derivatives as anti-infectives, (2013)
41. Ragle B E, Karginov V A, Bubeck Wardenburg J. *Antimicrob Agents Chemother*. 2010;54:298–304. doi: 10.1128/AAC.00973-09.
42. Duncan, M.C., Lington, R.G., Auerbuch, V.: Chemical inhibitors of the type three secretion system: Disarming bacterial pathogens, (2012)
43. Milla, C.E., Chmiel, J.F., Accurso, F.J., Vandevanter, D.R., Konstan, M.W., Yarranton, G., Geller, D.E.: Anti-PcrV antibody in cystic fibrosis: A novel approach targeting *Pseudomonas aeruginosa* airway infection. *Pediatric Pulmonology*. 49, 650–658 (2014). <https://doi.org/10.1002/ppul.22890>
44. François, B., Luyt, C.E., Dugard, A., Wolff, M., Diehl, J.L., Jaber, S., Forel, J.M., Garot, D., Kipnis, E., Mebazaa, A., Misset, B., Andreumont, A., Ploy, M.C., Jacobs, A., Yarranton, G., Pearce, T., Fagon, J.Y., Chastre, J.: Safety and pharmacokinetics of an anti-PcrV PEGylated monoclonal antibody fragment in mechanically ventilated patients colonized with *Pseudomonas aeruginosa*: A randomized, double-blind, placebo-controlled trial. *Critical Care Medicine*. 40, 2320–2326 (2012). <https://doi.org/10.1097/CCM.0b013e31825334f6>
45. Pereira S. G., Rosa A. C., Ferreira A. S., Moreira L. M., Proença D. N., Morais P. V. and Cardoso O. (2014) Virulence factors and infection ability of *Pseudomonas aeruginosa* isolates from a hydrophobic facility and respiratory infections, *Journal of Applied Microbiology*, 116(5), 1359–1368.
46. de Bentzmann, S. & Plésiat, P. The *Pseudomonas aeruginosa* opportunistic pathogen and 154 human infections. *Environ. Microbiol.* 13, 1655–1665 (2011).
47. Ro, U., Mling, È., Schmidt, K.D., Tu, B., Mmler, È.: Large Genome Rearrangements Discovered by the Detailed Analysis of 21 *Pseudomonas aeruginosa* Clone C Isolates Found in Environment and Disease Habitats. (1997)
48. Klockgether, J., Cramer, N., Wiehlmann, L., Davenport, C.F., Tümmler, B.: *Pseudomonas aeruginosa* genomic structure and diversity. *Frontiers in Microbiology*. 2, (2011). <https://doi.org/10.3389/fmicb.2011.00150>

49. Hauser, A.R.: *Pseudomonas aeruginosa*: So many virulence factors, so little time, (2011)
50. Alhede, M., Bjarnsholt, T., Jensen, P., Phipps, R.K., Moser, C., Christophersen, L., Christensen, L.D., van Gennip, M., Parsek, M., Høiby, N., Rasmussen, T.B., Givskov, M.: *Pseudomonas aeruginosa* recognizes and responds aggressively to the presence of polymorphonuclear leukocytes. *Microbiology*. 155, 3500–3508 (2009). <https://doi.org/10.1099/mic.0.031443-0>
51. Bhagirath, A.Y., Li, Y., Somayajula, D., Dadashi, M., Badr, S., Duan, K.: Cystic fibrosis lung environment and *Pseudomonas aeruginosa* infection. *BMC Pulmonary Medicine*. 16, (2016). <https://doi.org/10.1186/s12890-016-0339-5>
52. Anantharajah, A., Mingeot-Leclercq, M.P., van Bambeke, F.: Targeting the Type Three Secretion System in *Pseudomonas aeruginosa*, (2016)
53. Smyth, A., Elborn, J.S.: Exacerbations in cystic fibrosis: 3 · management, (2008)
54. McCarthy, R.R., Mooij, M.J., Reen, F.J., Lesouhaitier, O., O’Gara, F.: A new regulator of pathogenicity (bvIR) is required for full virulence and tight microcolony formation in *Pseudomonas aeruginosa*. *Microbiology (United Kingdom)*. 160, 1488–1500 (2014). <https://doi.org/10.1099/mic.0.075291-0>
55. Mulcahy, L.R., Isabella, V.M., Lewis, K.: *Pseudomonas aeruginosa* Biofilms in Disease. *Microbial Ecology*. 68, 1–12 (2014). <https://doi.org/10.1007/s00248-013-0297-x>
56. Raineri E., Porcella L., Acquarolo A., Crema L., Albertario F. and Candiani A. (2014) Ventilator-Associated Pneumonia Caused by *Pseudomonas aeruginosa* in Intensive Care Unit: Epidemiology and Risk Factors, *Journal of Medical Microbiology & Diagnosis*, 3(3).
57. Høiby N., Ciofu O. and Bjarnsholt T. (2010) *Pseudomonas aeruginosa* biofilms in cystic fibrosis, *Future Microbiology*, 5(11), 1663–1674.
58. Cantin, A.M., Hartl, D., Konstan, M.W., Chmiel, J.F.: Inflammation in cystic fibrosis lung disease: Pathogenesis and therapy, (2015)
59. Mowat E., Paterson S., Fothergill J. L., Wright E. A., Ledson M. J., Walshaw M. J., Brockhurst M. A. and Winstanley C. (2011) *Pseudomonas aeruginosa* Population Diversity and Turnover in Cystic Fibrosis Chronic Infections, *American Journal of Respiratory and Critical Care Medicine*, 183(12), 1674–1679.
60. Liu, C., Sun, D., Zhu, J., Liu, J., Liu, W.: The Regulation of Bacterial Biofilm Formation by cAMP-CRP: A Mini-Review, (2020)
61. Delcour, A.H.: Outer membrane permeability and antibiotic resistance, (2009)
62. Exner, M., Bhattacharya, S., Christiansen, B.: Antibiotic resistance: What is so special about multidrug-resistant Gram-negative bacteria? multiresistenten Bakterien?
63. UK Cystic Fibrosis Registry Annual data report 2012. (2013)
64. Stewart, Philip S, and William Costerton, J. “Antibiotic Resistance of Bacteria in Biofilms.” *The Lancet*. 358.9276 (2001): 135-38. Web.
65. Sabnis, A., Ledger, E.V.K., Pader, V., Edwards, A.M.: Antibiotic interceptors: Creating safe spaces for bacteria. *PLoS Pathogens*. 14, (2018). <https://doi.org/10.1371/journal.ppat.1006924>

66. Soto, S.M.: Role of efflux pumps in the antibiotic resistance of bacteria embedded in a biofilm. *Virulence*. 4, 223–229 (2013). <https://doi.org/10.4161/viru.23724>
67. Terzi, H.A., Kulah, C., Ciftci, İ.H.: The effects of active efflux pumps on antibiotic resistance in *Pseudomonas aeruginosa*. *World Journal of Microbiology and Biotechnology*. 30, 2681–2687 (2014). <https://doi.org/10.1007/s11274-014-1692-2>
68. Livermore D. M. (2002) Multiple Mechanisms of Antimicrobial Resistance in *Pseudomonas aeruginosa*: Our Worst Nightmare?, *Clinical Infectious Diseases*, 34(5), 634–640.
69. Nikaido, H., Pagès, J.M.: Broad-specificity efflux pumps and their role in multidrug resistance of Gram-negative bacteria, (2012)
70. Tankhiwale, S.: Beta-lactamases in *P. aeruginosa*: A threat to clinical therapeutics.
71. Pechère, J.C., Köhler, T.: Patterns and modes of  $\beta$ -lactam resistance in *Pseudomonas aeruginosa*. In: *Clinical Microbiology and Infection*. Decker Europe (1999)
72. Wright, G. Bacterial resistance to antibiotics: Enzymatic degradation and modification. *Adv. Drug Deliv. Rev.* 57, 1451–1470 (2005).
73. Lambert, P.A.: Bacterial resistance to antibiotics: Modified target sites, (2005)
74. Blanco, P., Hernando-Amado, S., Reales-Calderon, J., Corona, F., Lira, F., Alcalde-Rico, M., Bernardini, A., Sanchez, M., Martinez, J.: Bacterial Multidrug Efflux Pumps: Much More Than Antibiotic Resistance Determinants. *Microorganisms*. 4, 14 (2016). <https://doi.org/10.3390/microorganisms4010014>
75. Morita, Y., Komori, Y., Mima, T., Kuroda, T., Mizushima, T., Tsuchiya, T.: Construction of a series of mutants lacking all of the four major mex operons for multidrug efflux pumps or possessing each one of the operons from *Pseudomonas aeruginosa* PAO1: MexCD-OprJ is an inducible pump. *FEMS microbiology letters*. 202, 139–43 (2001)
76. Yelin, I., Kishony, R.: *Antibiotic Resistance*, (2018)
77. Peleg, A.Y., Hooper, D.C.: *Hospital-Acquired Infections Due to Gram-Negative Bacteria*. (2010)
78. Lee, J., Zhang, L.: The hierarchy quorum sensing network in *Pseudomonas aeruginosa*. *Protein and Cell*. 6, 26–41 (2014). <https://doi.org/10.1007/s13238-014-0100-x>
79. Pearson, J.P., Passadori, L., Iglewskit, B.H., Greenberg, E.P.: A second N-acylhomoserine lactone signal produced by *Pseudomonas aeruginosa* [autoinduction/gene activation/las genes/N-(tetrahydro-2-oxo-3-furanyl)butanamide/quorum sensing]. (1995)
80. Pearson, J.P., Gray, K.M., Passadort, L., Tuckert, K.D., Eberhard, A., Iglewskit, B.H., Greenberg, E.P.: Structure of the autoinducer required for expression of *Pseudomonas aeruginosa* virulence genes [density-dependent transcription/gene activation/las genes/N-acyl homoserine lactone/3-oxo-N-(tetrahydro-2-oxo-3-furanyl)dodecanamide]. (1994)
81. Pesci, E.C., Milbank, J.B.J., Pearson § ¶, J.P., Mcknight, S., Kende, A.S., Greenberg, E.P., Iglewski, B.H.: Quinolone signaling in the cell-to-cell communication system of *Pseudomonas aeruginosa*. (1999)

82. Lee J, Wu J, Deng Y, Wang J, Wang C, Wang J, Chang C, Dong Y, Williams P, Zhang LH (2013) A cell-cell communication signal integrates quorum sensing and stress response. *Nature Chem Biol* 9:339–343.
83. Murray, T.S., Ledizet, M., Kazmierczak, B.I.: Swarming motility, secretion of type 3 effectors and biofilm formation phenotypes exhibited within a large cohort of *Pseudomonas aeruginosa* clinical isolates. *Journal of Medical Microbiology*. 59, 511–520 (2010). <https://doi.org/10.1099/jmm.0.017715-0>
84. Overhage, J., Bains, M., Brazas, M.D., Hancock, R.E.W.: Swarming of *Pseudomonas aeruginosa* is a complex adaptation leading to increased production of virulence factors and antibiotic resistance. *Journal of Bacteriology*. 190, 2671–2679 (2008). <https://doi.org/10.1128/JB.01659-07>
85. Kearns, D.B.: A field guide to bacterial swarming motility, (2010)
86. Gellatly, S.L., Hancock, R.E.W.: *Pseudomonas aeruginosa*: New insights into pathogenesis and host defenses. *Pathogens and Disease*. 67, 159–173 (2013). <https://doi.org/10.1111/2049-632X.12033>
87. Koehler, T., Koehler, K., Curty, L.K., Barja, F., Delden, C. van, Peche`re, J.-C., Peche`re, P.: Swarming of *Pseudomonas aeruginosa* Is Dependent on Cell-to-Cell Signaling and Requires Flagella and Pili Downloaded from. (2000)
88. van 't Wout, E.F.A., van Schadewijk, A., van Boxtel, R., Dalton, L.E., Clarke, H.J., Tommassen, J., Marciniak, S.J., Hiemstra, P.S.: Virulence Factors of *Pseudomonas aeruginosa* Induce Both the Unfolded Protein and Integrated Stress Responses in Airway Epithelial Cells. *PLoS Pathogens*. 11, (2015). <https://doi.org/10.1371/journal.ppat.1004946>
89. O'May, C.Y., Sanderson, K., Roddam, L.F., Kirov, S.M., Reid, D.W.: Iron-binding compounds impair *Pseudomonas aeruginosa* biofilm formation, especially under anaerobic conditions. *Journal of Medical Microbiology*. 58, 765–773 (2009). <https://doi.org/10.1099/jmm.0.004416-0>
90. Singh, P.K., Parsek, M.R., Peter Greenberg, E., Welsh, M.J., Keck, W.M.: A component of innate immunity prevents bacterial biofilm development. (2002)
91. Abby, S.S., Rocha, E.P.C.: The Non-Flagellar Type III Secretion System Evolved from the Bacterial Flagellum and Diversified into Host-Cell Adapted Systems. *PLoS Genetics*. 8, (2012). <https://doi.org/10.1371/journal.pgen.1002983>
92. Brown, N.F., Finlay, B.: Potential origins and horizontal transfer of type III secretion systems and effectors. *Mobile Genetic Elements*. 1, 118–121 (2011). <https://doi.org/10.4161/mge.1.2.16733>
93. Pallen, M.J., Chaudhuri, R.R., Henderson, I.R.: Genomic analysis of secretion systems, (2003)
94. How Did T3S Evolve?
95. Hu, J., Worrall, L.J., Hong, C., Vuckovic, M., Atkinson, C.E., Caveney, N., Yu, Z., Strynadka, N.C.J.: Cryo-EM analysis of the T3S injectisome reveals the structure of the needle and open secretin. *Nature Communications*. 9, (2018). <https://doi.org/10.1038/s41467-018-06298-8>

96. Lunelli, M., Kamprad, A., Bürger, J., Mielke, T., Spahn, C.M.T., Kolbe, M.: Cryo-EM structure of the *Shigella* type III needle complex. *PLoS Pathogens*. 16, (2020). <https://doi.org/10.1371/journal.ppat.1008263>
97. Tosi, T., Estrozi, L.F., Job, V., Guilvout, I., Pugsley, A.P., Schoehn, G., Dessen, A.: Structural similarity of secretins from type II and type III secretion systems. *Structure*. 22, 1348–1355 (2014). <https://doi.org/10.1016/j.str.2014.07.005>
98. Burns, R.E., McDaniel-Craig, A., Sukhan, A.: Site-directed mutagenesis of the *Pseudomonas aeruginosa* type III secretion system protein PscJ reveals an essential role for surface-localized residues in needle complex function. *Microbial Pathogenesis*. 45, 225–230 (2008). <https://doi.org/10.1016/j.micpath.2008.05.002>
99. Lee, P.C., Rietsch, A.: Fueling type III secretion, (2015)
100. Lombardi, C., Tolchard, J., Bouillot, S., Signor, L., Gebus, C., Liebl, D., Fenel, D., Teulon, J.M., Brock, J., Habenstein, B., Pellequer, J.L., Faudry, E., Loquet, A., Attrée, I., Dessen, A., Job, V.: Structural and functional characterization of the type three secretion system (T3SS) needle of *pseudomonas aeruginosa*. *Frontiers in Microbiology*. 10, (2019). <https://doi.org/10.3389/fmicb.2019.00573>
101. Hauser, A.R.: The type III secretion system of *Pseudomonas aeruginosa*: Infection by injection, (2009)
102. Goure, J., Pastor, A., Faudry, E., Chabert, J., Dessen, A., Attree, I.: The V antigen of *Pseudomonas aeruginosa* is required for assembly of the functional PopB/PopD translocation pore in host cell membranes. *Infection and Immunity*. 72, 4741–4750 (2004). <https://doi.org/10.1128/IAI.72.8.4741-4750.2004>
103. Sundin, C., Wolfgang, M.C., Lory, S., Forsberg, Å., Frithz-Lindsten, E.: Type IV pili are not specifically required for contact dependent translocation of exoenzymes by *Pseudomonas aeruginosa*. *Microbial Pathogenesis*. 33, 265–277 (2002). <https://doi.org/10.1006/mpat.2002.0534>
104. Feltman, H., Schulert, G., Khan, S., Jain, M., Peterson, L., Hauser, A.R.: Prevalence of type III secretion genes in clinical and environmental isolates of *Pseudomonas aeruginosa*. (2001)
105. Pazos, M.A., Lanter, B.B., Yonker, L.M., Eaton, A.D., Pirzai, W., Gronert, K., Bonventre, J. v., Hurley, B.P.: *Pseudomonas aeruginosa* ExoU augments neutrophil transepithelial migration. *PLoS Pathogens*. 13, (2017). <https://doi.org/10.1371/journal.ppat.1006548>
106. Sawa, T., Hamaoka, S., Kinoshita, M., Kainuma, A., Naito, Y., Akiyama, K., Kato, H.: *Pseudomonas aeruginosa* Type III secretory toxin ExoU and its predicted homologs. *Toxins*. 8, (2016). <https://doi.org/10.3390/toxins8110307>
107. Cowell, B.A., Evans, D.J., Fleiszig, S.M.J.: Actin cytoskeleton disruption by ExoY and its effects on *Pseudomonas aeruginosa* invasion. *FEMS Microbiology Letters*. 250, 71–76 (2005). <https://doi.org/10.1016/j.femsle.2005.06.044>
108. Hritonenko, V., Mun, J.J., Tam, C., Simon, N.C., Barbieri, J.T., Evans, D.J., Fleiszig, S.M.J.: Adenylate cyclase activity of *Pseudomonas aeruginosa* ExoY can mediate bleb-niche formation in epithelial cells and contributes to virulence. *Microbial Pathogenesis*. 51, 305–312 (2011). <https://doi.org/10.1016/j.micpath.2011.08.001>

109. Yahr, T.L., Vallis, A.J., Hancock, M.K., Barbieri, J.T., Frank, D.W.: ExoY, an adenylate cyclase secreted by the *Pseudomonas aeruginosa* type III system. (1998)
110. Yahr, T.L., Wolfgang, M.C.: Transcriptional regulation of the *Pseudomonas aeruginosa* type III secretion system, (2006)
111. Rietsch, A., Mekalanos, J.J.: Metabolic regulation of type III secretion gene expression in *Pseudomonas aeruginosa*. *Molecular Microbiology*. 59, 807–820 (2006).  
<https://doi.org/10.1111/j.1365-2958.2005.04990.x>
112. Hayes, C.S., Aoki, S.K., Low, D.A.: Bacterial Contact-Dependent Delivery Systems. *Annual Review of Genetics*. 44, 71–90 (2010).  
<https://doi.org/10.1146/annurev.genet.42.110807.091449>
113. Kim, J., Ahn, K., Min, S., Jia, J., Ha, U., Wu, D., Jin, S.: Factors triggering type III secretion in *Pseudomonas aeruginosa*. *Microbiology*. 151, 3575–3587 (2005).  
<https://doi.org/10.1099/mic.0.28277-0>
114. Urbanowski, M.L., Brutinel, E.D., Yahr, T.L.: Translocation of ExsE into Chinese hamster ovary cells is required for transcriptional induction of the *Pseudomonas aeruginosa* type III secretion system. *Infection and Immunity*. 75, 4432–4439 (2007).  
<https://doi.org/10.1128/IAI.00664-07>
115. Brutinel, E.D., Yahr, T.L.: Control of gene expression by type III secretory activity, (2008)
116. Brutinel, E.D., Vakulskas, C.A., Yahr, T.L.: ExsD inhibits expression of the *Pseudomonas aeruginosa* type III secretion system by disrupting ExsA self-association and DNA binding activity. *Journal of Bacteriology*. 192, 1479–1486 (2010). <https://doi.org/10.1128/JB.01457-09>
117. Brutinel, E.D., Vakulskas, C.A., Brady, K.M., Yahr, T.L.: Characterization of ExsA and of ExsA-dependent promoters required for expression of the *Pseudomonas aeruginosa* type III secretion system. *Molecular Microbiology*. 68, 657–671 (2008).  
<https://doi.org/10.1111/j.1365-2958.2008.06179.x>
118. Brutinel, E.D., Vakulskas, C.A., Yahr, T.L.: Functional domains of ExsA, the transcriptional activator of the *Pseudomonas aeruginosa* type III secretion system. *Journal of Bacteriology*. 191, 3811–3821 (2009). <https://doi.org/10.1128/JB.00002-09>
119. Diaz, M.R., King, J.M., Yahr, T.L.: Intrinsic and extrinsic regulation of type III secretion gene expression in *Pseudomonas aeruginosa*. *Frontiers in Microbiology*. 2, (2011).  
<https://doi.org/10.3389/fmicb.2011.00089>
120. Shen, D.K., Filopon, D., Kuhn, L., Polack, B., Toussaint, B.: PsrA is a positive transcriptional regulator of the type III secretion system in *Pseudomonas aeruginosa*. *Infection and Immunity*. 74, 1121–1129 (2006). <https://doi.org/10.1128/IAI.74.2.1121-1129.2006>
121. Kang, Y., Lunin, V. v., Skarina, T., Savchenko, A., Schurr, M.J., Hoang, T.T.: The long-chain fatty acid sensor, PsrA, modulates the expression of rpoS and the type III secretion exsCEBA operon in *Pseudomonas aeruginosa*. *Molecular Microbiology*. 73, 120–136 (2009).  
<https://doi.org/10.1111/j.1365-2958.2009.06757.x>
122. Wolfgang, M.C., Lee, V.T., Gilmore, M.E., Lory, S.: Coordinate Regulation of Bacterial Virulence Genes by a Novel Adenylate Cyclase-Dependent Signaling Pathway These include

- two ADP-ribosyltransferases (ExoS and ExoT), a protein with host-specific adenylate cyclase activity (ExoY), and an acute cytotoxin (ExoU) (Finck-Bar-bancon et al Various biochemical and in silico approaches resulted. (2003)
123. Diaz, M.R., King, J.M., Yahr, T.L.: Intrinsic and extrinsic regulation of type III secretion gene expression in *Pseudomonas aeruginosa*. *Frontiers in Microbiology*. 2, (2011). <https://doi.org/10.3389/fmicb.2011.00089>
  124. Linares, J.F., Moreno, R., Fajardo, A., Martínez-Solano, L., Escalante, R., Rojo, F., Martínez, J.L.: The global regulator Crc modulates metabolism, susceptibility to antibiotics and virulence in *Pseudomonas aeruginosa*. *Environmental Microbiology*. 12, 3196–3212 (2010). <https://doi.org/10.1111/j.1462-2920.2010.02292.x>
  125. Leroux, M., Kirkpatrick, R.L., Montauti, E.I., Tran, B.Q., Peterson, S.B., Harding, B.N., Whitney, J.C., Russell, A.B., Traxler, B., Goo, Y.A., Goodlett, D.R., Wiggins, P.A., Mougous, J.D.: Kin cell lysis is a danger signal that activates antibacterial pathways of *Pseudomonas aeruginosa*. <https://doi.org/10.7554/eLife.05701.001>
  126. Broder, U.N., Jaeger, T., Jenal, U.: LadS is a calcium-responsive kinase that induces acute-to-chronic virulence switch in *Pseudomonas aeruginosa*. *Nature Microbiology*. 2, (2016). <https://doi.org/10.1038/nmicrobiol.2016.184>
  127. Moscoso, J.A., Jaeger, T., Valentini, M., Hui, K., Jenal, U., Filloux, A.: The diguanylate cyclase SadC is a central player in Gac/Rsm-mediated biofilm formation in *Pseudomonas aeruginosa*. *Journal of Bacteriology*. 196, 4081–4088 (2014). <https://doi.org/10.1128/JB.01850-14>
  128. Almlblad, H., Harrison, J.J., Rybtke, M., Groizeleau, J., Givskov, M., Parsek, M.R., Tolker-Nielsen, T.: The cyclic AMP-Vfr signaling pathway in *Pseudomonas aeruginosa* is inhibited by cyclic Di-GMP. *Journal of Bacteriology*. 197, 2190–2200 (2015). <https://doi.org/10.1128/JB.00193-15>
  129. Trampari, E., Stevenson, C.E.M., Little, R.H., Wilhelm, T., Lawson, D.M., Malone, J.G.: Bacterial rotary export ATPases are allosterically regulated by the nucleotide second messenger cyclic-di-GMP. *Journal of Biological Chemistry*. 290, 24470–24483 (2015). <https://doi.org/10.1074/jbc.M115.661439>
  130. Balasubramanian, D., Schneper, L., Kumari, H., Mathee, K.: A dynamic and intricate regulatory network determines *Pseudomonas aeruginosa* virulence, (2013)
  131. Alam, A., Tam, V., Hamilton, E., Dziejman, M.: vttRa and vttRB encode ToxR family proteins that mediate bile-induced expression of type three secretion system genes in a non-O1/non-O139 *Vibrio cholerae* strain. *Infection and Immunity*. 78, 2554–2570 (2010). <https://doi.org/10.1128/IAI.01073-09>
  132. Matsuda, S., Okada, R., Tandhavanant, S., Hiyoshi, H., Gotoh, K., Iida, T., Kodama, T.: Export of a *Vibrio parahaemolyticus* toxin by the Sec and type III secretion machineries in tandem, (2019)
  133. Nissim-Eliraz, E., Nir, E., Shoval, I., Marsiano, N., Nissan, I., Shemesh, H., Nagy, N., Goldstein, A.M., Gutnick, M., Rosenshine, I., Yagel, S., Shpigela, N.Y.: Type three secretion system-dependent microvascular thrombosis and ischemic enteritis in human gut xenografts infected with enteropathogenic *Escherichia coli*. *Infection and Immunity*. 85, (2017). <https://doi.org/10.1128/IAI.00558-17>

134. Berube, B.J., Murphy, K.R., Torhan, M.C., Bowlin, N.O., Williams, J.D., Bowlin, T.L., Moir, D.T., Hauser, A.R.: Impact of Type III Secretion Effectors and of Phenoxyacetamide Inhibitors of Type III Secretion on Abscess Formation in a Mouse Model of *Pseudomonas aeruginosa* Infection. (2017)
135. Sampaio, S.C.F., Moreira, F.C., Liberatore, A.M.A., Vieira, M.A.M., Knobl, T., Romão, F.T., Hernandez, R.T., Ferreira, C.S.A., Ferreira, A.P., Felipe-Silva, A., Sinigaglia-Coimbra, R., Koh, I.H.J., Gomes, T.A.T.: Analysis of the virulence of an atypical enteropathogenic *Escherichia coli* strain in vitro and in vivo and the influence of type three secretion system. *BioMed Research International*. 2014, (2014). <https://doi.org/10.1155/2014/797508>
136. Matz, C., Nouri, B., McCarter, L., Martinez-Urtaza, J.: Acquired type III secretion system determines environmental fitness of epidemic *Vibrio parahaemolyticus* in the interaction with bacterivorous protists. *PLoS ONE*. 6, (2011). <https://doi.org/10.1371/journal.pone.0020275>
137. Nakamura, K., Shinoda, N., Hiramatsu, Y., Ohnishi, S., Kamitani, S., Ogura, Y., Hayashi, T., Horiguchi, Y.: BspR/BtrA, an Anti- $\sigma$  Factor, Regulates the Ability of *Bordetella bronchiseptica* To Cause Cough in Rats. *mSphere*. 4, (2019). <https://doi.org/10.1128/msphere.00093-19>
138. Marteyn, B., West, N.P., Browning, D.F., Cole, J.A., Shaw, J.G., Palm, F., Mounier, J., Prévost, M.C., Sansonetti, P., Tang, C.M.: Modulation of *Shigella* virulence in response to available oxygen in vivo. *Nature*. 465, 355–358 (2010). <https://doi.org/10.1038/nature08970>
139. Stones, D.H., Fehr, A.G.J., Thompson, L., Rocha, J., Perez-Soto, N., Madhavan, V.T.P., Voelz, K., Krachler, A.M.: Zebrafish (*Danio rerio*) as a Vertebrate Model Host To Study Colonization, Pathogenesis, and Transmission of Foodborne *Escherichia coli* O157. *mSphere*. 2, (2017). <https://doi.org/10.1128/mspheredirect.00365-17>
140. Duncan, M.C., Lington, R.G., Auerbuch, V.: Chemical inhibitors of the type three secretion system: Disarming bacterial pathogens, (2012)
141. Browne, S.H., Hasegawa, P., Okamoto, S., Fierer, J., Guiney, D.G.: Identification of *Salmonella* SPI-2 secretion system components required for SpvB-mediated cytotoxicity in macrophages and virulence in mice. *FEMS Immunology and Medical Microbiology*. 52, 194–201 (2008). <https://doi.org/10.1111/j.1574-695X.2007.00364.x>
142. Hotinger, J.A., May, A.E.: Animal models of type III secretion system-mediated pathogenesis, (2019)
143. Kent, G., Iles, R., Bear, C.E., Huan, L.-J., Griesenbach, U., Mckerlie, C., Frndova, H., Ackerley, C., Gosselin, D., Radzioch, D., O'brodovich, H., Tsui, L.-C., Buchwald, M., Tanswell, A.K.: Lung Disease in Mice with Cystic Fibrosis lung mechanics • ion transport • obstructive airway disease • pulmonary fibrosis • chloride channels. (1997)
144. McCarron, A., Donnelley, M., Parsons, D.: Airway disease phenotypes in animal models of cystic fibrosis, (2018)
145. Grier, M.C., Garrity-Ryan, L.K., Bartlett, V.J., Klausner, K.A., Donovan, P.J., Dudley, C., Alekshun, M.N., Ken Tanaka, S., Draper, M.P., Levy, S.B., Kim, O.K.: N-Hydroxybenzimidazole inhibitors of ExsA MAR transcription factor in *Pseudomonas aeruginosa*: In vitro anti-virulence activity and metabolic stability. *Bioorganic and Medicinal Chemistry Letters*. 20, 3380–3383 (2010). <https://doi.org/10.1016/j.bmcl.2010.04.014>

146. Marsden, A.E., King, J.M., Spies, M.A., Kim, O.K., Yahr, T.L.: Inhibition of *Pseudomonas aeruginosa* ExsA DNA-Binding Activity by N-Hydroxybenzimidazoles. *Antimicrobial agents and chemotherapy*. 60, 766–76 (2016). <https://doi.org/10.1128/AAC.02242-15>
147. Yamazaki, A., Li, J., Zeng, Q., Khokhani, D., Hutchins, W.C., Yost, A.C., Biddle, E., Toone, E.J., Chen, X., Yang, C.H.: Derivatives of plant phenolic compound affect the type III secretion system of *Pseudomonas aeruginosa* via a GacS-GacA two-component signal transduction system. *Antimicrobial Agents and Chemotherapy*. 56, 36–43 (2012). <https://doi.org/10.1128/AAC.00732-11>
148. Wang, D., Zetterström, C.E., Gabrielsen, M., Beckham, K.S.H., Tree, J.J., Macdonald, S.E., Byron, O., Mitchell, T.J., Gally, D.L., Herzyk, P., Mahajan, A., Uvell, H., Burchmore, R., Smith, B.O., Elofsson, M., Roe, A.J.: Identification of bacterial target proteins for the salicylidene acylhydrazide Class of virulence-blocking compounds. *Journal of Biological Chemistry*. 286, 29922–29931 (2011). <https://doi.org/10.1074/jbc.M111.233858>
149. Gabrielsen, M., Beckham, K.S.H., Feher, V.A., Zetterström, C.E., Wang, D., Müller, S., Elofsson, M., Amaro, R.E., Byron, O., Roe, A.J.: Structural characterisation of Tpx from *Yersinia pseudotuberculosis* reveals insights into the binding of salicylidene acylhydrazide compounds. *PLoS ONE*. 7, (2012). <https://doi.org/10.1371/journal.pone.0032217>
150. Slepentin, A., Chu, H., Elofsson, M., Keyser, P., Peterson, E.M.: Protection of mice from a *Chlamydia trachomatis* vaginal infection using a salicylidene acylhydrazide, a potential microbicide. *Journal of Infectious Diseases*. 204, 1313–1320 (2011). <https://doi.org/10.1093/infdis/jir552>
151. Uusitalo, P., Hägglund, U., Rhöös, E., Scherman Norberg, H., Elofsson, M., Sundin, C.: The salicylidene acylhydrazide INP0341 attenuates *Pseudomonas aeruginosa* virulence in vitro and in vivo. *Journal of Antibiotics*. 70, 937–943 (2017). <https://doi.org/10.1038/ja.2017.64>
152. Enquist, P.A., Gylfe, Å., Hägglund, U., Lindström, P., Norberg-Scherman, H., Sundin, C., Elofsson, M.: Derivatives of 8-hydroxyquinoline - Antibacterial agents that target intra- and extracellular Gram-negative pathogens. *Bioorganic and Medicinal Chemistry Letters*. 22, 3550–3553 (2012). <https://doi.org/10.1016/j.bmcl.2012.03.096>
153. Anantharajah, A., Buyck, J.M., Sundin, C., Tulkens, P.M., Mingeot-Leclercq, M.P., van Bambeke, F.: Salicylidene acylhydrazides and hydroxyquinolines act as inhibitors of type three secretion systems in *Pseudomonas aeruginosa* by distinct mechanisms. *Antimicrobial Agents and Chemotherapy*. 61, (2017). <https://doi.org/10.1128/AAC.02566-16>
154. Tosi, T., Estrozi, L.F., Job, V., Guilvout, I., Pugsley, A.P., Schoehn, G., Dessen, A.: Structural similarity of secretins from type II and type III secretion systems. *Structure*. 22, 1348–1355 (2014). <https://doi.org/10.1016/j.str.2014.07.005>
155. Felise, H.B., Nguyen, H. v., Pfuetzner, R.A., Barry, K.C., Jackson, S.R., Blanc, M.P., Bronstein, P.A., Kline, T., Miller, S.I.: An Inhibitor of Gram-Negative Bacterial Virulence Protein Secretion. *Cell Host and Microbe*. 4, 325–336 (2008). <https://doi.org/10.1016/j.chom.2008.08.001>
156. Aiello, D., Williams, J.D., Majgier-Baranowska, H., Patel, I., Peet, N.P., Huang, J., Lory, S., Bowlin, T.L., Moir, D.T.: Discovery and characterization of inhibitors of *Pseudomonas aeruginosa* type III secretion. *Antimicrobial Agents and Chemotherapy*. 54, 1988–1999 (2010). <https://doi.org/10.1128/AAC.01598-09>

157. Bowlin, N.O., Williams, J.D., Knoten, C.A., Torhan, M.C., Tashjian, T.F., Li, B., Aiello, D., Meccas, J., Hauser, A.R., Peet, N.P., Bowlin, T.L., Moir, D.T.: Mutations in the *Pseudomonas aeruginosa* needle protein gene *pscF* confer resistance to phenoxyacetamide inhibitors of the type III secretion system. *Antimicrobial Agents and Chemotherapy*. 58, 2211–2220 (2014). <https://doi.org/10.1128/AAC.02795-13>
158. Williams, J.D., Torhan, M.C., Neelagiri, V.R., Brown, C., Bowlin, N.O., Di, M., McCarthy, C.T., Aiello, D., Peet, N.P., Bowlin, T.L., Moir, D.T.: Synthesis and structure-activity relationships of novel phenoxyacetamide inhibitors of the *Pseudomonas aeruginosa* type III secretion system (T3SS). *Bioorganic and Medicinal Chemistry*. 23, 1027–1043 (2015). <https://doi.org/10.1016/j.bmc.2015.01.011>
159. Berube, B.J., Murphy, K.R., Torhan, M.C., Bowlin, N.O., Williams, J.D., Bowlin, T.L., Moir, D.T., Hauser, A.R.: Impact of Type III Secretion Effectors and of Phenoxyacetamide Inhibitors of Type III Secretion on Abscess Formation in a Mouse Model of *Pseudomonas aeruginosa* Infection. (2017)
160. Frank, D.W., Vallis, A., Wiener-Kronish, J.P., Roy-Burman, A., Spack, E.G., Mullaney, B.P., Megdoud, M., Marks, J.D., Fritz, R., Sawa, T.: Generation and Characterization of a Protective Monoclonal Antibody to *Pseudomonas aeruginosa* PcrV.
161. Lynch, S. v., Flanagan, J.L., Sawa, T., Fang, A., Baek, M.S., Rubio-Mills, A., Ajayi, T., Yanagihara, K., Hirakata, Y., Kohno, S., Misset, B., Nguyen, J.C., Wiener-Kronish, J.P.: Polymorphisms in the *Pseudomonas aeruginosa* type III secretion protein, PcrV - Implications for anti-PcrV immunotherapy. *Microbial Pathogenesis*. 48, 197–204 (2010). <https://doi.org/10.1016/j.micpath.2010.02.008>
162. Imamura, Y., Yanagihara, K., Fukuda, Y., Kaneko, Y., Seki, M., Izumikawa, K., Miyazaki, Y., Hirakata, Y., Sawa, T., Wiener-Kronish, J.P., Kohno, S.: Effect of anti-PcrV antibody in a murine chronic airway *Pseudomonas aeruginosa* infection model. *European Respiratory Journal*. 29, 965–968 (2007). <https://doi.org/10.1183/09031936.00147406>
163. François B, Luyt CE, Dugard A, et al. Safety and pharmacokinetics of an anti-PcrV PEGylated monoclonal antibody fragment in mechanically ventilated patients colonized with *Pseudomonas aeruginosa*: a randomized, double-blind, placebo-controlled trial. *Crit Care Med*. 2012;40(8):2320-2326. doi:10.1097/CCM.0b013e31825334f6.
164. Ali, S.O., Yu, X.Q., Robbie, G.J., Wu, Y., Shoemaker, K., Yu, L., DiGiandomenico, A., Keller, A.E., Anude, C., Hernandez-Illas, M., Bellamy, T., Falloon, J., Dubovsky, F., Jafri, H.S.: Phase 1 study of MEDI3902, an investigational anti-*Pseudomonas aeruginosa* PcrV and Psl bispecific human monoclonal antibody, in healthy adults. *Clinical Microbiology and Infection*. 25, 629.e1-629.e6 (2019). <https://doi.org/10.1016/j.cmi.2018.08.004>
165. phase II trial PcrV.
166. DiGiandomenico, A., Keller, A.E., Gao, C., Rainey, G.J., Warrenner, P., Camara, M.M., Bonnell, J., Fleming, R., Bezabeh, B., Dimasi, N., Sellman, B.R., Hilliard, J., Guenther, C.M., Datta, V., Zhao, W., Gao, C., Yu, X.-Q., Suzich, J.A., Stover, C.K.: A multifunctional bispecific antibody protects against *Pseudomonas aeruginosa*.
167. Thaden, J.T., Keller, A.E., Shire, N.J., Camara, M.M., Otterson, L., Huband, M., Guenther, C.M., Zhao, W., Warrenner, P., Stover, C.K., Fowler, V.G., DiGiandomenico, A.: *Pseudomonas*

- aeruginosa bacteremic patients exhibit nonprotective antibody titers against therapeutic antibody targets PcrV and Psl exopolysaccharide. *Journal of Infectious Diseases*. 213, 640–648 (2016). <https://doi.org/10.1093/infdis/jiv436>
168. Arnoldo, A., Curak, J., Kittanakom, S., Chevelev, I., Lee, V.T., Sahebol-Amri, M., Kosciak, B., Ljuma, L., Roy, P.J., Bedalov, A., Giaever, G., Nislow, C., Merrill, R.A., Lory, S., Stagljar, I.: Identification of small molecule inhibitors of *Pseudomonas aeruginosa* exoenzyme S using a yeast phenotypic screen. *PLoS Genetics*. 4, (2008). <https://doi.org/10.1371/journal.pgen.1000005>
  169. Lee, V.T., Pukatzki, S., Sato, H., Kikawada, E., Kazimirova, A.A., Huang, J., Li, X., Arm, J.P., Frank, D.W., Lory, S.: Pseudolipasin A is a specific inhibitor for phospholipase A2 activity of *Pseudomonas aeruginosa* cytotoxin ExoU. *Infection and Immunity*. 75, 1089–1098 (2007). <https://doi.org/10.1128/IAI.01184-06>
  170. Kim, D., Baek, J., Song, J., Byeon, H., Min, H., Min, K.H.: Identification of arylsulfonamides as ExoU inhibitors. *Bioorganic and Medicinal Chemistry Letters*. 24, 3823–3825 (2014). <https://doi.org/10.1016/j.bmcl.2014.06.064>
  171. Marsden, A.E., King, J.M., Spies, M.A., Kim, O.K., Yahr, T.L.: Inhibition of *Pseudomonas aeruginosa* ExsA DNA-Binding Activity by N-Hydroxybenzimidazoles. *Antimicrobial agents and chemotherapy*. 60, 766–76 (2016). <https://doi.org/10.1128/AAC.02242-15>
  172. March-Vila, E., Pinzi, L., Sturm, N., Tinivella, A., Engkvist, O., Chen, H., Rastelli, G.: On the integration of in silico drug design methods for drug repurposing. *Frontiers in Pharmacology*. 8, (2017). <https://doi.org/10.3389/fphar.2017.00298>
  173. Danchin A, Medigue C, Gascuel O, Soldano H, Henaut A (1991). From data banks to data bases. *Res Microbiol* 142: 913–916.
  174. Sieburg HB (1990). Physiological studies in silico. *Studies in the Sciences of Complexity* 12: 321–342.
  175. Jorgensen, W.L.: *The Many Roles of Computation in Drug Discovery*. (2004)
  176. Drews, J.: *Drug Discovery: A Historical Perspective*. (2000)
  177. Wang, Y., Bryant, S.H., Cheng, T., Wang, J., Gindulyte, A., Shoemaker, B.A., Thiessen, P.A., He, S., Zhang, J.: PubChem BioAssay: 2017 update. *Nucleic Acids Research*. 45, D955–D963 (2017). <https://doi.org/10.1093/nar/gkw1118>
  178. Berman, H.M., Westbrook, J., Feng, Z., Gilliland, G., Bhat, T.N., Weissig, H., Shindyalov, I.N., Bourne, P.E.: The Protein Data Bank. (2000)
  179. Shameer, K., Glicksberg, B.S., Hodos, R., Johnson, K.W., Badgeley, M.A., Readhead, B., Tomlinson, M.S., O'Connor, T., Miotto, R., Kidd, B.A., Chen, R., Ma'ayan, A., Dudley, J.T.: Systematic analyses of drugs and disease indications in RepurposeDB reveal pharmacological, biological and epidemiological factors influencing drug repositioning. *Briefings in bioinformatics*. 19, 656–678 (2018). <https://doi.org/10.1093/bib/bbw136>
  180. Brown, A.S., Patel, C.J.: A standard database for drug repositioning. *Scientific Data*. 4, (2017). <https://doi.org/10.1038/sdata.2017.29>
  181. Stumpfe, D., Bajorath, J.: *Exploring activity cliffs in medicinal chemistry*, (2012)

182. Gimeno, A., Ojeda-Montes, M.J., Tomás-Hernández, S., Cereto-Massagué, A., Beltrán-Debón, R., Mulero, M., Pujadas, G., Garcia-Vallvé, S.: The light and dark sides of virtual screening: What is there to know?, (2019)
183. Cleves, A.E., Johnson, S.R., Jain, A.N.: Electrostatic-field and surface-shape similarity for virtual screening and pose prediction. *Journal of Computer-Aided Molecular Design.* 33, 865–886 (2019). <https://doi.org/10.1007/s10822-019-00236-6>
184. Dror, O., Schneidman-Duhovny, D., Inbar, Y., Nussinov, R., Wolfson, H.J.: Novel approach for efficient pharmacophore-based virtual screening: Method and applications. *Journal of Chemical Information and Modeling.* 49, 2333–2343 (2009). <https://doi.org/10.1021/ci900263d>
185. Pal, S., Kumar, V., Kundu, B., Bhattacharya, D., Preethy, N., Reddy, M.P., Talukdar, A.: Ligand-based Pharmacophore Modeling, Virtual Screening and Molecular Docking Studies for Discovery of Potential Topoisomerase I Inhibitors. *Computational and Structural Biotechnology Journal.* 17, 291–310 (2019). <https://doi.org/10.1016/j.csbj.2019.02.006>
186. Blaney, J.M., Martini, E.J.: Computational approaches for combinatorial library design and molecular diversity analysis. *Current Opinion in Chemical Biology.* 1, 54–59 (1997)
187. Lipinski, C.A.: Lead- and drug-like compounds: The rule-of-five revolution, (2004)
188. Free, S.M., Wilson, J.W.: Downloaded via UNIV OF CAMBRIDGE on. UTC (1964)
189. Korotcov, A., Tkachenko, V., Russo, D.P., Ekins, S.: Comparison of Deep Learning with Multiple Machine Learning Methods and Metrics Using Diverse Drug Discovery Data Sets. *Molecular Pharmaceutics.* 14, 4462–4475 (2017). <https://doi.org/10.1021/acs.molpharmaceut.7b00578>
190. Cronin, M.T.D., Schultz, T.W.: Pitfalls in QSAR.
191. Vigers, G.P.A., Rizzi, J.P.: Multiple Active Site Corrections for Docking and Virtual Screening. *Journal of Medicinal Chemistry.* 47, 80–89 (2004). <https://doi.org/10.1021/jm030161o>
192. Charifson, P.S., Corkery, J.J., Murcko, M.A., Walters, W.P.: Consensus scoring: A method for obtaining improved hit rates from docking databases of three-dimensional structures into proteins. *Journal of Medicinal Chemistry.* 42, 5100–5109 (1999). <https://doi.org/10.1021/jm990352k>
193. Fradera, X., Mestres, J.: Guided Docking Approaches to Structure-Based Design and Screening. *Current Topics in Medicinal Chemistry.* 4, 687–700 (2005). <https://doi.org/10.2174/1568026043451104>
194. Khan, M.T.H., Orhan, I., Şenol, F.S., Kartal, M., Şener, B., Dvorská, M., Šmejkal, K., Šlapetová, T.: Cholinesterase inhibitory activities of some flavonoid derivatives and chosen xanthone and their molecular docking studies. *Chemico-Biological Interactions.* 181, 383–389 (2009). <https://doi.org/10.1016/j.cbi.2009.06.024>
195. Ma, D.L., Chan, D.S.H., Leung, C.H.: Molecular docking for virtual screening of natural product databases, (2011)
196. Lee, K.W., Bode, A.M., Dong, Z.: Molecular targets of phytochemicals for cancer prevention, (2011)

197. Ehrh, C., Brinkjost, T., Koch, O.: Impact of Binding Site Comparisons on Medicinal Chemistry and Rational Molecular Design, (2016)
198. Manning, G., Whyte, D.B., Martinez, R., Hunter, T., Sudarsanam, S.: The Protein Kinase Complement of the Human Genome Author(s). (2002)
199. Zhang, Y.M., Cockerill, S., Guntrip, S.B., Rusnak, D., Smith, K., Vanderwall, D., Wood, E., Lackey, K.: Synthesis and SAR of potent EGFR/erbB2 dual inhibitors. *Bioorganic and Medicinal Chemistry Letters*. 14, 111–114 (2004). <https://doi.org/10.1016/j.bmcl.2003.10.010>
200. Huang, L., Fu, L.: Mechanisms of resistance to EGFR tyrosine kinase inhibitors, (2015)
201. Anighoro, A., Stumpfe, D., Heikamp, K., Beebe, K., Neckers, L.M., Bajorath, J., Rastelli, G.: Computational polypharmacology analysis of the heat shock protein 90 interactome. *Journal of Chemical Information and Modeling*. 55, 676–686 (2015). <https://doi.org/10.1021/ci5006959>
202. Jalencas, X., Mestres, J.: Chemoisosterism in the proteome. *Journal of Chemical Information and Modeling*. 53, 279–292 (2013). <https://doi.org/10.1021/ci3002974>
203. Mari, M., Gallegos, M.-T., Schleif, R., Robert, Bairoch, A., Hofmann, K., Ramos, J.L.: AraC/XylS Family of Transcriptional Regulators. (1997)
204. Childers, B.M., Cao, X., Weber, G.G., Demeler, B., Hart, P.J., Klose, K.E.: N-terminal residues of the *Vibrio cholerae* virulence regulatory protein ToxT involved in dimerization and modulation by fatty acids. *Journal of Biological Chemistry*. 286, 28644–28655 (2011). <https://doi.org/10.1074/jbc.M111.258780>
205. Egan, S.M.: Growing repertoire of AraC/XylS activators, (2002)
206. Ruíz, R., Marqués, S., Ramos, J.L.: Leucines 193 and 194 at the N-terminal domain of the XylS protein, the positive transcriptional regulator of the TOL meta-cleavage pathway, are involved in dimerization. *Journal of Bacteriology*. 185, 3036–3041 (2003). <https://doi.org/10.1128/JB.185.10.3036-3041.2003>
207. Rodgers, M.E., Holder, N.D., Dirla, S., Schleif, R.: Functional modes of the regulatory arm of AraC. *Proteins: Structure, Function and Bioinformatics*. 74, 81–91 (2009). <https://doi.org/10.1002/prot.22137>
208. Bowser, T.E., Bartlett, V.J., Grier, M.C., Verma, A.K., Warchol, T., Levy, S.B., Alekshun, M.N.: Novel anti-infection agents: small-molecule inhibitors of bacterial transcription factors. *Bioorganic & medicinal chemistry letters*. 17, 5652–5 (2007). <https://doi.org/10.1016/j.bmcl.2007.07.072>
209. Grzybowski, B.A., Ishchenko, A. v, Kim, C.-Y., Topalov, G., Chapman, R., Christianson, D.W., Whitesides, G.M., Shakhnovich, E.I.: Combinatorial computational method gives new picomolar ligands for a known enzyme.
210. Evers, A., Klabunde, T.: Structure-based drug discovery using GPCR homology modeling: Successful virtual screening for antagonists of the alpha1A adrenergic receptor. *Journal of Medicinal Chemistry*. 48, 1088–1097 (2005). <https://doi.org/10.1021/jm0491804>

211. Evers, A., Klebe, G.: Successful virtual screening for a submicromolar antagonist of the neurokinin-1 receptor based on a ligand-supported homology model. *Journal of Medicinal Chemistry*. 47, 5381–5392 (2004). <https://doi.org/10.1021/jm0311487>
212. Bhabha, G., Biel, J.T., Fraser, J.S.: Keep on moving: Discovering and perturbing the conformational dynamics of enzymes. *Accounts of Chemical Research*. 48, 423–430 (2015). <https://doi.org/10.1021/ar5003158>
213. Cockrell, G.M., Kantrowitz, E.R.: ViewMotions Rainbow: A new method to illustrate molecular motions in proteins. *Journal of Molecular Graphics and Modelling*. 40, 48–53 (2013). <https://doi.org/10.1016/j.jmglm.2012.12.012>
214. Flores, S.: The Database of Macromolecular Motions: new features added at the decade mark. *Nucleic Acids Research*. 34, D296–D301 (2006). <https://doi.org/10.1093/nar/gkj046>
215. Hospital, A., Goñi, J.R., Orozco, M., Gelpí, J.L.: *Molecular dynamics simulations: Advances and applications*, (2015)
216. Noé, F.: *Beating the millisecond barrier in molecular dynamics simulations*, (2015)
217. Voelz, V.A., Bowman, G.R., Beauchamp, K., Pande, V.S.: Molecular simulation of ab initio protein folding for a millisecond folder NTL9(1-39). *Journal of the American Chemical Society*. 132, 1526–1528 (2010). <https://doi.org/10.1021/ja9090353>
218. Author, D., Lamb, J., Crawford, E.D., Peck, D., Modell, J.W., Blat, I.C., Wrobel, M.J., Lerner, J., Brunet, J.-P., Subramanian, A., Ross, K.N., Reich, M., Hieronymus, H., Wei, G., Armstrong, S.A., Haggarty, S.J., Clemons, P.A., Wei, R., Carr, S.A., Lander, E.S., Golub, T.R.: The Connectivity Map: Using Gene-Expression Signatures to Connect Small Molecules. (2006)
219. Chang, M., Smith, S., Thorpe, A., Barratt, M.J., Karim, F.: Evaluation of phenoxybenzamine in the CFA model of pain following gene expression studies and connectivity mapping. *Molecular Pain*. 6, (2010). <https://doi.org/10.1186/1744-8069-6-56>
220. Butti, R., Das, S., Gunasekaran, V.P., Yadav, A.S., Kumar, D., Kundu, G.C.: Receptor tyrosine kinases (RTKs) in breast cancer: Signaling, therapeutic implications and challenges, (2018)
221. Rodgers, M.E., Schleif, R.: Solution structure of the DNA binding domain of AraC protein. *Proteins: Structure, Function and Bioinformatics*. 77, 202–208 (2009). <https://doi.org/10.1002/prot.22431>
222. Rhee, S., Martin, R.G., Rosner, J.L., Davies, D.R.: A novel DNA-binding motif in MarA: The first structure for an AraC family transcriptional activator. (1998)
223. Shrestha, M., Xiao, Y., Robinson, H., Schubot, F.D.: Structural analysis of the regulatory domain of ExsA, a key transcriptional regulator of the type three secretion system in *Pseudomonas aeruginosa*. *PLoS ONE*. 10, (2015). <https://doi.org/10.1371/journal.pone.0136533>
224. Zhang, Y., Skolnick, J.: Automated structure prediction of weakly homologous proteins on a genomic scale. *Proceedings of the National Academy of Sciences*. 101, 7594–7599 (2004). <https://doi.org/10.1073/pnas.0305695101>
225. PyMOL. <https://www.pymol.org/>

226. Ngan, C.H., Hall, D.R., Zerbe, B., Grove, L.E., Kozakov, D., Vajda, S.: FtSite: High accuracy detection of ligand binding sites on unbound protein structures. *Bioinformatics*. 28, 286–287 (2012). <https://doi.org/10.1093/bioinformatics/btr651>
227. Dolinsky, T.J., Nielsen, J.E., McCammon, J.A., Baker, N.A.: PDB2PQR: An automated pipeline for the setup of Poisson-Boltzmann electrostatics calculations. *Nucleic Acids Research*. 32, (2004). <https://doi.org/10.1093/nar/gkh381>
228. Vilar, S., Cozza, G., Moro, S.: Medicinal chemistry and the molecular operating environment (MOE): application of QSAR and molecular docking to drug discovery. *Current topics in medicinal chemistry*. 8, 1555–72 (2008)
229. Mysinger, M.M., Carchia, M., Irwin, J.J., Shoichet, B.K.: Directory of useful decoys, enhanced (DUD-E): better ligands and decoys for better benchmarking. *Journal of medicinal chemistry*. 55, 6582–94 (2012). <https://doi.org/10.1021/jm300687e>
230. Trott, O., Olson, A.J.: AutoDock Vina: Improving the speed and accuracy of docking with a new scoring function, efficient optimization, and multithreading. *Journal of Computational Chemistry*. 31, NA-NA (2009). <https://doi.org/10.1002/jcc.21334>
231. Jones, G., Willett, P., Glen, R.C., Leach, A.R., Taylor, R.: Development and validation of a genetic algorithm for flexible docking 1 Edited by F. E. Cohen. *Journal of Molecular Biology*. 267, 727–748 (1997). <https://doi.org/10.1006/jmbi.1996.0897>
232. Naylor, E., Arredouani, A., Vasudevan, S.R., Lewis, A.M., Parkesh, R., Mizote, A., Rosen, D., Thomas, J.M., Izumi, M., Ganesan, A., Galione, A., Churchill, G.C.: Identification of a chemical probe for NAADP by virtual screening. *Nature Chemical Biology*. 5, 220–226 (2009). <https://doi.org/10.1038/nchembio.150>
233. Cheeseright, T., Mackey PhD, M., Rose PhD, S., Vinter PhD, A.: Molecular field technology applied to virtual screening and finding the bioactive conformation. *Expert Opinion on Drug Discovery*. 2, 131–144 (2007). <https://doi.org/10.1517/17460441.2.1.131>
234. Morris, G.M., Goodsell, D.S., Halliday, R.S., Huey, R., Hart, W.E., Belew, R.K., Olson, A.J.: Automated docking using a Lamarckian genetic algorithm and an empirical binding free energy function. *Journal of Computational Chemistry*. 19, 1639–1662 (1998). [https://doi.org/10.1002/\(SICI\)1096-987X\(19981115\)19:14<1639::AID-JCC10>3.0.CO;2-B](https://doi.org/10.1002/(SICI)1096-987X(19981115)19:14<1639::AID-JCC10>3.0.CO;2-B)
235. Curtis, A.E., Smith, T.A., Ziganshin, B.A., Eleftheriades, J.A.: The Mystery of the Z-Score. *AORTA*. 4, 124–130 (2016). <https://doi.org/10.12945/j.aorta.2016.16.014>
236. Quan, L., Lv, Q., Zhang, Y.: STRUM: Structure-based prediction of protein stability changes upon single-point mutation. *Bioinformatics*. 32, 2936–2946 (2016). <https://doi.org/10.1093/bioinformatics/btw361>
237. Jacobs, M.A., Alwood, A., Thaipisuttikul, I., Spencer, D., Haugen, E., Ernst, S., Will, O., Kaul, R., Raymond, C., Levy, R., Chun-Rong, L., Guenther, D., Bovee, D., Olson, M. v, Manoil, C.: Comprehensive transposon mutant library of *Pseudomonas aeruginosa*. (2003)
238. Morita, Y., Komori, Y., Mima, T., Kuroda, T., Mizushima, T., Tsuchiya, T.: Construction of a series of mutants lacking all of the four major mex operons for multidrug efflux pumps or possessing each one of the operons from *Pseudomonas aeruginosa* PAO1: MexCD-OprJ is an

- inducible pump . FEMS Microbiology Letters. 202, 139–143 (2001).  
<https://doi.org/10.1111/j.1574-6968.2001.tb10794.x>
239. Fletcher, M.P., Diggle, S.P., Cámara, M., Williams, P.: Biosensor-based assays for PQS, HHQ and related 2-alkyl-4-quinolone quorum sensing signal molecules. *Nature Protocols*. 2, 1254–1262 (2007). <https://doi.org/10.1038/nprot.2007.158>
240. Steindler, L., Venturi, V.: Detection of quorum-sensing N-acyl homoserine lactone signal molecules by bacterial biosensors, (2007)
241. Westa, S.E.H., Schweizerb, H.P., Dall, C., Sample, A.K., Runyen-Janecky, L.J.: Recombinant DNA; broad-host-range expression vectors; plasmid replication; replication protein. (1994)
242. Winson, M.K., Swift, S., Fish, L., Throup, J.P., Jørgensen, F., Chhabra, S.R., Bycroft, B.W., Williams, P., Stewart, G.S.A.B.: Construction and analysis of luxCDABE -based plasmid sensors for investigating N -acyl homoserine lactone-mediated quorum sensing . FEMS Microbiology Letters. 163, 185–192 (1998). <https://doi.org/10.1111/j.1574-6968.1998.tb13044.x>
243. Fletcher, M.P., Diggle, S.P., Cámara, M., Williams, P.: Biosensor-based assays for PQS, HHQ and related 2-alkyl-4-quinolone quorum sensing signal molecules. *Nature Protocols*. 2, 1254–1262 (2007). <https://doi.org/10.1038/nprot.2007.158>
244. Choi, K.H., Gaynor, J.B., White, K.G., Lopez, C., Bosio, C.M., Karkhoff-Schweizer, R.A.R., Schweizer, H.P.: A Tn7-based broad-range bacterial cloning and expression system. *Nature Methods*. 2, 443–448 (2005). <https://doi.org/10.1038/nmeth765>
245. Harrison, F., Muruli, A., Higgins, S., Diggle, S.P.: Development of an ex vivo porcine lung model for studying growth Virulence, And signaling of pseudomonas aeruginosa. *Infection and Immunity*. 82, 3312–3323 (2014). <https://doi.org/10.1128/IAI.01554-14>
246. Thomson, J.J., Withey, J.H.: Bicarbonate increases binding affinity of *Vibrio cholerae* ToxT to virulence gene promoters. *Journal of Bacteriology*. 196, 3872–3880 (2014).  
<https://doi.org/10.1128/JB.01824-14>
247. Lowden, M.J., Skorupski, K., Pellegrini, M., Chiorazzo, M.G., Taylor, R.K., Kull, F.J.: Structure of *Vibrio cholerae* ToxT reveals a mechanism for fatty acid regulation of virulence genes. *Proceedings of the National Academy of Sciences of the United States of America*. 107, 2860–2865 (2010). <https://doi.org/10.1073/pnas.0915021107>
248. Ni, L., Tonthat, N.K., Chinnam, N., Schumacher, M.A.: Structures of the *Escherichia coli* transcription activator and regulator of diauxie, XylR: An AraC DNA-binding family member with a LacI/GalR ligand-binding domain. *Nucleic Acids Research*. 41, 1998–2008 (2013).  
<https://doi.org/10.1093/nar/gks1207>
249. Li, J., Wehmeyer, G., Lovell, S., Battaile, K.P., Egan, S.M.: 1.65 Å resolution structure of the AraC-family transcriptional activator ToxT from *Vibrio cholerae*. *Acta Crystallographica Section:F Structural Biology Communications*. 72, 726–731 (2016).  
<https://doi.org/10.1107/S2053230X1601298X>
250. Lowden, M.J., Skorupski, K., Pellegrini, M., Chiorazzo, M.G., Taylor, R.K., Kull, F.J.: Structure of *Vibrio cholerae* ToxT reveals a mechanism for fatty acid regulation of virulence genes. *Proceedings of the National Academy of Sciences of the United States of America*. 107, 2860–2865 (2010). <https://doi.org/10.1073/pnas.0915021107>

251. Woodbrey, A.K., Onyango, E.O., Pellegrini, M., Kovacicova, G., Taylor, R.K., Gribble, G.W., Jon Kull, F.: A new class of inhibitors of the AraC family virulence regulator *Vibrio cholerae* ToxT. *Scientific Reports*. 7, (2017). <https://doi.org/10.1038/srep45011>
252. Colombani, J., Bianchini, L., Layalle, S., Pondeville, E., Dauphin-Villemant, C., Antoniewski, C., Carré, C., Noselli, S., Léopold, P.: Antagonistic actions of ecdysone and insulins determine final size in *Drosophila*. *Science*. 310, 667–670 (2005). <https://doi.org/10.1126/science.1119432>
253. Plecha, S.C., Withey, J.H.: Mechanism for Inhibition of *Vibrio cholerae* ToxT activity by the unsaturated fatty acid components of bile. *Journal of Bacteriology*. 197, 1716–1725 (2015). <https://doi.org/10.1128/JB.02409-14>
254. Woodbrey, A.K., Onyango, E.O., Kovacicova, G., Kull, F.J., Gribble, G.W.: A Modified ToxT Inhibitor Reduces *Vibrio cholerae* Virulence in Vivo. *Biochemistry*. 57, 5609–5615 (2018). <https://doi.org/10.1021/acs.biochem.8b00667>
255. Shakhnovich, E.A., Hung, D.T., Pierson, E., Lee, K., Mekalanos, J.J.: Virstatin inhibits dimerization of the transcriptional activator ToxT. (2007)
256. Baker, N.A., Sept, D., Joseph, S., Holst, M.J., Andrew McCammon, J.: Electrostatics of nanosystems: Application to microtubules and the ribosome. (2001)
257. Whittle, M., Gillet, V.J., Willett, P., Loesel, J.: Analysis of data fusion methods in virtual screening: Similarity and group fusion. *Journal of Chemical Information and Modeling*. 46, 2206–2219 (2006). <https://doi.org/10.1021/ci0496144>
258. Whittle, M., Gillet, V.J., Willett, P., Loesel, J.: Analysis of data fusion methods in virtual screening: Theoretical model. *Journal of Chemical Information and Modeling*. 46, 2193–2205 (2006). <https://doi.org/10.1021/ci049615w>
259. Svensson, F., Karlén, A., Sköld, C.: Virtual screening data fusion using both structure- and ligand-based methods. *Journal of Chemical Information and Modeling*. 52, 225–232 (2012). <https://doi.org/10.1021/ci2004835>
260. Hert, J., Willett, P., Wilton, D.J., Acklin, P., Azzaoui, K., Jacoby, E., Schuffenhauer, A.: New methods for ligand-based virtual screening: Use of data fusion and machine learning to enhance the effectiveness of similarity searching. In: *Journal of Chemical Information and Modeling*. pp. 462–470 (2006)
261. Hellman, L.M., Fried, M.G.: Electrophoretic mobility shift assay (EMSA) for detecting protein-nucleic acid interactions. *Nature Protocols*. 2, 1849–1861 (2007). <https://doi.org/10.1038/nprot.2007.249>
262. Lee, P.C., Stopford, C.M., Svenson, A.G., Rietsch, A.: Control of effector export by the *Pseudomonas aeruginosa* type III secretion proteins PcrG and PcrV. *Molecular Microbiology*. 75, 924–941 (2010). <https://doi.org/10.1111/j.1365-2958.2009.07027.x>
263. Hornef, M.W., Roggenkamp, A., Geiger, A.M., Hogardt, M., Jacobi, C.A., Heesemann, J.: Triggering the ExoS regulon of *pseudomonas aeruginosa*: A GFP-reporter analysis of exoenzyme (Exo) S, ExoT and ExoU synthesis. *Microbial Pathogenesis*. 29, 329–343 (2000). <https://doi.org/10.1006/mpat.2000.0398>

264. Dolan, S.K., Pereira, G., Silva-Rocha, R., Welch, M.: Transcriptional regulation of central carbon metabolism in *Pseudomonas aeruginosa*. *Microbial Biotechnology*. 13, 285–289 (2020). <https://doi.org/10.1111/1751-7915.13423>
265. Diaz, M.R., King, J.M., Yahr, T.L.: Intrinsic and extrinsic regulation of type III secretion gene expression in *Pseudomonas aeruginosa*. *Frontiers in Microbiology*. 2, (2011). <https://doi.org/10.3389/fmicb.2011.00089>
266. Few antibiotics under development – ReAct. Available at: <https://www.reactgroup.org/toolbox/understand/how-did-we-end-up-here/few-antibiotics-under-development/>. (Accessed: 21st July 2017).
267. Tsai, C.J.Y., Loh, J.M.S., Proft, T.: *Galleria mellonella* infection models for the study of bacterial diseases and for antimicrobial drug testing, (2016)
268. Miyata, S., Casey, M., Frank, D.W., Ausubel, F.M., Drenkard, E.: Use of the *Galleria mellonella* caterpillar as a model host to study the role of the type III secretion system in *Pseudomonas aeruginosa* pathogenesis. *Infection and Immunity*. 71, 2404–2413 (2003). <https://doi.org/10.1128/IAI.71.5.2404-2413.2003>
269. Renwick, J., Reeves, E.P., Wientjes, F.B., Kavanagh, K.: Translocation of proteins homologous to human neutrophil p47phox and p67phox to the cell membrane in activated hemocytes of *Galleria mellonella*. *Developmental and Comparative Immunology*. 31, 347–359 (2007). <https://doi.org/10.1016/j.dci.2006.06.007>
270. Bergin, D., Reeves, E.P., Renwick, J., Wientjes, F.B., Kavanagh, K.: Superoxide production in *Galleria mellonella* hemocytes: Identification of proteins homologous to the NADPH oxidase complex of human neutrophils. *Infection and Immunity*. 73, 4161–4170 (2005). <https://doi.org/10.1128/IAI.73.7.4161-4170.2005>
271. Harrison, F., Diggle, S.P.: An ex vivo lung model to study bronchioles infected with *Pseudomonas aeruginosa* biofilms. *Microbiology (United Kingdom)*. 162, 1755–1760 (2016). <https://doi.org/10.1099/mic.0.000352>
272. Cools, F., Torfs, E., Aizawa, J., Vanhoutte, B., Maes, L., Caljon, G., Delputte, P., Cappoen, D., Cos, P.: Optimization and characterization of a *Galleria mellonella* larval infection model for virulence studies and the evaluation of therapeutics against *Streptococcus pneumoniae*. *Frontiers in Microbiology*. 10, (2019). <https://doi.org/10.3389/fmicb.2019.00311>
273. Angelo, F.D., Baldelli, V., Halliday, N., Pantalone, P., Polticelli, F., Fiscarelli, E., Williams, P., Visca, P., Leoni, L., Rampioni, G.: Identification of FDA-Approved Drugs as Antivirulence Agents Targeting the pqs Quorum-Sensing System of *Pseudomonas aeruginosa*. (2018). <https://doi.org/10.1128/AAC>
274. McLaughlin, H.P., Caly, D.L., McCarthy, Y., Ryan, R.P., Dow, J.M.: An orphan chemotaxis sensor regulates virulence and antibiotic tolerance in the human pathogen *Pseudomonas aeruginosa*. *PLoS ONE*. 7, (2012). <https://doi.org/10.1371/journal.pone.0042205>
275. Zhao, S., Huang, J.J., Sun, X., Huang, X., Fu, S., Yang, L., Liu, X.W., He, F., Deng, Y.: (1-aryloxy-2-hydroxypropyl)-phenylpiperazine derivatives suppress *Candida albicans* virulence by interfering with morphological transition. *Microbial Biotechnology*. 11, 1080–1089 (2018). <https://doi.org/10.1111/1751-7915.13307>

276. Paškevičius, Š., Starkevič, U., Misiūnas, A., Vitkauskienė, A., Gleba, Y., Ražanskienė, A.: Plant-expressed pyocins for control of *Pseudomonas aeruginosa*. *PLoS ONE*. 12, (2017). <https://doi.org/10.1371/journal.pone.0185782>
277. Andrejko, M., Zdybicka-Barabas, A., Cytryńska, M.: Diverse effects of *Galleria mellonella* infection with entomopathogenic and clinical strains of *Pseudomonas aeruginosa*. *Journal of Invertebrate Pathology*. 115, 14–25 (2014). <https://doi.org/10.1016/j.jip.2013.10.006>
278. Pustelny, C., Brouwer, S., Müsken, M., Bielecka, A., Dötsch, A., Nimtz, M., Häussler, S.: The peptide chain release factor methyltransferase PrmC is essential for pathogenicity and environmental adaptation of *Pseudomonas aeruginosa* PA14. *Environmental Microbiology*. 15, 597–609 (2013). <https://doi.org/10.1111/1462-2920.12040>
279. Tang, A., Caballero, A.R., Marquart, M.E., Bierdeman, M.A., O’callaghan, R.J.: Mechanism of *Pseudomonas aeruginosa* small protease (PASP), a corneal virulence factor. *Investigative Ophthalmology and Visual Science*. 59, 5993–6002 (2018). <https://doi.org/10.1167/iovs.18-25834>
280. Yanagihara, K., Tomono, K., Kaneko, Y., Miyazaki, Y., Tsukamoto, K., Hirakata, Y., Mukae, H., Kadota, J.I., Murata, I., Kohno, S.: Role of elastase in a mouse model of chronic respiratory *Pseudomonas aeruginosa* infection that mimics diffuse panbronchiolitis. *Journal of Medical Microbiology*. 52, 531–535 (2003). <https://doi.org/10.1099/jmm.0.05154-0>
281. Nouwens, A.S., Beatson, S.A., Whitchurch, C.B., Walsh, B.J., Schweizer, H.P., Mattick, J.S., Cordwell, S.J.: Proteome analysis of extracellular proteins regulated by the las and rhl quorum sensing systems in *Pseudomonas aeruginosa* PAO1, (2003)
282. Diggle, S.P., Winzer, K., Chhabra, S.R., Worrall, K.E., Cámara, M., Williams, P.: The *Pseudomonas aeruginosa* quinolone signal molecule overcomes the cell density-dependency of the quorum sensing hierarchy, regulates rhl-dependent genes at the onset of stationary phase and can be produced in the absence of LasR. *Molecular Microbiology*. 50, 29–43 (2003). <https://doi.org/10.1046/j.1365-2958.2003.03672.x>
283. Chen, F., Chen, C.C., Riadi, L., Ju, L.K.: Modeling rhl quorum-sensing regulation on rhamnolipid production by *Pseudomonas aeruginosa*. *Biotechnology Progress*. 20, 1325–1331 (2004). <https://doi.org/10.1021/bp049928b>
284. Mukherjee, S., Moustafa, D., Smith, C.D., Goldberg, J.B., Bassler, B.L.: The RhlR quorum-sensing receptor controls *Pseudomonas aeruginosa* pathogenesis and biofilm development independently of its canonical homoserine lactone autoinducer. *PLoS Pathogens*. 13, (2017). <https://doi.org/10.1371/journal.ppat.1006504>
285. Pena, R.T., Blasco, L., Ambroa, A., González-Pedrajo, B., Fernández-García, L., López, M., Bleriot, I., Bou, G., García-Contreras, R., Wood, T.K., Tomás, M.: Relationship between quorum sensing and secretion systems, (2019)
286. Wang, Y., Gao, L., Rao, X., Wang, J., Yu, H., Jiang, J., Zhou, W., Wang, J., Xiao, Y., Li, M., Zhang, Y., Zhang, K., Shen, L., Hua, Z.: Characterization of lasR-deficient clinical isolates of *Pseudomonas aeruginosa*. *Scientific Reports*. 8, (2018). <https://doi.org/10.1038/s41598-018-30813-y>
287. O’Loughlin, C.T., Miller, L.C., Siryaporn, A., Drescher, K., Semmelhack, M.F., Bassler, B.L.: A quorum-sensing inhibitor blocks *Pseudomonas aeruginosa* virulence and biofilm formation.

- Proceedings of the National Academy of Sciences of the United States of America. 110, 17981–17986 (2013). <https://doi.org/10.1073/pnas.1316981110>
288. Dasgupta, N., Wolfgang, M.C., Goodman, A.L., Arora, S.K., Jyot, J., Lory, S., Ramphal, R.: A four-tiered transcriptional regulatory circuit controls flagellar biogenesis in *Pseudomonas aeruginosa*. *Molecular Microbiology*. 50, 809–824 (2003). <https://doi.org/10.1046/j.1365-2958.2003.03740.x>
  289. Appelt, S., Heuner, K.: The flagellar regulon of *Legionella*-A review, (2017)
  290. Arora, S.K., Ritchings, B.W., Almira, E.C., Lory, S., Ramphal, R.: A Transcriptional Activator, FleQ, Regulates Mucin Adhesion and Flagellar Gene Expression in *Pseudomonas aeruginosa* in a Cascade Manner. (1997)
  291. Arora, S.K., Neely, A.N., Blair, B., Lory, S., Ramphal, R.: Role of motility and flagellin glycosylation in the pathogenesis of *Pseudomonas aeruginosa* burn wound infections. *Infection and Immunity*. 73, 4395–4398 (2005). <https://doi.org/10.1128/IAI.73.7.4395-4398.2005>
  292. Li, Y., Bai, F., Xia, H., Zhuang, L., Xu, H., Jin, Y., Zhang, X., Bai, Y., Qiao, M.: A novel regulator PA5022 (aefA) is involved in swimming motility, biofilm formation and elastase activity of *Pseudomonas aeruginosa*. *Microbiological Research*. 176, 14–20 (2015). <https://doi.org/10.1016/j.micres.2015.04.001>
  293. Toutain, C.M., Zegans, M.E., O'Toole, G.A.: Evidence for two flagellar stators and their role in the motility of *Pseudomonas aeruginosa*. *Journal of Bacteriology*. 187, 771–777 (2005). <https://doi.org/10.1128/JB.187.2.771-777.2005>
  294. Caiazza, N.C., Merritt, J.H., Brothers, K.M., O'Toole, G.A.: Inverse regulation of biofilm formation and swarming motility by *Pseudomonas aeruginosa* PA14. *Journal of Bacteriology*. 189, 3603–3612 (2007). <https://doi.org/10.1128/JB.01685-06>
  295. Tremblay, J., Richardson, A.P., Lépine, F., Déziel, E.: Self-produced extracellular stimuli modulate the *Pseudomonas aeruginosa* swarming motility behaviour. *Environmental Microbiology*. 9, 2622–2630 (2007). <https://doi.org/10.1111/j.1462-2920.2007.01396.x>
  296. Hutchison, M.L., Govan, J.R.W.: Pathogenicity of microbes associated with cystic fibrosis. (1999)
  297. Yeung, A.T.Y., Torfs, E.C.W., Jamshidi, F., Bains, M., Wiegand, I., Hancock, R.E.W., Overhage, J.: Swarming of *Pseudomonas aeruginosa* is controlled by a broad spectrum of transcriptional regulators, including MetR. *Journal of Bacteriology*. 191, 5592–5602 (2009). <https://doi.org/10.1128/JB.00157-09>
  298. Koehler, T., Koehler, K., Curty, L.K., Barja, F., Delden, C. van, Peche`re, J.-C., Peche`re, P.: Swarming of *Pseudomonas aeruginosa* Is Dependent on Cell-to-Cell Signaling and Requires Flagella and Pili Downloaded from. (2000)
  299. Kamatkar, N.G., Shrout, J.D.: Surface hardness impairment of quorum sensing and swarming for *pseudomonas aeruginosa*. *PLoS ONE*. 6, (2011). <https://doi.org/10.1371/journal.pone.0020888>
  300. Leighton, T.L., Buensuceso, R.N.C., Howell, P.L., Burrows, L.L.: Biogenesis of *Pseudomonas aeruginosa* type IV pili and regulation of their function, (2015)

301. Kazmierczak, B.I., Schniederberend, M., Jain, R.: Cross-regulation of *Pseudomonas* motility systems: The intimate relationship between flagella, pili and virulence, (2015)
302. Alarcon, I., Evans, D.J., Fleiszig, S.M.J.: The role of twitching motility in *Pseudomonas aeruginosa* exit from and translocation of corneal epithelial cells. *Investigative Ophthalmology and Visual Science*. 50, 2237–2244 (2009). <https://doi.org/10.1167/iovs.08-2785>
303. Talà, L., Fineberg, A., Kukura, P., Persat, A.: *Pseudomonas aeruginosa* orchestrates twitching motility by sequential control of type IV pili movements, (2019)
304. Kearns, D.B., Robinson, J., Shimkets, L.J.: *Pseudomonas aeruginosa* exhibits directed twitching motility up phosphatidylethanolamine gradients. *Journal of Bacteriology*. 183, 763–767 (2001). <https://doi.org/10.1128/JB.183.2.763-767.2001>
305. Pinzon, N.M., Ju, L.K.: Improved detection of rhamnolipid production using agar plates containing methylene blue and cetyl trimethylammonium bromide. *Biotechnology Letters*. 31, 1583–1588 (2009). <https://doi.org/10.1007/s10529-009-0049-7>
306. Dötsch, A., Klawonn, F., Jarek, M., Scharfe, M., Blöcker, H., Häussler, S.: Evolutionary conservation of essential and highly expressed genes in *Pseudomonas aeruginosa*. *BMC Genomics*. 11, (2010). <https://doi.org/10.1186/1471-2164-11-234>
307. Gambello, M.J., Iglewski, B.H.: Cloning and Characterization of the *Pseudomonas aeruginosa* lasR Gene, a Transcriptional Activator of Elastase Expression. (1991)
308. Pesci, E.C., Pearson, J.P., Seed, P.C., Iglewski, B.H.: Regulation of las and rhl Quorum Sensing in *Pseudomonas aeruginosa*. (1997)
309. Rumbaugh, K.P., Griswold, J.A., Iglewski, B.H., Hamood, A.N.: Contribution of Quorum Sensing to the Virulence of *Pseudomonas aeruginosa* in Burn Wound Infections. (1999)
310. Bondí, R., Messina, M., de Fino, I., Bragonzi, A., Rampioni, G., Leoni, L.: Affecting *Pseudomonas aeruginosa* phenotypic plasticity by quorum sensing dysregulation hampers pathogenicity in murine chronic lung infection. *PLoS ONE*. 9, (2014). <https://doi.org/10.1371/journal.pone.0112105>
311. Lesprit, P., Faurisson, F., Join-Lambert, O., Roudot-Thoraval, F., Foglino, M., Vissuzaine, C., Carbon, C.: Role of the Quorum-sensing System in Experimental Pneumonia due to *Pseudomonas aeruginosa* in Rats. *American Journal of Respiratory and Critical Care Medicine*. 167, 1478–1482 (2003). <https://doi.org/10.1164/rccm.200207-736BC>
312. Bru, J.-L., Rawson, B., Trinh, C., Whiteson, K., Molin Høyland-Krogsho, N., Siryaporn, A.: PQS Produced by the *Pseudomonas aeruginosa* Stress Response Repels Swarms Away from Bacteriophage and Antibiotics. (2019). <https://doi.org/10.1128/JB>
313. Li, W.R., Zeng, T.H., Xie, X.B., Shi, Q.S., Li, C.L.: Inhibition of the pqsABCDE and pqsH in the pqs quorum sensing system and related virulence factors of the *Pseudomonas aeruginosa* PAO1 strain by farnesol. *International Biodeterioration and Biodegradation*. 151, (2020). <https://doi.org/10.1016/j.ibiod.2020.104956>
314. Mcgowan, D.: Characterization of the Chp System of *Pseudomonas aeruginosa*. (2016)

315. Fulcher, N.B., Holliday, P.M., Klem, E., Cann, M.J., Wolfgang, M.C.: The *Pseudomonas aeruginosa* Chp chemosensory system regulates intracellular cAMP levels by modulating adenylate cyclase activity. *Molecular Microbiology*. 76, 889–904 (2010). <https://doi.org/10.1111/j.1365-2958.2010.07135.x>
316. Semmler, A.B.T., Whitchurch, C.B., Mattick, J.S.: A re-examination of twitching motility in *Pseudomonas aeruginosa*. (1999)
317. Whitchurch, C.B., Leech, A.J., Young, M.D., Kennedy, D., Sargent, J.L., Bertrand, J.J., Semmler, A.B.T., Mellick, A.S., Martin, P.R., Alm, R.A., Hobbs, M., Beatson, S.A., Huang, B., Nguyen, L., Commolli, J.C., Engel, J.N., Darzins, A., Mattick, J.S.: Characterization of a complex chemosensory signal transduction system which controls twitching motility in *Pseudomonas aeruginosa*. *Molecular Microbiology*. 52, 873–893 (2004). <https://doi.org/10.1111/j.1365-2958.2004.04026.x>
318. D’Argenio, D.A., Gallagher, L.A., Berg, C.A., Manoil, C.: *Drosophila* as a model host for *pseudomonas aeruginosa* infection. *Journal of Bacteriology*. 183, 1466–1471 (2001). <https://doi.org/10.1128/JB.183.4.1466-1471.2001>
319. letters to nature 98. (2000)
320. Mattick, J.S.: Type IV pili and twitching motility, (2002)
321. Stroml, M.S., Lory, S.: STRIFCTURE-FUNCTION AND BIOGENESIS OF THE TYPE IV PILI. (1993)
322. Whitchurch, C.B., Alm, R.A., Matrick, J.S.: The alginate regulator AlgR and an associated sensor FimS are required for twitching motility in *Pseudomonas aeruginosa*. (1996)
323. O’toole, G.A., Gibbs, K.A., Hager, P.W., Phibbs, P. v, Kolter, R.: The Global Carbon Metabolism Regulator Crc Is a Component of a Signal Transduction Pathway Required for Biofilm Development by *Pseudomonas aeruginosa*. (2000)
324. Beatson, S.A., Whitchurch, C.B., Sargent, J.L., Levesque, R.C., Mattick, J.S.: Differential regulation of twitching motility and elastase production by Vfr in *Pseudomonas aeruginosa*. *Journal of Bacteriology*. 184, 3605–3613 (2002). <https://doi.org/10.1128/JB.184.13.3605-3613.2002>
325. Darzins, A.: The pilG Gene Product, Required for *Pseudomonas aeruginosa* Pilus Production and Twitching Motility, Is Homologous to the Enteric, Single-Domain Response Regulator CheY. (1993)
326. Sampedro, I., Parales, R.E., Krell, T., Hill, J.E.: *Pseudomonas* chemotaxis, (2015)
327. Ortega, D.R., Fleetwood, A.D., Krell, T., Harwood, C.S., Jensen, G.J., Zhulin, I.B.: Assigning chemoreceptors to chemosensory pathways in *Pseudomonas aeruginosa*. *Proceedings of the National Academy of Sciences of the United States of America*. 114, 12809–12814 (2017). <https://doi.org/10.1073/pnas.1708842114>
328. Croft, L., Beatson, S.A., Whitchurch, C.B., Huang, B., Blakeley, R.L., Mattick, J.S.: An interactive web-based *Pseudomonas aeruginosa* genome database : discovery of new genes, pathways and structures. (2000)
329. Stover, C.K., Pham<sup>2</sup>, X.Q., Erwin, A.L., Mizoguchi, S.D., Warrenner, P., Hickey, M.J., Brinkman<sup>3</sup>, F.S.L., Hufnagle, W.O., Kowalik, D.J., Lagrou, M., Garber, R.L., Goltry, L., Tolentino, E.,

- Westbrock-Wadman, S., Yuan, Y., Brody, L.L., Coulter, S.N., Folger, K.R., Kas<sup>2</sup>, A., Larbig, K., Lim<sup>2</sup>, R., Smith<sup>2</sup>, K., Spencer<sup>2</sup>, D., Wong<sup>2</sup>, -S, Wu<sup>2</sup>, Z., Paulsenk, I.T., Reizer, J., Saier, M.H., Hancock<sup>3</sup>, R.E.W., Lory#, S., Olson<sup>2</sup>, M. v: Complete genome sequence of *Pseudomonas aeruginosa* PAO1, an opportunistic pathogen. (2000)
330. Inclan, Y.F., Persat, A., Greninger, A., von Dollen, J., Johnson, J., Krogan, N., Gitai, Z., Engel, J.N.: A scaffold protein connects type IV pili with the Chp chemosensory system to mediate activation of virulence signaling in *Pseudomonas aeruginosa*. *Molecular Microbiology*. 101, 590–605 (2016). <https://doi.org/10.1111/mmi.13410>
331. Fajardo, A., Martínez-Martín, N., Mercadillo, M., Galán, J.C., Ghysels, B., Matthijs, S., Cornelis, P., Wiehlmann, L., Tümmler, B., Baquero, F., Martínez, J.L.: The neglected intrinsic resistome of bacterial pathogens. *PLoS ONE*. 3, (2008). <https://doi.org/10.1371/journal.pone.0001619>
332. Breidenstein, E.B.M., Khaira, B.K., Wiegand, I., Overhage, J., Hancock, R.E.W.: Complex ciprofloxacin resistome revealed by screening a *Pseudomonas aeruginosa* mutant library for altered susceptibility. *Antimicrobial Agents and Chemotherapy*. 52, 4486–4491 (2008). <https://doi.org/10.1128/AAC.00222-08>
333. Dötsch, A., Becker, T., Pommerenke, C., Magnowska, Z., Jänsch, L., Häussler, S.: Genomewide identification of genetic determinants of antimicrobial drug resistance in *Pseudomonas aeruginosa*. *Antimicrobial Agents and Chemotherapy*. 53, 2522–2531 (2009). <https://doi.org/10.1128/AAC.00035-09>
334. Winey, M., Meehl, J.B., O’Toole, E.T., Giddings, T.H.: Conventional transmission electron microscopy, (2014)
335. Koehler, T., Koehler, K., Curty, L.K., Barja, F., Delden, C. van, Peche`re, J.-C., Peche`re, P.: Swarming of *Pseudomonas aeruginosa* Is Dependent on Cell-to-Cell Signaling and Requires Flagella and Pili Downloaded from. (2000)
336. Rashid, M.H., Kornberg, A.: Inorganic polyphosphate is needed for swimming, swarming, and twitching motilities of *Pseudomonas aeruginosa*.
337. Feldman, M., Bryan, R., Rajan, S., Scheffler, L., Brunnert, S., Tang, H., Prince, A.: Role of Flagella in Pathogenesis of *Pseudomonas aeruginosa* Pulmonary Infection. (1998)
338. Leech, A.J., Mattick, J.S.: Effect of site-specific mutations in different phosphotransfer domains of the chemosensory protein ChpA on *Pseudomonas aeruginosa* motility. *Journal of Bacteriology*. 188, 8479–8486 (2006). <https://doi.org/10.1128/JB.00157-06>
339. Shrout, J.D., Chopp, D.L., Just, C.L., Hentzer, M., Givskov, M., Parsek, M.R.: The impact of quorum sensing and swarming motility on *Pseudomonas aeruginosa* biofilm formation is nutritionally conditional. *Molecular Microbiology*. 62, 1264–1277 (2006). <https://doi.org/10.1111/j.1365-2958.2006.05421.x>
340. Murray, T.S., Kazmierczak, B.I.: FlhF Is required for swimming and swarming in *Pseudomonas aeruginosa*. *Journal of Bacteriology*. 188, 6995–7004 (2006). <https://doi.org/10.1128/JB.00790-06>

341. Toutain, C.M., Caizza, N.C., Zegans, M.E., O'Toole, G.A.: Roles for flagellar stators in biofilm formation by *Pseudomonas aeruginosa*. *Research in Microbiology*. 158, 471–477 (2007). <https://doi.org/10.1016/j.resmic.2007.04.001>
342. Egelman, E.H., Kaplan, M., Ghosal, D., Subramanian, P., Oikonomou, C.M., Kjaer, A., Pirbadian, S., Ortega, D.R., Briegel, A., El-Naggar, M.Y., Jensen, G.J.: The presence and absence of periplasmic rings in bacterial flagellar motors correlates with stator type. <https://doi.org/10.7554/eLife.43487.001>
343. Jyot, J., Sonawane, A., Wu, W., Ramphal, R.: Genetic mechanisms involved in the repression of flagellar assembly by *Pseudomonas aeruginosa* in human mucus. *Molecular Microbiology*. 63, 1026–1038 (2007). <https://doi.org/10.1111/j.1365-2958.2006.05573.x>
344. Chuang, S.K., Vrla, G.D., Fröhlich, K.S., Gitai, Z.: Surface association sensitizes *Pseudomonas aeruginosa* to quorum sensing. *Nature Communications*. 10, (2019). <https://doi.org/10.1038/s41467-019-12153-1>
345. Rodesney, C.A., Roman, B., Dhamani, N., Cooley, B.J., Katira, P., Touhami, A., Gordon, V.D.: Mechanosensing of shear by *Pseudomonas aeruginosa* leads to increased levels of the cyclic-di-GMP signal initiating biofilm development. *Proceedings of the National Academy of Sciences of the United States of America*. 114, 5906–5911 (2017). <https://doi.org/10.1073/pnas.1703255114>
346. Luo, Y., Zhao, K., Baker, A.E., Kuchma, S.L., Coggan, K.A., Wolfgang, M.C., Wong, G.C.L., O'Toole, G.A.: A hierarchical cascade of second messengers regulates *Pseudomonas aeruginosa* Surface Behaviors. *mBio*. 6, (2015). <https://doi.org/10.1128/mBio.02456-14>
347. Siryaporn, A., Kuchma, S.L., O'Toole, G.A., Gitai, Z., Ausubel, F.M.: Surface attachment induces *Pseudomonas aeruginosa* virulence. *Proceedings of the National Academy of Sciences of the United States of America*. 111, 16860–16865 (2014). <https://doi.org/10.1073/pnas.1415712111>
348. Bardoel, B.W., Hartsink, D., Vughs, M.M., de Haas, C.J.C., van Strijp, J.A.G., van Kessel, K.P.M.: Identification of an immunomodulating metalloprotease of *Pseudomonas aeruginosa* (IMP<sub>a</sub>). *Cellular Microbiology*. 14, 902–913 (2012). <https://doi.org/10.1111/j.1462-5822.2012.01765.x>
349. Tian, Z., Cheng, S., Xia, B., Jin, Y., Bai, F., Cheng, Z., Jin, S., Liu, X., Wu, W.: *Pseudomonas aeruginosa* ExsA Regulates a Metalloprotease, ImpA, That Inhibits Phagocytosis of Macrophages. (2019). <https://doi.org/10.1128/IAI>
350. Seo, J., Brencic, A., Darwin, A.J.: Analysis of secretin-induced stress in *Pseudomonas aeruginosa* suggests prevention rather than response and identifies a novel protein involved in secretin function. *Journal of Bacteriology*. 191, 898–908 (2009). <https://doi.org/10.1128/JB.01443-08>
351. Gicquel, G., Bouffartigues, E., Bains, M., Oxaran, V., Rosay, T., Lesouhaitier, O., Connil, N., Bazire, A., Maillot, O., Bénard, M., Cornelis, P., Hancock, R.E.W., Dufour, A., Feuilloley, M.G.J., Orange, N., Déziel, E., Chevalier, S.: The extra-cytoplasmic function sigma factor sigX modulates biofilm and virulence-related properties in *pseudomonas aeruginosa*. *PLoS ONE*. 8, (2013). <https://doi.org/10.1371/journal.pone.0080407>

352. Jarrell' And, K.F., Kropinski, A.M.: The Virulence of Protease and Cell Surface Mutants of *Pseudomonas aeruginosa* for the Larvae of *Galleria me/lone/la*. (1982)
353. Tsang, J., Hoover, T.R.: Themes and Variations: Regulation of RpoN-Dependent Flagellar Genes across Diverse Bacterial Species. *Scientifica*. 2014, 1–14 (2014).  
<https://doi.org/10.1155/2014/681754>